

Beyond Standard Neuthreenos

Fundamental physics in the neutrino sector from three perspectives: oscillations, astrophysics and cosmology.

Antoni Bertólez Martínez



Aquesta tesi doctoral està subjecta a la llicència <u>Reconeixement- NoComercial – CompartirIgual 4.0. Espanya de Creative Commons</u>.

Esta tesis doctoral está sujeta a la licencia <u>Reconocimiento - NoComercial – CompartirIgual</u> <u>4.0. España de Creative Commons.</u>

This doctoral thesis is licensed under the <u>Creative Commons Attribution-NonCommercial-ShareAlike 4.0. Spain License.</u>

PhD thesis

Beyond Standard Neuthreenos

Fundamental physics in the neutrino sector from three perspectives: oscillations, astrophysics and cosmology.

Antoni Bertólez Martínez



Beyond Standard Neuthreenos

Fundamental physics in the neutrino sector from three perspectives: oscillations, astrophysics and cosmology.

Memòria presentada per optar al grau de doctor per la Universitat de Barcelona

Programa de doctorat en Física

Toni Bertólez Martínez

Director: Dr. Jordi Salvadó Serra

> Tutor: Dr. Joan Soto

Departament de Física Quàntica i Astrofísica Institut de Ciències del Cosmos Universitat de Barcelona



A la mama i al papa, és clar.

Your science will be valueless, you'll find.
And learning will be sterile, if inviting.
Unless you pledge your intellect to fighting.
Against all enemies of all mankind.

- Bertolt Brecht

To the Students of the Workers' and Peasants' Faculty

Contents

Re	esum	- Abst	ract	iv			
Li	st of	publica	ations	ix			
Li	st of	abbrev	riations	xi			
1	Intr	oducti	on to this thesis	1			
I	Ne	utrin	os from the lab	5			
2	Wh	at we k	know from the lab: an introduction	7			
	2.1	The S	tandard Model	7			
		2.1.1	The SM Lagrangian I: massless fields	9			
		2.1.2	The SM Lagrangian II: Higgs SSB and massive fields	10			
		2.1.3	Neutrino interactions	12			
	2.2	Massi	ve neutrinos and how to get them	13			
		2.2.1	Right-handed-neutrinos: Dirac vs Majorana	14			
		2.2.2	The type-I see-saw mechanism	15			
	2.3	Neutr	ino oscillations	16			
		2.3.1	Wave packet formalism of neutrino oscillations	20			
		2.3.2	Neutrino oscillations experiments	22			
		2.3.3	Searching for the absolute neutrino mass scale	26			
3	lmp	act of	Wave Packet Separation in Low-Energy Sterile Neutrino Searches	31			
	3.1	1 Formalism					
	3.2	.2 Impact on neutrino experiments					
		3.2.1	DayaBay analisis	36			
		3.2.2	NEOS analysis	38			
		3.2.3	DayaBay+NEOS joint analysis	39			
		3.2.4	PROSPECT analysis	40			
		3.2.5	BEST analysis	41			
	3.3	Result	ts	42			
	3.4	Concl	usions	43			
H	N	eutri	nos from outer space	47			
4	The	dawn	of ultra-high-energy neutrino astrophysics	49			
			o crossover of multimossonger actrophysics	50			

		4.1.1	The origin of ultra-high-energy Cosmic Rays	51
		4.1.2	A common origin for CRs, gamma rays and neutrinos	53
		4.1.3	The GZK cut-off and cosmogenic neutrinos	54
		4.1.4	Ultra-high-energy neutrinos for BSM searches	54
	4.2	The ex	perimental search for UHE neutrinos	56
		4.2.1	Optical detection experiments	57
		4.2.2	Radio detection experiments	60
5	lceC	ube an	d the origin of ANITA-IV events	63
	5.1	Beyon	d the Standard Model explanation	65
		5.1.1	Number of expected events	66
		5.1.2	Details of the test statistic	68
		5.1.3	Transient sources vs diffuse flux	70
	5.2	ANITA	a-IV angular self-consistency	70
	5.3	Interpl	lay with IceCube	72
		5.3.1	Impact of T absorption	74
	5.4	Particl	e physics models	75
	5.5	Summ	ary and conclusions	77
П	IN	leutri	nos from the Universe	79
6	Wha	at we k	now of the Universe: an introduction	81
	6.1	An hor	mogeneous Universe, expanding	82
		6.1.1	The geometry of the Universe	83
		6.1.2	The content of the Universe	84
		6.1.3	The evolution of the Universe	85
		6.1.4	Geodesics and the Boltzmann equation	87
	6.2	The lin	nearly perturbed Universe	88
		6.2.1	Gauge invariance and transformations	89
		6.2.2	Initial conditions	90
		6.2.3	Evolution of perturbations	92
	6.3	The Co	osmic Microwave Background	93
		6.3.1	Temperature inhomogeneities	94
		6.3.2	From inhomogeneities to anisotropies	95
		6.3.3	A modified separation of the Sachs-Wolfe effects	99
	6.4	Big Ba	ng Nucleosynthesis	101
7	Orig	gin of co	osmological neutrino mass bounds: background versus perturbations	s 107
	7.1	Forma	lism	109
		7.1.1	Evolution of the background	109

		7.1.2	Evolution of perturbations	. 111
	7.2	Physic	al effects on the CMB	. 116
		7.2.1	Low multipoles ($\ell \lesssim 10$)	. 117
		7.2.2	Intermediate multipoles (10 $\lesssim \ell \lesssim$ 500)	. 118
		7.2.3	High multipoles ($\ell \gtrsim 500$)	
	7.3	Consti	raints from Planck18 CMB data	. 122
		7.3.1	Results	. 123
		7.3.2	Discussion	. 124
	7.4	Conclu	usions and Outlook	. 126
8	BBN	l bound	ds on neutrinophilic ultralight Dark Matter	131
	8.1	Forma	lism	. 132
		8.1.1	Dirac equation and effective fermion mass	. 133
		8.1.2	Pseudoscalar equation of motion	. 135
	8.2	Adiaba	atic approximation	. 137
	8.3	Pheno	menology	. 140
		8.3.1	Energy density and effective mass	. 140
		8.3.2	Pressure and equation of state	. 143
		8.3.3	Initial conditions	. 146
		8.3.4	Massive neutrinos and N_{eff}	. 148
		8.3.5	Impact on Big Bang Nucleosynthesis	. 149
	8.4	Result	s	. 152
	8.5	Conclu	usions and outlook	. 154
I۷	, C	Concli	usions and appendices	157
•			• •	150
9	Con	clusion	IS	159
Α	UHE	Epartic	le propagation inside the Earth	161
Bi	bliog	raphy		165
Ag	raïm	ents		203

Resum

Títol de la tesi: Més enllà dels neutrins estàndard. Física fonamental en el sector dels neutrins des de tres perspectives: oscil·lacions, astrofísica i cosmologia.

Si mirem la matèria que ens forma i forma l'Univers amb el màxim nivell de detall a què hem arribat, hi trobem les partícules fonamentals. La teoria física que les recull com una "taula periòdica" i que descriu com aquestes interaccionen és el Model Estàndard. De totes les partícules fonamentals del Model Estàndard, n'hi ha tres que no som capaços d'explicar del tot: els neutrins.

Segons el Model Estàndard de la física de partícules, els neutrins són partícules sense massa. És a dir, cap de les partícules que coneixem és capaç de proveir amb massa als neutrins, així com el Higgs ho fa amb la resta de partícules del Model Estàndard. Ara bé, en les darreres dècades hem descobert i comprovat experimental –amb una precisió que no deixa lloc al dubte– que els neutrins sí que tenen massa. Aquests experiments han mesurat les anomenades oscil·lacions de neutrins, que representen la primera prova directa experimental que el Model Estàndard, la física fonamental de partícules que coneixem, és incomplet. És a dir, calen noves partícules o forces que expliquin per què els neutrins tenen massa.

Aquesta, però, no és l'única manca del Model Estàndard. Alguns fenòmens, com la Matèria Fosca o l'Energia Fosca, no tenen explicació dins el Model Estàndard, i generalment requereixen física Més enllà del Model Estàndard: noves partícules, noves forces. Malgrat que la comunitat científica ha pensat moltes propostes que podrien resoldre aquests problemes, per ara la cerca no ha donat cap resultat positiu. Ja que els neutrins són les primeres partícules que ens han avisat experimentalment que el Model Estàndard està incomplet, per què no utilitzar-les per esbrinar què li falta exactament?

Aquesta tesi és un esforç en aquesta direcció. En concret, és un recull de tres maneres –diferents i complementàries – en què podem utilitzar els neutrins per a descobrir quina és la física Més enllà del Model Estàndard. En la primera part, ens endinsem en les oscil·lacions de neutrins i, en concret, en la cerca de neutrins estèrils en experiments a baixa energia. Revisitem la descripció de paquet d'ona d'aquestes oscil·lacions, i demostrem que –donat el coneixement experimental que tenim – la mida del paquet d'ona podria afectar els resultats de les cerques. En la segona part, passem de la baixa energia fins a les energies més altes que coneixem, la dels neutrins cosmogènics. Aquests són neutrins que es generarien degut a les partícules més energètiques mai mesurades, els rajos còsmics ultraenergètics. Reanalitzem les deteccions anòmales de neutrins ultraenergètics de l'antena ANITA-IV i analitzem com podrien els telescopis de neutrins del futur i del present restringir possibles extensions del Model Estàndard. Finalment, en

la tercera part, mirem com utilitzar la cosmologia per a calcular la massa dels neutrins relíquia de l'Univers, i la robustesa de la mesura davant de modificacions Més enllà de Model Estàndard. També, utilitzem la nucleosíntesi primordial per a entendre si els neutrins podrien interactuar amb Matèria Fosca molt lleugera.

Així doncs, aquesta tesi s'emmarca en la fenomenologia de física de partícules i la cerca de física Més enllà del Model Estàndard, en concret en el sector dels neutrins. El seu enfocament és un pont entre la física teòrica i l'experimental: l'anàlisi de models motivats teòricament a partir de les seves conseqüències en experiments presents i futurs. En concret, pretén fer entendre millor el potencial d'aquests experiments i fer repensar les hipòtesis convencionalment assumides darrere les seves conclusions.

Paraules clau: neutrins, física de partícules, astrofísica, cosmologia.

Abstract

If we look at the matter that forms the Universe with the highest level of detail we have reached, we find fundamental particles. The physical theory that collects these particles, like the "periodic table" did for the chemical elements, and that describes how they interact is the Standard Model (SM) of Particle Physics. Of all the fundamental particles of the SM, there are three of them that we cannot yet fully explain: neutrinos.

According to the SM, neutrinos are massless particles. That is, none of the particles that we know is capable of providing mass to the neutrinos, as the Higgs field does with the rest of the particles of the SM. However, in recent decades we have discovered and experimentally tested –with a precision that leaves no room for doubt—that neutrinos do have mass. These experiments have measured the so-called neutrino oscillations. These are the first direct experimental proof that the SM, or fundamental particle physics as we know it, is incomplete. That is, new particles or forces are required to explain why neutrinos have mass.

This, however, is not the only shortcoming of the SM. There are phenomena, such as Dark Matter (DM) and Dark Energy (DE), that the SM can hardly explain, and that generally require physics Beyond the Standard Model (BSM): new particles or new forces. While the scientific community has thought of many BSM extensions that could solve these shortcomings, as of today the search for them has not given positive results. Since neutrinos are the first particles that have experimentally warned us that the SM is incomplete, why not use them to find out exactly what is missing?

This thesis is an effort in this direction. Specifically, it is a compilation of three ways –different and complementary– in which we can use neutrinos to discover what physics is beyond the SM. In the first part, we delve into neutrino oscillations and, specifically, in the search for sterile neutrinos in low-energy experiments. We review the wave packet description and demonstrate that –for our current experimental knowledge– the wave packet width could affect the results of the searches. In the second part, we move from low energies to the highest energies we know, those of cosmogenic neutrinos. These are neutrinos which are produced by the most energetic particles we know of, ultra-high-energy (UHE) Cosmic Rays. We reanalyze the anomalous detections of UHE neutrinos by the ANITA-IV antenna and analyze how future and present neutrino telescopes could restrict possible BSM extensions. Finally, in the third part, we look at how to use cosmology to calculate the mass of the relic neutrinos of the Universe, as well as the robustness of the method against BSM. Furthermore, we use Big Bang Nucleosynthesis to constrain interactions between neutrinos and ultralight DM.

Thus, this thesis belongs to the phenomenology of particle physics and the search

for BSM physics, specifically in the neutrino sector. Its approach is a bridge between theoretical and experimental physics: the analysis of theoretically motivated models based on their consequences in present and future experiments. Specifically, it aims to better understand the potential of these experiments and to rethink the hypotheses conventionally assumed behind their measurements.

Keywords: neutrinos, particle physics, astrophysics, cosmology.

List of publications

The original contents of this thesis are based on the following publications.

Part I. Neutrinos from the lab

[1] C. A. Argüelles, T. Bertólez-Martínez, J. Salvadó. "Impact of wave packet separation in low-energy sterile neutrino searches", Phys.Rev.D 107 (2023) 3, 036004; arXiv: 2201.05108.

Part II. Neutrinos from outer space

[2] T. Bertólez-Martínez, C. A. Argüelles, I. Esteban, J. López-Pavón, I. Martínez-Soler, J. Salvadó. "IceCube and the origin of ANITA-IV events", JHEP 07 (2023), 005; arXiv: 2305.03746

Part III. Neutrinos from the Universe

[3] T. Bertólez-Martínez, I. Esteban, R. Hajjar, O. Mena, J. Salvado. "Origin of cosmological neutrino mass bounds: background *versus* perturbations", arXiv: 2411.14524.

T. Bertólez-Martínez, A. Burns, J. López-Sarrión, J. Salvadó. "BBN bounds on neutrinophilic ultralight DM", *To appear*.

The following publication has been developed in parallel to the content of this thesis, but it has not been included in this dissertation:

[4] Virgile Dandoy, Toni Bertólez-Martínez, Francesco Costa. "High Frequency Gravitational Wave Bounds from Galactic Neutron Stars", JCAP 12 (2024), 023; arXiv: 2402.14092.

Apart from the collaborators, the author would like to acknowledge Janet Conrad, Maria Concepcion Gonzalez-Garcia, John Hardin, Joachim Kopp and Alexei Smirnov for insightful discussions on [1], as well as the anonymous referees which improved the manuscripts. The author also thanks Dr. Alessio Bianchi for the original template of this thesis. The research from the author has been possible thanks to the Spanish grant PRE2020-091896, and has received support from the Spanish grants PID2019-108122GBC32, PID2019-105614GB-C21 and PID2022-126224NB-C21, from the European Union's Horizon 2020 research and innovation programme under the Marie Skłodowska-Curie grant agreement No 860881-HIDDeN and the Marie Skłodowska-Curie Staff Exchange grant agreement No 101086085-ASYMMETRY, and from the State Agency for Research of the Spanish Ministry of Science and Innovation through the "Unit of Excellence María de Maeztu 2020-2023" award to the Institute of Cosmos Sciences (CEX2019-000918-M).

List of abbreviations

Here follow the most repeated abbreviations within the thesis.

BAOs Baryon Accoustic Oscillations

BBN Big Bang Nucleosynthesis
BSM Beyond the Standard Model

CC (NC) Charged (Neutral)-Current interaction

CMB Cosmic Microwave Background

CR Cosmic Ray
DE Dark Energy
DM Dark Matter

FLRW Friedmann-Lemaître-Robertson-Walker metric

GZK Greisen-Zatsepin-Kuzmin, cut-off or flux

ACDM Cosmological constant-Cold Dark Matter model of cosmology

PW (WP) Plane Wave (Wave Packet) formalism

NO (IO) Normal (Inverted) Ordering

SM Standard Model

(I)SW (Integrated) Sachs-Wolfe effect

UHE Ultra-High-Energy (i.e., $E \gtrsim 100 \,\text{PeV}$)

ULDM UltraLight Dark Matter

1 Introduction to this thesis

Neutrins que tot ho travessen, a mils en micro-tempestes Petits, traspassen es cossos, atòmics, inclús no tan grossos Neutrins, pareix impossible, sou tot matèria intangible Neutrins, amics invisibles, sou indestructibles, tranquils

- Antònia Font - Neutrins

Our world is traversed by neutrinos. They come in threes: electron neutrinos v_e , muon neutrinos v_μ and tau neutrinos v_τ . In this thesis, I have also confronted them from three different perspectives: neutrino oscillations, neutrino ultra-high-energy astrophysics and neutrino cosmology. This triple approach to the three neutrinos, i.e., neuthreenos, explains the name of this thesis.

During the research that has lead to this thesis, I have approached these topics with a phenomenological approach. The current state of particle physics phenomenology lays on the shoulders of giants, many generation of researchers who have bridged the gap between theoretical models and their experimental realisation. The work presented here is inspired and lies on top of a great amount of theoretical work on particle extensions to the Standard Model (SM) of Particle Physics, commonly known as Beyond the Standard Model (BSM) theories. In particular, this thesis collects different research works which try to use neutrinos to experimentally constrain such BSM theories.

Neutrinos have long been carriers of New Physics. Indeed, their first proposal by Pauli [5] was a desperate attempt to keep energy conservation against the apparent missing energy of beta decay. Neutrinos were also necessary actors for the discovery of neutral currents in the Gargamelle chamber at CERN [6], which then lead to the discovery of the W and Z bosons [7–10]. However, the modern cornerstone of New Physics from the neutrino sector begun with the solar neutrino problem [11, 12] and the discovery of atmospheric neutrinos [13, 14]. These neutrinos from natural sources lead to the discovery of neutrino oscillations [15, 16], which were later confirmed by terrestrial experiments [17–19] and measured with higher precision. As of today, neutrino oscillations are the only direct experimental measurement that requires physics which is not within the particle content of the SM.

Then, neutrinos, and neutrino masses in particular, are currently our best reminder that the SM of Particle Physics is not yet complete. In other words, that there is still a lot of work to do to understand the fundamental pieces of matter. Since neutrino oscillations gave us the first hint, it is the natural place to search for more hints; and so this is the topic of part I. In this part, chapter 2 reviews the basics of the SM in

order to understand why neutrino masses are a BSM phenomenon¹, and the theoretical and experimental groundings of neutrino oscillations. Then, chapter 3 delves in sterile neutrino searches at low-energy experiments, and how going beyond the plane wave approximation may modify the results.

The neutrinos that gave us that first BSM hint came from the Sun and cosmic rays from the Universe. Apart from this, astrophysical phenomena provide a natural source for the most extremely energetic neutrinos, resulting into potential collisions at higher center-of-mass energies than the Large Hadron Collider at CERN. Once again, neutrinos from beyond the Earth can be the key to explore uncharted territory beyond the SM [20], and so part II explores the intriguing world of neutrino ultra-high-energy astrophysics. In this part, chapter 4 offers an introduction to astroparticle physics and multimessenger astronomy. It explains why are ultra-high-energy neutrinos expected to exist, how are we looking for them, and how could we use them to explore BSM physics. Then, in chapter 5 explores the first anomalies of the field, the so-called ANITA-IV anomalous events. Using their measurements, we quantitatively show how data from neutrino telescopes can be leveraged to constrain BSM.

Finally, even if neutrino oscillations require the extension of the SM with neutrino masses, they can not provide us with a measurement of their absolute value [21–23]. Even if neutrino masses were discovered on terrestrial experiments, our best shot to finally measure the absolute neutrino mass, a currently unknown BSM parameter, is within cosmology. Then, neutrino cosmology is the topic of part III. First, chapter 6 introduces the basics of cosmology and its two cornerstones: the Cosmic Microwave Background (CMB) and Big Bang Nucleosynthesis (BBN). Then, chapter 7 explains the physical meaning of the measurement of neutrino masses with the CMB, and tries to make it more robust. Finally, in chapter 8 we use BBN to constrain the interaction between neutrinos and ultralight Dark Matter.

As I will try to develop in this thesis, neutrino phenomenology is experiencing a very exciting time, and particularly in these three fields. There are feasible discoveries in the mid-term future (e.g., the neutrino mass hierarchy [24–28], the CP phase [29, 30], the absolute neutrino mass [31–34]) which will precisely complete the measurement of the known parameters in the neutrino sector. There are also long-term exciting challenges (e.g. the Dirac or Majorana nature of the neutrino [35–37], cosmogenic neutrinos and the GZK flux [20, 38], the measurement of the Cosmic Neutrino Background [39, 40]) to keep us motivated for many generations to come. In any of the three fields here

¹This is, in fact, not an agreed-upon consensus of the particle physics community. Whether to call neutrino masses BSM or not is simply a matter of notation and a *sterile* debate. If you would like to spend your time in such a way, you might as well ask yourself what is the onomatopeia of a neutrino (*skibidi-woof!*).

presented, there is plenty of short-term work that must be done before we can set our hands on the solutions to these mysteries.

This thesis is too a honest effort in this direction. In particular, it strives to explore the potential of current and future experiments to uncover BSM physics through the neutrino sector, and to shed light on the challenges in the way. This thesis' phenomenological approach into BSM has mainly been model-independent, i.e, undergoing a minimal set of assumptions on the underlying BSM theory. In this manner, the focus is cast on the generic BSM Physics properties that experiments are probing, which can then be applied to different extensions to the SM.

After working in these three very different fields, with very different expertises required, I expect this thesis to have the value of interdisciplinarity. I have tried to balance clarity and concision, while providing a broad perspective of the fields. This has required me to present three different introductions, one at the start of each part. I encourage the reader to jump over these if they are already familiar with the topic. Also, I have tried to acknowledge the work that precedes me, and illustrate the exciting research landscape in the three fields, which implies a long list of references. All in all, I hope that this thesis is able to transmit a sense of excitement towards the future of neutrino phenomenology.

Part I Neutrinos from the lab

2 What we know from the lab: an introduction

I have done a terrible thing, I have postulated a particle that cannot be detected.

- Wolfgang Pauli [5]

(also every other PhD student in modern Physics)

Particle Physics is the endeavor of studying the fundamental building blocks (i.e. degrees of freedom) that make up the past and present Universe. During the last century, their properties and interactions have been probed by high-energy experiments to unfathomable precision. All these measurements have been matched with equally precise predictions from the Standard Model (SM) of Particle Physics. In almost all observations, theory and experiments agree to great detail, thus making the SM the most robust theory of particle physics. However, there is a experimental signature which the SM cannot account for: neutrino oscillations. This part of the thesis is devoted to them. In order to understand how do neutrinos break the SM and their existence as a light into the unknown, we first must discuss what we know. And what we know is the Standard Model.

Many lines have been shed to explain the SM, as lecture series [41–45], books [46–48] and historical discussions [49–51]. It is neither possible for me nor my goal do to a better task at explaining the SM than the existing bibliography. In this chapter we will only shortly discuss the details of the SM which are relevant to neutrinos, and which justify that neutrino oscillations (and masses) are not explained within the SM. In general, for further insights into any of the statements of this chapter, please refer to the cited references.

2.1 The Standard Model

If I could remember the names of all these particles, I'd be a botanist.

- Enrico Fermi, presumably.

The SM is a renormalizable Quantum Field Theory in flat 3+1 spacetime, first proposed by Weinberg, Glashow and Salam [52–54]. As such, it "only" describes electroweak and strong interactions at a 10^{-11} level of accuracy [55], but does not include

gravitational effects. The SM accounts for these interactions by introducing the local symmetry group [52–54, 56–58]

$$SU(3)_{C} \times SU(2)_{L} \times U(1)_{Y}. \tag{2.1}$$

The SM is born from asking that the laws of physics are invariant under local transformations of this group, eq. (2.1) [42]. These are called gauge transformations, and thus the SM is a gauge theory. In order for local gauge transformations to leave the system invariant, it is necessary to introduce a gauge boson for each generator of the group. Thus the SM predicts the existence of gauge bosons, spin-one particles which mediate the interactions of the SM.

On the one hand, in eq. (2.1), $SU(3)_C$ is the gauge group which describes quantum chromodynamics, i.e., the strong interaction between quarks which makes up mesons and hadrons. It predicts color, an intrinsic degree of freedom which can take up to three values, and gluons, massless bosons through which colored particles can interact. Since neutrinos are colorless, i.e., singlets under $SU(3)_C$, neutrinos do not interact through the strong interaction. Admittedly, $SU(3)_C$ describes the structure of the nucleus, which is definitely relevant for neutrino-nucleus interactions. Still, this thesis will not delve into these further.

On the other hand, invariance under the symmetry group $SU(2)_L \times U(1)_Y$ introduces the electroweak sector of the SM. First, $SU(2)_L$ only applies to left-handed particles, while right-handed particles are singlets under its transformations. This describes an interaction which maximally violates parity by only interacting with left-handed particles, the weak interaction. Symmetries under this group predict two charged bosons, W^1 , W^2 , which allow charged currents that convert neutral leptons v_L into charged leptons ℓ_L . But $SU(2)_L$ has three generators, and thus a further neutral gauge boson is predicted, W^3 . This mediates neutral currents which do not convert neutrinos. The electroweak unification consists of describing weak and electromagnetic interactions within the unified group $SU(2)_L \times U(1)_Y$. To such purpose, the hypercharge is defined as a combination of the electric charge Q and the third generator of $SU(2)_L$, the weak isospin T_3 , as

$$Y = 2(T_3 - Q), (2.2)$$

leading to a fourth gauge boson, B. As we will see in the next section, the Higgs mechanism spontaneously breaks this electroweak symmetry into a residual symmetry $U(1)_{em}$ which predicts a massless photon, γ . Contrarily, the other three bosons become massive, now W^{\pm} and Z^{0} . These bosons mediate the weak interaction, and their non-zero mass explains the short range of the interaction.

$(SU(3)_{C}, SU(2)_{L}, U(1)_{Y})$					
$(1,2,-\frac{1}{2})$	$(3, 2, \frac{1}{6})$	(1, 1, -1)	$(3, 1, \frac{2}{3})$	$\left(3,1,-\frac{1}{3}\right)$	
$\ell_L^e = \begin{pmatrix} \nu_e \\ e \end{pmatrix}_L$	$Q_L^{1,i} = \begin{pmatrix} u^i \\ d^i \end{pmatrix}_L$	e_R	u_R^i	d_R^i	
$\ell_L^\mu = \begin{pmatrix} \nu_\mu \\ \mu \end{pmatrix}_L$	$Q_L^{2,i} = \begin{pmatrix} c^i \\ s^i \end{pmatrix}_L$	μ_R	c_R^i	s_R^i	
$\ell_L^{\tau} = \begin{pmatrix} \nu_{\tau} \\ \tau \end{pmatrix}_L$	$Q_L^{3,i} = \begin{pmatrix} t^i \\ b^i \end{pmatrix}_L$	$ au_R$	t_R^i	b_R^i	

Table 2.1: The three generations of the fermionic particle content in the Standard Model, or flavors. For $SU(2)_L$ and $SU(3)_C$, 1, 2 and 3 denote the single, doublet and triplet representations, respectively. For $U(1)_Y$, the hypercharge Y is given; and for $SU(3)_C$, i = R, G, G are the colors of the quarks. From left to right, left-handed leptons, left-handed quarks, right-handed charged leptons and right-handed quarks. *The SM contains only left-handed neutrinos*.

Once the gauge bosons predicted by eq. (2.1) have been defined, we are allowed to introduce the particle content, which must be in the irreducible representation of this group. The particles that we have discovered up to today, and which make up the SM, are listed in table 2.1. Additionally to the three generations of quarks and leptons, the SM contains a neutral scalar, the Higgs boson. The field associated to this particle is the responsible for giving mass to (almost) all particles in the SM.

2.1.1 The SM Lagrangian I: massless fields

Once the particle content of the SM is defined, its dynamics are described by the most general renormalizable Lagrangian density invariant under eq. (2.1). First, in the gauge sector we have

$$\mathcal{L}_{\text{gauge}} = -\frac{1}{4} G^{a}_{\mu\nu} G^{a\mu\nu} - \frac{1}{4} W^{a}_{\mu\nu} W^{a\mu\nu} - \frac{1}{4} B_{\mu\nu} B^{\mu\nu} . \tag{2.3}$$

Here, $G_{\mu\nu}^a$, $W_{\mu\nu}^a$, $B_{\mu\nu}$ are the field strength tensors of SU(3)_C, SU(2)_L and U(1)_Y, respectively. In these equations, and in the remaining of the thesis, the Einstein summation notation is assumed, i.e., repeated indices are summed over. $\mathcal{L}_{\text{gauge}}$ describes the kinetic energies of the gauge fields and their self-interactions. If gauge bosons were massless and isolated, these would be the only terms in the Lagrangian.

Second, in the fermion sector we have

$$\mathcal{L}_{\text{fermion}} = \sum_{f} \bar{f}(i\gamma^{\mu}D_{\mu})f, \qquad (2.4)$$

where the sum on f runs over the 15 fermion multiplets in table 2.1, γ^{μ} are the Dirac

matrices, and D_{μ} is the covariant derivative

$$D_{\mu} = \partial_{\mu} - ig_{s}G_{\mu}^{i}t^{i} - igW_{\mu}^{i}\tau^{i} - ig'YB_{\mu}. \tag{2.5}$$

Here,

- The second term introduces the coupling between quarks and gluons through the coupling constant g_s . G^i_{μ} are the gluon fields, t^i are the generators from SU(3)_C, with $i=1,\ldots,8$.
- The third term involves the SU(2)_L part of the electroweak sector, with g the corresponding coupling constant, W^i_μ the gauge bosons and τ^i the group generators, for $i=1,\ldots,3$.
- The last term belongs to the $U(1)_Y$ part, with g' the coupling constant and Y the hypercharge of the fermion.

Then, $\mathcal{L}_{\text{fermion}}$ describes the dynamics of the SM fermions as if they were massless and interacting with the gauge bosons. However, we know that SM fermions are massive. We need something else.

2.1.2 The SM Lagrangian II: Higgs SSB and massive fields

Given the particle content of the SM from table 2.1, one can introduce a mass term for the electron as $m_e \bar{e}_L^c e_R$ or $m_e \bar{e}_R^c e_R$. This term conserves electric charge, but is not invariant under the subgroup $SU(2)_L$. Explicitly introducing a mass term for charged leptons is inconsistent with the symmetries of the SM, eq. (2.1). At the same time, precisely because the electron has a mass, we know that the $SU(2)_L$ symmetry must not be realized at low energies. The way to solve the inconsistency between the electron mass and the symmetry group is through the Higgs mechanism, which spontaneously breaks the $SU(2)_L \times U(1)_Y$ symmetry. That is, the fundamental theory describing the dynamics satisfies this symmetry, but the ground state of the system does not.

In the Higgs or ABEGHHK'tH¹ mechanism [59–61], we introduce the Higgs scalar Φ , which is a complex scalar doublet under SU(2)_L. The Higgs sector of the SM lagrangian is given by

$$\mathcal{L}_{\text{Higgs}} = D_{\mu} \Phi D^{\mu} \Phi - V(\phi), \qquad (2.6)$$

where $V(\phi)$ is the Higgs potential energy density, usually written as

$$V(\phi) = \mu^2 |\Phi|^2 + \lambda |\Phi|^4, \tag{2.7}$$

¹Fair but unutterable acronym for Anderson, Brout, Englert, Guralnik, Hagen, Higgs, Kibble, and 't Hooft.

with μ , λ parameters describing the shape of the potential. If $\mu^2 < 0$ and $\lambda > 0$, then this potential has a mexican hat shape and a minimum at $\Phi = \langle \Phi \rangle e^{i \arg \Phi}$, with

$$\langle \Phi \rangle = \frac{1}{\sqrt{2}} \begin{pmatrix} 0 \\ v \end{pmatrix},\tag{2.8}$$

where the Higgs vacuum expectation value (vev), v, is given by

$$v = \sqrt{-\frac{\mu^2}{\lambda}} \,. \tag{2.9}$$

Each $\arg \Phi$ gives a minimum of the potential which breaks the total electroweak group $SU(2)_L \times U(1)_Y$, but leaves the ground state symmetric under an electromagnetic group $U(1)_{\rm em}$. The breaking of the symmetry happens once a non-zero minimum is realized, which for simplicity we pick to be $\arg \Phi = 0$. Then, the scalar field around the minimum is

$$\Phi(x) = \frac{1}{\sqrt{2}} \begin{pmatrix} 0 \\ v + h(x) \end{pmatrix} \exp\left\{i \frac{\vec{\sigma} \cdot \vec{\xi}}{v}\right\}, \qquad (2.10)$$

where ξ_i are Goldstone bosons associated with excitations along the ring of the mexican hat. However, since these bosons can be gauged away through an SU(2)_L transformation, they are not physical. The only observable excitation is the Higgs field, h(x), discovered at CERN in 2012 [62, 63].

Then, while W^i_{μ} , B_{μ} were the weak eigenstates of $SU(2)_L \times U(1)_Y$, the mass eigenstates after symmetry breaking become

$$W_{\mu}^{\pm} = \frac{1}{\sqrt{2}} \left(W_{\mu}^{1} + W_{\mu}^{2} \right) ,$$

$$Z_{\mu} = \cos \theta_{w} W_{\mu}^{3} - \sin \theta_{w} B_{\mu} ,$$

$$A_{\mu} = \sin \theta_{w} W_{\mu}^{3} + \cos \theta_{w} B_{\mu} ,$$
(2.11)

where $\theta_w = \arctan(g'/g)$ is the Weinberg angle [46]. The mass terms to these gauge bosons comes from the kinematic term of the Higgs potential,

$$\mathcal{L}_{\text{Higgs}} \supset \frac{g^2 v^2}{4} W_{\mu}^+ W^{\mu -} + \frac{1}{2} \frac{(g^2 + {g'}^2) v^2}{4} Z_{\mu} Z^{\mu}. \tag{2.12}$$

We can read $m_W = gv/2$ and $m_Z = \sqrt{g^2 + {g'}^2}v/2$, while A_μ , the photon field, remains massless. Furthermore, the potential energy becomes $V(h) \supset \mu^2 h^2$, where we read $m_H = \sqrt{2}\mu$.

This is a beautiful result, which amazes me every time I revisit it. However, this does not answer yet how does the Higgs mechanism explain fermion masses. While a mass term like $m_e \bar{e}_L e_R$ is forbidden by our symmetry group, Yukawa interaction terms with Φ are not. For instance, for the first generation of fermions we can write

$$\mathcal{L}_{\text{Yukawa}} \supset y_e \bar{\ell}_L \Phi e_R + y_u \bar{q}_L \tilde{\Phi} u_R + y_d \bar{q}_L \Phi d_R + \text{h.c.}, \qquad (2.13)$$

where y_i are the Yukawa couplings of each of the SM fermions defined in table 2.1 (except neutrinos) and $\tilde{\Phi} = i\tau_2\Phi^*$. These interaction terms are invariant under SU(2)_L. After the Higgs field acquires a non-zero vev, these Yukawa interactions give the following mass terms,

$$\mathcal{L}_{\text{Yukawa}} \supset y_e \frac{v}{\sqrt{2}} \bar{e}_L e_R + y_u \frac{v}{\sqrt{2}} \bar{u}_L u_R + y_d \frac{v}{\sqrt{2}} \bar{d}_L d_R. \qquad (2.14)$$

Where we can identify the mass of the SM fermions, $m_i = y_i v / \sqrt{2}$. Not having enough with unifying electromagnetism and the weak interaction, the Higgs mechanism simultaneously solves the problem of fermion masses, all in one.

Fermion masses through the Higgs mechanism work because right-handed electrons exist. However, the SM does not include right-handed neutrinos, v_R . In fact, if such right-handed neutrinos existed, they would be a singlet of all SM interactions. Since right-handed neutrinos are not included in the SM, the Yukawa interaction lagrangian from eq. (2.13) does not lead to a mass term for neutrinos in the SM, as is the case of the charged fermions in eq. (2.14). No other term which respects the SM symmetry group from eq. (2.1) can lead to a mass term for neutrinos. In conclusion, within the SM, neutrinos should be strictly massless.

2.1.3 Neutrino interactions

The only term in the SM relevant which directly involves neutrinos is $\mathcal{L}_{\text{fermion}}$. After spontaneous symmetry breaking, neutrinos interact only with the weak gauge bosons, W^{\pm} and Z^{0} . This leads to charged-current (CC) and neutral-current (NC) interactions, respectively. On the one hand, CC interactions are given by

$$\mathcal{L}_{CC} = -\frac{g}{2} \left(\bar{\ell}_L \gamma^\mu \nu_L W_\mu^- + \text{h.c.} \right) . \tag{2.15}$$

CC interactions transform a neutrino of a given flavor, i.e., v_e , v_μ , v_τ ; with the corresponding charged lepton of the same flavor, e, μ , τ . That is, neutrino flavors are precisely defined through their interaction in charged currents.

On the other hand, NC interactions are described by

$$\mathcal{L}_{NC} = -\frac{g'}{2\cos\theta_{w}} \left(\bar{\nu}_{L} \gamma^{\mu} \nu_{L} Z_{\mu} + \text{h.c.} \right) . \tag{2.16}$$

NC interactions leave the neutrino flavor unchanged and are flavor-blind. In fact, it is through the Z boson that we know that there are only three active neutrinos, $(\nu_e, \nu_\mu, \nu_\tau)$. By looking at the decay $Z \to f\bar{f}$, the branching ratio into invisible particles is proportional to the number of active neutrinos (i.e., which participate in weak interactions through eq. (2.16)), N_ν , as

$$\Gamma_{\rm inv} = \Gamma(Z \to \nu \,\bar{\nu}) N_{\nu} = \frac{G_F m_Z^3}{12 \sqrt{2} \pi} N_{\nu} \,.$$
 (2.17)

LEP measured $N_{\nu} = 2.9840 \pm 0.0082$ [64], which discards the existence of more undiscovered active neutrinos.

Before closing this section, notice that all terms in the SM Lagrangian, and eqs. (2.15) and (2.16) in particular, conserve lepton flavor number. That is, if an initial state contains an electron neutrino v_e , the final state must also carry a net electron flavor (whether in the form of e or v_e); and analogously for muon and tau lepton flavors. Therefore, within the SM, lepton flavor number is conserved.

2.2 Massive neutrinos and how to get them

We have now learned that, in the SM, neutrinos should be massless and conserve lepton flavor number. However, nature does not know what is the SM, and needs not realize it. Three decades ago, it was neutrino physicists who measured the first deviation from SM predictions. From that time on, a plethora of neutrino oscillations experiments have measured that lepton flavor number is not conserved, e.g., [15–17, 24, 25, 65, 66]. For instance, we have seen how solar neutrinos (which should only contain electron neutrinos) measured in the Earth also contain muon and tau neutrinos [16]. Neutrinos do not conserve their flavor during their propagation, and this has been independently proven among: many different experiments, from many different sources, looking at many different channels, with many different energies and at many different propagation distances. Furthermore, the energy-dependence of this oscillations has been measured to be in excellent agreement with neutrinos having a mass.

In other words, *neutrinos are massive and the SM is not exactly realized in nature*. This is a fact, as the 2015 Nobel Prize in Physics shows, awarded to Takaaki Kajita and Arthur B. McDonald, from the Super-Kamiokande [15] and SNO [16] collaborations,

for the discovery of neutrino oscillations, which shows that neutrinos have mass. In this section we will introduce an example on how can we extend the SM to explain neutrino masses, while in the next section (section 2.3) we will describe the phenomenology of neutrino oscillations. For further insights into both of them, we refer the reader to [55, 67–69].

2.2.1 Right-handed-neutrinos: Dirac vs Majorana

In eq. (2.14) we have seen that electrons receive their mass from their Yukawa interaction with the Higgs field, which is possible due to existence of right-handed electrons. In particular, electrons in the SM are Dirac fermions, since their particle and antiparticle states are different. A possibility to extend the SM, which is analogous to the charged lepton sector, is to introduce right-handed-neutrinos (RHNs), ν_R , such that

$$\mathcal{L}_{\text{Dirac}} = -Y_{ij} \bar{\nu}_{Ri} \tilde{\Phi} \nu_{Lj}. \tag{2.18}$$

Here, we have added a total of m RHNs, v_{Ri} , and a Yukawa couplings matrix, Y_{ij} , of dimension $m \times 3$. After symmetry breaking, this would lead to neutrinos having a mass term

$$\mathcal{L}_{\text{Dirac}} = -M_{Dij}\bar{\nu}_{Ri}\nu_{Lj}, \quad \text{with } M_{Dij} = Y_{ij}\frac{v}{\sqrt{2}}. \tag{2.19}$$

Here we have defined the Dirac mass matrix M_{Dij} , of dimension $m \times 3$. If this were the neutrino sector Lagrangian, then neutrinos would also be Dirac fermions, with neutrinos and antineutrinos being different particles. This term can break lepton flavor number, but *Dirac neutrinos conserve the total lepton number*.

This scenario, while conceptually simple, holds two major caveats. First, in order to get sub-eV neutrino masses [21], one would require to have a Yukawa coupling, $y_{ij} \lesssim 10^{-12}$, which is six orders of magnitude smaller than the electron one. This huge separation of scales is unexplained by this minimal extension. Second, and most importantly, once we have added a RHN, the symmetries from the SM as in eq. (2.1) allow us to include also a Majorana mass term,

$$\mathcal{L}_{\text{Majorana}} = -\frac{1}{2} M_{Nij} \bar{v}_{Ri} v_{Rj}^{c} + \text{h.c.}, \qquad (2.20)$$

where $v^c = C\bar{v}^T$ is the neutrino charge conjugated field, with C the charge conjugation operator. Here, M_N is a symmetric $m \times m$ matrix, the Majorana mass matrix. Since RHNs are singlets of the SM gauge groups, there is no a priori reason not to include this term. The consequent need to fine-tune $M_N \to 0$ makes this minimal extension not very natural.

Apart from breaking lepton flavor, the Majorana mass term from eq. (2.20) breaks total lepton number by two unities. This is possible because the mass eigenstates would be Majorana fermions, fulfilling $v^c = v$. Since such neutrinos are their own antiparticle, they can annihilate and break lepton number by two unities. As a consequence, this mass term predicts processes like neutrinoless double beta decay, where a nucleus decays by emitting two electrons and no electron antineutrinos [70].

One could also try to define a Majorana mass term without introducing RHNs, e.g., $m\bar{\nu}_L \nu_L^c$. However, this term is not invariant under the SM gauge group and therefore can not be UV complete. One must go to higher order in SM Effective Field Theory (SMEFT) and write a higher-dimensional operator in terms of the SM fields which does introduce a Majorana mass term for the neutrino [71, 72]. In fact, SMEFT only has one 5-dimensional operator, the Weinberg operator [73],

$$\mathcal{L}_{\text{Weinberg}} = \frac{C_{\alpha\beta}}{\Lambda} \bar{\ell}_L^{\alpha} \tilde{\Phi} \tilde{\Phi}^T \ell_L^{\beta c}. \tag{2.21}$$

Here, $C_{\alpha\beta}$ is a matrix of coefficients, and Λ is the cut-off scale where New Physics is expected. After Higgs symmetry breaking, this becomes

$$\mathcal{L}_{\text{Weinberg}} = C_{\alpha\beta} \frac{v^2}{2\Lambda} \bar{v}_{L\alpha} v_{L\beta}^c \,, \tag{2.22}$$

which precisely acts as a Majorana mass term. Then, any UV completion whose IR realization is eq. (2.21) would make neutrinos Majorana, with their mass suppressed by Λ , and break total lepton number. Let us look into a particularly natural realization of such UV extensions (albeit definitely not the only one).

2.2.2 The type-I see-saw mechanism

Let us rewrite $\mathcal{L}_{mass} = \mathcal{L}_{Dirac} + \mathcal{L}_{Majorana}$ as

$$\mathcal{L}_{\text{mass}} = \frac{1}{2} \begin{pmatrix} \vec{v}_L^c, \ \vec{v}_R \end{pmatrix} \begin{pmatrix} 0 & M_D^T \\ M_D & M_N \end{pmatrix} \begin{pmatrix} \vec{v}_L \\ \vec{v}_R^c \end{pmatrix} + \text{h.c.} \equiv \vec{v}^c M_v \vec{v} + \text{h.c.}, \qquad (2.23)$$

where $\vec{v} = (\vec{v}_L, \vec{v}_R^c)^T$ is a (3+m)-dimensional vector, composed of 3 active neutrinos and m RHNs. The diagonalisation of M_v leads into 3+m mass eigenstates $v_{\rm mass}$ which are Majorana. In particular, if $M_N \gg M_D$, then this leads to 3 light eigenstates of mass

$$m_{\text{light}} \sim M_D M_N^{-1} M_D^T \,, \tag{2.24}$$

which are mostly left-handed; and m heavy eigenstates of mass $\sim M_N$ which are mostly right-handed. Such kind of heavy RHN are expected in SM extensions such as SO(10) GUTs [74, 75] or left-right symmetric models [76], and usually predict that the scale of New Physics, $\Lambda \sim M_N$, is much larger than the electroweak scale. Then, this mechanism naturally explains the lightness of neutrino masses, and is commonly known as the type-I see-saw mechanism [70, 73, 76, 77]. Indeed, integrating-out the heavy RHNs out of eq. (2.23) leads into a Weinberg operator as in eq. (2.21) with $\Lambda \sim M_N$. Other realisations of the see-saw mechanism also exist, without necessarily requiring RHN. For instance, the so-called type-II see-saw extends the SM with scalar triplets with hypercharge Y = 2 [78]; and the type-III see-saw extends it with fermionic triplets with no hypercharge [79].

2.3 Neutrino oscillations

We have introduced neutrino mass eigenstates, $|v_{\text{mass},i}\rangle \equiv |v_i\rangle = \{v_1, v_2, v_3, ..., v_n\}$, with n=3+m. These mass eigenstates need not be the same as the flavor (or interaction) eigenstates, $|v_{\alpha}\rangle = \{v_{Le}, v_{L\mu}, v_{L\tau}, v_{R1}, ..., v_{Rm}\}$. In general, these two basis of neutrino eigenstates are related by a mixing matrix $U_{\alpha i}$,

$$|\nu_{\alpha}\rangle = \sum_{i} U_{\alpha i}^{*} |\nu_{i}\rangle. \tag{2.25}$$

From eq. (2.15), a charged-current interaction will always produce a neutrino with defined flavor α . After travelling for a time t, the neutrino state will evolve to

$$|v(t)\rangle = e^{-i\hat{H}t}|v_{\alpha}\rangle, \tag{2.26}$$

where \hat{H} is the Hamiltonian operator. As a first step, we can assume that all the mass eigenstates are described by plane waves, with energy

$$E_i = \sqrt{p_i^2 + m_i^2} \simeq p_i + \frac{m_i^2}{2p_i} \simeq E + \frac{m_i^2}{2E}.$$
 (2.27)

Here, we have used that neutrinos are ultrarelativistic, and thus $p_i \simeq p_j \equiv p \simeq E$. Then, what differentiates the energy of the mass eigenstates is their squared mass, m_i^2 . Removing the part of the Hamiltonian which is proportional to the identity (which only introduces a global phase), the Hamiltonian in the mass base is

$$\hat{H}_m = \frac{1}{2E} \text{diag}\left(m_1^2, m_2^2, \dots, m_n^2\right)$$
 (2.28)

Then, the evolution of the neutrino in eq. (2.26) becomes

$$|v(t)\rangle = e^{-i\hat{H}t}|v_{\alpha}\rangle = \sum_{i=1}^{n} U_{\alpha i}^{*} \exp\left\{-i\frac{m_{i}^{2}L}{2E}\right\}|v_{i}\rangle. \tag{2.29}$$

Here, L = ct is the travelled distance, usually called the baseline length.

Now, in general $|v(t)\rangle$ does not remain as a $|v_{\alpha}\rangle$, but has some possibility of undergoing a charged-current interaction into a charged lepton state ℓ_{β} . We would associate this process to a final interaction state $|v_{\beta}\rangle$. The probability for such a transition is given by [55, 80–86]

$$P_{\alpha\beta} = \left| \langle v_{\beta} | e^{-i\hat{H}t} | v_{\alpha} \rangle \right|^{2} = \left| \sum_{i=1}^{n} U_{\alpha i}^{*} U_{\beta i} \exp\left\{ -i \frac{m_{i}^{2} L}{2E} \right\} \right|^{2} =$$

$$= \delta_{\alpha\beta} - 4 \sum_{i < j}^{n} \operatorname{Re} \left[U_{\alpha i}^{*} U_{\beta i} U_{\alpha j} U_{\beta j}^{*} \right] \sin^{2} \frac{\Delta m_{ij}^{2} L}{4E} + 2 \sum_{i < j}^{n} \operatorname{Im} \left[U_{\alpha i}^{*} U_{\beta i} U_{\alpha j} U_{\beta j}^{*} \right] \sin \frac{\Delta m_{ij}^{2} L}{2E} ,$$

$$(2.30)$$

where we have used the orthogonality of mass eigenstates, $\langle v_i | v_j \rangle = \delta_{ij}$, and have defined the squared-mass difference, $\Delta m_{ij}^2 = m_i^2 - m_j^2$. If we had followed the same approach for antineutrinos, we would have needed to replace $U \to U^*$, thus changing the sign of the last term.

Equation (2.30) tells us that, if neutrinos have different masses ($\Delta m_{ij} \neq 0$), and their mass eigenstates are not aligned with their interaction eigenstates ($U_{\alpha i}U_{\beta i}\neq 0$), then a neutrino with original flavor α has a non-zero probability of producing a charged lepton of flavor β after travelling some distance L. The oscillatory shape of this probability, shown in fig. 2.1, gave this transition the name of *neutrino oscillations*. It is useful to define the oscillation length as

$$L_{ij}^{\rm osc} = \frac{4\pi E}{|\Delta m_{ij}^2|} \tag{2.31}$$

as the characteristic length at which this oscillation happens. Equation (2.30) has two limits,

- If $L \ll L_{ij}^{\text{osc}}$, $P_{\alpha\beta} = \delta_{\alpha\beta}$. As expected, if the neutrino does not travel for a sufficiently long distance, the oscillation does not happen.
- If $L \gg L_{ij}^{\rm osc}$, then the \sin^2 in the second term averages out to 1/2, and the transition probability is constant

$$P_{\alpha\beta} = \delta_{\alpha\beta} - 2\sum_{i < j}^{n} \operatorname{Re}\left[U_{\alpha i}^{*} U^{\beta i} U_{\alpha j} U_{\beta j}^{*}\right]. \tag{2.32}$$

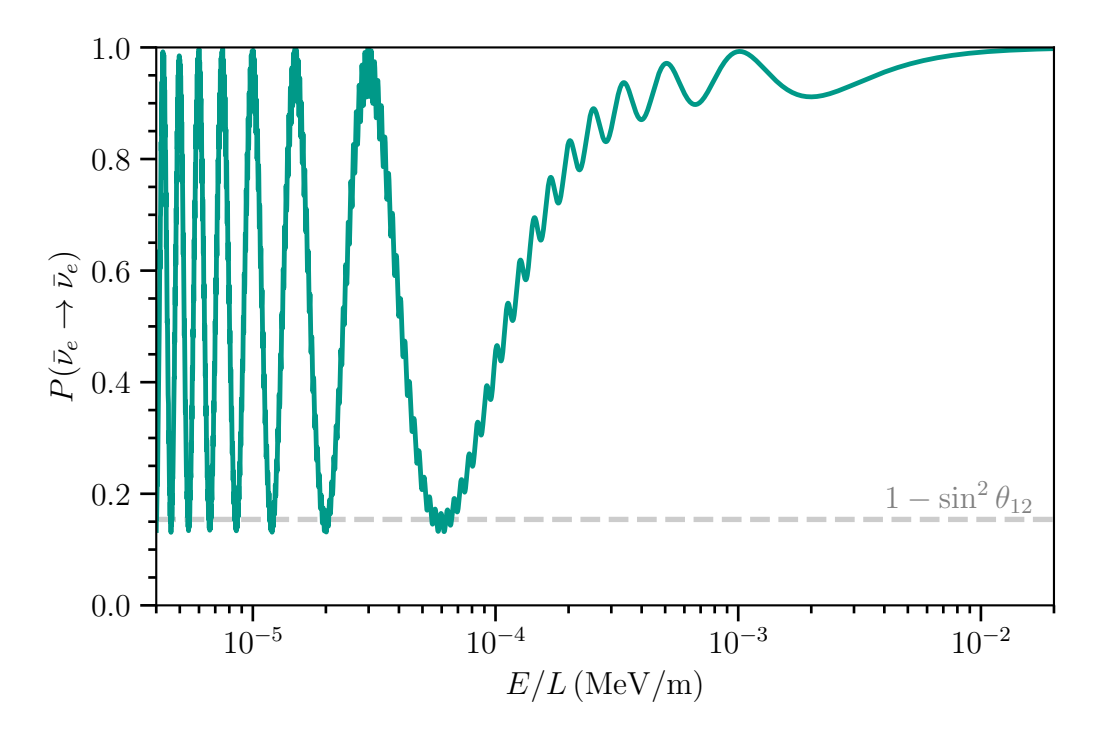


Figure 2.1: The 3-neutrino oscillation probability for electron antineutrino survival, as a function of the E/L ratio. This is the important probability for reactor experiments, where antineutrinos are produced from beta decay and observed by inverse beta decay. The parameters for this figure are taken from [21].

In this limit, many oscillations have happened on the baseline length, and only its average effect remains.

Real sources and detectors have non-monochromatic spectra, finite lengths and finite energy resolution. Neutrino oscillations must be integrated within spatial and energy uncertainties and as a consequence get (partly) averaged.

Three-neutrino oscillations

Equation (2.30) has been tested to great detail between the three known active neutrino eigenstates, $\{v_e, v_\mu, v_\tau\}$. If we reduce the description to these 3 states, U can be described with only six independent parameters: three mixing angles and three phases. Conventionally, it is parametrized as the Pontecorvo-Maki-Nakagawa-Sakata (PMNS) mixing matrix [87, 88]

$$U = \begin{pmatrix} 1 & 0 & 0 \\ 0 & c_{23} & s_{23} \\ 0 & -s_{23} & c_{23} \end{pmatrix} \begin{pmatrix} c_{13} & 0 & s_{13}e^{-i\delta_{CP}} \\ 0 & 1 & 0 \\ -s_{13}e^{i\delta_{CP}} & 0 & c_{13} \end{pmatrix} \begin{pmatrix} c_{21} & s_{12} & 0 \\ -s_{12} & c_{12} & 0 \\ 0 & 0 & 1 \end{pmatrix} \begin{pmatrix} e^{i\eta_{1}} & 0 & 0 \\ 0 & e^{i\eta_{2}} & 0 \\ 0 & 0 & 1 \end{pmatrix}, \quad (2.33)$$

where $c_{ij} = \cos \theta_{ij}$ and $s_{ij} = \sin \theta_{ij}$, with $\theta_{ij} \in [0, \pi/2]$ the mixing angles. Now, $\delta_{\text{CP}} \in [0, 2\pi)$ is the CP phase, responsible for CP violation in the neutrino sector; and $\eta_i \in [0, 2\pi)$ are the Majorana phases. If neutrinos are Dirac, η_i can be absorbed in the neutrino states and these phases are non-physical. Most importantly, even if neutrinos are Majorana and $\eta_i \neq 0$, the dependence of $P_{\alpha\beta}$ on η_i cancels out. In other words, it is not possible to measure Majorana phases from oscillation experiments.

As of 2024, neutrino oscillation experiments have measured the mass-squared differences Δm_{ij}^2 and the mixing angles θ_{ij} with great precision [21],

$$\begin{split} \Delta m_{21}^2 &\equiv \Delta m_{\rm sol}^2 = (7.49 \pm 0.19) \times 10^{-5} \, \text{eV}^2 \,, \\ |\Delta m_{3j}|^2 &\equiv \Delta m_{\rm atm}^2 = (2.534^{+0.025}_{-0.023}) \times 10^{-3} \, \text{eV}^2 \,, \\ \sin^2 \theta_{12} &= 0.307^{+0.012}_{-0.011} \,, \\ \sin^2 \theta_{23} &= 0.561^{+0.012}_{-0.015} \,, \\ \sin^2 \theta_{13} &= 0.02195^{+0.00054}_{-0.00058} \,. \end{split} \tag{2.34}$$

Other global fits find consistent results [22, 89]. Shown explicitly as $|\Delta m_{3j}|^2$, experiments have not yet reached the necessary precision to resolve the sign of the squared-mass difference between m_3 and m_1 (and m_2). As a consequence, we don't know if the lightest mass eigenstate is m_1 or m_3 . This leads to two possible ways of ordering neutrino mass eigenstates (or neutrino mass hierarchy), as shown in fig. 2.2. Namely, in normal ordering (NO) $m_1 < m_2 < m_3$ (the electron neutrino is mainly formed by the lightest state), while in inverted ordering (IO) $m_3 < m_1 < m_2$ (the lightest state has the least electron neutrino mixing). Experiments in the mid-term future will be able to distinguish between these two scenarios [26–28]. Then, values in eq. (2.34) are obtained under the assumption of normal ordering, but are similar to those from inverted ordering [21]. This is not the case for $\delta_{\rm CP}$ due to the current tension between the NOvA and T2K experiments, which does not lead to a clear image for $\delta_{\rm CP}$ [24, 25]. The best-fit value depends largely on the assumed ordering, with $\delta_{\rm CP} = (177^{+19}_{-20})^\circ$ in NO and $\delta_{\rm CP} = (285^{+25}_{-28})^\circ$ in IO [21].

Neutrino oscillations in matter

In general, neutrino oscillations do not happen in vacuum, but in matter. The crosssection of incoherent neutrino-nucleon scattering at the characteristic energies of neutrino oscillations (MeV to GeV) is quite small,

$$\sigma \sim G_F^2 s \sim 10^{-43} \,\mathrm{cm}^2 \left(\frac{E}{\mathrm{MeV}}\right)^2 \,. \tag{2.35}$$

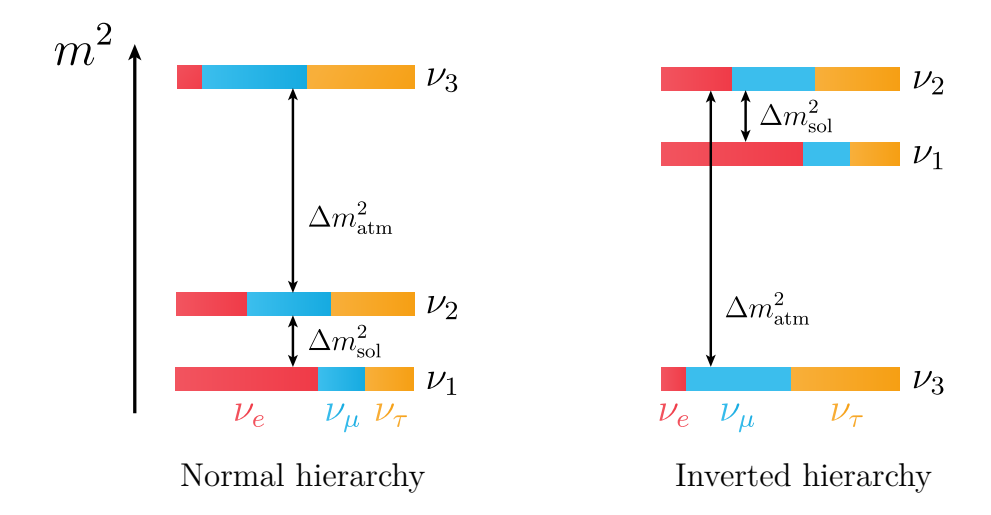


Figure 2.2: There are only two ways of ordering the neutrino mass eigenstates by mass, the normal hierarchy and the inverted hierarchy. For each mass eigenstate v_i , red is the composition of v_e , $|U_{ie}|^2$, blue for v_μ , $|U_{i\mu}|^2$, and orange for v_τ , $|U_{i\tau}|^2$. Values for the mixings taken from [21].

However, neutrinos propagating in matter can interact with the medium coherently. In this case, both the medium and the neutrino remain unchanged, so the scatter and unscattered neutrino waves can interfere. This enhances the effect of the interaction, which becomes proportional to G_F and not to G_F^2 . At the practical level, this requires to add an effective potential to the evolution Hamiltonian at eq. (2.28). In the SM and through ordinary matter, this is given by

$$H = H_m + U^{\dagger}VU$$
, with $V = \operatorname{diag}\left(\pm\sqrt{2}G_F n_e(x), 0, 0\right)$, (2.36)

where $n_e(x)$ is the electron number density at the position x in the medium. Here, + applies to neutrinos, and - to antineutrinos. Characteristic values of the potentials in the Earth core are $V \sim 10^{-13}$ eV, while at the solar core are $V \sim 10^{-12}$ eV. For neutrino oscillations studied in this thesis, matter effects are negligible.

2.3.1 Wave packet formalism of neutrino oscillations

In the previous section, we have obtained the transition probability $P_{\alpha\beta}$ as in eq. (2.30) assuming that neutrinos are in states with unique, well-defined, energy and momentum, i.e., that they propagate as plane waves. This is in contradiction to the kinematics of any neutrino production process, and furthermore neutrinos propagating between a source and a detector are localized. Nonetheless, the plane wave derivation of the oscillation formula leads to the correct result in the regime where the effect of the wave packet

width is negligible [90].

Opposite to the plane wave (PW) formalism, the wave packet (WP) formalism describes the state $|\nu_{\alpha}(t)\rangle$ by

$$|\nu_{\alpha}(t)\rangle = \sum_{i=1}^{n} U_{\alpha i}^{*} \int dp \ \psi_{i}(p) e^{-iE_{i}(p)t} |\nu_{i}(p)\rangle. \tag{2.37}$$

Here the produced state is a superposition of mass eigenstates with different momenta, described by the wave function in momentum space, $\psi_i(p)$. This quantum state is localized in space and describes the physics of a propagating neutrino. In order to reach an analytical result, we assume the evolution to be one dimensional and the momentum distribution to be Gaussian.

After its propagation, the produced neutrino v_{α} can be detected at some detector in a position L at time T through a charged-current interaction $v_{\alpha}X \to l_{\beta}Y$, with l_{β} a lepton of flavor β . The amplitude for this process in the WP formalism is [80]

$$A_{\alpha\beta} \propto \sum_{i=1}^{n} U_{\alpha i}^{*} U_{\beta i} \exp\left\{-iE_{i}^{0} T + iP_{i}L - \frac{(L - v_{i}T)}{4\sigma_{x}^{2}}\right\}. \tag{2.38}$$

Here P_i is the central linear momentum of each mass eigenstate wave packet, $E_i^0 = \sqrt{P_i^2 + m_i^2}$ its central energy and $v_i = \partial E_i(p)/\partial p|_{p=P_i}$ its group velocity. Finally, σ_x is a length scale which parametrizes the dampening of the oscillations and that can be referred as the wave packet size [80–86]. This wave packet size depends on the neutrino production and detection mechanisms.

Experiments do not measure T and oscillation periods are always much smaller than the operation time of the detector, then the total probability $P_{\alpha\beta}(L) = \int_0^\infty \mathrm{d}T |A_{\alpha\beta}|^2$ depends only on L,

$$P_{\alpha\beta} = \sum_{i=1}^{n} |U_{\alpha i}|^{2} |U_{\beta i}|^{2} + 2\operatorname{Re} \sum_{i < j} U_{\alpha i} U_{\alpha j}^{*} U_{\beta i}^{*} U_{\beta j} \exp \left\{ -2\pi i \frac{L}{L_{\text{osc}}^{ij}} - 2\pi^{2} \left(\frac{\sigma_{x}}{L_{\text{osc}}^{ij}} \right)^{2} - \left(\frac{L}{L_{\text{coh}}^{ij}} \right)^{2} \right\}.$$
(2.39)

Here we have imposed *a posteriori* the conservation of probability $\sum_{\alpha} P_{\alpha\beta} = 1$ and have defined

$$L_{\text{osc}}^{ij} = \frac{4\pi E}{|\Delta m_{ii}^2|}$$
 and $L_{\text{coh}}^{ij} = \frac{4\sqrt{2}E^2\sigma_x}{|\Delta m_{ii}^2|}$, (2.40)

the oscillation and coherence lengths, respectively. This formula can be obtained in a more consistent manner in the QFT formalism [84, 91–93], without any *a posteriori*

conservation of probability (and an additional energy dependence). Furthermore, the QFT formalism introduces the wave functions ψ_i in the incoming (outgoing) particle in the source (detector) vertex, not in the unobserved propagation neutrino.

Note that eq. (2.39) is the usual oscillation probability, with two additional terms in the exponential, which dampen the oscillation and only appear if we follow the WP formalism. The term $(\sigma_x/L_{\rm osc}^{ij})^2$ inside the exponential in eq. (2.39) is significant when $\sigma_x \sim L_{\rm osc}^{ij}$. In this regime, the wave packet width from production and/or detection is so large that it does not allow distinguishing between mass eigenstates. This results in washed-out oscillations. Most experiments, such as the ones studied in this thesis, work in the limit $\sigma_x \ll L_{\rm osc}^{ij}$, such that this term is negligible. Therefore, we will ignore it from here on.

On the other hand, the term $(L/L_{\rm coh}^{ij})^2$ is significant when $L\gtrsim L_{\rm coh}^{ij}$. This term can be understood as the decoherence arising from the separation of the mass eigenstates during their propagation at different velocities. The larger L, the more separation, the more decoherence and the more dampening of the oscillations. This term may be absorbed in the response function of the detector and thus could also be interpreted as a worsening of its energy resolution [94]. Note from (2.40) that the dampening increases with smaller σ_x and larger Δm_{ji}^2 . As we will see in chapter 3, this effect may be important when studying mass-squared differences which are orders of magnitude larger than the standard ones.

2.3.2 Neutrino oscillations experiments

As we have learned from eq. (2.30), the transition probability peaks at $E/L \sim \Delta m_{ij}^2$. In other words, in order to be sensitive to a particular energy splitting, the baseline between the source and the detector must be chosen adequately, given the energy of the neutrino source. Figure 2.3 shows the different (E,L) for past, present and some future experiments. These experiments may be classified in five families: solar, atmospheric, nuclear reactor, accelerator-based and gallium experiments. In this section we briefly review their properties, sources and (if any) anomalies.

Solar neutrino experiments. The Sun provides us with the largest natural flux of neutrinos. These neutrinos (originally v_e) are produced during nuclear fusion processes, which in the Sun are dominated by the pp chain. This includes reactions such as $p+p \to d+e^+v_e$ or $p+e^-+p \to d+v_e$ (here, d stands for deuterium). The neutrinos released by these reactions carry an energy between $\mathcal{O}(0.1-10)\,\text{MeV}$. The energy and flux intensity of these neutrinos are computed using the Standard Solar Model [95, 96]. When travelling from the neutrino core to the end of the photosphere, solar neutrinos cross an adiabatic resonance due to the matter potential. This is called the Mihheev-

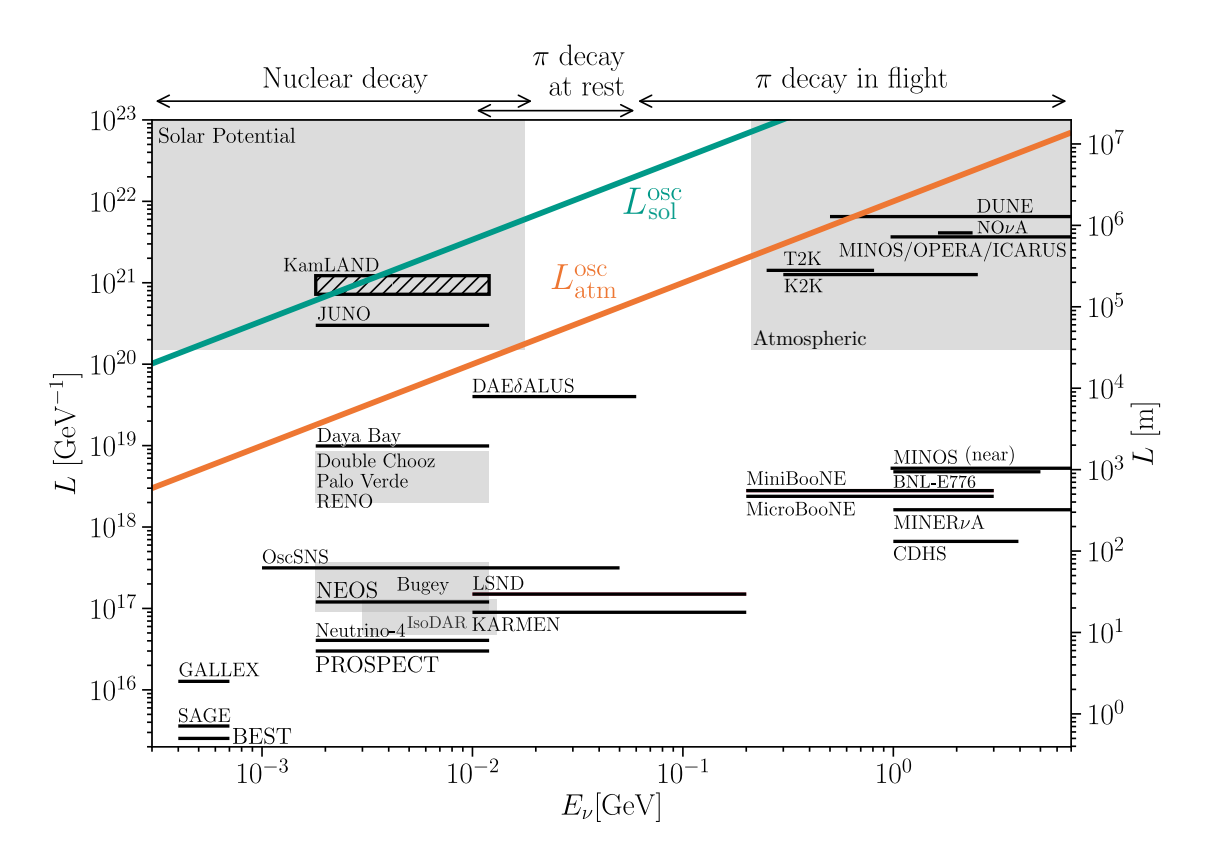


Figure 2.3: Neutrino experiments and characteristic scales as a function of the baseline and energy. $L_{\rm sol}^{\rm osc}$ (teal) and $L_{\rm atm}^{\rm osc}$ (orange) are computed from eq. (2.40) using eq. (2.34). Neutrino oscillation with mass-spliting Δm^2 are relevant close to the corresponding $L^{\rm osc}$ lines: far below oscillations do not have time to start, while far above they are averaged out. Matter effects important for solar oscillations in the Sun are under the region so-called solar potential, while the atmospheric regions covers the entire flux and baselines of atmospheric oscillations.

Smirnov-Wolfenstein (MSW) effect, which plays a fundamental role in explaining the observed deficit of solar neutrinos [97, 98]. Inside the Sun, this resonance happens at energies that allow for solar neutrino experiments to probe the value and sign of Δm_{21}^2 with great detail. Therefore, this is usually called the solar squared-mass splitting. In chronological order, experiments which have studied solar neutrinos are Homestake [99], SAGE [100], GALLEX [101], Kamiokande [102], SNO [103], KamLAND [104] and Borexino [105]. The next generation experiment which will soon reach new levels of precision is JUNO, which will also work as a reactor experiment [26].

Atmospheric neutrino experiments. The Earth is not only showered by particles from the Sun, but also it is constantly receiving highly energetic cosmic rays. These cosmic rays collide with nucleons in the top of the atmosphere, and produce particle cascades. These cascades involve charged mesons, mostly pions and kaons, that decay

to charged leptons and neutrinos, mostly through [46]

$$\pi^{\pm} \to \mu^{\pm} + \nu_{\mu} (\bar{\nu}_{\mu}),$$

$$\mu^{\pm} \to e^{\pm} + \bar{\nu}_{\mu} (\nu_{\mu}) + \nu_{e} (\bar{\nu}_{e}).$$
(2.41)

The energies of these neutrinos range from 100 MeV to TeV, and travel distances as long as the Earth's diameter. More precisely, neutrinos coming from different zenithal angles travel different distances. As shown in fig. 2.3, these neutrinos have been used to determine Δm_{31}^2 , usually called the atmospheric squared-mass splitting. In chronological order, experiments which have measured atmospheric neutrinos are IMB [106], Kamiokande [107], MACRO [108], Soudan-2 [109], Super-Kamiokande [15] and Ice-Cube [66]. In the future, these will be complemented by IceCube-Gen2 [38], Hyper-Kamiokande [27] and KM3NeT [110, 111].

Accelerator neutrino experiments Particle accelerators provide high-energy protons which can be collided against a target to produce pions and kaons. These mesons can decay, either in-air or after being stopped, producing a flux which is mostly v_{μ} or \bar{v}_{μ} , as shown in eq. (2.41). Magnetic horns can also be used to keep only positive or negative pions, and thus generate a beam of neutrinos and antineutrinos, respectively. Carefully choosing the design of the experiment allows to produce neutrino fluxes with a very narrow energy spectrum, centered at energies around $\mathcal{O}(1-20)$ GeV. This is the case of K2K [18], MINOS [19], T2K [24] or NO ν A [25], and will be followed by Hyper-Kamiokande [27] and DUNE [29].

Baselines of $\mathcal{O}(500)$ km allow to measure the atmospheric mass splitting. These are usually called long-baseline detectors. However, many experiments also place detectors at baselines $\mathcal{O}(1)$ km. These short-baseline detectors allow to reduce systematic uncertainties by measuring the neutrino flux before neutrinos have oscillated. Since short and long-baseline detectors have a similar or identic design, systematics and cross-section uncertainties are equivalent, and mostly cancel out for their event ratios.

Precisely, the short-baseline detector of the Liquid Scintillator Neutrino Detector (LSND) experiment studied neutrinos from stopped pion decay in the mid-1990s. While neutrinos should be mostly ν_{μ} , $\bar{\nu}_{\mu}$ or ν_{e} , the experiment reported an excess of $\bar{\nu}_{\mu} \rightarrow \bar{\nu}_{e}$ appearance [112, 113]. In the 2010s, the MiniBooNE experiment at Fermilab [114, 115] measured a low-energy excess of $\bar{\nu}_{e}$ with a 4.7 σ tension to standard oscillations. A possible explanation for such excess is the introduction of a sterile neutrino with $\Delta m^{2} \sim 1 \, \mathrm{eV}$, as we will discuss in chapter 3. While this still remains a valid explanation for LSND and MiniBooNE excesses, the absence of similar signals in other experiments difficults this explanation in the global picture.

On a sidenote, particle accelerators are also now producing the first signals of neutrinos from high-energy collisions. By placing a detector close to the vertex points of colliders, the FASER experiment at CERN announced in 2023 the detection of the first neutrino coming from such a collision event [116]. Even more recently, in 2024, the NA62 experiment announced the detection of the first neutrino tagged experiment from a collision [117]. The measurement of tagged neutrinos will allow to reconstruct the kinematics of LHC collisions that have a neutrino in the final state with improved precision [118].

Reactor antineutrino experiments. The most luminous artificial source of neutrinos are nuclear reactors, both commercial and research-oriented. The electron antineutrinos from nuclear fission processes have energies $\mathcal{O}(\text{MeV})$ and are detected by inverse beta decay (IBD),

$$\bar{\nu}_e + p \to e^+ + n \,. \tag{2.42}$$

The annihilation of the positron with an electron in the detector produces two photons which allow to precisely measure the positron energy E_p , and thus the antineutrino energy $E_{\nu} \simeq E_p + 0.8 \, \text{MeV}$. The lower energy threshold from IBD sets a cut for the minimum energy that can be detected, $E_{\nu}^{\min} = 1.806 \, \text{MeV}$.

Commercial nuclear reactors hold a mix of different heavy isotopes, usually 235 U, 238 U, 239 U, 241 U, and research reactors usually contain 235 U only. The reactor antineutrino flux is the result from the superposition of produced neutrinos from thousand of different beta-decay branches. Ab initio theoretical calculations are only available for the antineutrino flux from 238 U [119]. Current state-of-the-art calculations for 235 U, 239 U and 241 U are based in the inversion of the known spectra of beta-decay electrons, measured in the 1980s at the Institut-Laue-Langevin [120–123]. However, these calculations predicted a $\sim 5\%$ flux than that which was measured in reactor experiments such as DayaBay [124] and STEREO [125], which was dubbed the "reactor antineutrino anomaly" [126]. While this anomaly could be solved by an sterile neutrino with $\Delta m^2 \sim \mathcal{O}(1) \, \mathrm{eV^2}$, new measurements at the National Research Centre Kurchatov Institute refined the experimental input for the theoretical calculations, and the new predicted flux has become in good agreement with observations [127, 128]. However, the reactor antineutrino flux still shows an unexplained excess around 5 MeV, the so-called "5 MeV bump" [129].

While the vanishing of the reactor antineutrino anomaly washed out the necessity for a sterile neutrino explanation [129], many nuclear reactor experiments have looked

for $\Delta m^2 \sim \mathcal{O}(1)\,\mathrm{eV}^2$ oscillations. In chapter 3 we will discuss DayaBay [130], NEOS [131] and PROSPECT [132], but DANSS [133], STEREO [134] and Neutrino-4 [135] have also searched for them. Results vary from non-observation to 2σ detections [136, 137].

Radionuclei experiments. Radioactive nuclei, even if in smaller quantities, can also be used as a source of electron antineutrinos. Apart from studying solar neutrinos, the SAGE, GALLEX and –more recently– BEST experiments have been used as very-short-baseline experiments. In particular, the BEST experiment consists of a 51 Cr nucleus and two gallium targets 71 Ga [138]. The radioactive nucleus produces a $\bar{\nu}_e$ which undergoes IBD in the target,

71
Ga + $\bar{\nu}_e \rightarrow ^{71}$ Ge + e^+ . (2.43)

Then, the atoms of ⁷¹Ge are chemically extracted and counted. This is a measure of the total number of events, integrated both in time and energy.

The baseline between the source and the targets are separated at less than 3 meters, too close for $\Delta m_{\rm sol}^2$ and $\Delta m_{\rm atm}^2$ to produce any disappearance of $\bar{\nu}_e$. After accounting for the background from solar neutrinos, all SAGE, GALLEX and BEST have reported a deficit of events in the target. The ratio to the predicted number of events is 0.80 ± 0.05 , which means a 4σ discrepancy with standard three-neutrino oscillations [139, 140]. This is the so-called "Gallium anomaly", which was already present in the SAGE [141, 142] and GALLEX [143–145] in the 1990s and has been reaffirmed by BEST in 2022 [138, 146, 147]. One possible solution to explain this deficit is, again, the introduction of a sterile neutrino with $\Delta m^2 \sim \mathcal{O}(1)\,\mathrm{eV}$. However, the U_{es} mixing necessary to explain it is "surprisingly large", and in a tension with reactor and solar experiments which is of the same order of the anomaly itself [140, 147].

2.3.3 Searching for the absolute neutrino mass scale

Neutrino oscillations only depend on Δm^2 . For a 3-neutrino space with $\{m_1, m_2, m_3\}$, this means that from them we can only measure two independent quantities, namely $\Delta m_{21}^2 \equiv m_2^2 - m_1^2$ and $\Delta m_{31}^2 \equiv m_3^2 - m_1^2$. Then, there is an absolute mass scale which is not measurable by oscillations, for instance the lightest mass m_{light} . As seen in fig. 2.2, for normal ordering $m_{\text{light}} = m_1$, and for inverted ordering $m_{\text{light}} = m_3$.

Measuring the absolute mass of neutrinos is not an easy task. We expect it to be $m_i \lesssim \mathcal{O}(1)\,\mathrm{eV}$, much smaller than any other particle of the SM. However, the lowest-energy neutrinos that we have measured have energies $\mathcal{O}(10^5)\,\mathrm{eV}$ [148]. Then, neutrino masses only give corrections to the neutrino energy of at most $m/E \sim \mathcal{O}(10^{-5})$, which requires excellent relative energy resolution.

The current best direct bounds on the neutrino masses come from the KATRIN experiment [149, 150]. KATRIN studies the beta decay of tritium,

$${}^{3}\text{H} \rightarrow {}^{3}\text{He} + e^{-} + \bar{\nu}_{e}$$
 (2.44)

Tritium beta decay is a superallowed transition, and thus the nuclear matrix elements are energy independent. Then, the spectrum of the outgoing electron is given only by phase space kinematics,

$$\frac{\mathrm{d}N}{\mathrm{d}E} = C(E) \sum_{i} |U_{ei}|^2 \sqrt{(E_0 - E)^2 - m_i^2} \,\Theta(E_0 - E - m_i),\,\,(2.45)$$

where C(E) contains all m_i -independent factors and E_0 is the mass difference between the initial and final nuclei. The Heaviside function $\Theta(E_0 - E - m_i)$ expresses the fact that the neutrino mass eigenstate m_i can only be produced if there is enough available energy, $E_0 - E > m_i$. Assuming than $E_0 - E \gg m_i$, then we can write this energy spectrum in terms of a single parameter, $m_{\beta,\nu}$, [55]

$$m_{\beta,\nu} = \sqrt{\sum_{i} m_{i}^{2} |U_{ei}|^{2}} = \begin{cases} \sqrt{m_{\text{light}}^{2} + \Delta m_{21}^{2} (1 - c_{13}^{2} c_{12}^{2}) + \Delta m_{32}^{2} s_{13}^{2}} \ge 0.0085 \,\text{eV} & \text{NO} \\ \sqrt{m_{\text{light}}^{2} + \Delta m_{21}^{2} c_{13}^{2} c_{12}^{2} - \Delta m_{32}^{2} c_{13}^{2}} \ge 0.048 \,\text{eV} & \text{IO} \end{cases},$$

$$(2.46)$$

where the lower bounds are found setting $m_{\text{light}} = 0$. In conclusion, neutrino masses modify the electron energy spectrum to

$$\frac{\mathrm{d}N}{\mathrm{d}E} = C(E) \sum_{i} |U_{ei}|^2 \sqrt{(E_0 - E)^2 - m_{\beta,\nu}^2}.$$
 (2.47)

A non-zero mass will slightly move the endpoint of the electron spectrum to lower energies. The KATRIN experiment has not found this shortening of order $m_{\beta,\nu}/E \sim \mathcal{O}(10^{-5})$, and therefore has placed an upper bound on the effective mass [150]

$$m_{\beta,\nu} \le 0.45 \,\text{eV} \quad (95\% \,\text{C.L.}).$$
 (2.48)

While KATRIN holds the best direct bound on m_{ν} , the best indirect bounds come from cosmology. As we will explain in chapter 7, massive neutrinos modify cosmology in a distinct way, which allows us to use cosmological observations to place upper bounds on the sum of neutrino masses,

$$\sum_{i} m_{i} = \begin{cases} m_{\text{light}} + \sqrt{m_{\text{light}}^{2} + \Delta m_{21}^{2}} + \sqrt{m_{\text{light}}^{2} + \Delta m_{31}^{2}} > 0.059 \,\text{eV} & \text{NO}, \\ m_{\text{light}} + \sqrt{m_{\text{light}}^{2} + |\Delta m_{32}^{2}|} + \sqrt{m_{\text{light}}^{2} + |\Delta m_{32}^{2}|} - \Delta m_{21}^{2}} > 0.0099 \,\text{eV} & \text{IO}. \end{cases}$$
(2.49)

No cosmological survey has reported yet the observation of neutrino masses, and therefore only report upper bounds, which vary depending on the datasets used. For instance,

$$\sum_{i} m_{i} < 0.24 \text{ eV} \qquad \text{CMB} + \text{lensing [151]},$$

$$\sum_{i} m_{i} < 0.12 \text{ eV} \qquad \text{CMB} + \text{lensing} + \text{BAO [151]},$$

$$\sum_{i} m_{i} < 0.07 \text{ eV} \qquad \text{CMB} + \text{lensing} + \text{DESI BAO [152]},$$

$$(2.50)$$

at the 95% C.L. We show these constrains in fig. 2.4. Even if the latest cosmological results from DESI point towards the exclusion of IO [152–154], the measurement of neutrino masses in cosmology is indirect and model-dependent. A further investigation of this topic is required before jumping to conclusions, as discussed in chapter 7.

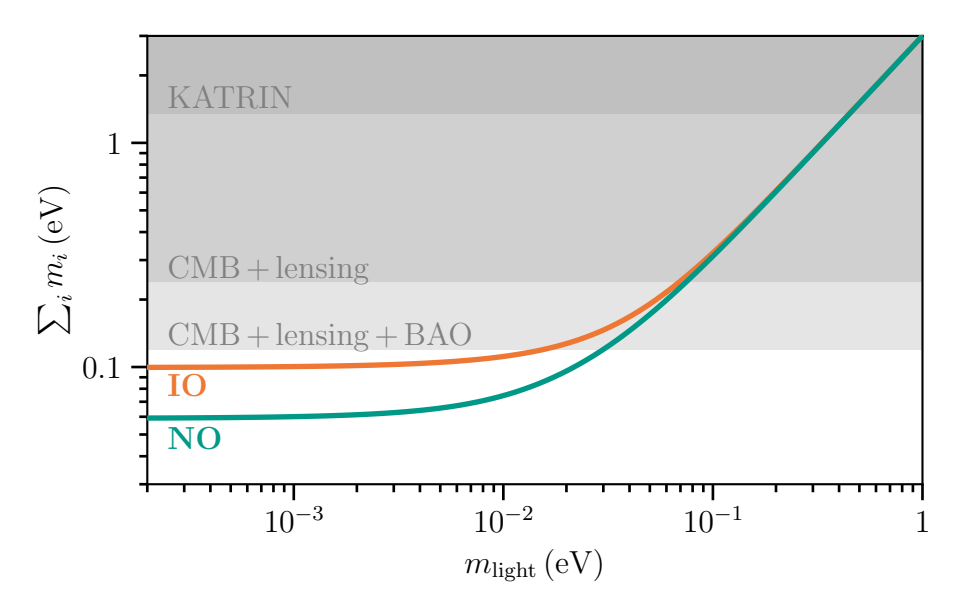


Figure 2.4: Current constraints on the sum of the neutrino masses, as shown in eq. (2.50). Teal and orange lines show $\sum_i m_i$ in terms of the lightest neutrino mass for the normal and inverted orderings, respectively, as in eq. (2.49). Cosmological constraints are closing up on the minimum total neutrino mass allowed by oscillations.

Concluding remarks

In this first chapter we have learned (or remembered) that

- 1. neutrinos oscillate and at least two of them have a non-zero mass,
- 2. this is unexplained by the particle content within the SM and requires to extend it in some manner,

- 3. we have measured to great precision the parameters of the neutrino flavor sector (eq. (2.34)), but the measurement of $\delta_{\rm CP}$, of the octant of θ_{23} and of the neutrino ordering is still missing,
- 4. we have not yet measured the absolute neutrino mass, but cosmology promises an observation in the following decade (or to rule out neutrino oscillations)².

Two big-picture conclusions can be drawn from what we have seen. First, we expect New Physics to be connected in some manner with the neutrino sector. Second, even if such New Physics is not reachable in the short-term future, there are still interesting questions which can be addressed and successfully answered. Obtaining these answers is necessary to attain a complete description of the known Physics of the SM.

In the same manner that neutrino oscillations were not the main initial objective of the Kamiokande experiment (these were proton decay and GUTs), New Physics can be found serendipitously. That is, as an unexpected result of another research line. While we try to measure with great precision the parameters from neutrino oscillations, we might encounter unexpected behaviour. In 3-neutrino oscillations, this is usually described in terms of Non-Standard neutrino Interactions (NSIs) [155–160]. However, as we have learned, new (sterile) neutrino species are physically motivated and would require to go beyond this paradigm.

This is the case for $\mathcal{O}(1)\,\mathrm{eV}$ sterile neutrinos. Signals that could be interpreted as $\Delta m^2 \sim 1\,\mathrm{eV}^2$ have been detected in multiple experiments and, while the global picture does not favor the sterile neutrino explanation, the anomaly remains unexplained. In the following section, chapter 3, we present the results from [1], where we address low-energy sterile neutrino searches and their robustness against a finite wave packet width. Understanding such robustness is necessary to undoubtedly discard the sterile neutrino hypothesis.

²I am not entirely sure of which scenario I would prefer.

3 Impact of Wave Packet Separation in Low-Energy Sterile Neutrino Searches

The observation of an excess of electron antineutrino events in the Liquid Scintillator Neutrino Detector (LSND) [112, 113] in the mid-1990s started a broad experimental program to confirm this signal. The simplest explanation of the excess is that it is due to the presence of a fourth neutrino, whose flavor state does not participate in the Standard Model weak interactions, and whose mass splitting is on the order of $1\,\mathrm{eV}^2$. Given this as the explanation of the LSND observation, we then expect that correlated signals should be present at different baselines and energies but at a similar ratio of baseline-to-energy of approximately $1\,\mathrm{GeV/km}$.

Experiments searching for these signatures have been performed with energies ranging from MeV to TeV and baselines from a few meters to the diameter of the Earth, as shown in fig. 2.3. These experiments use neutrinos produced predominantly by three means: nuclear decay in the MeV range, pion decay at rest at the 100 MeV scale, and pion or kaon decay in flight in the highest energy range. In the lowest energy range, gallium experiments study the production rate of inverse beta decay on 71Ga from an intense electron neutrino source [138, 139, 141-143, 161]. Also at MeV energies, reactor experiments have performed searches for the presence of electron antineutrino disappearance by comparing observations to theoretical predictions of the rates [126] or by searching for oscillatory patterns in measurements performed at different positions [65, 130-133, 135, 146, 162-165]. All these low-energy experiments have yielded confirmatory signals that range in significance from ~ 2 to more than 5 sigma but at the same time have yielded constraints that contradict these observations, specially when taking into account solar neutrino analysis [137, 166]. In the intermediate energy range, the MiniBooNE [114, 115] experiment has reported the appearance of electron-neutrino-like events compatible with the LSND observation at a significance of 4.8 sigma. Operating in the same beam, recently the MicroBooNE collaboration has published measurements of electron neutrino events under various interaction channels [167-170]. When this data is interpreted in the context of a light sterile neutrino, weak signals for electronneutrino disappearance are observed [171] and weak constraints on the MiniBooNE region are obtained [172, 173]. Finally, in the highest energy range, the MINOS+ collaboration has placed very strong constraints on muon-neutrino disappearance, while the IceCube Neutrino Observatory observes a mild signal [174-177]. This is a very confusing situation that, when studied in the context of global fits, results in the conclusion that the inconsistencies between the datasets rule out the light sterile neutrino interpretation of LSND [178-181].

In this chapter, we point out that the above-mentioned conclusion, specifically about the apparent contradiction between reactor experiments and radioactive sources, has overlooked an important fact that could resolve the tension. When deriving the results quoted above, the experiments assume that the neutrino state is a plane wave. It is wellknown that the plane-wave (PW) theory of neutrino oscillations [182-184] is a simplified framework that upon careful inspection contains apparent paradoxes [90, 185, 186]. These can be resolved by introducing the wave packet (WP) formalism [80-86, 143], as explained in section 2.3.1. The applicability of the plane-wave approximation has been studied in detail for the standard mass-squared differences [84, 90, 187-189] and has been shown to be a good approximation for current and future neutrino experiments. However, this has not been shown to be the case for mass-squared differences relevant to the LSND observation [112]. The correctness of the PW approximation depends on the wave packet width, which varies with the neutrino production and detection processes. For example, in the case of pion decay in flight the wave packet size has been quantitatively estimated [190], and as such it is inconsequential to the light sterile neutrino analyses. This is seen in fig. 3.1, where we compare the oscillation length and the coherence length. In the case of pion decay at rest or production from nuclear reactors or radioactive sources, this has not been precisely calculated. In particular, for nuclear reactors, it has been suggested that the relevant scales for the neutrino wave packet width could be [191]: the typical size of the beta-decaying nuclei ($\sim 10^{-5} \mathrm{nm}$), the interatomic spacing that characterizes the fuel ($\sim 0.01 - 1 \,\mathrm{nm}$ for uranium), or the inverse of the antineutrino energy ($\sim 10^{-4}$ nm), or the mean free path of the parent nucleus $(\sim 10^2 \text{nm})$ [94]. Most of these values are not definitive quantitative results [192]. As a matter of fact, a recent study following the formalism of open quantum systems states that the wave packet width should lie in the 0.01 – 0.4nm range [193]. Taking an agnostic viewpoint, our current knowledge is limited to bounds from experiments measuring the standard oscillation scales, which set it to be no smaller than 2.1×10^{-4} nm [191, 194].

In this work, we focus on the low-energy region, where searches using electron antineutrinos from nuclear reactors and radioactive sources are performed [65, 130–132, 138, 164]. We will show how the plane wave approximation breaks for values of the wave packet size currently allowed [194] and how introducing this formalism produces observable effects. It is worth mentioning that the damping of oscillations in neutrino physics is not exotic but an expected phenomenon in some scenarios. On the one hand, a precise enough measurement of the kinematics of the final states in the production region may effectively measure the mass of the outgoing neutrino. This effect is referred to as quantum damping and is believed to be very small for the production of neutrinos [195]. On the other hand, the wave packets may separate during propagation due

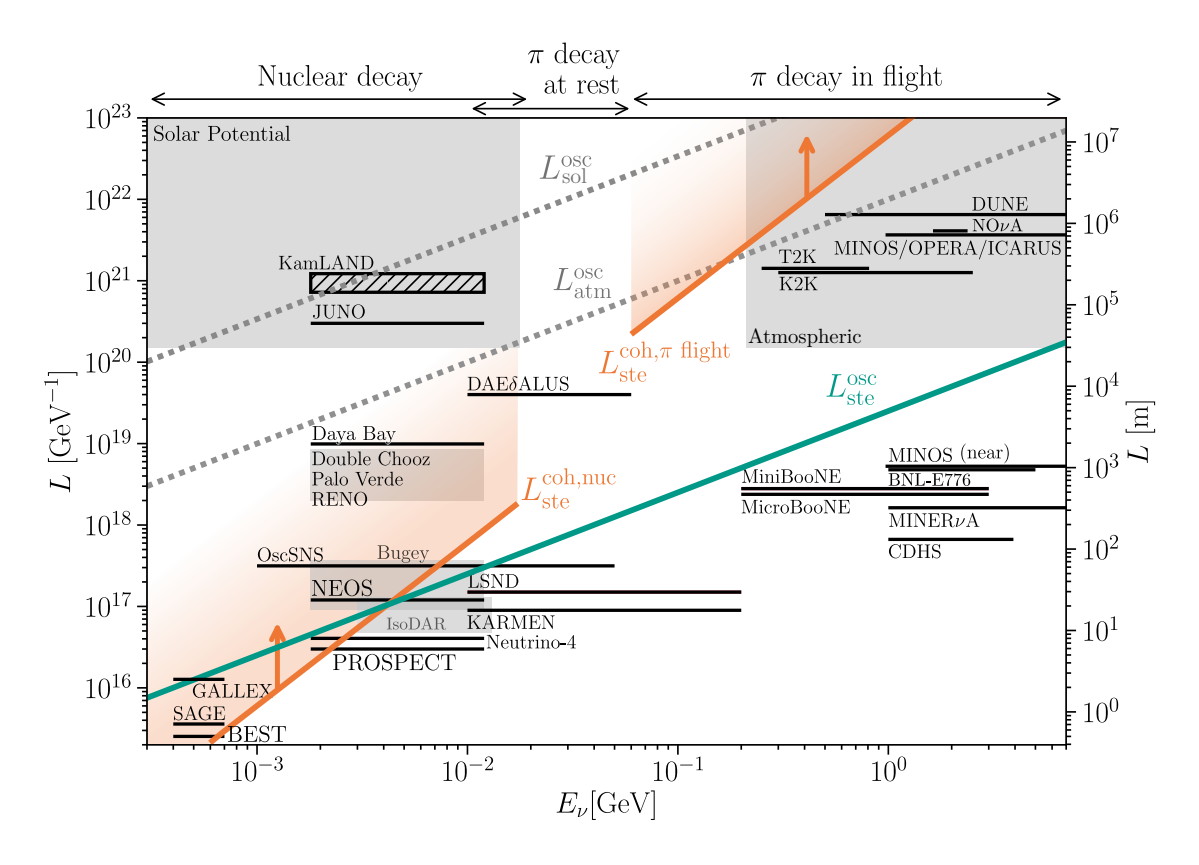


Figure 3.1: Characteristic scales for sterile neutrino oscillations and decoherence, analogously to fig. 2.3. $L^{\rm osc}$ (dotted gray and solid teal) and $L^{\rm coh}$ (solid orange) are computed from eq. (2.40) using $\Delta m_{41}^2 = 1\,{\rm eV}^2$ and $\sigma_x = 2.1\times 10^{-4}$ nm for $L_{\rm ste}^{\rm coh,nuc}$, and $\sigma_x = 10^{-11}$ m for $L_{\rm ste}^{\rm coh,\pi}$ flight [190]. Observable decoherence effects are expected at $L\gtrsim L^{\rm coh}$ (shaded orange gradient). Low-energy experiments, i.e., nuclear reactor and radionuclei decay, are the most affected by sterile neutrino decoherence.

to their different masses. This effect of decoherence is strictly equivalent to taking into account the proper energy uncertainty in the production and detection processes [94]. The latter is related to the spatial and time localization of the interaction or, equivalently, the uncertainty in the measurement of the neutrino energy. Since both these phenomena are physically indistinguishable, in this work we consider the energy resolution claimed by experiments and add a decoherence effect that introduces a damping of the oscillations. This addition can either be understood as a separation of the wave packets or as an underestimation of the energy uncertainties claimed by experiments. Finally, the macroscopical production and detection regions averaging also produces the same effect but is already considered in experimental analyses.

Caveats or fundamental physics unknowns in the wave packet size estimations or any exotic physics can enlarge the damping effect. For this reason, we choose the smallest wave packet size allowed by present bounds obtained from studies of standard oscillations in nuclear reactor experiments [191, 194]. Notice then that this must be robust under the most exotic scenario since it involves the same production and detection process and does not rely on any assumptions. Moreover, the chosen value is preferred by experiments at 90% C.L. [194].

The allowed size of the wave packet, together with the larger sterile mass value, brings us to the main points of this chapter. First: experimental results may need to consider the decoherence effects arising from the WP formalism, which might produce damped oscillations. Second: these effects may modify both signals from radioactive sources and exclusion regions from nuclear reactors and can indeed alleviate part of the tension between them.

The remainder of this chapter is organized in the following sections: *Formalism*, where we particularise the wave packet formalism to nuclear reactor experiments; *Impact on neutrino experiments*, where we show the impact of the finite wave packet size from sterile neutrino searches by the Daya Bay, NEOS, BEST, and PROSPECT experiments and we discuss the results; and, finally, in *Conclusions*, where we summarize our main findings.

3.1 Formalism

In the plane wave formalism, a propagating neutrino is modeled with perfectly defined momentum. However, this approximation cannot fully convey the physics effects we mention earlier. As explained in section 2.3.1, we are going to parametrize the damping of the oscillations by a length scale σ_x that is usually referred to as the wave packet size [80–86, 196, 197].

Nuclear decay experiments study $P(v_e \rightarrow v_e) \equiv P_{ee}$, the electron antineutrino survival probability. Following from eq. (2.39), this is given by

$$P_{ee} = 1 - \sin^{2} 2\theta_{12} \cos^{4} \theta_{13} \cos^{4} \theta_{14} \Delta_{21}$$

$$- \sin^{2} 2\theta_{13} \cos^{4} \theta_{13} (\cos^{2} \theta_{12} \Delta_{31} + \sin^{2} \theta_{12} \Delta_{32})$$

$$- \sin^{2} 2\theta_{14} \left[\cos^{2} \theta_{13} \cos^{2} \theta_{12} \Delta_{41} + \cos^{2} \theta_{13} \sin^{2} \theta_{12} \Delta_{42} + \sin^{2} \theta_{13} \Delta_{43} \right],$$
(3.1)

where we have defined, similarly to [80],

$$\Delta_{ji} = \frac{1}{2} \left(1 - \cos \frac{L\Delta m_{ji}^2}{2E} \exp \left\{ -\frac{L^2 (\Delta m_{ji}^2)^2}{32E^4 \sigma_x^2} \right\} \right). \tag{3.2}$$

While in the PW limit, $\Delta_{ji} = \sin^2(L\Delta m_{ji}^2/4E)$. Then, this is the analogous result to Ref. [130], but taking into account decoherence effects. The difference between both

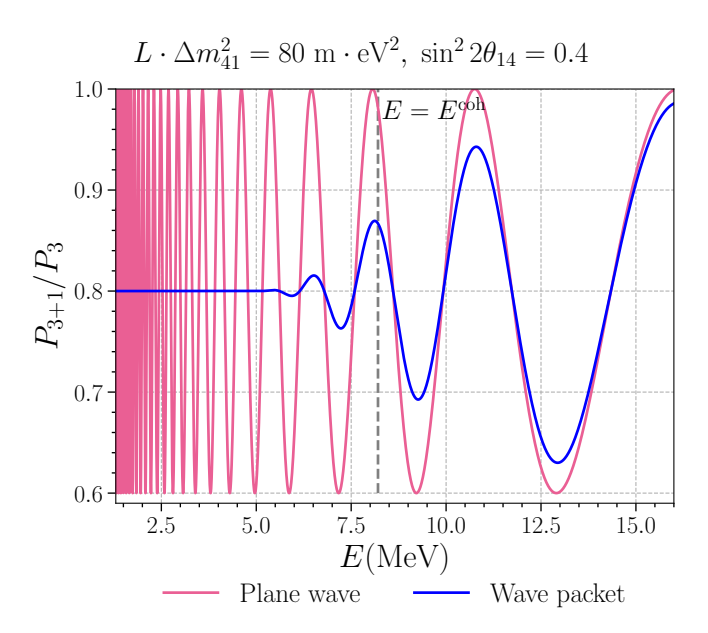


Figure 3.2: Illustration of the wave packet effect. Plot of the oscillation probability ratio for $\sigma_x = 2.1 \times 10^{-4}$ nm. The y axis represents the ratio between the 3+1 and the 3 neutrino oscillation probabilities, in the PW formalism (pink) and in the WP one (blue). The effect demonstrated here would appear for $\mathcal{O}(0.1 \text{ eV}^2)$ sterile at the Daya Bay baselines, or $\mathcal{O}(1 \text{ eV}^2)$ sterile at the NEOS or PROSPECT baselines. The energy where $L_{\text{ste}}^{\text{coh}} = L_{\text{ste}}^{\text{osc}}$ is defined as $E_{\text{ste}}^{\text{coh}}$ and is independent of the sterile neutrino mass. This energy is indicated as a vertical dashed line.

results with and without decoherence effects are shown in fig. 3.2 for parameters motivated by the LSND observation and wave packet at the current constraints. For illustration purposes, we show with a vertical line the energy

$$E_{\rm coh} = \sqrt{\frac{L|\Delta m_{ji}^2|}{4\sqrt{2}\sigma_x}} \tag{3.3}$$

for which the exponential argument of the coherence suppression term is equal to 1. Three different regimes can be clearly distinguished. At low energies, oscillations are very fast and cannot be resolved given the experimental energy resolution, resulting in averaging of the oscillations that cannot be distinguished from the decoherence effect. At energies close to $E^{\rm coh}$, decoherence can produce an observable effect that in principle can be measured and distinguished from other oscillation features. Finally, at high energies, the decoherence effect becomes less important and eventually is a small correction to the oscillation amplitude.

In order to understand the potential impact of the decoherence effect, it is useful to compare the different relevant scales. Figure 3.1 shows several oscillation experiments compared to the sterile oscillation scale ($L_{\text{ste}}^{\text{osc}}$) and the decoherence scale ($L_{\text{ste}}^{\text{coh}}$); in both

cases the parameters correspond to the $\Delta m_{41}^2=1\,\mathrm{eV}^2$ and the current best constrain for $\sigma_x=2.1\times10^{-4}\mathrm{nm}$ [194]. For experiments with baselines smaller than $L_{\mathrm{ste}}^{\mathrm{coh}}$, decoherence can be neglected, while experiments with large baselines will experience complete decoherence. Notice that the effect of not resolving fast oscillations experimentally is from an observational point of view identical to a decoherence effect, meaning that an experiment far above the $L_{\mathrm{ste}}^{\mathrm{osc}}$ line would also be effectively decoherent, and no effect due to $L_{\mathrm{ste}}^{\mathrm{coh}}$ would be manifest. This narrows the region of interest for the decoherence of light sterile neutrinos to the low-energy region and in particular to the reactor and radioactive sources experiments.

3.2 Impact on neutrino experiments

To show the impact of the wave packet separation we choose the smallest value allowed for the wave packet size, $\sigma_x = 2.1 \times 10^{-4} \mathrm{nm}$ [194], and perform analyses searching for sterile neutrinos with and without the plane wave approximation. In this work, we use this bound both in reactor and gallium experiments for simplicity, even though they need not have the same wave packet size. In our global analysis, we consider the null results from Daya Bay [65, 130], NEOS [131], and PROSPECT [132] and the anomalous results observed from radioactive sources by BEST [138]. This is not an exhaustive list of affected experiments, but they are sufficient to cover the regions of interest illustrated in fig. 3.1. The aim of this chapter is not to perform a global fit in the WP formalism, but to illustrate its phenomenology in low-energy sterile searches in the context of decoherence effects. Here we explain the details of the different data analysis undertaken.

3.2.1 DayaBay analisis

The Daya Bay experiment data has been fit using a test statistic ($\mathcal{TS}^{\text{DayaBay}}(\theta_{14}, \Delta m_{41}^2, \vec{\alpha})$) based on a Poisson log-likelihood,

$$\mathcal{T}S^{\text{DayaBay}}(\Delta m_{41}^{2}, \theta_{14}, \vec{\alpha}) = -2\sum_{d} \sum_{i=1}^{35} \left(O_{i}^{d} - \left[\alpha_{i} N_{i}^{d} (\Delta m_{41}^{2}, \theta_{14}) + B_{i}^{d} \right] + O_{i}^{d} \log \frac{\alpha_{i} N_{i}^{d} (\Delta m_{41}^{2}, \theta_{14}) + B_{i}^{d}}{O_{i}^{d}} \right).$$

$$(3.4)$$

This statistic is defined from the Poisson probability $P(k,\lambda) = e^{-\lambda} \lambda^k / k!$ and already takes into account statistical uncertainties, which are dominant in the Daya Bay experiment. In eq. (3.4) O_i^d , B_i^d , N_i^d are the observed, background, and predicted data in the

energy bin i and experimental hall d = EH1, EH2, EH3, respectively.

The reactor flux in which the analysis is built is taken from the theoretical predictions of Huber and Mueller [119, 120], even though there are known anomalies to them [198]. Then, $\vec{\alpha}$ are nuisance parameters that accommodate the uncertainties in this flux. These are different for each energy bin but the same for each experimental hall and minimize eq. (3.4),

$$\alpha_i = \frac{\sum_d O_i^d - B_i^d}{\sum_d N_i^d} \,. \tag{3.5}$$

With these nuisance parameters, the source flux and its normalization are free and the same for the three experimental halls. Only relative differences between detectors (*e.g.*, neutrino oscillations) will be manifest.

 O^d , B^d are taken from the Supplemental Material of [65], while N_i^d is computed following [199]

$$N_{i}^{d} = \mathcal{N}^{d} \sum_{r} \frac{\epsilon^{d}}{L_{r,d}^{2}} \int_{E_{i}^{\text{rec}}}^{E_{i+1}^{\text{rec}}} dE^{\text{rec}} \int_{0}^{\infty} dE_{\nu} \, \sigma(E_{\nu}) \, \phi(E_{\nu}) \, P_{ee}^{r,d}(E_{\nu}) \, R(E^{\text{rec}}, E_{\nu}). \tag{3.6}$$

Here,

- \mathcal{N}^d is a normalization constant which takes into account the number of target protons in the detector. Note that this factor is accommodated in eq. (3.4) by the free nuisance parameters $\vec{\alpha}$ and therefore plays no role. However, we choose it such that our prediction of the expected events without oscillations match the corresponding data from Daya Bay.
- r runs over the different reactor neutrino sources.
- ϵ^d is the detection efficiency of the experimental hall (averaged over all the detectors in the experimental hall), taken from Table VI in [65].
- $L_{r,d}$ is the mean distance between the reactor and the detectors in the experimental hall, taken from Table I in [65].
- E^{rec} , E_{ν} stand for the reconstructed and true neutrino energies.
- $\sigma(E_{\nu})$ is the inverse beta decay cross section [200].
- $\phi(E_{\nu})$ is the Huber-Mueller flux [119, 120],

$$\phi(E_{\nu}) = \sum_{\text{isotope}} f_{\text{isotope}} \, \phi^{\text{isotope}}(E_{\nu}) \,, \tag{3.7}$$

with $f_{\rm isotope}$ the mean fission fraction of isotope = 235 U, 238 U, 239 Pu, 241 Pu.

• $P_{ee}^{r,\text{exp}}$ is the survival probability from eq. (2.39).

• $R(E^{\text{rec}}, E_{\nu})$ is the response matrix of the Daya Bay detectors [65].

Note that in this analysis (and all the following) the standard oscillation parameters are not free but fixed at the values of [201]. A more rigorous treatment would marginalize θ_{13} and Δm_{31}^2 . However, the effect would be small even in the worst-case scenario and thus the present work does not consider this marginalization.

3.2.2 NEOS analysis

Our NEOS experiment analysis is based on the procedure in Ref. [131, 199] and using a χ^2 function as its test statistic ($\mathcal{TS}^{\text{NEOS}}(\theta_{14}, \Delta m_{41}^2, \vec{\alpha})$).

$$\mathcal{TS}^{\text{NEOS}}(\theta_{14}, \Delta m_{41}^2, \vec{\alpha}) = \sum_{i,j=1}^{60} \left(R_i - \frac{N_i(\Delta m_{41}^2, \theta_{14}) + B_i}{N_i^{\text{SM}} + B_i} \right) (V^{-1})_{ij} \left(R_j - \frac{N_j(\Delta m_{41}^2, \theta_{14}) + B_j}{N_j^{\text{SM}} + B_j} \right) . \tag{3.8}$$

Here, R_i is the ratio data from Fig. 3(c) in [131], B_i is the background events from Fig. 3(a), V_{ij} is the NEOS covariance matrix, and $N_j(\Delta m_{41}^2, \theta_{14})$, N_j^{SM} are the expected events at NEOS with a 3+1 and a 3 neutrino model, respectively. Since there is only one detector, the nuisance parameters are fixed to unity. As in Ref. [131, 199], we have used the electron-antineutrino spectrum measured in the Daya Bay experiment [124] as the source flux.

The expected number of values are obtained using

$$N_{i} = \mathcal{N} \int_{L_{\text{min}}}^{L_{\text{max}}} \frac{dL}{L^{2}} \int_{E^{\text{rec}}}^{E^{\text{rec}}_{i+1}} dE^{\text{rec}} \int_{0}^{\infty} dE_{\nu} \, \sigma(E_{\nu}) \, \phi^{\text{DB}}(E_{\nu}) \, P_{ee}(L, E_{\nu}) \, R(E^{\text{rec}}, E_{\nu}) \,. \tag{3.9}$$

Here,

- The normalization factor \mathcal{N} is free and adjusted to match the total number of observed events from Fig. 3(a) in [131] for any $(\Delta m_{41}^2, \theta_{14})$, taking into account the background.
- Since the baseline is short, finite-size effects of the detector need to be taken into account by integrating between $L_{\min} = 22.14$ m and $L_{\max} = 25.14$ m.
- $\sigma(E_{\nu})\phi^{DB}(E_{\nu})$ is the Daya Bay antineutrino flux weighted by the inverse beta decay cross section, taken from Table 12 in [124]. As noted in [199], this spectrum is computed under the assumption of three-flavor oscillations, and thus these oscillations, although small, should be unfolded for a rigorous analysis. This effect is only corrected in the Daya Bay + NEOS joint analysis.
- The response matrix $R(E^{rec}, E_{\nu})$ is not provided by the NEOS collaboration, and therefore has to be reproduced from [202, 203] using the same technique as in [198].

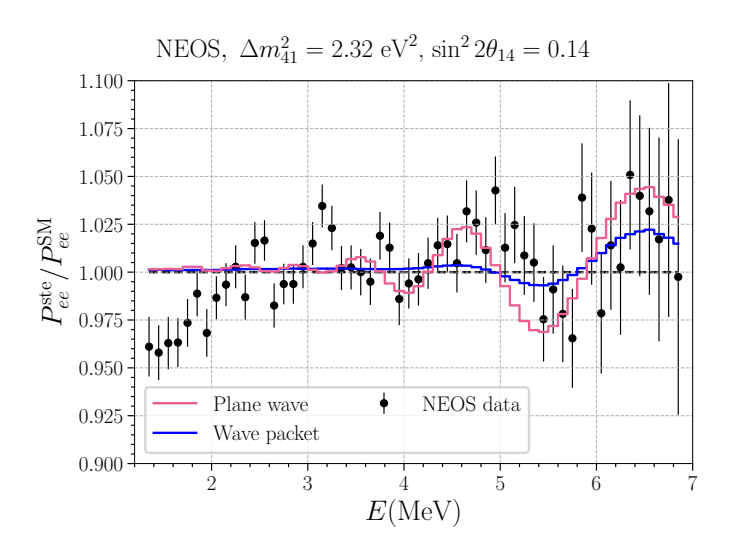


Figure 3.3: Example of the effect in NEOS. A figure of the decoherence effect, for $\sigma_x = 2.1 \times 10^{-4}$ nm, with the reactor antineutrino anomaly best-fit parameters [131]: $\Delta m_{41}^2 = 2.32 \, \text{eV}^2$ and $\sin^2 2\theta_{14} = 0.14$. The y axis represents the ratio between the 3+1 and the 3 expected events for the Daya Bay-NEOS joint analysis.

Finally, to build V_{ij} we have digitized the correlation matrix from [202], which has unity diagonal elements. Then, this matrix is rescaled such that its diagonal elements match the quadratic sum of the systematical and statistical errors digitized from Fig. 3(c) in [131]. We take this rescaled matrix to be the covariance matrix V_{ij} in (3.8).

Figure 3.3 shows the ratio between the expected events from a 3+1 model and from a 3 model at the NEOS baseline in this joint fit. Here, the decoherence effect of the wave packet formalism is clearly manifest.

3.2.3 DayaBay+NEOS joint analysis

Now NEOS is treated as if it was a fourth Daya Bay detector. That is, we have computed the expected events using the same Huber-Mueller flux for both Daya Bay and NEOS, and accommodated the flux uncertainties using a common vector of nuisance parameters.

However, we must take into account that the energy bins for Daya Bay and NEOS are different. On the one hand, Daya Bays energy range is $E_{\rm DB}^{\rm rec} \in (0.7, 12.0) {\rm MeV}$, with energy binning $\Delta E_{\rm DB}^{\rm rec} = 0.2$ MeV. On the other hand, NEOS measures in $E_{\rm NEOS}^{\rm rec} \in (1.0, 10.0) {\rm MeV}$ and with bins of width $\Delta E_{\rm NEOS}^{\rm rec} = 0.1$ MeV. Therefore, we pick the conservative choice to only consider the energy bins that are well defined in both experiments and that share the same energy bin edges, *i.e.*, $E_{\rm DB}^{\rm rec} \in (1.3, 6.9) {\rm MeV}$. Since NEOS has twice as many bins as Daya Bay, the nuisance parameter α_i of Daya Bay's energy bin i is applied to two consecutive energy bins in NEOS.

Taking all this into account, the test statistic to minimize for $\vec{\alpha}$ is

$$\mathcal{T}S^{\text{DB+NEOS}}(\Delta m_{41}^{2}, \theta_{14}, \vec{\alpha}) = -2 \sum_{d} \sum_{i=2}^{29} \left(O_{i}^{d} - \left[\alpha_{i} N_{i}^{d} + B_{i}^{d} \right] + O_{i}^{d} \log \frac{\alpha_{i} N_{i}^{d} + B_{i}^{d}}{O_{i}^{d}} \right) +$$

$$+ \sum_{i,j=4}^{59} \left(R_{i} - \frac{\alpha_{\text{floor}(i/2)} N_{i}^{\text{NEOS}} + B_{i}}{N_{i}^{\text{SM}} + B_{i}} \right) (V^{-1})_{ij} \left(R_{j} - \frac{\alpha_{\text{floor}(j/2)} N_{j}^{\text{NEOS}} + B_{j}}{N_{j}^{\text{SM}} + B_{j}} \right),$$
(3.10)

where $N_i^d = N_i^d(\Delta m_{41}^2, \theta_{14})$, and the test statistic is $\mathcal{TS}^{\mathrm{DB+NEOS}} = \min_{\vec{\alpha}} \mathcal{TS}^{\mathrm{DB+NEOS}}(\vec{\alpha})$. This minimization can only be done numerically.

3.2.4 PROSPECT analysis

The PROSPECT data has also been analyzed following [132], where the detector is divided into different subsegments with different baselines, and using a χ^2 function as its test statistic ($\mathcal{T}S^{\text{PROSPECT}}(\theta_{14}, \Delta m_{41}^2)$) with a covariance provided by the experiment. Since our PROSPECT analysis uses ratios, it is independent of the reactor flux model. The analysis of the PROSPECT data [132] is independent from those of Daya Bay and NEOS, since PROSPECT's neutrino source only contains 235 U. The PROSPECT detector is subdivided onto independent segments at difference distances to the nuclear reactor. These segments are capable of measuring neutrino propagation in different baselines, and are sensitive to a $1\,\text{eV}^2$ sterile neutrino oscillation.

The test statistic to minimize is the χ^2 function

$$\mathcal{T}\mathcal{S}^{\text{PROSPECT}}(\theta_{14}, \Delta m_{41}^2) = \vec{x} \cdot V^{-1} \cdot \vec{x}, \qquad (3.11)$$

where V is the PROSPECT covariance matrix, and \vec{x} is a 160-dimensional vector that describes the discrepancy between data and prediction. Namely, it contains this information at each of the 16 energy bins of each of the 10 different baselines, ordered in increasing length, and then in increasing energy. For each baseline l and energy bin e, it is defined as

$$x^{l,e} = M^{l,e} - M^e \frac{P^{l,e}}{P^e}. (3.12)$$

Here, $M^{l,e}$, $P^{l,e}$ are the observed and the predicted data at baseline l and energy bin e, respectively. Then, M^e , P^e represent the total observed and predicted data, respectively, summing for all baselines. That is,

$$M^e = \sum_{l=1}^{10} M^{l,e}$$
 and $P^e = \sum_{l=1}^{10} P^{l,e}$. (3.13)

The test statistic in eq. (3.11) minimizes the effect of source flux uncertainties and is independent of its normalization. Therefore, we use the Hubber-Mueller flux for 235 U only, ϕ_{235U} [120]. The prediction is computed as

$$P^{l,e} = \mathcal{N} \sum_{\text{seg} \in l} \epsilon^{\text{seg}} \int_{L_{\text{seg}} - \delta L}^{L_{\text{seg}} + \delta L} \frac{dL_{\text{seg}}}{L_{\text{seg}}^2} \int_0^{\infty} dE_{\nu} \sigma(E_{\nu}) \phi_{235U}(E_{\nu}) P_{ee}(L_{\text{seg}}, E_{\nu}) R(E^e, E_{\nu}), \quad (3.14)$$

where E^e is the central energy of the energy bin e, $L_{\rm seg}$ is the baseline of the segment, $e^{\rm seg}$ its efficiency, R the response matrix provided by the collaboration, and the sum is done for all segments in the same baseline [132]. We also perform a fast integration in $L_{\rm seg}$ to consider the finite width of the reactor and the segments, with $\delta L = 0.25$ cm. Although the normalization constant $\mathcal N$ plays no role in eq. (3.11), it is computed such that our predicted data without oscillations matches the analogous PROSPECT results at each baseline.

Finally, the combined test statistic used in the joint fit of Daya Bay, NEOS, and the PROSPECT is

$$\mathcal{T}S^{\text{Joint}}(\theta_{14}, \Delta m_{41}^2) = \mathcal{T}S^{\text{PROSPECT}}(\theta_{14}, \Delta m_{41}^2) + \mathcal{T}S^{\text{DB+NEOS}}(\theta_{14}, \Delta m_{41}^2),$$
 (3.15)

obtained by adding the individual test statistics and minimizing over the correlated nuisance parameters.

3.2.5 BEST analysis

Again, the analysis on the Baksan Experiment on Sterile Transition data [138] is independent from the rest of experiments. BEST uses a 51 Cr radioactive source, which emits neutrinos in only four discrete energies, namely $E_i = 747, 427, 752, 432 \,\text{keV}$. Their fission fractions are $f_i = 0.8163, 0.0895, 0.0849, 0.0093$, respectively.

Our χ^2 only takes into accounts two points, namely

$$\chi_{\text{BEST}}^2(\Delta m_{41}^2, \theta_{14}) = \frac{(r_{\text{meas}}^{\text{in}} - r_{\text{pred}}^{\text{in}})^2}{\epsilon_{\text{in}}^2} + \frac{(r_{\text{meas}}^{\text{out}} - r_{\text{pred}}^{\text{out}})^2}{\epsilon_{\text{out}}^2}.$$
 (3.16)

Here, ϵ are the statistical and systematic uncertainties, and r are the measured and predicted production mean rates. The predicted rate $r_{\rm pred}$ is computed as

$$r_{\text{pred}} = \xi_{\text{in/out}} \frac{n\sigma A_0}{4\pi} \int_{V_{\text{in/out}}} \frac{\sum f_i P_{ee}(L, E_i)}{L^2} dV, \qquad (3.17)$$

with $n=(2.1001\pm0.0008)\times10^{22}/\mathrm{cm}^3$ the ⁷¹Ga number density of the detector, $\sigma=$

 $(5.81^{+0.21}_{-0.16}) \times 10^{-45}$ cm² [138, 161] the neutrino capture cross section, $A_0 = (3.414 \pm 0.008)$ Ci the initial activity of the ⁵¹Cr source, and the integration is done for the whole volume of the inner or the outer detector. The geometry of the inner and outer detectors are not exactly known and are subject to experimental details such as the quantity of ⁷¹Ga or the position of tubes inside the detector. Therefore, we add two geometric correction factors $\xi_{\rm in/out}$. The BEST data provide the values of the integrals in eq. (3.17) when $P_{ee} = 1$. We pick $\xi_{\rm in/out}$ to match these values, and neglect its dependence on P_{ee} .

In eq. (3.16) the production rate predictions are compared with the $r_{\rm meas}$ from Table I in [138]. Namely, $r_{\rm meas}^{\rm in}=54.9^{+2.5}_{-2.4}$ and $r_{\rm meas}^{\rm out}=55.6^{+2.7}_{-2.6}$. Finally, ϵ^2 are computed as the square sum of statistical uncertainties (taken from Table I [138]), systematic uncertainties ($\sim 2\%$) and the cross section uncertainty.

3.3 Results

We assume that the test statistic satisfies Wilk's theorem and draw the two-sigma exclusion contours in fig. 3.4, which represent the main result of this chapter. Here, the solid pink line shows the exclusion regions at two sigma for the plane wave approximation, while the solid blue and solid yellow lines are analogous with $\sigma_x = 2.1 \times 10^{-4} \text{nm}$ and $\sigma_x = 5.0 \times 10^{-4}$ nm in the wave packet formalism, respectively. Finally, the BEST experiment has been fit with a two-point χ^2 function, using the mean absorption rates for the inner and outer targets of the detector. These rates can then be predicted as a function of the oscillation probability of the model. The positive hint regions at two sigma by BEST are shown in fig. 3.4 as filled regions. Again, pink is used for the plane wave approximation and blue and yellow for the wave packet formalism results. A couple of effects of decoherence can be noticed. First, the suppression of oscillations connects the two separated regions around $\Delta m_{41}^2 = 2 \, \mathrm{eV}^2$, making both results compatible for values of Δm_{41}^2 that were excluded before. Notice that in the lower Δm_{41}^2 part, the suppression of the event rate comes from a slow oscillation, and large values of $\sin^2 2\theta_{14}$ are needed to compensate for the decoherence effect. Second, in the large Δm_{41}^2 region, the suppression of the event rate comes from the fast oscillations and therefore cannot be distinguished from a full decoherence effect. For completeness, fig. 3.5 shows the results for each of the measured experiments.

In this work, we have addressed only the tension between reactor and gallium experiments. Aside from having a common energy range, this tension is specially interesting because both neutrino sources come from nuclear decay within a controlled environment, and systematic uncertainties are under control. However, this is not the strongest tension in this energy range. As can be seen in fig. 3.4, recent solar analysis excludes a

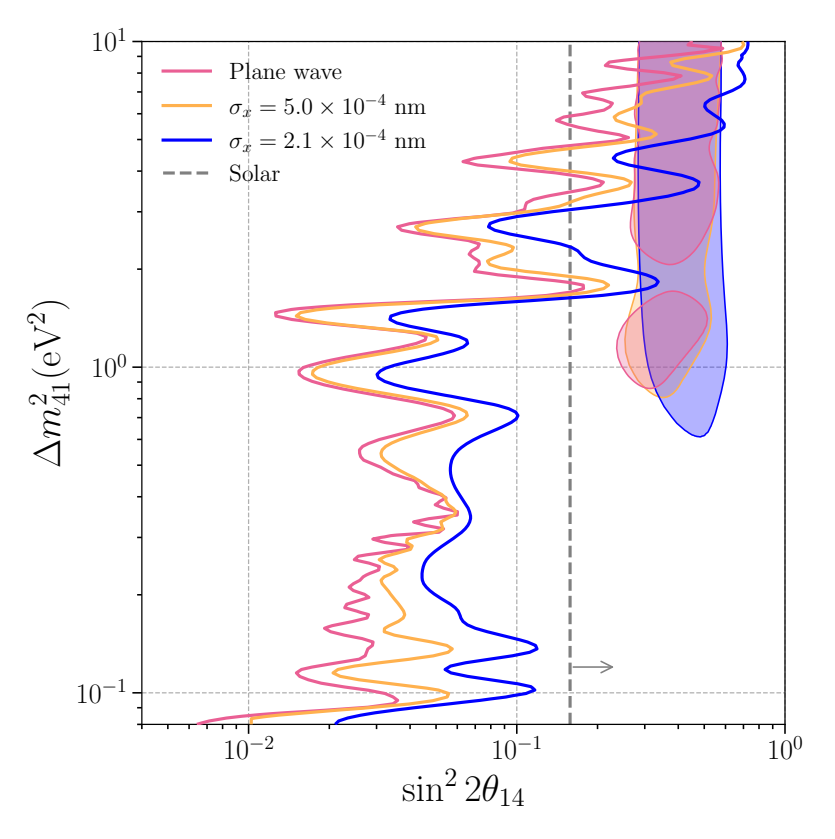


Figure 3.4: Effect of finite wave-packet size on all the electron-neutrino disappearance experiments together. While the solid pink contour bounds the exclusion region at two sigma in the PW formalism, the solid yellow and solid blue contours are computed in the WP formalism with $\sigma_x = 5.0 \times 10^{-4} \mathrm{nm}$ and $\sigma_x = 2.1 \times 10^{-4} \mathrm{nm}$ [194], respectively. The preferred region at two sigma for the BEST experiment is shaded for the plane wave approximation (pink) and the wave packet formalism (yellow and blue). Notably, the region close to the global best fit point, $\Delta m_{41}^2 \sim 2 \, \mathrm{eV}$, is now allowed as well as a larger fraction of large mass-squared difference solutions. A gray dashed line marks the 2 sigma bounds from solar neutrino experiments [137, 166].

wide range of the allowed parameter space by reactor experiments, and are in tension with gallium experiments around three sigma. We do not expect a finite wave packet size to affect this tension, and thus it is not addressed in this work.

3.4 Conclusions

In this chapter, we studied the impact of the oscillation damping phenomena within the wave packet formalism in low-energy searches of sterile neutrinos. Estimations of the wave packet sizes are currently larger than the experimental lower bound; however, these estimations are not without caveats. We found that within the bounds for the wave packet sizes the effects are important in both the exclusion regions from nuclear reactors and the anomalous observations from radioactive sources measurements.

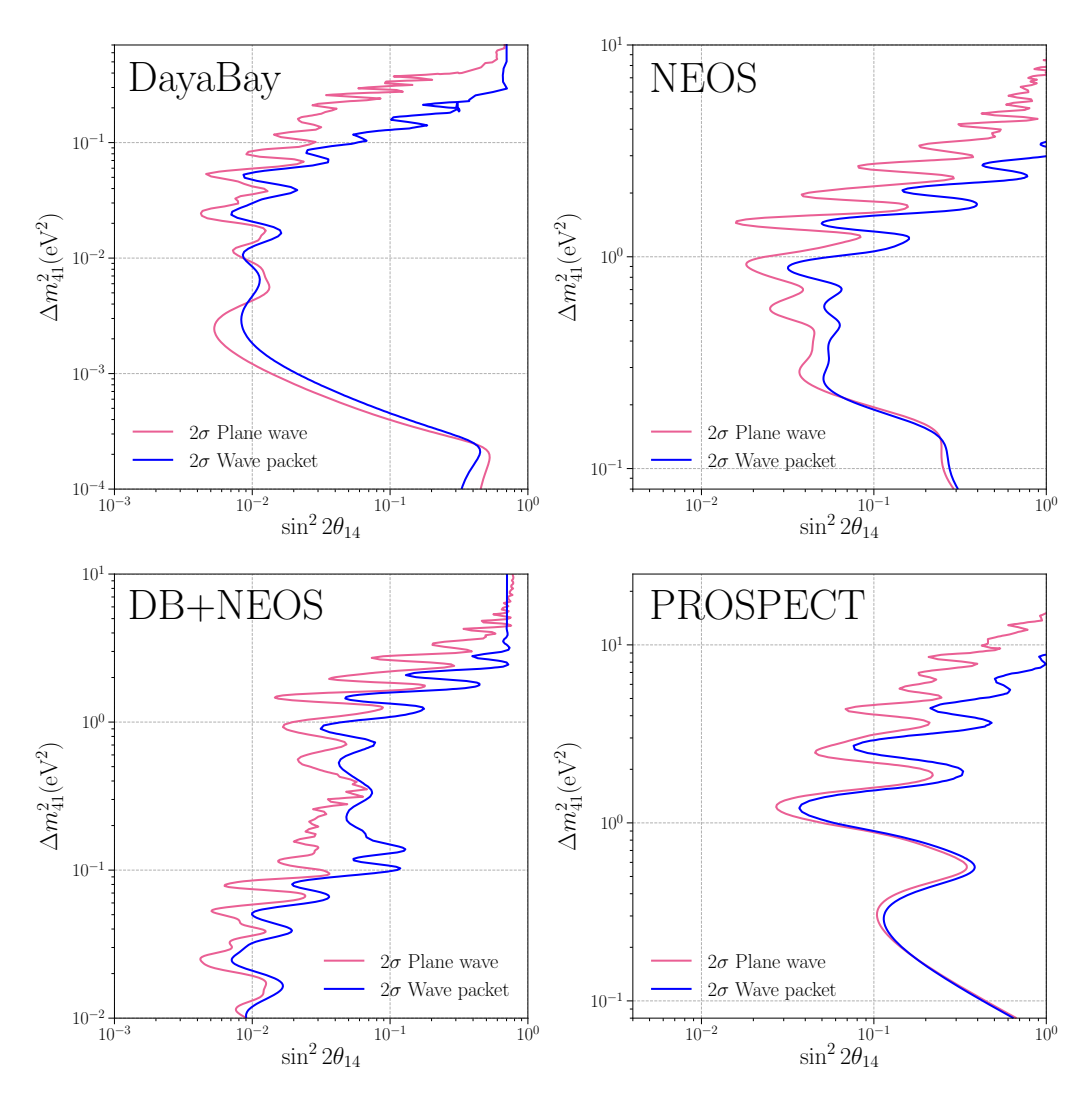


Figure 3.5: Effect of finite wave packet size on different electron neutrino disappearance experiments and their combination. The solid pink and solid blue contours bound the exclusion region at two sigma for the PW and WP formalisms, respectively. All WP contours are obtained using $\sigma_x = 2.1 \times 10^{-4}$ nm [194], and are drawn with respect to the null hypothesis.

When setting the wave packet size at the current constraints, we find that the null observations using event ratios and the anomalous observations by BEST can be resolved. The results become compatible not only at large values of Δm_{41}^2 but also at the region around $\Delta m_{41}^2 = 2 \, \mathrm{eV}^2$. The work performed in this chapter does not necessarily include additional new physics beyond a light sterile neutrino; instead, it highlights the importance of validating the plane wave approximation.

Our chapter implies that further experimental work ought to be performed to understand decoherence effects in neutrino production and detection, and to constrain the size of the wave packet, since its impact is significant in sterile neutrino oscillations. Additionally, we encourage calculations of the neutrino wave packet in the spirit of [190]

for the relevant experimental contexts. Our work additionally motivates the importance of understanding the reactor neutrino flux and the use of radioactive sources, whose fluxes are better predicted. This is, there could be a scenario where the ratio experiments see null results in the presence of a sterile neutrino due to the effect mentioned, and the sterile neutrino could only be observed by comparing results to absolute flux predictions. Finally, our code is available at this URL \mathbf{Q} . The experiments here analysed can be easily reproduced using arbitrary probabilities.

Further insights in the wave packet width

In retrospect, it seems like this publication [1] sparked new interest in the question of the wave packet width of neutrinos. This is not the case, *of course*, but the interest is due to the expected sensitivity of the upcoming JUNO experiment, which will improve the bound on σ_x by an order of magnitude [204]. As shown in fig. 3.4, a non-observation of σ_x would wash out our proposed solution. But, more interestingly, a possible observation of decoherence would require to understand its agreement with the SM.

The SM calculations, however, are not yet in agreement among themselves. In particular, there is no consensus on what is the limiting distance scale for neutrino coherence. On the one hand, [94, 205, 206] claim that coherence is interrupted by collisions of the parent atom with the surrounding atoms on the medium, thus leading to $\sigma_x \sim \mathcal{O}(10^{-7})\,\mathrm{m}$. This would make decoherence effect unobservable at reactor experiments, and JUNO in particular. On the other hand, [192, 193] claim that the limiting distance is sub-nuclear, from the nucleon-nucleon correlation length to the diameter of the parent nucleus. This leads to $\sigma_x \sim \mathcal{O}(10^{-15})\,\mathrm{m}$. While much closer to the value used here, it would still be unobservable by JUNO and would wash out our prediction. Finally, [207] claimed to have directly measured $\sigma_x \gtrsim \mathcal{O}(10^{-12})\,\mathrm{m}$. However, the neutrino production process studied is electron capture, not beta decay, and hence the limit does not apply [208].

All in all, the possibility of New Physics narrowing the wave packet width is still open [209, 210], and the experimental search for σ_x is very much well motivated [211–213]. In the end, neutrino decoherence is tightly related to the theory of measurement in open quantum systems, and thus the measurement of the neutrino wave packet width would represent a fundamental test of it [193].

Chapter 3 Impact of Wave Packet Separation in Low-Energy Sterile Neutrino Searches					

Part II Neutrinos from outer space

4 The dawn of ultra-high-energy neutrino astrophysics

just one more collider bro. i promise bro just one more collider and we'll find all the particles bro. it's just a bigger collider bro. please just one more. one more collider and we'll figure out dark matter bro. bro cmon just give me 22 billion dollars and we'll solve physics i promise bro. bro bro please we just need to build one more collider t

- Internet meme, anonymous

As we have seen in the previous Part, laboratory particle accelerators and colliders have been an absolutely successful scientific program, setting all the stones for the SM and starting the search beyond it. However, terrestrial experiments have not been able to predict nor explain the existence of Dark Matter (DM) and Dark Energy (DE). Terrestrial scales have not yet been sufficient for understanding the microscopical description of these components. Their discovery has only been possible by looking at astrophysical and cosmological scales, which so far only has taught us about their macroscopical behaviour. The question is, then, natural: is there any way to exploit these scales for microphysics searches?

In this chapter and for the rest of this Thesis, we leave behind terrestrial experiments and gaze beyond Earth. Our intention is to understand how can we use astrophysics (and, later on, cosmology) to complement laboratory and collider BSM searches. Coincidentially, our first direct hint of BSM physics, neutrino oscillations, came from extraterrestrial particles: solar neutrinos and cosmic rays impacting in the atmosphere.

In particular, in this second Part we will address a very specific field, ultra-high energy (UHE) neutrino astrophysics. That is, the study of extraterrestrial neutrinos with $E_{\nu} \gtrsim 100\,\text{PeV}$. As we will understand in this chapter, the motivation for this research area is two-fold, both from astronomy and from particle physics. While still a dawning field, it bears great scientific potential and it is already raising its first questions and BSM searches. We will show an example of possible BSM searches in chapter 5 [2]. Then, let us first explore the foundations of the field of ultra-high-energy neutrinos, following [20, 214, 215]. First, in section 4.1 we explore the physical processes behind UHE processes, and their potential use for BSM searches. Then, in section 4.2 we review the experimental setups that allow to measure UHE neutrinos. As usual, if you're familiar with these you're welcome to skip the chapter.

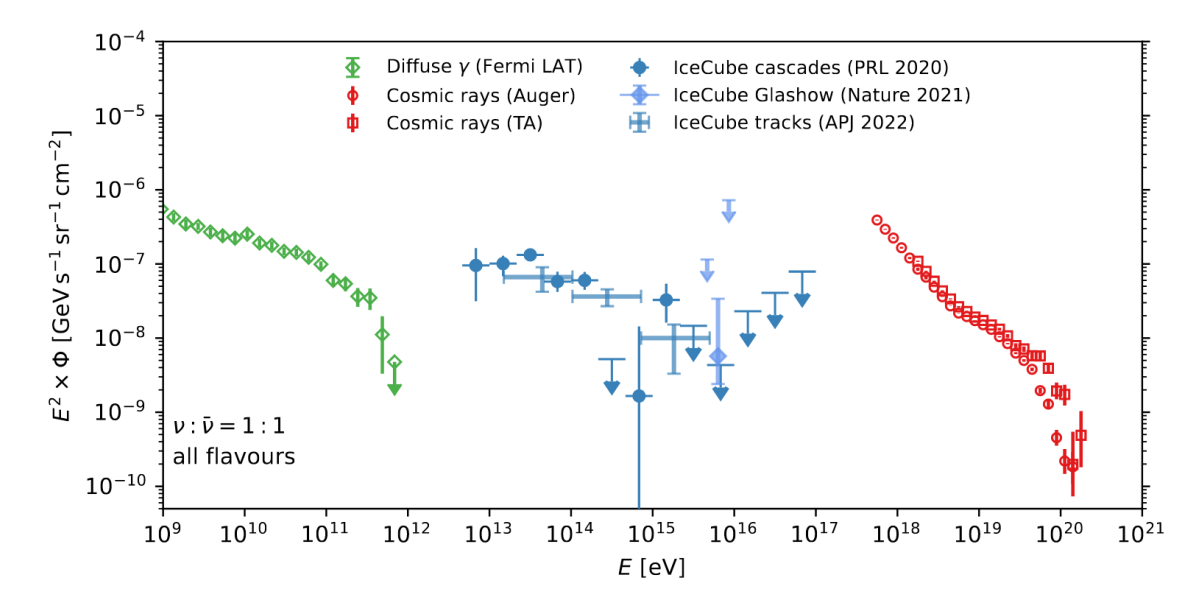


Figure 4.1: As of July of 2022, a selection of the measurements of high-energy gamma rays by Fermi-LAT [216] (green), high-energy neutrinos by IceCube [217–219] (blue), and ultra-high-energy cosmic rays by the Pierre Auger Observatory [220] and the Telescope Array (TA) [221] (red). Three different measurement datasets are shown: contained cascades (dots) [218], Glashow resonance (diamonds) [217] and through-going muons (crosses) [219]. Error bars and upper limits represent 68% C.L. intervals. Figure extracted from [20].

4.1 At the crossover of multimessenger astrophysics

The history of astronomy and astrophysics is founded in electromagnetic waves. From radio to gamma-rays, the electromagnetic spectrum has allowed to observe and understand the Universe with incredible precision (in astrophysical standards). However, light is not a perfect astrophysical messenger. At energies larger than hundreds of TeV, the photon-photon ($\gamma\gamma \to e^+e^-$) cross-section with the interstellar and intergalactic media stops the propagation of high-energy photons, and cascades them down to lower energies [222]. In fact, gamma-ray events with energies larger than the PeV are not expected to arrive from long distances. Gamma-ray events as measured by Fermi-LAT are shown in fig. 4.1 and have energies up to $E=1\,\mathrm{TeV}=10^{12}\,\mathrm{eV}$. Recently, the LHAASO detector has seen more energetic gamma-ray events, up to $E=2.5\,\mathrm{PeV}=2.5\times10^{15}\,\mathrm{eV}$ [223–226].

In any case, we know that the Universe is full of particle colliders which reach energies far beyond the PeV. As shown in fig. 4.1, we have measured Cosmic Ray (CR) events with energies up to $E=320\,\mathrm{EeV}=3.2\times10^{20}\,\mathrm{eV}$, the so-called Oh-My-God particle [227]. Such a particle carries an energy $\mathcal{O}(10^7)$ times higher than LHC protons. However, since CR collisions with protons in the atmosphere are fixed target experiments, the available

¹That is around 50 joules in a single particle.

energy is only the center-of-mass energy,

$$E_{\rm com} = \sqrt{2Em_p} \,. \tag{4.1}$$

For the Oh-My-God particle this gives 750 TeV, which is *only* $\mathcal{O}(50)$ times more energetic than proton-proton collisions at the LHC. Immediately, this motivates the use of CRs for BSM searches, which produce heavier states than in the LHC. However, CR measurements are plagued with the systematic uncertainties from hadronic interactions and are hard to control experimentally. While CRs can constrain the parameter space of some BSM theories [228, 229], their existence poses a question which might have a closer answer: where are these ultra-high-energy cosmic rays (UHECRs) coming from? That is, what are the cosmic accelerators which are capable of producing such ultra-high-energy particles? Also, through which mechanisms do they manage to do so? Unluckily, the electric charge of CRs which allows to accelerate them also deflects them as they travel through galactic and intergalactic magnetic fields. Even if the CRs are heavier nuclei or have higher energies, such that they are less deflected, we have not managed to trace them back to their cosmic sources [228, 229].

Even if we do not know too much about them, the existence of UHECRs is a guarantee for the existence of an ultra-high-energy flux of neutrinos, which could point straight back to their sources and might give clearer signals with which to look for BSM Physics. To understand this, we need to go back to the origin. In particular, to the origin of Cosmic Rays.

4.1.1 The origin of ultra-high-energy Cosmic Rays

The general requirements for the acceleration of CRs to ultra-high-energies date back to the seminal paper by Hillas [230]. Regardless of the acceleration mechanism with produces such ultra-high-energy particles, the CR source must have a magnetic field B which confines the particle for a sufficiently long time. Within this magnetic field, the particle will spin in a circular orbit with a radius given by their Larmor radius. For an ultrarelativistic charged particle with energy E and atomic number E, this is

$$r_{\text{Lar}}(E) = \frac{E}{ZeB} = 1.08 \frac{1}{Z} \left(\frac{E}{\text{PeV}}\right) \left(\frac{1 \,\mu\text{G}}{B}\right) \text{ pc}.$$
 (4.2)

The maximum energy that a particle can reach then depends on the size of the region where the magnetic field is extended, *R*. That is, the particle will not be contained

anymore when $r_{Lar}(E_{max}) > R$. This is the so-called Hillas criterion,

$$E_{\text{max}} \simeq Z \left(\frac{B}{1\,\mu\text{G}}\right) \left(\frac{R}{1\,\text{kpc}}\right) \text{ EeV}.$$
 (4.3)

This criterion already tells us that the Milky way cannot be at the origin of the highest-energy CRs that we have measured. Furthermore, the incoming direction of these CRs do not show the anisotropy that the emission from the Galactic plane would predict. Within astrophysical uncertainties, the consensus is that CRs energies larger than 3 EeV have an extragalactic origin [214]. This energy also corresponds to the so-called "ankle" of the CR spectrum, where the CR flux becomes steeper, compatible with a change on the source population.

The Hillas criterion is a very intuitive physical argument, necessary for the acceleration of UHECRs, but not sufficient. In particular, we also require that the acceleration mechanism is efficient enough to overcome energy losses, to reach the right energy within the lifetime of the source and before the particle escapes the source. The most popular mechanism for CR acceleration is the first-order Fermi shock acceleration [231, 232]. In this mechanism, particles are accelerated through multiple crossings of a shock wave which is expanding at non-relativistic speeds. At each one of these crossings, the particle extracts energy from the varying magnetic field of the shock wave,

$$\left\langle \frac{\Delta E}{E} \right\rangle = \frac{4}{3}\beta\,,\tag{4.4}$$

where β is approximately the velocity of the shock wave. Then, after n encounters, the energy will be given by

$$E = E_{\rm ini} \left(1 + \frac{4}{3}\beta \right)^n \,, \tag{4.5}$$

with $E_{\rm ini}$ the initial energy of the particle. This kind of acceleration mechanism leads to the energy spectrum of the CRs to follow a power-law

$$\frac{\mathrm{d}N(E)}{\mathrm{d}E} = \Phi_0 \left(\frac{E}{E_0}\right)^{-\gamma} , \qquad (4.6)$$

where γ is the spectral index and E_0 , Φ_0 an arbitrary pivot energy and normalization, respectively. In particular, first-order Fermi acceleration in shock waves predicts $\gamma \sim 2$, with the value varying depending on the velocity of the shock. This is remarkably close to the power-law behaviour observed in the CR spectrum.

4.1.2 A common origin for CRs, gamma rays and neutrinos

While we have good theoretical guesses on the possible CR sources and their acceleration mechanisms, we do not yet have observational evidence. The deflection of CR hinders the search. However, gamma rays and neutrinos share a common origin with CRs, and so this opens two new messengers with which to understand their origin.

As we have seen, magnetic fields are required for confining protons while they are accelerated. As a consequence, all charged particles in the media (i.e., electrons and protons) will lose energy through synchrotron radiation, in the form of high-energy photons. Both electrons and photons will then start electromagnetic cascades, which will cascade down the energy spectrum of gamma rays to energies where their absorption by pair production is negligible [214, 233]. Then, this population of photons acts as a target for the accelerating protons, which can undergo photohadronic interactions such as

$$p + \gamma \rightarrow n + \pi^0 + \text{stuff},$$
 (4.7)

to produce more gamma rays through

$$\pi^0 \to \gamma + \gamma \,, \tag{4.8}$$

among other mechanisms such as inverse Compton scattering [234] or *pp* collisions. UHE gamma rays point back to their origin and are a useful messenger to determine the origin of UHECRs. However, as we have said, their mean free path in the intergalactic medium is short. In this thesis, we are interested in neutrinos. Then, we need to look into the analogous processes with charged pions in the final state, e.g.,

$$p + \gamma \rightarrow n + \pi^{\pm} + \text{stuff}$$
 (4.9)

The produced neutrons can beta-decay and inject \bar{v}_e , but the neutron abundance will be disminished by subsequent photohadronic interactions with other γ . However, the π^{\pm} will produce neutrinos through its decay

$$\pi^{\pm} \to \mu^{\pm} + \nu_{\mu} (\bar{\nu}_{\mu}) \mu^{\pm} \to e^{\pm} + \bar{\nu}_{\mu} (\nu_{\mu}) + \nu_{e} (\bar{\nu}_{e}).$$
 (4.10)

That is, if UHE protons exist, photohadronic interactions predict that the same source must produce a flux of ultra-high-energy neutrinos, which will escape the source and arrive to Earth in a straight line.

Taking all this into account, one can use the observation of the CR flux to con-

strain the intensity of the expected neutrino flux. This was first done by Waxmann and Bahcall [233, 235], reporting an upper bound on the neutrino flux of $E_{\nu}^2 \Phi_{\nu} \lesssim 2 \times 10^{-8} \, \text{GeV cm}^{-2} \, \text{s}^{-1} \, \text{sr}^{-1}$, as long as the sources are optically thin to photohadronic processes. The measured flux by IceCube is consistent with this Waxmann-Bahcall bound, which reinforces the idea that CRs and neutrinos have a common origin [236].

4.1.3 The GZK cut-off and cosmogenic neutrinos

Photohadronic interactions in the environment of a CR source have a ~PeV energy threshold due to the high energy carried by the photons in the environment. However, as soon as CRs leave the source, these target photons are now unavailable, and photohadronic interactions are not possible for PeV protons. Still, the intergalactic medium is filled with photons of the Cosmic Microwave Background (with energies ~ 10^{-3} eV) or interstellar light. Now, protons with energy $E_p \gtrsim 7 \times 10^{19}$ eV can undergo photohadronic interactions as in eq. (4.9) with these low-energy photons, which unavoidably fill up the entire Universe. These photohadronic interactions cascade down the protons to lower energies, and as a consequence we do not expect protons with $E_p \gtrsim 7 \times 10^{19}$ eV from further away of 75–150 Mpc [214]. This is the so-called Greisen-Zatsepin-Kuzmin (GZK) cut-off [237, 238]. Above this region, we expect about one CR event per square kilometer per century. A suppression of the CR flux above 6×10^{19} eV has indeed been measured, but it is not yet clear whether this is the GZK cut-off or the maximum energy that accelerators can reach [214].

As a byproduct of the pion decay from eq. (4.10), the GZK cut-off predicts the existence of a flux of ultra-high-energy neutrinos, usually called GZK neutrinos or cosmogenic neutrinos. The intensity and shape of this flux is subject to many astrophysical uncertainties, such as the chemical composition of the CR (e.g., if CR were only nuclei, this flux would be greatly suppressed). While experiments are improving their sensitivities to this expected flux, cosmogenic neutrinos have not been measured yet.

4.1.4 Ultra-high-energy neutrinos for BSM searches

We have understood that UHE neutrinos are expected to exist, and they can hold the key to solve a central question in astrophysics: what is the origin of Cosmic Rays? However, the search for UHE neutrinos is also well-motivated from the perspective of Particle Physics. In particular, the discovery of UHE neutrinos will expand the energy frontiers for high-energy-physics.

Firstly, the center-of-mass energy in their collisions with nucleons, namely eq. (4.1), can reach $E_{\rm com} \gtrsim 30\,{\rm TeV}$ for neutrinos with energy $E_{\nu} \gtrsim 1\,{\rm EeV}$. Therefore, they can

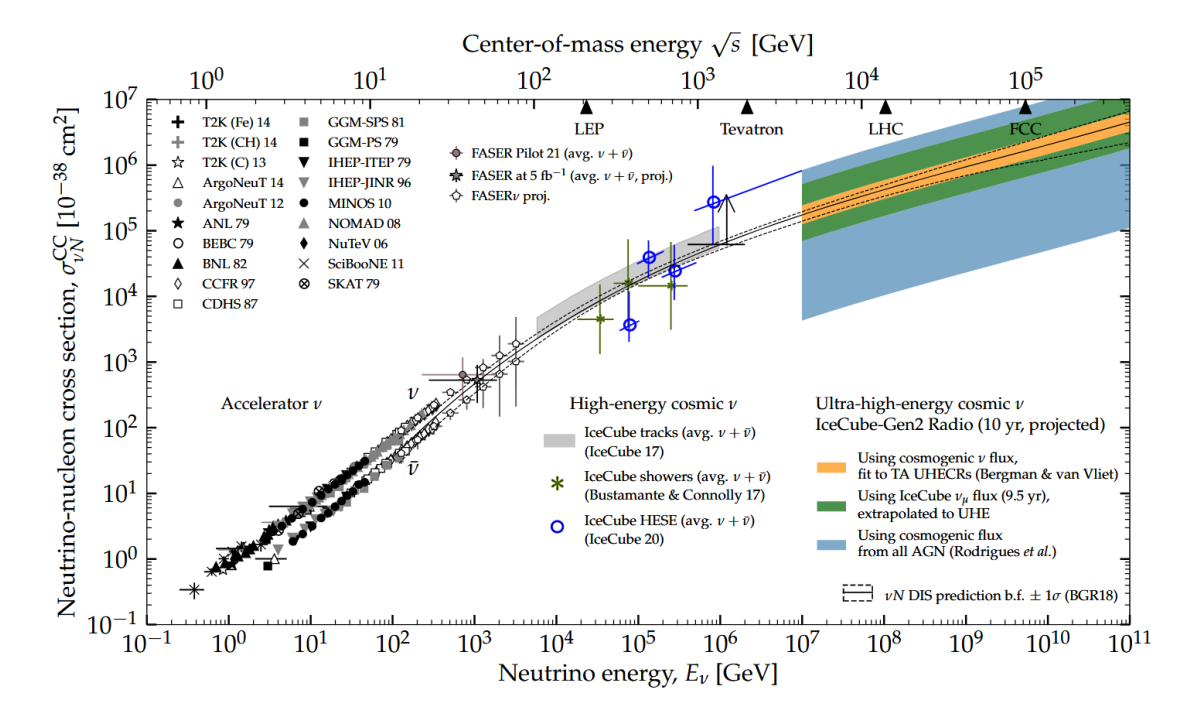


Figure 4.2: Neutrino-nucleon cross section measurements and DIS predictions [244], as a function of energy. Yellow, green and blue bands show the projected sensitivity for 10 years of measurements at IceCube-Gen2 radio, for different cosmogenic fluxes, assuming 10% energy resolution and 2° angular resolution. Figure extracted from [20], adapted from [240]. UHE neutrinos will be able to measure the DIS cross-section at energies not reachable by LHC, and constrain BSM contributions.

serve to measure neutrino-nucleus cross-section at unprecedented energies [239–241]. In particular, UHE neutrinos will test models of nuclear structure [242–245] and new physics in the neutrino-nucleon interactions [246–250], since undiscovered heavy degrees of freedom could lie at these high-energies. In fact, next-generation experiments will be able to put good constraints on neutrino-nucleon cross-section with modest energy and angular resolution, even in the low-statistics regime (10 events per energy decade), and rule out extra dimension or leptoquark models [240].

Secondly, measured UHE neutrinos –of extragalactic origin– will have travelled Mpc distances. As a consequence, they will be able to probe fundamental properties of neutrinos that only manifest at high energy and at the propagation through cosmological scales. Among others, this would be the case for neutrino self-interactions [251–264], neutrino-DM interaction [263–274], neutrino-DE interaction [275, 276] or neutrino decay [265, 277–282]. The propagation of neutrinos might also be flavor-dependent, and thus measuring the flavor composition of the neutrino flavor would probe the flavor structure of the leptonic sector at ultra-high-energies [265, 274, 275, 283–293].

Finally, UHE neutrinos will also be able to test DM models which produce neutrinos

through annihilation or decay [266, 294–319]. In chapter 5, we present an example into the capabilities of UHE experiments to constrain general high-energy BSM extensions. To such purpose, let us review these experiments.

4.2 The experimental search for UHE neutrinos

As we learned in section 2.3, neutrinos can interact either through CC interactions, via the exchange of an W^{\pm} , or through NC interactions, via Z^{0} . One the one hand, CC interactions, namely

$$\nu_l(\bar{\nu}_l) + N \to l^{\dagger} + X, \tag{4.11}$$

are flavour dependent. Thus, the detection of the secondary charged lepton l allows for the identification of the neutrino flavor. However, in UHE experiments l^+ and l^- leave very similar traces, and thus this process does not allow to distinguish between neutrinos and antineutrinos, except for inelasticity measurements [320] and the Glashow resonance [321]. That is, only electron antineutrinos are able to produce an on-shell W^- through

$$\bar{\nu}_e + e^- \rightarrow W^- \rightarrow \text{stuff},$$
 (4.12)

which peaks at energies $E_{\nu}=6.3\,\mathrm{PeV}$. The IceCube experiment first measured this resonance in [217].

On the other hand, NC interactions, namely

$$\nu_l(\bar{\nu}_l) + N \to \nu_l(\bar{\nu}_l) + X, \tag{4.13}$$

are flavour-blind. Since they do not produce any charged lepton, they are only detectable by the energy they deposit in the detector, which is independent of the original neutrino flavour. Thus, flavor identification with NC interactions is impossible.

In both cases, neutrino-matter interactions are in the Deep Inelastic Scattering (DIS) limit. The extrapolation to EeVs for the corresponding cross-sections are [239]

$$\sigma_{\nu N}^{\rm CC} \simeq 2.35 \times 10^{-32} \text{ cm}^2 \left(\frac{E_{\nu}}{10 \text{ EeV}}\right)^{0.363},$$

$$\sigma_{\nu N}^{\rm NC} \simeq 9.85 \times 10^{-33} \text{ cm}^2 \left(\frac{E_{\nu}}{10 \text{ EeV}}\right)^{0.363}.$$
(4.14)

These cross-sections gives a mean free path for UHE neutrinos

$$\lambda = \frac{1}{n_N(\sigma_{\nu N}^{\text{CC}} + \sigma_{\nu N}^{\text{NC}})} = 176.9 \left(\frac{2.835 \,\mathrm{g \, cm^{-3}}}{\rho}\right) \left(\frac{10 \,\mathrm{EeV}}{E_\nu}\right)^{0.363} \,\mathrm{km}\,,\tag{4.15}$$

where n_N is the nucleon number density, ρ the mass density, and we have used the average value of Earth's crust density, $2.835\,\mathrm{g\,cm^{-3}}$. As a consequence, the Earth is quite opaque to UHE neutrinos, i.e., they cannot travel more than hundreds of kilometers inside the Earth.

Therefore, UHE neutrinos are not detectable for the whole 4π solid angle sphere, but are instead expected to come nearly horizontal, so-called Earth-skimming neutrinos. While this narrows the available window for cosmogenic neutrinos searches, it also allows for targeted searches. Current and future experiments are mainly based in two different technologies, optical and radar. Let us look into them.

4.2.1 Optical detection experiments

ANTARES [322], IceCube [323, 324] and KM3NeT [110] can detect neutrinos via the optical Cherenkov light by neutrino-induced showers and tracks. Figure 4.3 shows the topology of cascades and tracks in an optical detector (IceCube in particular). These are,

- Cascade-like events [218] deposit all their energy in a localized point. Cherenkov light then diffuses in all directions, forming a spherical topology. These are formed by NC interactions from all flavors, which deposit energy in the nucleus, and by CC interactions from v_e and v_τ . In particular, v_e produce an electron which loses energy very efficiently before it propagates, and v_τ produces a tau lepton which decays before it propagates.
- Track-like events [219] are formed by particles which cross the instrumented volume (either starting inside the detector or crossing it from side to side) and deposit energy around their linear trajectory. This are formed by CC interactions from v_{μ} . Since its much more massive, the resulting muon loses energy less efficiently and can travel a long distance without being absorbed or decaying.
- Ultra-high-energy v_{τ} interactions can also produce double-cascade topologies, where two cascades happen at different points within the detector. This is because, at such energies, the boost factor of the produced tau lepton is sufficient to separate the collision and the decay points. These have not been measured yet, but future larger arrays will increase the sensitivity to them [38].

In general, track-like events give a much better angular reconstruction than cascades. However, since the track is not contained in the detector, their energy losses are harder to quantify and energy reconstruction is worse. Instead, cascade-like events have

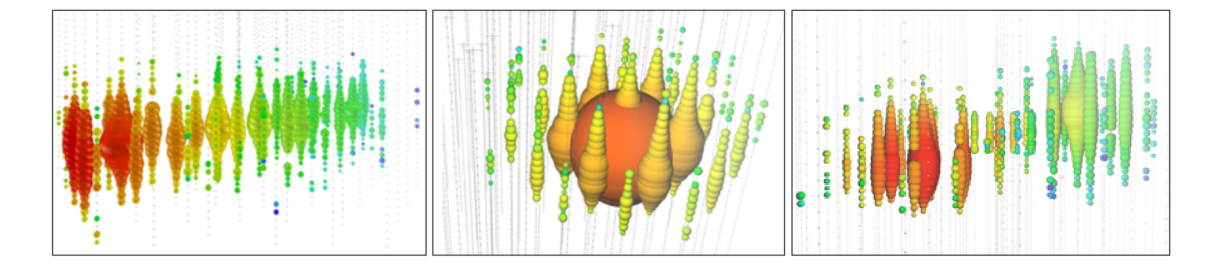


Figure 4.3: Event topologies at an optical Cherenkov detector. Here, in particular, at IceCube. From left to right: a track, a cascade and a double cascade. Each sphere is a detector, the size of the sphere shows the amount of light acquired and the color marks the time of the detection (early signals are red, late signals blue). Extracted from [38]. *Each event topology reconstructs better a different quantity, and their differences can allow for flavour identification.*

a very good energy reconstruction. The main background for astrophysical (and cosmogenic) neutrino searches are atmospheric neutrinos and muons. Since these fall more steeply with energy, at sufficiently high energies ($E_{\nu} \gtrsim 100\,\mathrm{TeV}$) the flux is mainly astrophysical [325]. Another way to remove the background is to look at up-going events, i.e., events which have crossed the Earth before arriving to the detector. As a consequence, the hemisphere where the detector is placed determines in which directions of the sky the signal-to-noise ratio is better. For this reason, KM3NeT (located in the northern hemisphere) is better at looking towards the Galactic Center than IceCube (located in the southern hemisphere).

IceCube

IceCube, located in the geographical South Pole, is the world-leading telescope for high-energy neutrinos. It consists of a cubic kilometer of instrumented ice buried between 1.45 and 2.45 kilometers below the surface, just on top of the Anctartic bedrock. It is also formed by IceTop, a surface array for CR searches. IceCube started operations in 2010, when it observed its first atmospheric neutrinos [326], and in 2013 first reported the observation of astrophysical neutrinos [325].

As explained above, IceCube is excellent in looking at TeV astrophysical sources in the Northern Sky, where atmospheric backgrounds are reduced. These events are called Northern Sky Tracks (NST) [219]. In this portion of the sky, the good angular resolution from muon tracks (roughly 1°) can locate sources with good precision. This led to the discovery of the first steady sources of neutrinos, namely TXS 0506+056 [327] and NGC 1068 [328]. In fact, the discovery of the former was the first and unique multimessenger detection including neutrinos, since a gamma-ray flare was also observed [329].

However, IceCube also looks into the TeV Southern sky. In order to do so, it uses the outer instrumented volume as veto, and trigger out any event which does not start in

the detector. This reduces its effective volume, but it benefits from an inner region of the detector with a higher density of detectors, the DeepCore component. Events detected in this manner are called High-Energy Starting Events (HESE) [330] and provide a better sensitivity to low-energy neutrinos, with hundreds of TeVs. The first detection of astrophysical neutrinos was in this manner [325], and the reconstruction of contained cascade-like events was essential for the discovery of neutrino emission from the Galactic plane [331].

After a decade of observing data, IceCube has been able to characterize the astrophysical diffuse neutrino flux up to the PeV, measuring its normalization Φ_0 and its spectral index γ , defined as in eq. (4.6). As a matter of fact, a slight tension exists between the preferred power law from NST and HESE measurements [219, 330]. Still, IceCube has not yet measured any neutrino above 10 PeV.

KM3NeT

KM3NeT [110] is a gigaton water Cherenkov detector deployed at the bottom of the Mediterranean Sea. It consists of two sub-detectors: the Astroparticle Research with Cosmics in the Abyss (ARCA) and the Oscillation Research with Cosmics in the Abyss (ORCA). On the one hand, ARCA is located south of Sicily, at a depth of 3.5 kilometers, and it consists of two building blocks with increased spacing between photomultipliers (PMTs). This allows for improved sensitivity to high-energy astrophysical neutrinos. On the other hand, ORCA is a single block located south of France. It plans to study the oscillations of 1-100 GeV atmospheric neutrinos. In both cases, string of PMTs are attached to the seabed and located using acoustic positioning [332]. While both detectors are currently still under construction, the KM3NeT collaboration has already reported the detection of a 220 PeV neutrino [333], which is in $2.5 - 3.5\sigma$ tension with lceCube [333–335].

Photon scattering is less efficient in water than in ice [234], and thus photons keep direction better². As a consequence, the ARCA detector will have better angular resolution than IceCube, around 0.1° for PeV tracks, and 1° for cascades. This will be specially useful to study the Southern Sky and, in particular, the Galactic Plane. For instance, its sensitivity to Southern-Sky point-like sources will improve IceCube's by an order of magnitude in only three years of data-taking. The diffuse flux from the Galactic Plane will be detected with 5σ significance after only four years of observations.

Apart from IceCube and KM3NeT, other Cherenkov detectors are planned in the future: IceCube-Gen2 [38], Baikal-GVD [336], P-ONE [337] and TRIDENT [338]. These telescopes, which will be finished in the next 10-20 years, will form a global network

²In all fairness, photon absorption is more efficient in water than ice.

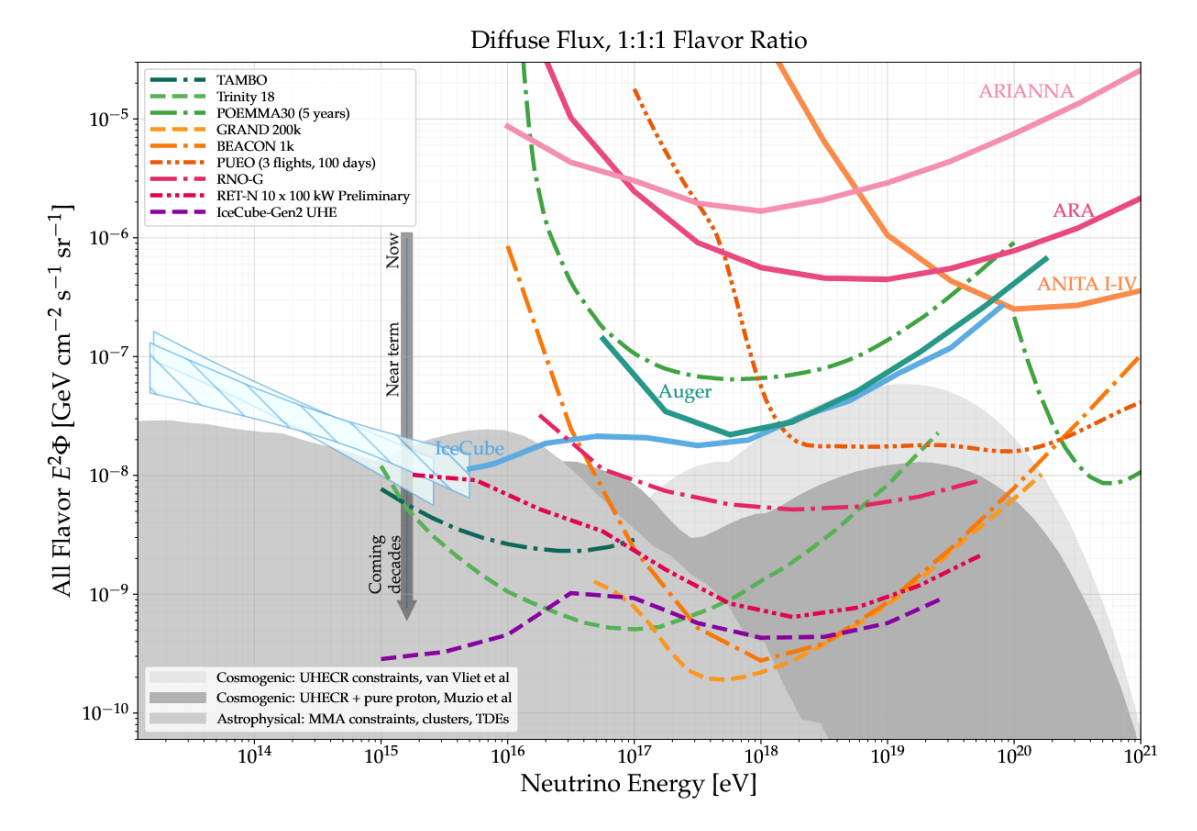


Figure 4.4: Differential 90% C.L. sensitivities for UHE neutrino experiments to an all-flavor diffuse neutrino flux in decade-wide energy bins, assuming 10 years of observation (unless stated otherwise). Solid lines are present experiments, dashed lines are future ones. Gray bands show different cosmogenic [340, 341] and astrophysical neutrino models [340]. Light blue bands show the measurements from IceCube using tracks (hatched [219]) and cascades (solid [330]). For references on the different experiments, see main text. Figure extracted from [20]. Future experiments have the potential to discover the UHE cosmogenic neutrino flux.

capable of continously monitoring the entire sky and increasing the rate of neutrino detection by an order of magnitude [339] and as shown in fig. 4.4. While optical telescopes pose an exciting future to look forward to, the detection of UHE neutrinos will also benefit from another kind of telescopes, radio detectors.

4.2.2 Radio detection experiments

Since the neutrino flux falls at higher energies, we require big effective areas to catch UHE neutrinos, and thus to instrument a big volume. However, photons propagating in water or ice get absorbed at distances $\mathcal{O}(100)\,\mathrm{m}$, so the spacing between detectors cannot be much larger than few hundreds of meters. As a consequence, to increase the experiment's volume, experiments are switching to radio detection techniques, where signals from UHE neutrinos are also expected. Radio detectors are cheap and radio waves attenuate at $\mathcal{O}(2)\,\mathrm{km}$ in ice, thus allowing to instrument a larger volume with the

same number of detectors.

Neutrinos can produce radio signals in many ways. First, neutrino scatterings initiate an electromagnetic shower. In a dense dielectric (such as ice, but also e.g. rock or lunar regolith), positrons are quickly annihilated and the shower acquires a net electric charge $\sim 10^6 e$. If the wavelength of the electromagnetic waves is larger than $\mathcal{O}(10)$ cm, then the emission of all electrons is coherent, i.e., the shower effectively acts as a point charge. This is called Askaryan radiation [342–344]. Aditionally, if these electromagnetic showers propagate within a magnetic field (such as the Earth's), this separates positrons and electrons and creates a non-zero polarization, which emits polarized radio waves [345–347].

Finally, the CC scattering of v_{τ} produces a τ lepton. At ultra-high-energies, this τ can travel large distances,

$$d_{\tau} \simeq 51 \left(\frac{E_{\tau}}{1 \,\text{EeV}} \right) \,\text{km} \,.$$
 (4.16)

Therefore, if the scattering and production of the τ lepton happens close enough below the surface, it can escape the rock or ice, and decay in the atmosphere. This produces an up-going electromagnetic shower, which in the presence of a magnetic field, emits coherent, impulsive, polarized radio waves [348, 349].

Multiple experiments are looking for neutrinos in the radio frequency. For Askaryan radiation in ice, ARA [350] and ARIANNA [351] are setting the ground for the underground radio array of IceCube-Gen2 [38] and RNO-G [352]. Aerial experiments such as ANITA [353] and, in the near-future, PUEO [354] look at Askaryan radiation in Antarctica from a high altitude, and also τ -emerging showers. From the ground, these are also looked at by Auger [349] in the present, and by BEACON [355], TAROGE [356], GRAND [357], TAMBO [358], TRINITY [359] and POEMMA [360] in the future.

ANITA

The Antarctic Impulsive Transient Antenna (ANITA) is a balloon-borne experiment which has done four flights above Anctartica, for a total of four months between 2006 and 2016. In each of these flights, ANITA has had an instantaneous effective area of $\mathcal{O}(200)\,\mathrm{km}^2$ to Askaryan radiation and electromagnetic showers from τ decay.

The signals are as explained above: short and impulsive pulses, of nanosecond duration, horizontally polarized by the vertical Earth magnetic field. The phase from these pulses distinguish an upward-going shower from a reflected down-going shower (from a CR), rephased by reflection in the ice. While human activity usually produces noise in the radio band, the Antarctic region is very much radio-free and the experimental collaboration claims that the background control is manageable [353].

In its first and third flights, ANITA has measured one τ -shower-like event per flight, with energies $\mathcal{O}(1)$ EeV [361]. The reconstructed direction is well below the horizon, 27° and 35° respectively. If these events came from a τ decay, the primary v_{τ} should have crossed $\mathcal{O}(6000)$ km, much larger than the neutrino mean free path shown in eq. (4.15). This small survival probability of such neutrinos ($\lesssim 10^{-6}$) strongly disfavours a SM interpretation of these events [362]. Several BSM models have tried to explain these events in various degrees of *exoticness* [363–371], but those which require high-energy extensions are hard to explain within a diffuse flux explanation [364].

However, in its fourth flight, ANITA measured four similar events, also with $\mathcal{O}(1)$ EeV energies, but from directions much more closer to the horizon. These could be explained by ν_{τ} , but are again in tension with IceCube and Auger. In chapter 5 we explore a possible BSM explanation for these events which relieves the tension [2].

Concluding remarks

We finish this introduction to UHE neutrino astrophysics with the taste that it is a field which will bring exciting discoveries in the mid-term future. This is because,

- The origin of UHE Cosmic Rays is unknown, but their existence implies a flux of UHE neutrinos which might point straight to their source.
- This is a question of great astrophysical interest which justifies the ongoing international investment in developing an array of multiple telescopes around the Earth to explore the extreme Universe with neutrinos.
- The energies and scales that concerns these neutrinos allows to probe physical processes which could not be feasible in laboratory experiments, such as neutrino interactions at energies larger than the LHC, or the existence of neutrinophilic Dark Matter, among many others.

While the future of the field is bright, the present brings a lot of questions. We are in the dawn of a new epoch, and as such a lot of work is necessary from both the experimental and theory sides. Since we will be in the low-statistic regime for a long time, it will be essential to have systematics and theoretical uncertainties under control. In the following chapter, we study the first –anomalous– signals measured by UHE experiments, namely the ANITA-IV events. Are they a hint of New Physics at the highest energies, or an unidentified background? We advocate for the former, in order to learn about the potential of UHE data to constrain BSM physics [2]. The reader is left to decide, only time (i.e., more observational exposure) will tell.

5 IceCube and the origin of ANITA-IV events

It has been over a decade since the IceCube Neutrino Observatory, located at the geographical South Pole, opened a new window to observe the Universe by detecting high-energy astrophysical neutrinos with energies up to 6 PeV [217]. This decade has witnessed the progress from observing a flux compatible with an isotropic distribution [325], the so-called diffuse flux; to the discovery of first sources [328, 329]. The confidence of these observations as astrophysical neutrinos is extremely high, not only because the sample sizes have grown to hundreds over the last decade, but also because systematic uncertainties are controlled by in-situ measurements. IceCube first measured the atmospheric neutrino flux [326], proving that it could constrain its backgrounds and that the event reconstructions were reliable, and then discovered the astrophysical component on top of this one.

As we venture into this new decade, radio detectors place themselves as a promising technology to extend the observations of IceCube to Ultra-High Energies (UHE). This requires surmounting significant technological and logistical challenges. Among the challenges, one stands out. Unlike IceCube or ANTARES [322], where the detectors can calibrate and test their selection procedures and reconstructions on the well-understood atmospheric neutrino flux, in this upcoming generation such calibration is much more challenging. Fortunately, the sensitivity of present UHE experiments is comparable with IceCube limits, so current observations can be cross-checked with existing or future IceCube data.

First results are showing up. The ANITA-IV experiment, a balloon flying over Antarctica, has observed four events with energies ~ 1 EeV and incident directions $\sim 1^\circ$ below the horizon with a significance $\sim 3\sigma$ [372, 373], that we depict in Figure 5.1. The directions are compatible with a neutrino origin, which would make them the highest-energy neutrinos ever observed. However, a Standard Model (SM) explanation is in tension with non-observations from Auger [373] and, as we show below, IceCube.

It is pressing to understand the origin of these events, whether novel physics or background, in order to guarantee the success of other UHE detectors with better sensitivity than ANITA. If they are background, further work is needed to understand their origin and filter them out to avoid overwhelming the neutrino signal. If they have a Beyond the Standard Model (BSM) origin, we must robustly understand which particle models can explain them and their predictions in different detectors, to fully confirm this hypothesis.

In this Chapter, we exploit the aforementioned connection with IceCube to diagnose if these detections correspond to neutrinos or to some BSM scenario, focusing on the

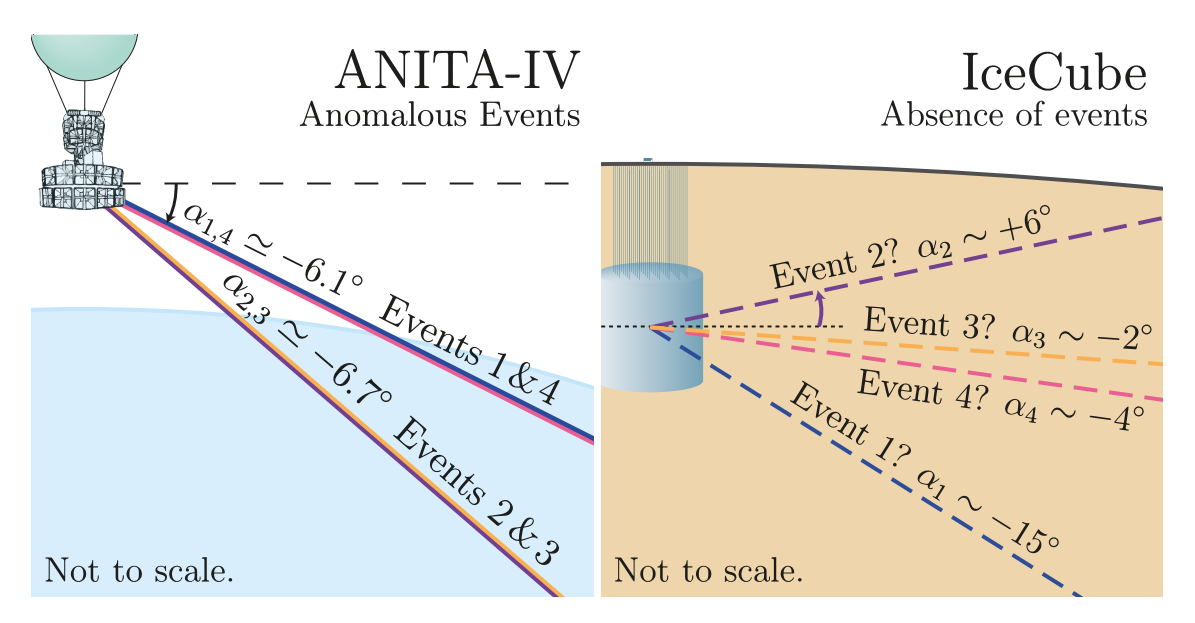


Figure 5.1: Directions of the Anomalous Events as viewed from ANITA (left) and IceCube (right). Particle physics models that explain the ANITA observations are challenged by the absence of signals at IceCube.

latter. By exploring an energy scale never reached before with fundamental particles, ANITA is opening a new window to such scenarios [240, 374–376]. We perform a model-independent analysis, leaving most details to model builders, but we briefly comment on specific models and encourage the reader to read Refs. [363–371, 377–388] for proposed models on UHE anomalous events.

Our method extends beyond ANITA and IceCube, since these are expected to be accompanied soon by a family of optical — such as KM3NeT [110], P-ONE [337], or Baikal-GVD [336] —, radio — such as PUEO [354], GRAND [357], TAROGE [356], BEACON [389], RET [390], or RNO-G [352] —, or even acoustic neutrino detectors — such as ANDIAMO [391]. We do not discuss here the connection with Earth-skimming experiments — such as TAMBO [358], TRINITY [359] or POEMMA [360] —, since they have not yet reached the sensitivity to detect neutrinos, but we expect them to also provide important information as they look at the region of Earth that is mostly transparent to neutrinos.

The rest of this Chapter is organized as follows. In section 5.1, we introduce our model-independent parametrization of generic BSM models; in section 5.1.3 we discuss the source properties; in section 5.2 we study the inner consistency of ANITA's data; in section 5.3 we report on the consistency between ANITA and IceCube observations; in section 5.4 we give the reader a brief discussion of potential models; and in section 5.5 we conclude.

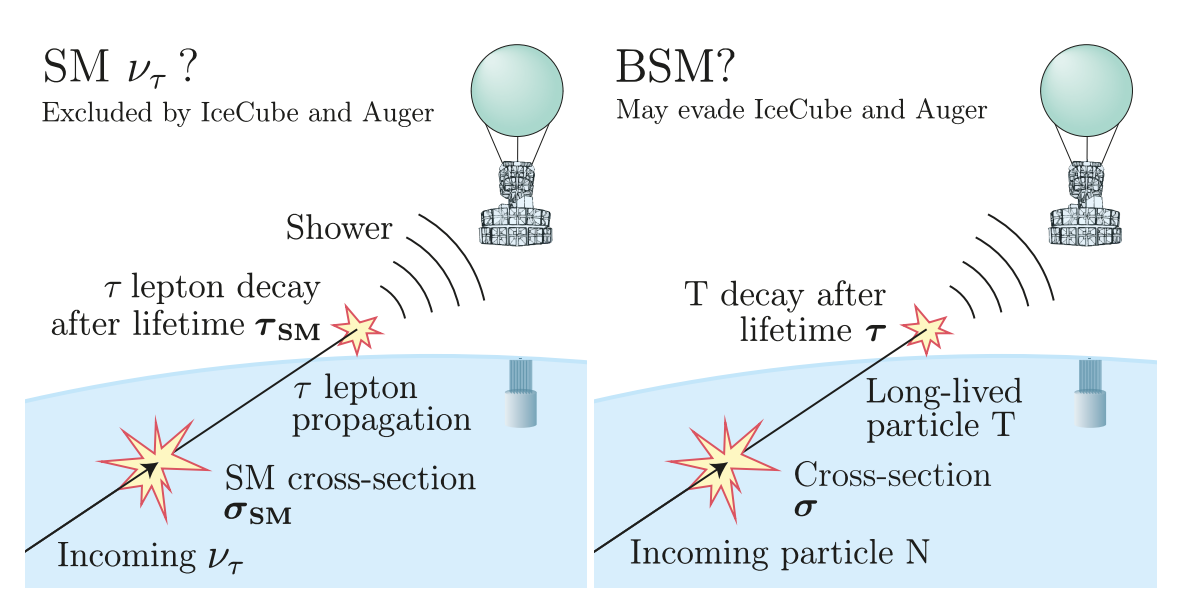


Figure 5.2: Possible origins of the ANITA anomalous events. In the SM, v_{τ} produce a τ lepton that decays in-air (left). We parametrize a class of BSM models by incoming particles that produce, with cross section σ , long-lived particles that decay with lifetime τ (right). Event distributions only depend on σ and τ .

5.1 Beyond the Standard Model explanation

In this section, following a model independent approach, we parametrize a class of BSM models that could explain the anomalous events detected by ANITA. We seek generic modeling, showing that few parameters capture the main physics.

Figure 5.2 shows how anomalous events can be generated. In the SM, an incoming ν_{τ} flux interacts with Earth nucleons, producing τ leptons that decay and generate a shower observed by ANITA. In BSM, we consider an incoming flux of particles, denoted as N, that interact with Earth nucleons with cross section σ producing long-lived particles, denoted as T, that decay with lab-frame lifetime τ and generate a shower observed by ANITA.

Our simplified BSM models are fully determined by three parameters: the incoming N flux, Φ ; the N-nucleon interaction cross section, σ ; and the lab-frame T lifetime, τ . When σ is the SM neutrino-nucleon cross section and τ the τ -lepton lifetime, this parametrization approximates the SM. Although a SM explanation is inconsistent with Auger UHE neutrino limits [373] (and IceCube, as we show below), different σ and τ modify the event morphologies in those experiments, leading to potentially weaker constraints as we explore below.

This parametrization is a proof-of-principle of scenarios where particle showers produce the events. It does not exhaustively explore all BSM models, and more detailed

model-by-model studies can still be done; we comment on this in section 5.4. There are also models for previous UHE anomalous events that do not invoke particle showers [363], and hence do not fall under our parametrization.

We seek a minimal, conservative approach, assuming an incoming flux *only* at the energies where ANITA has observed the anomalous events. We also ignore effects that would redistribute particle energies — including T or N energy losses, or different energies of T at production —, as the detection efficiencies of IceCube and ANITA are quite flat at the energies we consider [373, 392]. We assume T absorption by Earth with the production cross section σ , expected from the time-reversal invariance of the production process. As we show in section 5.3.1, our conclusions do not change if T is not absorbed by Earth.

5.1.1 Number of expected events

We parametrize the incoming flux by a normalization constant, the energy spectrum and the angular distribution,

$$\Phi(\Omega, E) = \Phi_0 f_E(E) f_{\Omega}(\Omega), \qquad (5.1)$$

where E is energy, Ω the solid angle ($d\Omega = \sin \theta \, d\theta \, d\phi$), and Φ_0 the flux per unit area, time, solid angle, and energy. The expected number of events per unit solid angle and energy is

$$\frac{\mathrm{d}N(\theta)}{\mathrm{d}\Omega\,\mathrm{d}E} = \Phi_0\,\Delta t\,f_E(E)\,f_\Omega(\Omega)\,\mathcal{A}(\Omega,E)\,. \tag{5.2}$$

Here Δt is the total observation time; and \mathcal{A} includes the geometric area of the detector, detection efficiency, the absorption of the flux inside Earth, and the probability for the flux to produce a detectable signal. It encodes all the details of the propagation and absorption models, as we explain next. We assume \mathcal{A} has axial symmetry and does not depend strongly on energy [373, 392]. Then, $\mathcal{A}(\Omega, E) = \mathcal{A}(\theta)$.

We are interested in the expected number of events per solid angle Ω , so we integrate over a narrow energy bin which encloses all ANITA-IV events,

$$\frac{\mathrm{d}N(\theta)}{\mathrm{d}\Omega} = \left(\Phi_0 \int_{E_{\mathrm{min}}}^{E_{\mathrm{max}}} \mathrm{d}E \, f_E(E)\right) f_{\Omega}(\Omega) \, \Delta t \, \mathcal{A}(\theta) \equiv \Phi \, f_{\Omega}(\Omega) \, \Delta t \, \mathcal{A}(\theta) \,. \tag{5.3}$$

Experiments do not perfectly reconstruct the true angle of the incoming particle, θ^{true} . To take this into account, we assume Gaussian angular uncertainty $\Delta\theta$. For ANITA-IV, $\Delta\theta$ is reported in Ref. [372]. Then, the expected number of events per unit solid angle

as a function of the reconstructed angle θ^{rec} is given by

$$\frac{d\bar{N}(\theta^{\text{rec}})}{d\Omega} = \int d\theta^{\text{true}} \frac{1}{\sqrt{2\pi}\Delta\theta} \exp\left[-\frac{(\theta^{\text{rec}} - \theta^{\text{true}})^{2}}{2(\Delta\theta)^{2}}\right] \frac{dN(\theta^{\text{true}})}{d\Omega} =
= \frac{\Phi\Delta t}{\sqrt{2\pi}\Delta\theta} \int d\theta^{\text{true}} f_{\Omega}(\theta^{\text{true}}, \varphi) \mathcal{A}(\theta^{\text{true}}) \exp\left[-\frac{(\theta^{\text{rec}} - \theta^{\text{true}})^{2}}{2(\Delta\theta)^{2}}\right].$$
(5.4)

Absorption and detection processes

There are four signals that the scenario we consider can produce. First, a shower is produced when T decays, which generates the signals at ANITA. Second, a shower produced when N interacts with Earth to produce T. (This signal can be avoided if the hadronic part of the interaction between N and nuclei to produce T is very elastic, which may happen for instance in models with light mediators [393].) Third, a shower produced if T gets absorbed by Earth. Fourth, a track if T is charged. Since the last signal can only be detected by IceCube and is easily avoided if T is electrically neutral, we conservatively ignore it.

We separate these contributions as $\mathcal{A}=\mathcal{A}_T^{dec}+\mathcal{A}_T^{int}+\mathcal{A}_N$. On the one hand, T decays are quantified by

$$A_{\rm T}^{\rm dec}(\theta) = P_{\rm exit}^{\rm T}(\theta) P_{\rm decay}^{\rm T}(\theta) A_{\rm eff}(\theta). \tag{5.5}$$

Here $A_{\rm eff}(\theta)$ is the area to which the detector is sensitive, including detection efficiency. For ANITA, the geometric area and trigger efficiency have been extracted from Figure 10 in Ref. [373]. For IceCube, we have set the geometric area to 1 km² and the detection efficiency has been extracted from Ref. [394]. Then, $P_{\rm decay}^{\rm T}(\theta) \equiv 1 - e^{-d(\theta)/\tau}$ is the probability for T to decay inside the effective volume of length $d(\theta)$. For ANITA, $d(\theta) \sim \mathcal{O}(500)$ km is the distance between the exit point and the radio antenna, detailed in appendix A. For IceCube, we set $d(\theta) = 1$ km. Finally, $P_{\rm exit}^{\rm T}(\theta)$ is the probability for T to be produced and arrive to the effective volume, that we compute in appendix A.

Altogether, the total number of expected events from T decay per unit solid angle is

$$\frac{dN_{\rm T}^{\rm dec}(\theta)}{d\Omega} = \Phi f_{\Omega}(\Omega) \, \mathcal{A}_{\rm T}^{\rm dec}(\theta) \, \Delta t = \Phi f_{\Omega}(\Omega) \, P_{\rm exit}^{\rm T}(\theta) \, P_{\rm decay}^{\rm T}(\theta) \, A_{\rm eff}(\theta) \, \Delta t \,. \tag{5.6}$$

We assume that the direction of the shower at ANITA corresponds to the incoming direction of T and N, i.e., that all particles are relativistic.

As mentioned above, interaction of N or T with Earth can also lead to a visible

shower. Their contribution is

$$A_{\rm T}^{\rm int}(\theta) = P_{\rm exit}^{\rm T}(\theta) N_{\rm targets} \, \sigma \, \varepsilon \, , \qquad (5.7)$$

$$A_{\rm N}(\theta) = P_{\rm evit}^{\rm N}(\theta) N_{\rm targets} \, \sigma \, \varepsilon \,, \tag{5.8}$$

respectively. Here, N_{targets} is the number of targets in the detector, ε the detection efficiency, and $P_{\text{exit}}^{\text{N}}(\theta)$ is the probability for an N particle to arrive to the effective volume that we compute in appendix A. Then, the number of expected events from T and N interactions per unit of solid angle is

$$\frac{\mathrm{d}N_{\mathrm{T}}^{\mathrm{int}}(\theta)}{\mathrm{d}\Omega} = \Phi f_{\Omega}(\Omega) \,\mathcal{A}_{\mathrm{T}}^{\mathrm{int}}(\theta) \,\Delta t = \Phi f_{\Omega}(\Omega) \,P_{\mathrm{exit}}^{\mathrm{T}}(\theta) \,N_{\mathrm{targets}} \,\sigma \,\varepsilon \,\Delta t \,, \tag{5.9}$$

$$\frac{\mathrm{d}N_{\mathrm{N}}(\theta)}{\mathrm{d}\Omega} = \Phi f_{\Omega}(\Omega) \, \mathcal{A}_{\mathrm{N}}(\theta) \, \Delta t = \Phi f_{\Omega}(\Omega) \, P_{\mathrm{exit}}^{\mathrm{N}}(\theta) \, N_{\mathrm{targets}} \, \sigma \, \varepsilon \, \Delta t \,, \tag{5.10}$$

respectively. The total number of events is

$$\frac{dN(\theta)}{d\Omega} = \frac{dN_{T}^{\text{dec}}(\theta)}{d\Omega} + \frac{dN_{T}^{\text{int}}(\theta)}{d\Omega} + \frac{dN_{N}(\theta)}{d\Omega}.$$
 (5.11)

5.1.2 Details of the test statistic

In this section, we describe our statistical analysis. As data is scarce, an unbinned Poisson likelihood is well-suited. This test statistic is given, up to constants, by

$$\mathcal{TS}(\Phi, \sigma, \tau) = 2 \int d\varphi \, d\theta \sin \theta \, \mu(\theta, \varphi; \Phi, \sigma, \tau) - 2 \sum_{i=1}^{N} \log \tilde{\mu}(\theta_i^{\text{rec}}; \Phi, \sigma, \tau), \qquad (5.12)$$

where $\mu \equiv dN/d\Omega$, $\tilde{\mu}(\theta^{\rm rec}) \equiv \sin\theta^{\rm rec} \int_0^{2\pi} d\varphi \, d\tilde{N}/d\Omega(\theta^{\rm rec}, \varphi)$, and $\theta_i^{\rm rec}$ are the reconstructed angles of the N observed events.

Since the ANITA-IV flight has detected 4 anomalous events,

$$\mathcal{TS}^{\text{ANITA}}(\Phi, \sigma, \tau) = 2 \int d\varphi \, d\theta \sin \theta \, \mu(\theta, \varphi; \Phi, \sigma, \tau) - 2 \sum_{i=1}^{4} \log \tilde{\mu}(\theta_i^{\text{rec}}; \Phi, \sigma, \tau). \quad (5.13)$$

For an isotropic flux, $f_{\Omega}(\Omega) = (4\pi)^{-1}$. Then, integrating over φ

$$\mathcal{TS}^{\text{ANITA}}(\Phi, \sigma, \tau) = -2 \sum_{i=1}^{4} \log \left(\frac{\Phi \Delta t}{2} \sin \theta_{i}^{\text{rec}} \,\overline{\mathcal{A}}(\theta_{i}^{\text{rec}}, \Delta \theta_{i}; \sigma, \tau) \right) +$$

$$+ \Phi \Delta t \int d\theta \, \sin \theta \, \mathcal{A}(\theta; \sigma, \tau) \,.$$
(5.14)

Here we have defined

$$\overline{\mathcal{A}}(\theta^{\text{rec}}, \Delta\theta; \sigma, \tau) = \int d\theta \,\mathcal{A}(\theta; \sigma, \tau) \frac{1}{\sqrt{2\pi}\Delta\theta} \exp\left[-\frac{(\theta^{\text{rec}} - \theta)^2}{2(\Delta\theta)^2}\right]. \tag{5.15}$$

The best-fit value of Φ for this likelihood is

$$\Phi_{\text{ANITA}}^{\text{BF}} = \frac{2 \times 4}{\Delta t \int d\theta \sin \theta \, \mathcal{A}(\theta; \sigma, \tau)},$$
(5.16)

that only depends on the total number of observed and expected events. We can then insert Equation (5.16) in Equation (5.14) to obtain the ANITA test statistic profiled over Φ_{ANITA} ,

$$\mathcal{TS}^{\text{ANITA}}(\sigma, \tau) = \sum_{i} -2 \log \left(\frac{\sin \theta_{i}^{\text{rec}} \overline{\mathcal{A}}(\theta_{i}^{\text{rec}}; \sigma, \tau)}{\int d\theta \sin \theta \, \mathcal{A}(\theta; \sigma, \tau)} \right), \tag{5.17}$$

up to constant terms. The best-fit values of (σ, τ) must maximize the argument of the logarithm. That is, they must concentrate the flux around θ_i^{rec} . This way, the probability for the events to happen at θ_i^{rec} and not elsewhere is maximal.

In turn, IceCube has not observed any event in the energy range of the ANITA anomalous events. Then,

$$\mathcal{TS}^{\mathsf{IC}}(\Phi, \sigma, \tau) = 2 \int d\varphi \, d\theta \sin \theta \, \mu(\theta, \varphi; \Phi, \sigma, \tau). \tag{5.18}$$

This test statistic is twice the total number of expected events in IceCube. The bigger the expected number of events, the worse the fit. For a diffuse flux, this gives

$$\mathcal{TS}^{\mathsf{IC}}(\Phi, \sigma, \tau) = \Phi \,\Delta t \, \int \,\mathrm{d}\theta \sin\theta \,\mathcal{A}(\theta; \sigma, \tau) \,. \tag{5.19}$$

The total test statistic for both experiments contains the likelihoods from eqs. (5.14) and (5.19),

$$\mathcal{T}S(\Phi, \sigma, \tau) = -2 \sum_{i=1}^{N} \log \left(\frac{\Phi \Delta t_{A}}{2} \sin \theta_{i}^{\text{rec}} \overline{\mathcal{A}}_{A}(\theta_{i}^{\text{rec}}, \Delta \theta_{i}; \sigma, \tau) \right) + \Phi \Delta t_{A} \int d\theta \sin \theta \, \mathcal{A}_{A}(\theta; \sigma, \tau) + \Phi \Delta t_{I} \int d\theta \sin \theta \, \mathcal{A}_{I}(\theta; \sigma, \tau),$$
(5.20)

where the A, I subscripts stand for ANITA and IceCube, respectively. This test statistic can be analytically profiled over Φ , which gives

$$\mathcal{T}S(\sigma,\tau) = -2\sum_{i=1}^{4} \log \left(\frac{\sin \theta_{i}^{\text{rec}} \overline{\mathcal{A}}_{A}(\theta_{i}^{\text{rec}}; \sigma, \tau)}{\Delta t_{A} \mathcal{A}_{A}^{\text{tot}} + \Delta t_{I} \mathcal{A}_{I}^{\text{tot}}} \right), \tag{5.21}$$

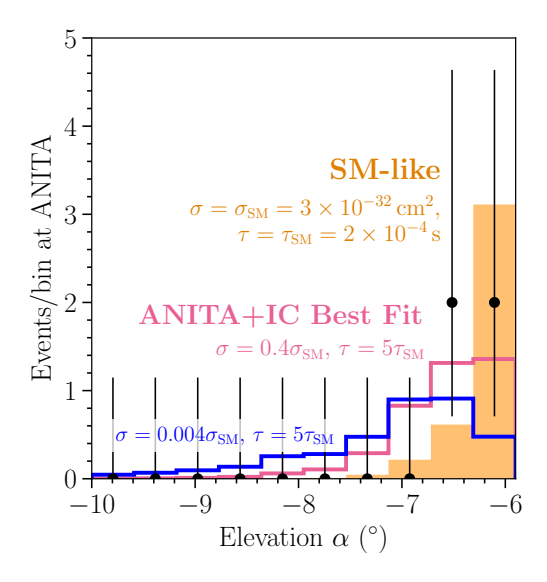


Figure 5.3: Angular event distribution at ANITA for different values of σ and τ under the diffuse-flux hypothesis. σ controls the angular event distribution, whereas τ mostly controls the normalization (see text). The incoming directions at ANITA enforce cross sections around the SM value.

up to constant terms. We have abbreviated $\mathcal{A}^{tot} = \int d\theta \sin \theta \, \mathcal{A}(\theta; \sigma, \tau)$. The best-fit flux is

$$\Phi(\sigma, \tau)^{BF} = \frac{2 \times 4}{\Delta t_A \, \mathcal{A}_A^{\text{tot}} + \Delta t_I \, \mathcal{A}_I^{\text{tot}}}.$$
 (5.22)

5.1.3 Transient sources vs diffuse flux

There are two scenarios for the incoming particle flux — v_{τ} for SM, N for BSM. It can be transient, i.e., the flux is non-zero only in some time window; or it can be diffuse, i.e., the flux is produced by many sources and is constant in time.

As the IceCube effective area is a factor $\sim 10^2$ smaller than that of ANITA [373, 392], a transient origin for the events cannot be tested by IceCube as long as four transient sources activated *only* in the month that ANITA-IV was flying and *never again* in the nine years of IceCube operation (as the transient rate increases, the flux becomes diffuse). This admittedly baroque hypothesis would allow even a SM explanation of the anomalous events [373]. For the rest of the Chapter, we focus on the more realistic diffuse flux hypothesis.

5.2 ANITA-IV angular self-consistency

In this section, we show that, despite the small sample size, the observed angular distribution at ANITA provides information on BSM parameters.

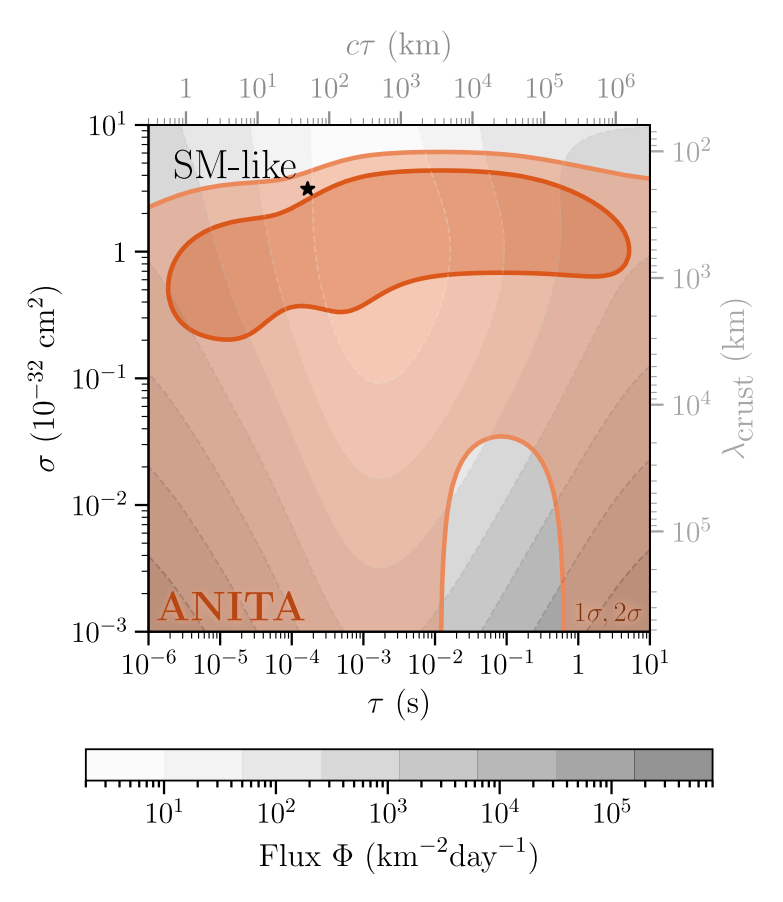


Figure 5.4: Allowed BSM parameters from ANITA data under the diffuse-flux hypothesis, together with the required incoming N flux. We also show the mean free path of N in the Earth crust, λ_{crust} ; and the average distance travelled by the long-lived particle T, $c\tau$.

Figure 5.3 shows how the N cross section, σ , modifies the event distribution. Reduced σ increases the distance that N can travel inside Earth, making the outgoing T distribution more isotropic. Generically, the distribution peaks at angles where the chord length inside Earth equals the mean free path of N. The distributions are normalized to predict four events at ANITA.

The impact of τ is less significant. If $\sigma \gtrsim \sigma_{SM}$, the distribution of outgoing T is quite anisotropic, and τ only controls the probability for them to exit Earth and decay before ANITA, which is degenerate with the overall flux normalization. Explicitly, very small τ requires large fluxes because of the suppressed probability to exit Earth, and so do very large τ because of the suppressed probability to decay before ANITA. If $\sigma \ll \sigma_{SM}$, the distribution of T is more isotropic, and large τ implies a more isotropic event distribution.

We quantify the agreement with observations through the unbinned likelihood analysis described in Section 5.1.2. Figure 5.4 shows that the ANITA angular distribution implies a preferred region of BSM parameters. The star signals the parameters where

the BSM sector approximates the SM,

$$\sigma \sim \sigma_{\text{SM}} \simeq 3 \times 10^{-32} \text{ cm}^2,$$

$$\tau \sim \tau_{\text{SM}} \simeq 2 \times 10^{-4} \text{ s}.$$
(5.23)

Although the approximation is not exact due to the simplifications described in section 5.1, the phenomenology is similar. We also show the N flux Φ that would predict four events at ANITA, which is always comparable to or greater than UHE cosmic-rays fluxes ($\sim 1\,\mathrm{km}^{-2}\mathrm{day}^{-1}$ at 1 EeV [220]). As described above, the flux is strongly correlated with τ ; slightly increasing τ with respect to τ_{SM} reduces the required flux by an order of magnitude.

ANITA data excludes large σ , because the events would peak closer to the horizon. For small σ , $10^{-2}\,\mathrm{s} \lesssim \tau \lesssim 1\,\mathrm{s}$ is excluded because the event distribution would be too isotropic. $\tau \gtrsim 1\,\mathrm{s}$ is allowed for small σ because most T decay after ANITA, and the events are produced by interactions of N with the atmosphere at the expense of very large fluxes.

We conclude that a large region of parameter space in our model independent framework, including the SM-like scenario, is consistent with ANITA data. Below, we show that this is challenged by null observations from IceCube.

5.3 Interplay with IceCube

The IceCube experiment is sensitive to the same flux that produces events in ANITA [395–397]. Although IceCube has a smaller effective volume, its larger angular aperture and observation time allow to test the origin of the ANITA events. In this section, we describe such a test, pointing out the parameter region where both experiments could be compatible.

Figure 5.5 shows that explanations of the ANITA events are challenged by the lack of observations at IceCube [398]. We show the expected event distribution at IceCube, for the same σ and τ as fig. 5.3 and the flux normalization that predicts four events at ANITA.

Most of the events predicted at IceCube are due to interactions of N with Earth (as we assume that such interactions generate showers), and for SM-like or larger cross sections, they are dominantly downgoing because of Earth attenuation. The sensitivity of IceCube to τ is indirect but key for its compatibility with ANITA's measurements. As described above, slightly increasing τ with respect to $\tau_{\rm SM}$ reduces the required flux, and the predictions are then compatible with null observations at IceCube. For extremely

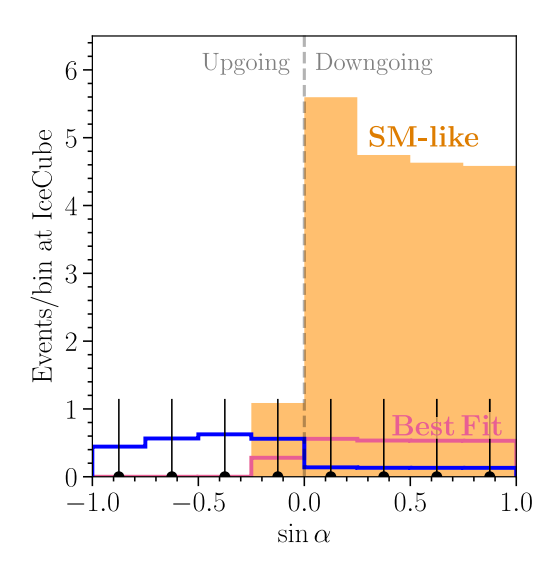


Figure 5.5: Same as fig. 5.3, but for IceCube. The normalizations are fixed to predict 4 events at ANITA. *IceCube is mostly sensitive to the flux normalization required to explain 4 events in ANITA.*

low values of σ (blue histogram), the contribution from N interactions in IceCube is suppressed, and most of the events are generated by upgoing T-s produced by interactions of N with Earth.

Figure 5.6 shows how the correlation between lifetime and flux affects the interplay between ANITA and IceCube, with only some values of τ allowing Φ consistent both with the observations at ANITA and the lack of events at IceCube. We show the allowed values of τ and Φ for fixed σ , obtained using an unbinned likelihood described in section 5.1.2. For ANITA, Φ is always comparable to or higher than the cosmic-ray flux as mentioned above. As the figure shows, IceCube is mostly sensitive to interactions of N, i.e., to its flux Φ . In turn, ANITA mostly detects T decays, and Φ is very correlated with τ because T must exit Earth *and* decay before ANITA: small τ spoil the former and large τ spoil the latter.

Figure 5.7 shows the ranges of σ and τ allowed by a combined analysis of ANITA and IceCube, together with the best-fit flux Φ . From fig. 5.4, non-observation of events at IceCube only allows regions with small Φ , which implies $\tau \sim 10^{-3} \, \mathrm{s}$. There is also some information on σ because it controls both the angular distribution at ANITA and the number of events at IceCube due to N interactions. Altogether, this implies closed allowed regions up to $\sim 2\sigma$ (we recall that the significance of the anomalous events is $\sim 3\sigma$ [372, 373]), with the best-fit point at $\sigma = 8.9 \times 10^{-33} \, \mathrm{cm}^2$, $\tau = 1.3 \times 10^{-3} \, \mathrm{s}$, and $\Phi = 1.8 \, \mathrm{km}^{-2} \, \mathrm{day}^{-1}$. The best-fit parameters predict 1.2 events at IceCube after nine years of operation, and the best-fit flux at every point in the parameter space predicts at least 0.9 events.

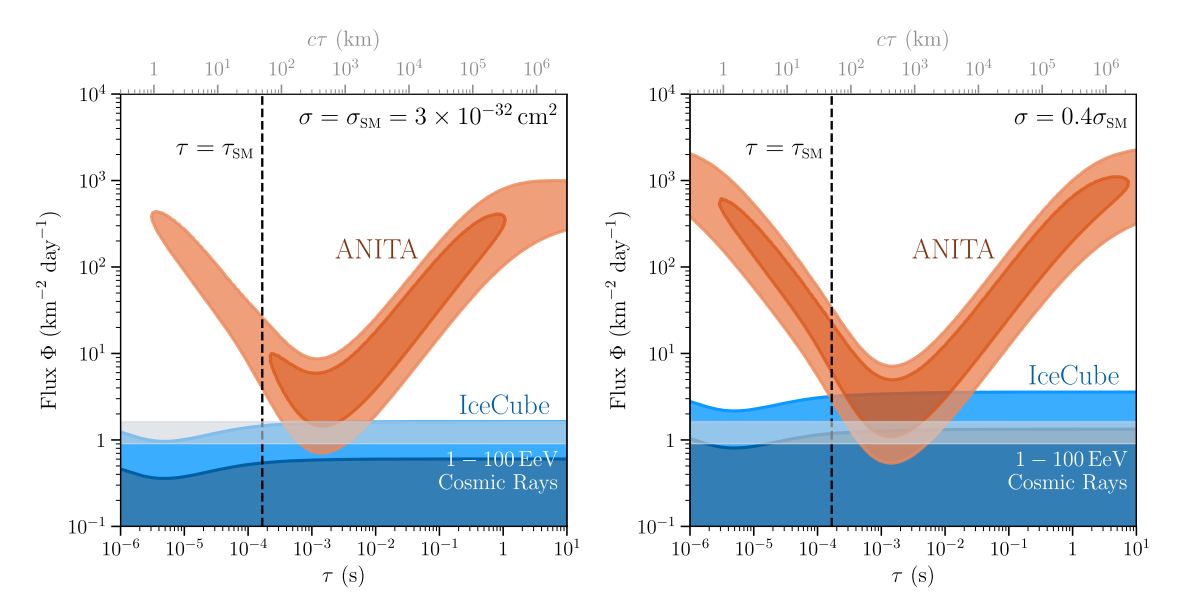


Figure 5.6: Allowed regions for τ and the flux normalization Φ from ANITA and IceCube independently. We show for orientation the UHE Cosmic Ray flux [220]. τ and Φ are strongly correlated in ANITA, while IceCube is insensitive to τ . The BSM parameters can partially alleviate the tension.

Overall, a BSM interpretation relaxes the tension between the ANITA anomalous events and IceCube, but does not fully remove it. The combined allowed regions always predict $\mathcal{O}(1)$ events at IceCube, so if the anomalous events have a particle physics origin parametrized by our set of BSM models, the signal should be observable in the future.

5.3.1 Impact of T absorption

Up to now, we have assumed that T interacts with Earth with the same cross section that produces it, σ . This is to be expected in the simplest BSM extensions. However, the N absorption cross section σ_N and the T absorption cross section σ_T could in principle be different. In particular, $\sigma_T = 0$ would maximize the compatibility between ANITA and IceCube. The number of events in ANITA would increase due to fewer T particles being absorbed by the Earth, and the number of events in IceCube would slightly decrease due to fewer interaction of T particles with the detector.

Figure 5.8 shows the results obtained following the same procedure as in Figures 5.4 and 5.7 but setting $\sigma_T=0$. The left panel shows the results including only ANITA-IV data. There are some qualitative differences with respect to the $\sigma_N=\sigma_T$ case in fig. 5.4. For $10^{-3}\,\mathrm{s} \lesssim \tau \lesssim 1\,\mathrm{s}$, larger σ is allowed because, even though N is always absorbed, T can exit Earth and generate the anomalous events. However, data disfavors too long lifetimes because the event distribution would be too isotropic.

In the right panel we show the results with both ANITA and IceCube data. The

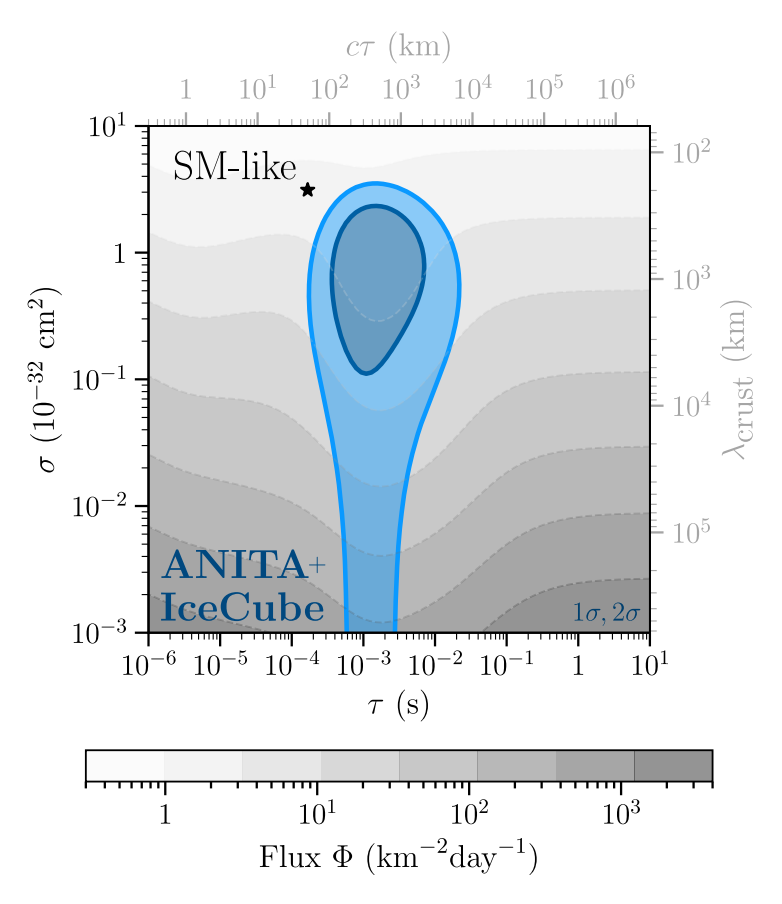


Figure 5.7: Allowed BSM parameters the combination of ANITA and IceCube (blue) under the diffuse-flux hypothesis, together with the required incoming particle flux. The best fit predicts 1.2 events after 9 years of IceCube operation. Although the SM-like scenario is excluded at $\sim 3\sigma$, BSM models may explain the ANITA anomalous events, and signals would be observable in IceCube-Gen2.

combination leads to an allowed region similar to the one shown in fig. 5.7 for the scenario with $\sigma_T = \sigma_N$. This is because the large- σ_N region that is allowed by ANITA if $\sigma_T = 0$ would produce too many downgoing events in IceCube. We thus conclude that the results obtained above are robust against assuming that T does not interact with Earth.

5.4 Particle physics models

Above, we have demonstrated in a model independent approach that BSM scenarios could accommodate the ANITA observations and the absence of any signal in IceCube. In this section, we discuss explicit particle physics models that can provide the required ingredients.

As our best fit is not very far from the SM-like prediction, an appealing possibility is

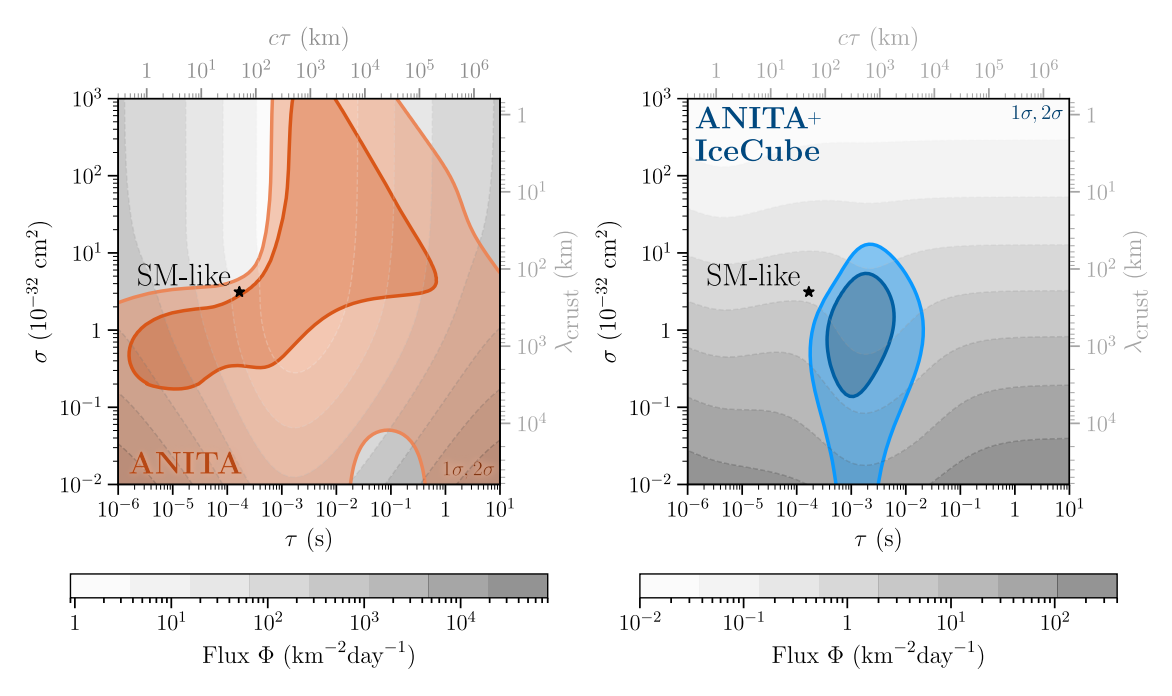


Figure 5.8: Allowed BSM parameters from ANITA (left, red) and the combination of ANITA and IceCube (right, blue) under the diffuse-flux hypothesis, together with the required incoming particle flux, if we remove interactions of T with Earth. Note that, by neglecting T absorption, the "SM-like" point resembles less the SM than the choice in the main text. *ANITA alone is sensitive to T interaction with matter, but its combination with IceCube is mostly not.*

to consider BSM models related to neutrinos, such as scenarios involving heavy neutral leptons that mix with the SM neutrinos and further couple to other fields belonging to a richer Dark Sector. In such scenarios, the SM neutrinos could play the role of N.

However, one of the main issues in searching for a successful particle physics model is the origin of the flux of N particles. Current neutrino flux limits are $\Phi \lesssim 0.1 \, \mathrm{km^{-2} \, day^{-1}}$, well below the required N flux (see fig. 5.7) [349, 398]. Thus, a more exotic primary particle is generically required. A DM origin is probably the less exotic possibility. Such option has been recently put forward [364, 365, 377, 386] to explain the two upgoing highly anomalous events previously observed by ANITA [361, 399]. The decay of extremely heavy DM (in the EeV range) to N can produce very large fluxes [400]

$$\Phi_{\rm N} = \frac{1}{\tau_{\rm DM} m_{\rm DM}} \int \rho_{\rm DM} \, \mathrm{d}s \,, \tag{5.24}$$

where $\tau_{\rm DM} > 10^{19}\,{\rm s}$ [401] is the DM lifetime and $m_{\rm DM}$ its mass, and the integral is along the line of sight s. Numerically, $\int \rho_{\rm DM}\,{\rm d}s \sim 5\times 10^{22}\,{\rm GeV/cm^2}$ [400]. If $m_{\rm DM}=1\,{\rm EeV}$, then $\Phi_{\rm N}$ can be as large as $10^{12}\,{\rm km^{-2}\,day^{-1}}$, well in agreement with fig. 5.7.

Following this idea, we consider a toy model involving a dark sector that includes an

extremely heavy DM candidate and two dark fermions playing the role of our N and T particles. Adding an extra $U_X(1)$ gauge symmetry in the Dark Sector, we introduce a new dark boson X_μ that mixes with the SM photon via kinetic mixing [402, 403], allowing the dark fermions to interact with ordinary matter and have nonzero σ and τ .

In more detail, the DM can be a scalar SM singlet ϕ that decays via a Yukawa coupling to a stable fermion χ_1 , a SM singlet that would play the role of N. The role of T would be played by a second fermion singlet χ_2 (heavier than χ_1) which, choosing the dark charges of both fermions appropriately, couples to X_{μ} just via a $g_D \bar{\chi}_2 \gamma^{\mu} \chi_1 X_{\mu}$ term in the Lagrangian. This way, χ_1 interacts with Earth nuclei via kinetic mixing generating a χ_2 , which subsequently decays via $\chi_2 \rightarrow \chi_1$ + shower, the shower being originated through kinetic mixing with the ordinary photon. The same model was proposed to fit the previous ANITA anomalous events [386]. Following Ref. [386], we find that for $g_D = 1.1$, particle masses $m_X = 1.5$ GeV, $m_{\chi_2} = 0.7$ GeV, $m_{\chi_1} = 0.5$ GeV, and kinetic mixing $\epsilon = 7 \cdot 10^{-3}$, the values of σ and τ are in the right ballpark in agreement with fig. 5.7 (these are different from the values considered in Ref. [386] to explain the previous anomalous events). These parameter values are currently allowed (see, e.g., Fig. 5.1 in Ref. [404]). The constraints on this scenario are weaker than for minimal dark photon scenarios — where the dark photon decays predominantly either into SM visible particles (visible dark photons) or into missing energy (invisible dark photons) — because X_{μ} decays involve both SM and dark particles (semi-visible dark photons).

The proposal considered here is an extension of the so-called inelastic DM models [405]. In such models χ_1 constitutes the thermal DM relic, and there are typically no new scalars such as our singlet ϕ . The $g_{\mu}-2$ anomaly can also be accommodated [406], but it has been shown recently that both phenomena cannot be simultaneously explained in most part of the parameter space [404] (see also a review of semi-visible light dark photon models in Ref. [407]). Instead, in the model considered here the DM is mainly composed of a super-heavy scalar singlet ϕ , while χ_1 is a subdominant component. This super-heavy DM can be generated for instance via freeze-in [408] or at the end of inflation [409–412].

5.5 Summary and conclusions

The fourth flight of ANITA found four upgoing UHE events coming from about a degree below the horizon. Explaining these events within the SM implies a flux of v_{τ} inconsistent with the non-observations in Auger or IceCube. Here, we have performed a model-independent analysis of IceCube and ANITA-IV results for BSM scenarios. We consider a conservative approach assuming an incoming flux of generic particles N only

at the energy window where ANITA has observed the anomalous events. The N particles interact with Earth nucleons — with cross section σ — generating primary showers along with long lived particles T that decay — with lifetime τ — producing another shower (see fig. 5.2). Such formalism can be applied to better understand the origin of any future observation.

Therefore, the set of models under consideration are determined by three parameters: the flux (Φ) of the incoming N particles, their cross section with nucleons (σ), and the lifetime (τ) of the secondary long-lived T particles produced after the interaction. Performing a statistical analysis of the four events observed by ANITA, we found that the low statistics allows large ranges for σ and τ compatible with a SM-like explanation of the signals. The angular distribution of the events excludes $\sigma \gtrsim 5 \times 10^{-32} \, \mathrm{cm}^2$, where the events would peak closer to the horizon, together with $\sigma \lesssim 5 \times 10^{-34} \, \mathrm{cm}^2$ and $10^{-2} \, \mathrm{s} \lesssim \tau \lesssim 1 \, \mathrm{s}$, where the distribution would be too isotropic.

The large observation time and its large angular acceptance makes IceCube an excellent candidate to explore the flux observed by ANITA. The main sensitivity of IceCube to this set of models comes from interactions of N with Earth. Null results in IceCube are compatible with ANITA for $\tau \sim 10^{-3}$ s and $\sigma \lesssim 3 \times 10^{-32}$ cm² at 2σ .

Finally, we provide a concrete scenario based on super-heavy scalar Dark Matter that can explain ANITA-IV and IceCube data. The decay of the Dark Matter into a stable dark fermion χ_1 , via a Yukawa coupling, can account for the large fluxes needed ($\Phi \gtrsim 1 \text{ km}^{-2} \text{day}^{-1}$). In the scenario considered in this work, the Dark Sector is also enlarged by an unstable dark fermion χ_2 , heavier than χ_1 , which plays the role of T. Adding, an extra $U_X(1)$ dark gauge symmetry, we also introduce a dark boson with a non diagonal coupling to the dark fermions and kinetic mixing with the SM photon. This allows χ_1 to interact with Earth nucleons, generating a χ_2 which subsequently decays via $\chi_2 \to \chi_1$ + shower with the shower generated through kinetic mixing. Previously proposed as an explanation of the anomalous events observed by ANITA in previous flights [386], this scenario can account for the new anomalous events with large kinetic mixings ($\sim 10^{-2}$), and masses around the GeV scale ($m_X \sim 2 \text{ GeV}$, $m_{\chi_2} \sim 1 \text{ GeV}$, $m_{\chi_1} \sim 0.5 \text{ GeV}$). Further model-building work can explore other options.

The ANITA experiment is starting to probe uncharted land. First results are already anomalous, and understanding their BSM or background origin is pressing to ensure the success of future, more ambitious, UHE neutrino detectors. As we have shown, BSM explanations predict that anomalous events should be observed in other experiments too. The upcoming flight of PUEO [354], with a detection principle similar to ANITA, and the future IceCube-Gen2 upgrade [38] will thus be unique opportunities to gain insight into the potential signals and backgrounds of the UHE landscape.

Part III Neutrinos from the Universe

6 What we know of the Universe: an introduction

[The Big Bang is] followed by what? By a dull-as-ditchwater expansion which degrades itself adiabatically until it is incapable of doing anything at all. The notion that galaxies form, to be followed by an active astronomical history, is an illusion. Nothing forms, the thing is as dead as a door-nail.

- Fred Hoyle [413]

Pioneer in stellar nucleosynthesis, he coined the term "Big Bang" while clearly disliking the theory.

The Universe did not start with a Bang, and neither did the Big Bang Theory. Just like the expanding cosmos, our progress on our understanding of the Universe has been slow and steady, both in the theoretical and observational sides. In its early years, cosmology was largely speculative, and it was not even clear whether it could evolve into a rigorous scientific discipline [414]. Now, just a century after Alexander Friedmann solved General Relativity for a homogeneous Universe [415], we have achieved the era of precision cosmology, which has turned cosmology into a rigorous, data-driven research. This has come with some surprises.

By probing the observable Universe as our research object we have discovered phenomena which are unexplained by terrestrial experiments, namely (Cold) Dark Matter (DM) and Dark Energy. The distances and time scales of the Universe bring afloat the gravitational effects of these species, which have not been found to interact in any other manner with ordinary matter, i.e., the SM. No particle within the SM can account for the properties of these "dark sector". Then, with the exception of neutrino oscillations, cosmology remains our best reminder that the SM is not all there is.

Cosmology has provided us with a precise description of the macroscopical properties of this dark sector, the so-called Λ -Cold Dark Matter (Λ CDM) model of cosmology. However, its microscopical description still remains a challenge, and the BSM opportunities lie in this precise challenge. In order to uncover what is missing in our current picture of fundamental physics, two paths open up in front of us.

First, it is imperative to challenge the Λ CDM paradigm and look for deviations from it. This requires new observations with increasing precision and statistics, but also theoretical developments to interpret them and boost the reach of observations beyond its original scope. The Hubble tension [151, 416–418], the hints of dynamical Dark Energy [153, 419, 420] or "negative neutrino masses" [152, 421, 422], even if they end up

vanishing in the air, are anomalies that make us think how BSM intercedes in some particular cosmological observations. Chapter 7 provides an example on the challenge of neutrino masses to cosmology [3].

Second, as we have seen in the previous part, the Universe provides us with extreme environments where to test our theories, for free. In the case of the early Universe, this is large energies and large number densities; in the late Universe, it is long distances and large volumes. BSM properties that are invisible in terrestrial experiments may become apparent when looking at the Universe. This is specially interesting for Dark Matter (production, annihilation and/or decay) [423], but also for the neutrino sector [55, 424]. New manners of looking into the Cosmos, or the refinement of old ones, may open unexpected windows to New Physics. In this case, chapter 8 describes a research work which explores the Early Universe to constrain BSM properties.

Before we delve in these two examples, however, we need to present the basics of cosmology. To such purpose, in this chapter we first introduce the basic description of a homogeneous (section 6.1) and a linearly perturbed Universe (section 6.2). Then, we describe the physical processes behind the key pillars of cosmology: the Cosmic Microwave Background (section 6.3) and Big Bang Nucleosynthesis (section 6.4). This chapter mostly follows [424–427]. If you are already familiar with these topics, you are welcome to skip to chapter 7.

6.1 An homogeneous Universe, expanding

We live in an expanding Universe. It started approximately 13.79×10^9 years ago, when it was in a hot and dense plasma of particles, and has been expanding since then. We know this from the observation of the recession of galaxies, the measurement of the Cosmic Microwave Background (section 6.3) and the observation of light element abundances (section 6.4).

We live in a (quite) homogeneous and isotropic Universe too. While the Universe is clearly not homogeneous at the scales of galaxies and of galaxy clusters, it is at the scales of the Large Scale Structure of the Universe. The primordial Universe was also extremely homogeneous, with relative inhomogeneities of size $\mathcal{O}(10^{-5})$. This observation has led into the cosmological principle, which states that there is no privileged point nor direction in the Universe, i.e., it is homogeneous and isotropic. This assumption, in good agreement with current observations, puts great constrains on the dynamics of the Universe. In this section, we write down the equations governing the expansion of a homogeneous Universe.

6.1.1 The geometry of the Universe

In the framework of general relativity, a metric $g_{\mu\nu}$ describes the space-time structure of the Universe and, thus, gravity and the dynamics of objects within it. Under the constraints imposed by the cosmological principle, the most general metric is the Friedmann-Lemaître-Roberston-Walker (FLRW),

$$ds^{2} = g_{\mu\nu}dx^{\mu}dx^{\nu} = -dt^{2} + a(t)^{2} \left(\frac{dr^{2}}{1 - kr^{2}} + r^{2}d\Omega^{2}\right).$$
 (6.1)

Here, $\mathrm{d}s^2$ is the proper-time interval and t is the cosmological proper time, defined as the time measured by an observer moving along the Hubble flow. Then, Ω is the solid angle and r is the comoving distance, which refers only to the coordinate grid with which we map the Universe space-time. Finally, k=+1,0,-1 for open, flat and closed space-times, and a(t) is the scale factor which follows the Universe expansion.

In order to simplify some expressions, one usually defines the conformal time $d\eta = a(t)dt$, which turns the standard FLRW metric into

$$ds^{2} = a(t)^{2} \left(-d\eta^{2} + \frac{dr^{2}}{1 - kr^{2}} + r^{2} d\Omega^{2} \right).$$
 (6.2)

This new time coordinate can be understood as the comoving distance that light travels (in the absence of interactions) in a time interval dt. Another useful time variable is the redshift

$$1 + z = \frac{a_0}{a(t)},\tag{6.3}$$

where $a_0 \equiv 1$ is the scale factor today. In the popular interpretation, photons emitted from distant sources in the past are stretched as they travel to us through an expanding Universe, resulting in redshift. However, this popular belief contradicts that spacetime must be locally Minkowskian, and thus cosmological redshift is better understood as the accumulation of infinitesimal Doppler shifts along the line of sight between the source and the observer [428]. In any case, the further the source, the more the Universe has expanded, and the larger redshift z we measure.

Even if it can be parametrised in terms of many different time variables, the metric of the homogeneous Universe requires only one parameter to be described, here the scale factor a. The expansion history of the Universe, encoded in a(t), is governed by the Einstein equations of general relativity,

$$G_{\mu\nu} = 8\pi G T_{\mu\nu} \,. \tag{6.4}$$

Here, G is Newton's constant, $G_{\mu\nu}$ is the Einstein tensor and $T_{\mu\nu}$ is the total energy-momentum tensor in the Universe. Equation (6.4) describes how the curvature of the Universe influences the evolution of the matter content within it, and vice versa. We leave $T_{\mu\nu}$ for the following section, and briefly comment on $G_{\mu\nu}$ now.

The spacetime of the Universe is a four-dimensional curved manifold described by the metric in eq. (6.1). In such a spacetime, each point belongs to a different tangent space and thus we require an affine connection between tangent spaces, given by the Christoffel symbols

$$\Gamma^{\sigma}_{\mu\nu} = \frac{1}{2} g^{\sigma\rho} \left(\partial_{\mu} g_{\nu\rho} + \partial_{\nu} g_{\mu\rho} - \partial_{\rho} g_{\mu\nu} \right) . \tag{6.5}$$

For the FLRW metric from eq. (6.1), the only non-vanishing Christoffel symbols are

$$\Gamma^{0}_{ij} = \frac{\dot{a}}{a} g_{ij},$$

$$\Gamma^{j}_{0i} = \Gamma^{j}_{i0} = \frac{\dot{a}}{a} \delta^{j}_{i},$$
(6.6)

where a dot denotes a derivative with respect to proper time. This affine connection allows to define parallel transport along a vector field and, thus, the covariant derivative ∇_{μ} . Once $\Gamma^{\sigma}_{\mu\nu}$ are defined, the Ricci tensor

$$R_{\mu\nu} = \partial_{\sigma} \Gamma^{\sigma}_{\mu\nu} - \partial_{\mu} \Gamma^{\sigma}_{\nu\sigma} + \Gamma^{\sigma}_{\sigma\rho} \Gamma^{\rho}_{\mu\nu} - \Gamma^{\sigma}_{\mu\rho} \Gamma^{\rho}_{\sigma\nu}$$
 (6.7)

measures the local curvature, i.e., how much does spacetime locally differs from Euclidean spactime. The trace of this tensor, $R=g^{\mu\nu}R_{\mu\nu}$, is the Ricci scalar. Finally, the Einstein's tensor $G_{\mu\nu}$ which relates the curvature of spacetime to its content is

$$G_{\mu\nu} = R_{\mu\nu} - \frac{1}{2} g_{\mu\nu} R \,. \tag{6.8}$$

The Einstein tensor fulfills the Bianchi identities, $\nabla_{\mu}G^{\mu\nu}=0$, which immediately implies the conservation of the energy-momentum tensor, $\nabla_{\mu}T^{\mu\nu}=0$.

6.1.2 The content of the Universe

Under the cosmological principle of homogeneity and isotropy, the energy-momentum tensor for matter is that of a perfect fluid,

$$T_{\mu}^{\nu} = p g_{\mu}^{\nu} + (\rho + p) u_{\mu} u^{\nu} \equiv \operatorname{diag}(-\rho, p, p, p),$$
 (6.9)

with u^{μ} the four-velocity of the fluid, ρ its energy density and p its pressure. An important quantity of a perfect fluid is the equation of state,

$$w = \frac{p}{\rho} \,. \tag{6.10}$$

The equation of state is a thermodynamical quantity which relates pressure and internal energy and governs how does the energy of a system evolve as it expands. This will become clear in the following section. Important benchmarks are w = 1/3 for an ultrarelativistic gas (usually called radiation), w = 0 for a non-relativistic gas (matter or dust) and w = -1 for a cosmological constant (Λ).

6.1.3 The evolution of the Universe

Once the geometry and content of the Universe are defined through eqs. (6.1) and (6.9), we use eq. (6.4) to obtain the Friedmann equations [415]

$$H^2 \equiv \left(\frac{\dot{a}}{a}\right)^2 = \frac{8\pi G}{3}\rho - \frac{k}{a^2},\tag{6.11}$$

$$\frac{\ddot{a}}{a} = -\frac{4\pi G}{3}(\rho + 3p). \tag{6.12}$$

Equation (6.11) defines the Hubble parameter $H = \dot{a}/a$, i.e., the expansion rate of the Universe. p and ρ correspond to the total pressure and energy density of the Universe, respectively. In a matter-dominated Universe ($w \approx 0$) or a radiation-dominated Universe ($w \approx 1/3$), larger energy densities decrease the acceleration of the Universe, i.e., tend to slow down the expansion. However, a Universe dominated by a cosmological constant Λ ($w \sim -1$) is in an ever-expanding acceleration.

The current value of the Hubble parameter is called the Hubble constant, H_0 , and is usually quantified as

$$H_0 = 100h \,\mathrm{km} \,\mathrm{s}^{-1} \mathrm{Mpc}^{-1}$$
, (6.13)

with h the reduced Hubble constant, $h=0.6766\pm0.0042$ [151] from early-Universe measurements. If working in terms of the conformal time, it is convenient to define the conformal Hubble rate $\mathcal{H}=a'/a$, which is related to the Hubble rate as $\mathcal{H}=aH$.

The evolution of the Universe must conserve the energy and momentum tensor,

$$\nabla_{\mu}T^{\mu}_{\ \nu} = \partial_{\mu}T^{\mu}_{\ \nu} + \Gamma^{\mu}_{\ \mu\sigma}T^{\sigma}_{\ \nu} - \Gamma^{\sigma}_{\ \mu\nu}T^{\mu}_{\ \sigma}. \tag{6.14}$$

In the case of a perfect fluid, conservation of energy and momentum implies

$$\dot{\rho} = -3H(\rho + p) = -3H\rho(1 + w), \tag{6.15}$$

which can also be written as

$$\frac{1}{\rho} \frac{d\rho}{d\log a} = -3(1+w). \tag{6.16}$$

Then, the variation of the energy density of the Universe is given by its equation of state. This is also true for the energy density of a decoupled species which does not interact with the rest of the Universe. Importantly, eqs. (6.11), (6.12) and (6.15) are not linearly independent, only two of them are. It is typical to work with eqs. (6.11) and (6.15).

For a constant equation of state, eq. (6.16) can be solved to

$$\rho \sim a^{-3(1+w)} = \begin{cases} a^{-4} & \text{radiation} \\ a^{-3} & \text{matter} \\ \text{ct.} & \text{cosmological constant} \end{cases}$$
 (6.17)

Furthermore, under the constant w approximation, one can solve eq. (6.11) and obtain the scaling of a(t) with time,

$$a(t) \propto \begin{cases} t^{1/2} & \text{radiation domination} \\ t^{2/3} & \text{matter domination} \end{cases}$$
 (6.18)
 $e^{tH} & \Lambda \text{ domination}$

For every species i that the Universe has, with energy density ρ_i , one can define a density parameter

$$\Omega_i = \frac{\rho_i}{\rho_c} \,, \tag{6.19}$$

where ρ_c is the critical density

$$\rho_c = \frac{3H_0^2}{8\pi G} = 5.53 \times 10^{41} h^2 \,\mathrm{kg} \,\mathrm{Mpc}^{-3} \,. \tag{6.20}$$

Then, Friedmann eq. (6.11) can be written in the more compact manner

$$H^{2} = H_{0}^{2} \left[\Omega_{r,0} a^{-4} + \Omega_{m,0} a^{-3} + \Omega_{k,0} a^{-2} + \Omega_{\Lambda,0} \right] . \tag{6.21}$$

Here, $\Omega_{i,0}=\Omega_i(a_0)$ is the density parameter today and, in particular, $\Omega_{k,0}=k\,H_0^{-2}$ and

 $\Omega_{\Lambda,0}=\Lambda/3$. The most recent analysis of Planck18 (with Baryon Accoustic Oscillations) provides the best measurement of spatial curvature, $\Omega_{k,0}=0.001\pm0.002$ [151], which is consistent with spatially flat Universe. Therefore, we will work with k=0 for the rest of this thesis.

The conformal dictionary

To simplify expressions, in the rest of this thesis we will work with conformal time η instead of the proper time t, which are related through $dt = ad\eta$, and

$$\frac{\mathrm{d}}{\mathrm{d}t} = \frac{1}{a}\frac{\mathrm{d}}{\mathrm{d}\eta}, \qquad \frac{\mathrm{d}^2}{\mathrm{d}t^2} = \frac{1}{a^2}\frac{\mathrm{d}^2}{\mathrm{d}\eta^2} - \frac{\mathcal{H}}{a^2}\frac{\mathrm{d}}{\mathrm{d}\eta}, \qquad \mathcal{H} = \frac{a'}{a} = aH = \dot{a}. \tag{6.22}$$

Here, a prime denotes a derivative with respect to η . In conformal time, eqs. (6.11), (6.12) and (6.15) respectively rewrite to

$$\mathcal{H} = \frac{8\pi G a^2}{3} \rho - k \,, \tag{6.23}$$

$$\mathcal{H}' = -\frac{4\pi G a^2}{3} (\rho + 3p), \qquad (6.24)$$

$$\rho' = -3\mathcal{H}(\rho + p). \tag{6.25}$$

The non-vanishing Christoffel symbols are

$$\Gamma^{0}_{00} = \frac{a'}{a},$$

$$\Gamma^{0}_{ij} = \frac{a'}{a} g_{ij},$$

$$\Gamma^{j}_{0i} = \Gamma^{j}_{i0} = \frac{a'}{a} \delta^{j}_{i}.$$
(6.26)

6.1.4 Geodesics and the Boltzmann equation

In the previous definitions, we have introduced a macroscopic description of the content of the Universe, through $T_{\mu\nu}$. However, most species of the Universe require the microscopical description from a gas of particles. For these species, we begin by defining the phase space distribution function $f(x^i, P_j, \eta)$, which gives the number of particles per unit of phase space volume at the point (x^i, P_j) of the phase space and at time η . Here, P_μ is the conjugate momentum to x^μ , and is related to the 4-momentum of the particle P^ν by $P_\mu = g_{\mu\nu}P^\nu$, and to the physical momentum $p^i = p_i$ as $P_i = ap_i$. Then, the

4-momentum of the particle is described by the geodesic equation

$$P^{0} \frac{\mathrm{d}P^{\mu}}{\mathrm{d}\eta} + \Gamma^{\mu}_{\ \nu\rho} P^{\nu} P^{\rho} = 0. \tag{6.27}$$

In a homogeneous Universe, this returns that the physical linear momentum, $p_i = P_i/a$, decreases as a^{-1} as the Universe expands. In this thesis, we will mostly work with the comoving linear momentum, $q_i = ap_i$, which we describe in terms of its magnitude and direction, $q_i = qn_i$.

From this microscopical description of the species, in terms of $f(x^i, P_j, \eta)$, it is possible to recover the macroscopical description in terms of the energy-momentum tensor through

$$T_{\mu\nu} = \int \frac{\mathrm{d}P_1 \,\mathrm{d}P_2 \,\mathrm{d}P_3}{\sqrt{-\det g}} \frac{P_{\mu}P_{\nu}}{P^0} f(x^i, P_j, \eta), \qquad (6.28)$$

where det g denotes the determinant of the metric $g_{\mu\nu}$. For the conformal homogeneous FLRW metric, $\sqrt{-\det g}=a^4$.

Then, the distribution $f(x^i, q, n_j, \eta)$ evolves according to the Boltzmann equation

$$\frac{Df}{d\eta} = \frac{\partial f}{\partial \eta} + \frac{dx^i}{d\eta} \frac{\partial f}{\partial x^i} + \frac{dq}{d\eta} \frac{\partial f}{\partial q} + \frac{dn_i}{d\eta} \frac{\partial f}{\partial n_i} = \frac{\partial f}{\partial \eta} \bigg|_{C}.$$
 (6.29)

Here, the right-hand side describes the changes on the distribution function due to collisions. For a decoupled species with constant mass in a homogeneous Universe, $dq/d\eta=0$, $dn_i/d\eta=0$ and $\partial f/\partial x^i=0$, which leads to $\partial f/\partial \eta=0$. This means that any distribution function which depends on q=pa is a solution to the homogeneous collisionless Boltzmann equation. That is, $f(x^i,P_j,\eta)=f_0(q)$, which will maintain its shape and only have the physical momenta redshifted by p=q/a.

6.2 The linearly perturbed Universe

Luckily for us, the Universe is not homogeneous. While inhomogeneities at galactic scales are large, there are scales of cosmological interest where inhomogeneities are sufficiently small to be analytically treated. At the time of recombination, as seen in the Cosmic Microwave Background, these are $\delta T_{\gamma}/T_{\gamma} \sim \mathcal{O}(10^{-5})$. The Large Scale Structure of the Universe, presents overdensities at most $\delta \rho/\rho \sim \mathcal{O}(10^{-2})$ [424, 426]. These inhomogeneities can be described by perturbing the FLRW metric eq. (6.1) to linear order. Following the notation from [425],

$$ds^{2} = a^{2}(\eta) \left(-(1 + 2\psi) d\eta^{2} + (1 - 2\phi) \left[dr^{2} + r^{2} d\Omega^{2} \right] \right). \tag{6.30}$$

Here, $\psi = \psi(\vec{x}, \eta)$ is a generalization of the conformal Newtonian potential [427] (and coincides with it for non-relativistic bodies at scales much smaller than the Hubble radius), while $\phi = \phi(\vec{x}, \eta)$ is a correction to the spatial curvature, which can also be understood as a small correction to time dilation. This parametrisation of scalar linear perturbations is the so-called Newtonian (or longitudinal) gauge. We will describe perturbations in Fourier space, with

$$\psi(\vec{x}, \eta) = \int d^{3}\vec{k} \, e^{i\vec{k}\cdot\vec{x}} \psi(\vec{k}, \eta), \qquad \phi(\vec{x}, \eta) = \int d^{3}\vec{k} \, e^{i\vec{k}\cdot\vec{x}} \phi(\vec{k}, \eta). \tag{6.31}$$

Here, \vec{k} is the comoving wavenumber of the perturbation. A perturbation of comoving wavenumber \vec{k} varies within a characteristic comoving scale $\lambda = 2\pi k^{-1}$. The Newtonian gauge is not the unique way of describing perturbations of a FLRW universe. However, it is the best suited to study scalar perturbations [425]. Gauge freedom is further discussed in section 6.2.1.

In the same manner that we perturb the geometry, we must also admit perturbations in the matter content. The perturbed energy-momentum tensor is

$$T_0^0 = -(\rho + \delta \rho), \tag{6.32}$$

$$T_{i}^{0} = (\rho + p)v_{i}, (6.33)$$

$$T^{i}_{j} = (p + \delta p)\delta^{i}_{j} + \Sigma^{i}_{j}. \tag{6.34}$$

Here, $\delta \rho$ is the overdensity, δp the overpressure, v_i the three-velocity of the fluid and $\Sigma^i_{\ j} = T^i_{\ j} - \delta^i_{\ j} T^k_{\ k}/3$ the traceless component of $T^i_{\ j}$. For scalar perturbations, the necessary variables are the divergence of the fluid velocity θ and the anisotropic stress or shear σ ,

$$\theta = ik^{j}v_{j}, \qquad (\rho + p)\sigma = -\left(k_{i}k_{j} - \frac{1}{3}\delta_{ij}\right)\Sigma^{i}_{j}. \tag{6.35}$$

Physically, θ represents the divergence of the bulk velocity of energy perturbations; and δP and σ the isotropic and anisotropic components of the linear momentum flux, respectively.

6.2.1 Gauge invariance and transformations

General Relativity allows the freedom to choose the system of coordinates to describe spacetime. In the case of a homogeneous Universe, the choice of coordinates is imposed by the symmetries of the system. However, this symmetry disappears when considering inhomogeneous perturbations, and there is not a preferred system of coordinates to describe them. The different systems of coordinates are related between them through

gauge transformations, defined as in [425]

$$\eta \to \eta + \alpha(\vec{x}, \eta),$$
 (6.36)

$$\vec{x} \to \vec{x} + \vec{\nabla} \beta(\vec{x}, \eta) + \vec{\epsilon} (\vec{x}, \eta).$$
 (6.37)

Here, $\vec{\nabla}\beta$ is a longitudinal component and $\vec{\epsilon}$ ($\vec{\nabla} \cdot \vec{\epsilon} = 0$) is a transversal component. For instance, matter perturbations transform under these gauge transformations as [425]

$$\delta \to \delta - \alpha \rho' / \rho$$
, (6.38)

$$\theta \to \theta - \alpha k^2$$
, (6.39)

$$\delta P \to \delta P - \alpha P'$$
, (6.40)

$$\sigma \to \sigma$$
. (6.41)

This means that –broadly defined– δ , θ and δP are not gauge-invariant quantities, but σ is. As a consequence, one can always transform from a system of coordinates with no real inhomogeneities (e.g., $\delta=0$) to a system of coordinates where $\delta\neq0$, i.e., where a fictitious inhomogeneity appears. In order to distinguish between fictitious and real perturbations, it is standard to work in the Newtonian (or longitudinal) gauge. This is because gauge-invariant metric, energy and velocity fluctuations correspond to their values in the Newtonian gauge. Therefore calculations in these coordinates are identical to calculations in terms of the gauge-invariant variables [427].

6.2.2 Initial conditions

The origin of perturbations goes back to quantum fluctuations in the inflaton field. In the standard single-field inflationary paradigm, the value of the scalar field is the only clock in the Universe. Then, all fluctuations are understood as local time shifts $\delta \eta(\vec{x})$ with respect to the average time η [424]. As a consequence, densities and pressures must obey

$$\lim_{k \to 0} (p + \delta p)(\eta) = p(\eta + \delta \eta) = p(\eta) + p'(\eta)\delta\eta, \qquad (6.42)$$

$$\lim_{k \to 0} (\rho + \delta \rho)(\eta) = \rho(\eta + \delta \eta) = \rho(\eta) + \rho'(\eta)\delta\eta, \qquad (6.43)$$

where, as we will describe now, the $k \to 0$ limit indicates initial conditions. The existence of a single clock also implies that all species must have the same $\delta \eta(\vec{x})$. Then, density

perturbations for a species i is

$$\frac{\delta \rho_i}{\rho_i + p_i} = \frac{\rho_i'}{\rho_i + p_i} \delta \eta(\vec{x}) = -3\mathcal{H} \delta \eta(\vec{x}), \qquad (6.44)$$

where we have used eq. (6.15). Since this does not depend on the species, every species i is originated with the same fractional density perturbation, and analogously for velocities. Another consequence is that pressure perturbations will fulfill

$$\lim_{k \to 0} \frac{\delta p}{\delta \rho} = \frac{p'}{\rho'} = w - \frac{w'}{3\mathcal{H}(1+w)} \equiv c_{\text{ad}}^2, \qquad (6.45)$$

where we have defined the adiabatic sound speed, $c_{\rm ad}$. These kind of initial conditions, where a single clock is at the origin of fluctuations, are called adiabatic initial conditions. Planck18 has precisely measured that cosmological perturbations are adiabatic, constraining non-adiabatic perturbations to less than a percent-level fraction [151]. Therefore, in what follows we assume only adiabatic perturbations.

The initial period of fast inflationary expansion makes the fluctuations in the scalar field grow beyond the horizon, $k < \mathcal{H}$. At such scales, perturbations are not causally connected and remain frozen. This is what we define as "initial conditions". In particular, if they are adiabatic, superhorizon perturbations must correspond to the background Universe with a local time shift correction. Quantitatively, adiabatic initial conditions predict that the comoving curvature perturbation [424, 426]

$$\mathcal{R} = \phi + \frac{1}{\mathcal{H}} \frac{\theta}{k^2},\tag{6.46}$$

is conserved for superhorizon modes [424, 426]. \mathcal{R} receives its name from the fact that, in a gauge comoving with the fluid (i.e., $\theta = 0$), it exactly matches the curvature perturbation $\mathcal{R} = \phi$. Adiabatic initial conditions imply [425],

$$\delta_{\gamma} = -2\psi, \qquad \delta_{c} = \delta_{b} = \frac{3}{4}\delta_{\nu} = \frac{3}{4}\delta_{\gamma},$$

$$\theta_{\gamma} = \theta_{\nu} = \theta_{c} = \theta_{b} = \frac{1}{2}(k^{2}\eta)\psi,$$

$$\sigma_{\nu} = \frac{1}{15}(k\eta)^{2}\psi.$$
(6.47)

Here, c stands for CDM, b for baryons and v for (ultrarelativistic) neutrinos.

All equations are then solved using R = 1 as an arbitrary initial condition, and

plugging afterwards the power primordial spectrum $\mathcal{P}_{\mathcal{R}}(k)$,

$$\left\langle \mathcal{R}(\eta_{\rm in}, \vec{k}), \mathcal{R}(\eta_{\rm in}, \vec{k}') \right\rangle = \frac{2\pi^2}{k^3} \mathcal{P}_{\mathcal{R}}(k) \, \delta^{(3)}(\vec{k} - \vec{k}'), \tag{6.48}$$

with η_{in} is an initial time when modes are sufficiently super-horizon. One of the main predictions of inflation is a nearly scale-invariant power spectrum as

$$\mathcal{P}_{\mathcal{R}}(k) = A_s \left(\frac{k}{k_0}\right)^{n_s - 1},\tag{6.49}$$

where n_s is the spectral index, slightly below unity, and A_s is the primordial spectrum amplitude at the arbitrary pivot scale k_0 , usually taken to be $k_0 = 0.5 \,\mathrm{Mpc^{-1}}$. From Planck18, $n_s = 0.9665 \pm 0.0038$ and $A_s = (2.105 \pm 0.030) \times 10^{-9}$ [151].

Another useful property of adiabatic initial conditions, as we will see in the next chapter, is that in the $k \to 0$ limit,

$$k^2 \delta = 3\mathcal{H}(1+w)\theta. \tag{6.50}$$

First of all, from eqs. (6.38) to (6.41), this identity is gauge-invariant. Then, super-horizon adiabatic initial conditions in the radiation-domination regime correspond to $\delta = -2\psi$, $\theta = k^2\eta\psi/2$, w = 1/3, $a'/a = \eta^{-1}$ [425]; which satisfy eq. (6.50). Equation (6.50) is also maintained by super-horizon evolution: using eqs. (6.56) and (6.57) with $k \to 0$ (where $\theta \to 0$ and $\sigma \to 0$), as well as the Friedmann and perturbed Einstein equations [425], we obtain

$$\frac{\mathrm{d}}{\mathrm{d}\eta} \left[\frac{3\mathcal{H}(1+w)\theta}{k^2} + \delta \right] = \mathcal{H} \left[-\frac{3}{2} \left(1 + \frac{p}{\rho} \right) + 3w \right] \left[\frac{3\mathcal{H}(1+w)\theta}{k^2} + \delta \right], \quad (6.51)$$

Since the right-hand side vanishes for the initial conditions, super-horizon evolution keeps the identity true at all times, even if \mathcal{H} or w change with time. This is also fulfilled by decoupled neutrino perturbations.

6.2.3 Evolution of perturbations

Eventually, as the Hubble horizon grows with time, a mode will enter the horizon (k > H), become causally connected and evolve according to Einstein's eq. (6.4). Then, modes with $k > H_0$ remain always frozen, but these are larger than the observable Universe

and are not observable. From eqs. (6.30) and (6.32), Einstein's equation returns

$$k^{2}\phi + 3\mathcal{H}\left(\phi' + \mathcal{H}\psi\right) = -4\pi G a^{2}\delta\rho, \qquad (6.52)$$

$$k^{2}\left(\phi'+\mathcal{H}\psi\right)=4\pi Ga^{2}(\rho+p)\theta\,,\tag{6.53}$$

$$\phi'' + \mathcal{H}(\psi' + 2\phi') + 2\left(2\frac{a''}{a} - \mathcal{H}^2\right)\psi + \frac{k^2}{3}(\phi - \psi) = \frac{4\pi}{3}Ga^2\delta p \tag{6.54}$$

$$k^{2}(\phi - \psi) = 12\pi Ga^{2}(\rho + p)\sigma$$
. (6.55)

Deep inside Hubble's radius ($k \gg \mathcal{H}$), eq. (6.52) gives the Poisson equation for ϕ . Furthermore, eq. (6.55) shows that $\phi = \psi$ in the absence of anisotropic stress. While this is true to a good approximation in a neutrinoless Universe, neutrinos may carry a nonnegligible σ and eq. (6.55) needs to be treated with caution.

In addition, conservation of energy and momentum as in eq. (6.14) leads to

$$\delta' = -(1+w)\left(\theta - 3\phi'\right) - 3\mathcal{H}\left(\frac{\delta p}{\delta \rho} - w\right) \tag{6.56}$$

$$\theta' = -\mathcal{H}(1 - 3w)\theta - \frac{w'}{1 + w}\theta + \frac{\delta p/\delta \rho}{1 + w}k^2\delta - k^2\sigma + k^2\psi, \qquad (6.57)$$

where we have defined the density contrast $\delta = \delta \rho/\rho$. Physically, the first three terms in eq. (6.56) correspond to energy dilution due to bulk motions, gravitational redshift, and the expansion of the Universe; respectively. In eq. (6.57), the first term corresponds to drag due to the expansion of the Universe; the second and third terms to isotropic and anisotropic momentum flow, respectively; and the fourth term to gravitational forces. These equations must be fulfilled by any uncoupled species, and by the mass-averaged δ , θ of the total Universe. Equipped with the knowledge of cosmological linear perturbation theory, let us study the CMB.

6.3 The Cosmic Microwave Background

The Cosmic Microwave Background (CMB) is a cornerstone of modern cosmology, providing a snapshot of the universe approximately 380,000 years after the Big Bang. At this epoch, the universe had cooled sufficiently for electrons and protons to combine into neutral hydrogen, a process known as recombination. This event marked the transition from an opaque plasma to a transparent universe, allowing photons to travel freely. The CMB is the relic radiation from this last-scattering surface, which has a nearly isotropic blackbody spectrum with a temperature of $T_{\gamma,0} = (2.27255 \pm 0.00057)$ K [429].

Prior to recombination, the universe was dominated by a tightly coupled baryon-

photon fluid, with small inhomogeneities seeded by primordial density fluctuations from inflation. The interplay between photon pressure and baryon gravity led to acoustic oscillations in the fluid, approximately described by [430]

$$m_{\rm eff}\Theta_{\gamma 0}^{\prime\prime} + k^2 \frac{\Theta_{\gamma 0}}{3} \simeq -m_{\rm eff} \left(k^2 \frac{\psi}{3} - \phi^{\prime\prime} \right) ,$$
 (6.58)

Here, $m_{\rm eff} \equiv 1 + \frac{\rho_b + p_b}{\rho_\gamma + p_\gamma} \simeq 1 + 3\rho_b/(4\rho_\gamma)$; with ρ_b , p_b , ρ_γ , and p_γ the baryon energy density, baryon pressure, photon energy density, and photon pressure, respectively. Equation (6.58) is the equation of a forced harmonic oscillator, with the gravitational potentials playing the role of an external force. These oscillations, which propagate with a sound speed $c_{s,\gamma}$, created regions of compression (overdensities) and rarefaction (underdensities) in both the photon and baryon distributions. The characteristic scale of these oscillations is set by the sound horizon at recombination,

$$r_s(\eta) = \int_{\eta_{\rm in}}^{\eta} c_{s,\gamma}(\eta') \mathrm{d}\eta', \qquad (6.59)$$

the maximum distance sound waves could travel in the baryon-photon fluid before the universe became transparent. Here, $\eta_{\rm in} \ll \eta$ is an arbitrary initial time.

The power spectrum of the CMB temperature anisotropies, shown in fig. 6.1, reflects the imprint of these acoustic oscillations. The peaks and troughs in the spectrum correspond to different oscillation modes that entered the horizon prior to recombination. The first peak represents the mode that underwent exactly one compression at the time of last scattering, while subsequent peaks correspond to modes that experienced multiple compressions and rarefactions. The CMB tail is damped due to photon diffusion, which homogeneizes the temperature for modes which entered the horizon soon enough. An excellent review on the information that can be extracted from the relative heights and positions of these peaks can be found in [424, 426]. In the following sections we introduce the basic ingredients we need to understand the CMB, so that then we can understand how neutrinos impact it.

6.3.1 Temperature inhomogeneities

The perturbed phase space distribution for a photon gas is given by

$$f_{\gamma}(\eta, \vec{x}, \vec{p}) = \left[\exp\left(\frac{|\vec{p}|}{T_{\gamma}(\eta) \left\{1 + \Theta_{\gamma}(\eta, \vec{x}, \hat{n})\right\}}\right) - 1 \right]^{-1}, \tag{6.60}$$

with $\Theta_{\gamma} = \delta T_{\gamma}/T_{\gamma}$ the relative photon temperature shift. We can plug this f_{γ} in the Boltzmann equation eq. (6.29), and obtain

$$\Theta_{\nu}' + \hat{n} \cdot \vec{\nabla} \Theta_{\nu} - \phi' + \hat{n} \cdot \vec{\nabla} \psi = a n_e \sigma_T (\Theta_{\nu,0} - \Theta_{\nu} + \hat{n} \cdot \vec{v}_B). \tag{6.61}$$

The right-hand term corresponds to the collision term between photons and baryons, and thus n_e is the number density of free electrons, σ_T the Thomson cross-section and \vec{v}_B the bulk velocity of the baryon-electron fluid. Here, $\Theta_{\gamma,0}$ is the temperature perturbation monopole (i.e., the average of Θ_{γ} over all directions \hat{n}). The collision term tries to make Θ_{γ} approach thermal equilibrium, with a unique temperature $\Theta_{\gamma,0} + \hat{n} \cdot \vec{v}_B$, i.e., the average temperature with a Doppler shift from the velocity of the fluid. In the tight-coupling limit ($\sigma_T \to \infty$), this forces the anisotropies to be only a sum of a monopole and a dipole, and vanishes higher multipoles.

To solve this equation we work in Fourier space of \vec{k} . Afterwards, we would need to expand $\Theta_{\gamma}(\eta, \vec{k}, \hat{n})$ in two-dimensional spherical harmonics. However, eq. (6.61) only depends in \vec{k} through $\mu \equiv \hat{n} \cdot \vec{k}$, and initial conditions of Θ_{γ} correspond to tightly coupled-photons, which only depend on \hat{n} through a monopole or a dipole. Then, we can consider $\Theta_{\gamma} = \Theta_{\gamma}(\eta, \vec{k}, \mu)$ and work in one-dimensional Legendre space instead,

$$\Theta_{\gamma}(\eta, \vec{k}, \mu) = \sum_{\ell} (-i)^{\ell} (2\ell + 1) \Theta_{\gamma, \ell}(\eta, \vec{k}) P_{\ell}(\mu), \qquad (6.62)$$

where the index ℓ tags the Legendre multipole. Most importantly, we can relate the coefficients $\Theta_{\gamma,\ell}$ to the variables just defined, through

$$\delta_{\gamma} = 4\Theta_{\gamma,0}, \qquad \theta_{\gamma} = 3k\Theta_{\gamma,1}, \qquad \sigma_{\gamma} = 2\Theta_{\gamma,2}.$$
 (6.63)

Again, in the tightly-coupled limit, $\Theta_{\gamma,\ell} = 0$ for $\ell \geq 2$.

6.3.2 From inhomogeneities to anisotropies

Now we want to compute the temperature anisotropy observed today $(\eta = \eta_0)$, at the Earth's position $\vec{x} = \vec{o}$, for photons coming to us (in the $-\hat{n}$ direction), $\Theta_{\gamma}(\eta_0, \vec{o}, -\hat{n})$. This temperature anisotropy can be now expanded in spherical harmonics $Y_{\ell m}(\hat{n})$,

$$\Theta_{\gamma}(\eta_0, \vec{o}, -\hat{n}) = \sum_{\ell,m} a_{\ell m} Y_{\ell m}(\hat{n}), \qquad (6.64)$$

where, from eq. (6.62),

$$a_{\ell m} = (-i)^{\ell} \int \frac{\mathrm{d}^{3} k}{2\pi^{2}} Y_{\ell m}(\vec{k}) \Theta_{\gamma, \ell}(\eta_{0}, \vec{k}).$$
 (6.65)

Assuming that first-order cosmological perturbations are gaussian and that the Universe is isotropic, then all the information of CMB anisotropies can be described by the two-point correlation functions

$$C_{\ell} = \langle a_{\ell m} a_{\ell m}^* \rangle . \tag{6.66}$$

The harmonic power spectrum coefficients C_ℓ are currently the best measured quantities of CMB anisotropies, as shown in fig. 6.1. The fundamental property by which low multipoles have more (statistical) uncertainty is called cosmic variance. Assuming ergodicity, we can understand causally disconnected points to be independent realizations of the same observable. Then, we can take advantage of the independence of C_ℓ on m, and average over all two-point functions with the same ℓ and different m. Since $-\ell \leq m \leq \ell$, we have more statistical power for large ℓ , and thus the measurement of the corresponding C_ℓ has less statistical error.

Using eqs. (6.65) and (6.66) and the properties of $Y_{\ell m}$, we retrieve the useful formula

$$C_{\ell} = \frac{1}{2\pi^2} \int \frac{\mathrm{d}k}{k} \left[\Theta_{\gamma,\ell}(\eta_0, k) \right]^2 \mathcal{P}_{\mathcal{R}}(k). \tag{6.67}$$

The transfer functions $\Theta_{\gamma,\ell}$ can be computed by solving eq. (6.61) numerically. Since this is computationally costly, it is more convenient to use a line-of-sight integral, where we trace the evolution of CMB photons from the last-scattering surface to the Earth today. In this approach,

$$\Theta_{\gamma,\ell}(\eta_0, k) = \int_{\eta_{\text{in}}}^{\eta_0} d\eta \left[g \left(\Theta_{\gamma,0} + \psi \right) + \left(g k^{-2} \theta_b \right)' + e^{-\tau} \left(\phi' + \psi' \right) \right] j_{\ell} [k(\eta_0 - \eta)] , \quad (6.68)$$

where $j_{\ell}(x)$ are the spherical Bessel functions and θ_b the velocity divergence of baryons. We have also introduced the optical depth

$$\tau(\eta) = \int_{\eta}^{\eta_0} \mathrm{d}\eta \, a n_e \sigma_T \,, \tag{6.69}$$

which is the integrated scattering rate from a time η until today. Then, the visibility function

$$g(\eta) = -\tau(\eta)' e^{-\tau(\eta)} \tag{6.70}$$

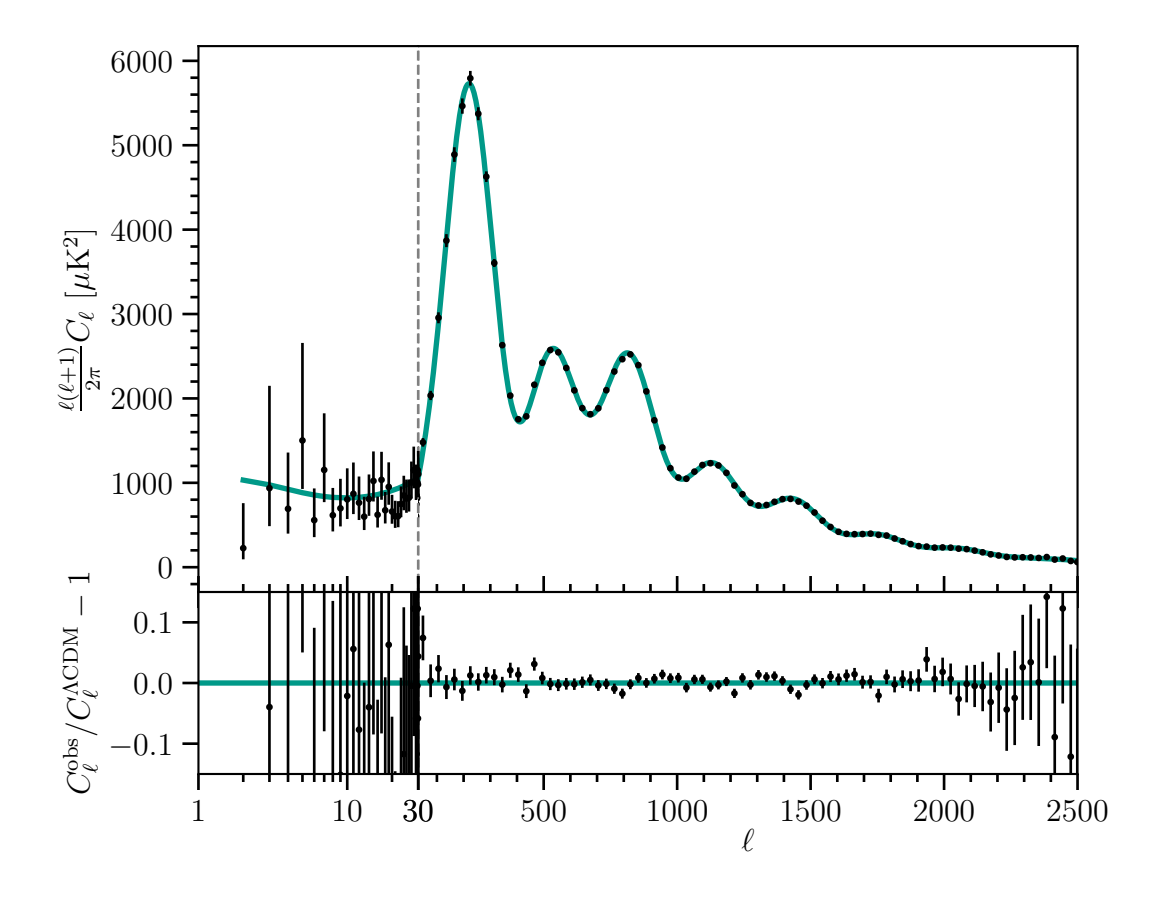


Figure 6.1: Power spectrum of the temperature anisotropies of the Cosmic Microwave Background. Black dots show observed data, while the teal solid line shows the best fit to the data from the 6 parameters of the ΛCDM model (with massless neutrinos). Namely, $100\theta_s = 1.04172$, $\omega_b = 0.02237$, $\omega_{\rm cdm} = 0.1200$, $\log(10^{10}A_s) = 3.044$, $n_s = 0.9649$, $\tau_{\rm reio} = 0.0544$.

is the probability that a photon, which has arrived to us, has experienced its last scattering at a time η . Both functions are plotted in fig. 6.2. In the instantaneous decoupling approximation, $e^{-\tau(\eta)}$ is a step-function which equals one after the last-scattering time η_{LS} , and $g(\eta)$ a delta function centered at η_{LS} .

Equation (6.68) offers a very intuitive way to understand the different effects that contribute to CMB anisotropies. In particular,

- The term $g\left(\Theta_{\gamma,0} + \psi\right)$ is the effect from the intrinsic temperature anisotropy of the photon-baryon fluid at the time of recombination $\Theta_{\gamma,0}$, redshifted by the local gravitational potential ψ . This is the usually called Sachs-Wolfe (SW) effect [431].
- The term $e^{-\tau} (\phi' + \psi')$ is the accumulated gravitational redshift as CMB photons travels from recombination to us, which is conventionally called the Integrated

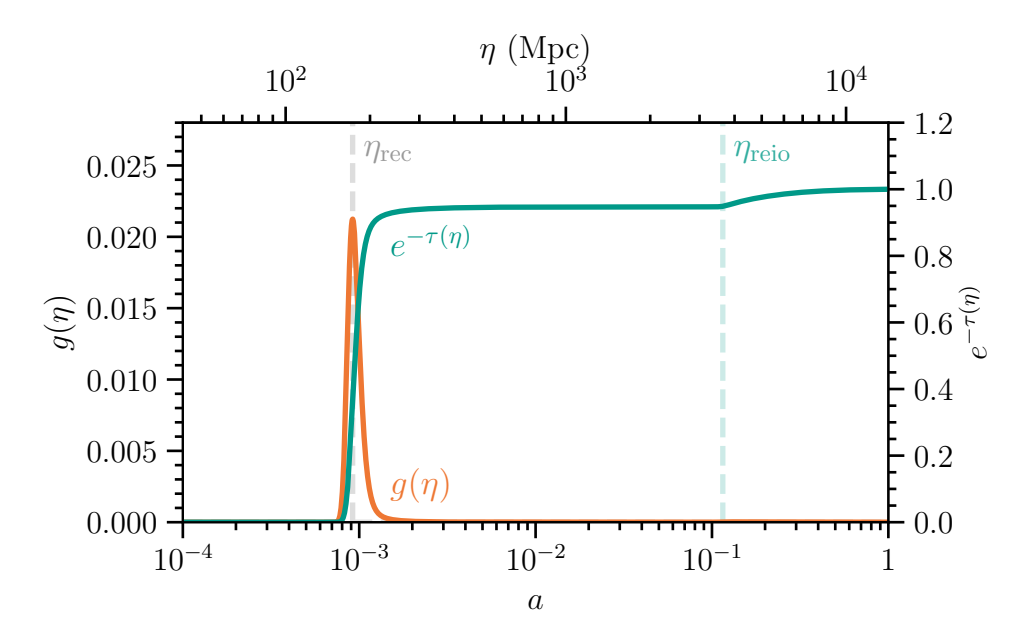


Figure 6.2: Evolution of the visibility function $g(\eta)$ and the exponential of the optical depth $e^{-\tau(\eta)}$. The visibility function is narrow, its peak marks the time of recombination $\eta_{\rm rec}$. On the contrary, $e^{-\tau(\eta)}$ grows close to unity just after recombination. Then, $n_e = 0$ and the optical depth remains constant until the reionization time $\eta_{\rm reio}$. In eq. (6.68), terms with $g(\eta)$ are evaluated only around recombination, while terms with $e^{-\tau(\eta)}$ are only evaluated at times just after recombination.

Sachs-Wolfe (ISW) effect [431]. Notice that a photon crossing a static potential well would experience a blueshift and a redshift exactly equal when entering and exiting the potential well, respectively. Then, in order to make a net effect on the photon, the gravitational potentials must evolve while the photon is inside them. Technically, the term ψ' accounts for gravitational redshift, while ϕ' accounts for the time dilation redshift. Potentials can only decay if the Universe is *not* matter-dominated [426]. Then, the ISW is usually split in an early ISW contribution, due to residual radiation left shortly after recombination; and a late ISW, due to the Λ -accelerated expansion.

• The term $(gk^{-2}\theta_b)'$ is an anisotropic Doppler shift due to the different peculiar velocities of the photon-emitting baryons at the last-scattering surface.

Furthermore, on their way to Earth, CMB photons get randomly deflected by the gravitational pull of the large-scale structure of the Universe [426, 432]. This weak gravitational lensing is a second-order non-linear effect, since it is a perturbative deflection of perturbative anisotropies, but with the precision of current data it is detectable. Lensing has two observable features on CMB anisotropies, that are more prominent at high multipoles. First, it smoothes out the power spectrum, since it mixes photons coming from different points in the last scattering surface. Second, it transfers power from large

scales to small scales, due to its non-linear nature. This leads to increased anisotropies at high ℓ .

6.3.3 A modified separation of the Sachs-Wolfe effects

While artificial, the standard separation between the SW and ISW effects provides an intuitive explanation for the different contributions to CMB anisotropies. However, this separation is not particularly appropriate to study the impact of neutrinos. In particular, both $(\Theta_{\gamma 0} + \psi)$ and $(\phi' + \psi')$ depend on the anisotropic stress σ even at super-horizon scales [425], which can be non-negligible in the presence of neutrinos. Thus, the SW contribution to modes that are much larger than the horizon would depend on σ ; and, as σ changes with time, there would be an ISW effect even for modes that are well outside the horizon. This would contradict the expected super-horizon behavior of adiabatic perturbations: as $k \to 0$, these perturbations behave as background and their evolution cannot depend on perturbation-related quantities such as σ .

Indeed, one can numerically check that the $\ell \to 0$ limit of eq. (6.68) is independent of the anisotropic stress around recombination, even if the SW and ISW terms separately are not. Technically, the SW term can be integrated by parts, leading to terms proportional to $e^{-\tau}$ that may as well be interpreted as an ISW contribution. Physically, as argued by Bardeen in his seminal paper on gauge-invariant cosmological perturbations [433], there is an ambiguity of what one means by a temperature or metric perturbation at scales comparable to or bigger than the horizon.

To facilitate physical understanding, below we redefine the separation between SW (understood as the temperature fluctuation at recombination, redshifted by the local gravitational potential) and ISW (understood as the accumulated gravitational redshift from recombination until today) contributions, so that they both depend only on background quantities in the $k \to 0$ limit [3].

To such purpose, we split the last term in eq. (6.68) as

$$\phi + \psi = \frac{6(1+w)}{5+3w} \left[\phi + \frac{2}{3(1+w)} \left(\psi + \frac{\phi'}{\mathcal{H}} \right) \right] - \frac{1+3w}{5+3w} \left(\phi - \psi + \frac{2}{3} \frac{\phi'}{\mathcal{H}} \frac{6}{1+3w} \right). \tag{6.71}$$

We identify the comoving curvature perturbation

$$\mathcal{R} \equiv \phi + \frac{k^{-2}\theta}{\mathcal{H}} = \phi + \frac{2}{3(1+w)} \left(\psi + \frac{\phi'}{\mathcal{H}}\right), \tag{6.72}$$

where we have used eq. (6.53) to express ϕ and ψ in terms of θ . Thus, we can rewrite

eq. (6.71) as

$$\phi + \psi = \frac{6(1+w)}{5+3w} \mathcal{R} - \frac{1+3w}{5+3w} \left(\phi - \psi + \frac{2}{3} \frac{\phi'}{\mathcal{H}} \frac{6}{1+3w} \right). \tag{6.73}$$

Then, we have separated $\phi + \psi$ in a first term which is conserved on super-horizon scales (except for the background variation of w), and a term which explicitly depends on the shear (see eq. (6.55)). Substituting eq. (6.73) in the third term in eq. (6.68), and integrating by parts the second term in eq. (6.73), we obtain

$$\Theta_{\gamma\ell}(\eta_0, k) = \int_{\eta_{\text{in}}}^{\eta_0} \left\{ g(\eta) \Theta_{\gamma\ell}^{\text{SW}} + \left[g(\eta) k^{-2} \theta_b \right]' j_\ell \left[k \left(\eta_0 - \eta \right) \right] + e^{-\tau} \Theta_{\gamma\ell}^{\text{ISW}} \right\} d\eta, \qquad (6.74)$$

with

$$\Theta_{\gamma\ell}^{SW} \equiv \left[\Theta_{\gamma 0} + \psi + \frac{1+3w}{5+3w} \left(\phi - \psi + \frac{2}{3} \frac{\phi'}{H} \frac{6}{1+3w} \right) \right] j_{\ell} \left[k \left(\eta_{0} - \eta \right) \right] = \\
= \left[\frac{1+3w}{5+3w} \mathcal{R} + \left(\Theta_{\gamma 0} + \frac{k^{-2}\theta}{H} \right) \right] j_{\ell} \left[k \left(\eta_{0} - \eta \right) \right] ,$$
(6.75)

where we have used the Einstein equations to go from the first to the second line; and

$$\Theta_{\gamma\ell}^{\text{ISW}} \equiv \left(\frac{6(1+w)}{5+3w}\mathcal{R}\right)' j_{\ell}[k(\eta_{0}-\eta)]
-\frac{1+3w}{5+3w}\left(\phi-\psi+\frac{4}{1+3w}\frac{\phi'}{\mathcal{H}}\right)k j_{\ell}'[k(\eta_{0}-\eta)].$$
(6.76)

This definition of the SW and ISW contributions are shown and compared to the standard definitions in fig. 6.3. The first term in eq. (6.75) is, on super-horizon scales, explicitly σ -independent. Since on such scales $\mathcal R$ is conserved, it only depends on the background quantity w—the amplitude of super-horizon perturbations does depend on the background equation of state [427, 434]—, and provides the $\ell \to 0$ SW plateau of the CMB power spectrum [426, 431],

$$\lim_{\ell \to 0} \ell(\ell+1) C_{\ell}^{\text{SW}} \approx 8 \left[\frac{1 + 3w(\eta_{\text{rec}})}{5 + 3w(\eta_{\text{rec}})} \right]^2 A_s.$$
 (6.77)

This coincides with the standard result $\ell(\ell+1)C_\ell^{\rm SW} \approx 8A_s/25$ for matter domination, $w_{\rm tot}(\eta_{\rm rec}) = 0$ [426, 431]. The second term in eq. (6.75) is zero for super-horizon scales and adiabatic perturbations (see section 6.2.2). It corresponds to one of the gauge-invariant density perturbations defined by Bardeen [433], and it represents the photon temperature perturbations in a gauge comoving with matter.

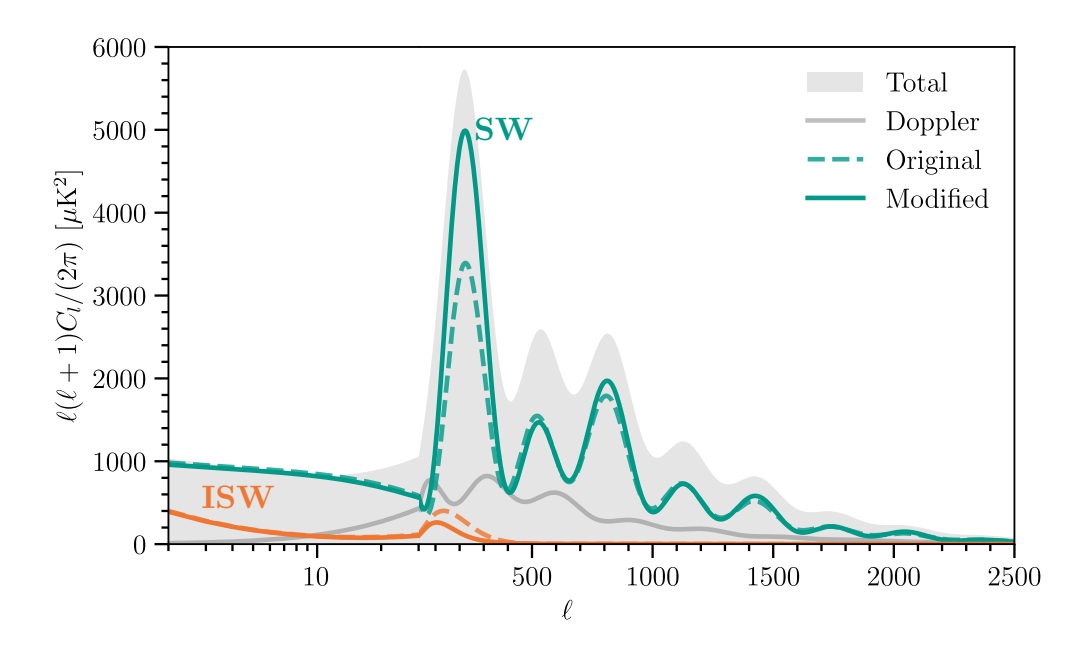


Figure 6.3: Decomposition of the CMB temperature anisotropies in the Sachs-Wolfe effects. Solid lines show our modified definitions of the SW (teal, eq. (6.75)) and ISW (orange, eq. (6.76)), while dashed lines show their original definitions (eq. (6.68)). The gray filled region and the gray solid line show the total C_{ℓ} and the Doppler term, respectively, which remain unmodified. As expected from its definition in eq. (6.67), the different C_{ℓ} are not directly additive.

The first term in eq. (6.76) is also, on super-horizon scales, explicitly σ -independent. It only introduces an ISW effect if w changes, which would affect the super-horizon gravitational potentials. The second term in eq. (6.76) is explicitly suppressed as $k \to 0$.

6.4 Big Bang Nucleosynthesis

Big Bang Nucleosynthesis (BBN) is the process by which the primordial light elements are formed in the first twenty minutes of the Universe. Mainly, 2 H (deuterium), 3 He, 4 He and 7 Li. Thanks to CMB observations, we know that the primordial Universe was thermal, dense and hot enough for nuclear reactions to take place. Furthermore, from CMB measurement that the particle content of the very early Universe was vastly dominated by photons, with the baryon-to-photon ratio $\eta \sim \mathcal{O}(10^{-10})$, measured with percent precision [55]. For going beyond this section, we recommend [424, 435].

Initially, at energies GeV $\gtrsim T_{\gamma} \gtrsim 2\,\mathrm{MeV}$, the matter content of the universe is in the form of free nucleons, i.e., protons and neutrons. Neutrinos are still in thermal

equilibrium with the plasma through the processes

$$n + \nu \leftrightarrow p + e^{-},$$

 $n + e^{+} \leftrightarrow p + \nu,$
 $n \leftrightarrow p + e^{-} + \nu,$ (6.78)

and thus $T_{\nu} = T_{\gamma}$. These equations maintain the equilibrium abundances between neutrons and protons, which we describe as

$$X_i = A_i \frac{n_i}{n_B}, (6.79)$$

with A_i the mass number, n_i the volume density of the species $i=p,n,{}^2\mathrm{H},{}^3\mathrm{He},...,$ and $n_B=\sum_i A_i n_i$ the total baryon volume density. From the processes in eq. (6.78), the neutron-to-proton ratio at $T_\gamma\sim 2\,\mathrm{MeV}$ is set to $X_n/X_p\sim 0.37$ [424]. This is different from equality since neutrons and protons have a mass difference $\Delta=m_n-m_p\simeq 1.29333\,\mathrm{MeV}$ [435], which unbalances the processes. In general, a given reaction will cease to be efficient when its decay rate Γ is slower than the Hubble rate, that is, when,

$$\Gamma \lesssim H$$
. (6.80)

For neutrino interactions this happens at $T\sim 2\,\mathrm{MeV}$, and thus then neutrinos decouple. Still, equilibrium between neutrons and protons can still be maintained by

$$n + v \leftarrow p + e^{-},$$

$$n + e^{+} \rightarrow p + v,$$

$$n \rightarrow p + e^{-} + v,$$
(6.81)

At $T_{\gamma} \sim 0.8$ MeV, weak interactions fulfill eq. (6.80). At this point, the neutron-to-proton abundances are fixed to $X_n \simeq 0.17$ and from now on these are only reduced by neutron decay, to $X_n \simeq 0.135$ when nucleosynthesis starts. At $T_{\gamma} \sim 0.5$ MeV, electrons and positrons annihilate into photons and increase T_{γ} , but not T_{ν} (since they are decoupled). Then, at $T_{\gamma} \simeq 0.078$ MeV, deuterium can be formed efficiently because photons are not energetic enough for deuterium photodissociation to be efficient. This starts a chain of nuclear reactions which ends up producing the light elements until $T \sim 0.01$ MeV, when nucleosynthesis ends.

⁴He abundance can be measured by observing low-metallicity stars in primitive galaxies [436–440]. Deuterium abundance is obtained from the observation of a few cosmological clouds at high redshift which absorb the light of even more distant quasars

on their line of sight, e.g., [441–444]. ³He has not yet been observed outside our Galaxy and therefore only an upper bound exists [445, 446]. ³Li is also obtained by looking at old galaxies, e.g., [447–449], but its modelisation is tricky and the current measurement is in tension with the SM prediction, the so-called "lithium anomaly" [450]. Strictly speaking this ⁷Li abundance should be considered a lower bound [55]. All in all, we will use the reference values from the PDG [55],

$$Y_{\rm P} \equiv X_{^{4}\rm He} = 0.245 \pm 0.003 \,,$$

$$D/H \equiv n_{\rm D}/n_{^{1}\rm H} = (2.547 \pm 0.025) \times 10^{-5} \,,$$

$$^{3}\rm He/H \equiv n_{^{3}\rm He}/n_{^{1}\rm H} < (1.1 \pm 0.2) \times 10^{-5} \,[435] \,,$$

$$^{7}\rm Li/H \equiv n_{^{7}\rm Li}/n_{^{1}\rm H} = (1.6 \pm 0.3) \times 10^{-10} \,.$$

$$(6.82)$$

These observed values are shown in fig. 6.4 as yellow boxes. Light element abundances are extremely sensitive to the details of BBN. For instance, in the SM, the predicted values depend finely in the baryon-to-photon ratio. A joint fit with CMB provides an excellent agreement between the two cosmological probes at $\eta \equiv n_b/n_\gamma = (6.143 \pm 0.190) \times 10^{-10}$ [55]. The excellent agreement with the SM also makes BBN a powerful probe of BSM physics in the very-early Universe. For instance, a modification of the amount of radiation in the early Universe will modify its expansion rate, the duration of the different BBN epochs and the observed abundances. Additional radiation is usually written in terms of the number of relativistic degrees of freedom,

$$N_{\text{eff}} = \frac{\rho_{\text{rad}} - \rho_{\gamma}}{\frac{7}{8} \left(\frac{4}{11}\right)^{4/3} \rho_{\gamma}},\tag{6.83}$$

where $\rho_{\rm rad}=3p_{\rm tot}$ is the amount of radiation energy density. In the Standard Model, $N_{\rm eff}=3.044$, which corresponds to the three active neutrinos plus corrections from non-instantaneous decoupling and non-equilibrium neutrino heating [451–453]. $N_{\rm eff}$ is constrained by the CMB to $N_{\rm eff}=2.99^{+0.34}_{-0.33}$ [151] and by BBN to $N_{\rm eff}=2.843\pm0.154$ [55, 454], both of which are greatly compatible with the standard scenario. Then, the measurement of $N_{\rm eff}$ allows to strongly constrain models which predict non-standard relativistic species in the early Universe.

Concluding remarks

In this introduction to cosmology, we have had but a glance of the theoretical development required to bring cosmology to its precision era. From all the things that we have learned, I would like to emphasize three of them,

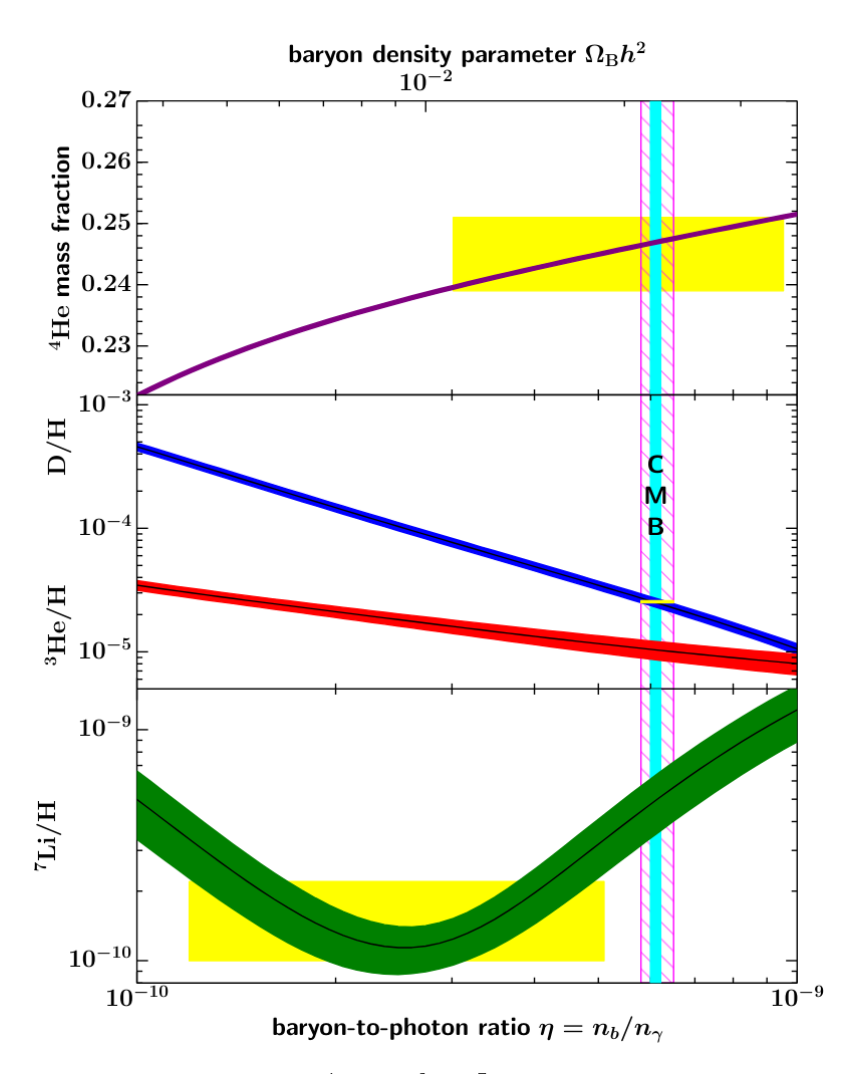


Figure 6.4: Primordial abundances of 4 He, D, 3 He, 7 Li as a function of η. Yellow boxes indicate the observed values, as in eq. (6.82), while bands show the 95% C.L. predictions from the SM. The cyan vertical band shows the measurement from CMB, while the hatched band shows the region where the measurements of deuterium and 4 He are compatible (both at 95% C.L.).

- The energy-momentum tensor T^{μ}_{ν} is the essential quantity which determines the evolution of the Universe, both at the background and perturbation levels. While it is a macroscopical quantity, we need microscopical assumptions in order to compute it.
- Perturbations are perturbations of something. Thus, there are some consistency laws between the variables that describe perturbations, i.e., δ , θ , c_s^2 and σ ; and the background evolution, i.e., w.
- The CMB is an integrated observable. That is, the CMB we observe today is not only dependent on the physics at recombination, but also in the evolution of the

gravitational potentials from recombination until today, specially of weak lensing.

With this knowledge in mind, we are ready to delve into neutrino cosmology. As a first step, the next chapter dissects the effects of neutrino masses in cosmology, in order to physically understand the meaning of cosmological bounds on them [3].

7 Origin of cosmological neutrino mass bounds: background *versus* perturbations

Negative masses? I am not bothered anymore, I would suggest to just analytically extend them to imaginary masses, and see what does the fit prefer.

Jordi Salvadó

Neutrinos are hot thermal relics, permeating the Universe and being the most abundant particles after Cosmic Microwave Background (CMB) photons. As we have seen in the first part of the thesis, neutrino masses have meant the first departure from the Standard Model (SM), where no gauge-invariant renormalizable neutrino mass term can be written. Yet neutrino oscillation experiments have robustly measured two squared-mass differences, $|\Delta m_{31}^2| \equiv |m_3^2 - m_1^2| \simeq 2.5 \cdot 10^{-3} \, \text{eV}^2$ and $\Delta m_{21}^2 \equiv m_2^2 - m_1^2 \simeq 7.5 \cdot 10^{-5} \, \text{eV}^2$ [21, 22, 89], confirming that neutrinos are massive and that the SM must be extended. Two mass orderings are possible, *normal* (NO, $\Delta m_{31}^2 > 0$) and *inverted* (IO, $\Delta m_{31}^2 < 0$), and oscillation experiments aim to determine it [24–28].

The absolute neutrino mass scale, however, remains unknown, as oscillations are only sensitive to mass differences. Oscillation results constrain $\sum m_{\nu} > 0.06$ eV for NO and $\sum m_{\nu} > 0.1$ eV for IO [21], and direct searches in the KATRIN experiment imply $\sum m_{\nu} < 1.35$ eV [150]; where $\sum m_{\nu} \equiv m_1 + m_2 + m_3$ is the total neutrino mass. This is shown in fig. 2.4. Even if neutrino masses are tiny, determining them is a mandatory first step to understand not only the origin of the particle masses and hierarchies, but also the Universe's evolution and structure formation—neutrinos are, so far, the only known form of (hot) dark matter.

In the early Universe, neutrinos are relativistic and behave as radiation, constituting up to 40% of the total energy density. At temperatures \lesssim MeV, their weak-interaction rate with the primordial plasma falls below the expansion rate of the Universe. Then, they decouple and stream freely, with their momentum being redshifted by the expansion. When neutrino momenta fall below their mass, neutrinos move at non-relativistic speeds, contributing to the Universe's matter energy density.

Due to their abundance, neutrinos leave a measurable imprint on cosmological observables. This leads to upper bounds on the total neutrino mass that are around $\sum m_{\nu} \lesssim 0.05$ –0.3 eV [153, 154, 455–457], potentially raising a tension between oscillation results and cosmological observations. As cosmological datasets grow, the neutrino mass will soon be either measured or a bound in clear conflict with oscillation

experiments will be placed [31-34].

Cosmological inferences, however, are indirect. The cosmological neutrino-mass bound is known to be correlated with, among others, the equation of state of dark energy [458–480]; the Hubble constant H_0 [151, 416, 417, 481] and the amplitude parameter σ_8 [151, 482, 483], which are in tension among different datasets [484–489]. The bound is also correlated with CMB lensing [421, 422, 466, 490–494], where some observations are anomalous [151, 495–497]. Finally, new physics in the neutrino sector could also modify the bound [498–519].

To clarify the robustness of cosmological neutrino-mass determinations, and the complementarity with direct searches, it is key to understand the physical effects of neutrino masses that cosmology is most sensitive to [424, 520–522]. Is current and upcoming data only sensitive to the background energy in neutrino masses, degenerate with other sources of energy and cosmological unknowns? Or is it sensitive to a characteristic scale-dependent imprint, induced by neutrinos not moving at the speed of light?

In this Chapter, we explicitly separate background neutrino-mass effects, which capture the evolution of the average neutrino energy density; from perturbations effects, which capture "kinematic" scale-dependent effects directly related to the neutrino velocity. As a first step, we focus on their impact on CMB anisotropies, which is sensitive to both background and perturbations effects. To gain intuition, we study in detail the physical origin of detectable effects. Finally, we carry out an analysis of current CMB data, finding out that it mostly constraints background neutrino-mass effects. In turn, the limit on perturbations effects is significantly weaker than the standard bounds.

Our results provide insight into the physical origin of cosmological neutrino-mass bounds, and serve as a benchmark of extended models that could affect them. As one direct consequence, we find that any change on the background expansion history that is degenerate with the impact of neutrino masses can strongly affect the cosmological neutrino-mass determination. Our definitions of background and perturbations effects are not tied to particular observables (e.g., CMB anisotropies are perturbations, but their evolution is sensitive to the background expansion rate), providing a generic framework to understand the cosmological effects of neutrino masses.

The structure of this chapter is as follows. In section 7.1, we describe our formalism to separate background and perturbations effects. In section 7.2, we examine and illustrate their physical effects on CMB anisotropies at different angular scales. In section 7.3, we present our statistical analysis together with the cosmological constraints on the key parameters of this study. Finally, we draw our conclusions in section 7.4.

7.1 Formalism

After decoupling from the primordial plasma, neutrinos only affect cosmological observables via gravity, i.e., via their stress-energy tensor T^{μ}_{ν} that enters the Einstein equations. In this Section, we set up the formalism to separate background and perturbations effects. We start from the most general parametrization, and compute the relevant quantities for the specific case of massive, non-interacting neutrinos. On top of establishing our framework, this identifies the neutrino-mass effects that cosmology can be sensitive to, enabling a better understanding of the cosmological neutrino-mass determination.

7.1.1 Evolution of the background

At the background level, neutrinos enter in the Friedmann eq. (6.11) explicitly as

$$\mathcal{H}^{2} = \frac{8\pi G}{3} a^{2} (\rho_{\gamma} + \rho_{b} + \rho_{cdm} + \rho_{\nu} + \rho_{\Lambda}). \tag{7.1}$$

We make explicit that, in this Section, we include photons, baryons, cold dark matter, neutrinos and a cosmological constant. Then, ρ_i the background energy density of each species i. This is the only equation where neutrinos modify the background evolution of the Universe.

As we have seen in eq. (6.16), the covariant conservation of the neutrino stress-energy tensor (eq. (6.14)) leads to the time dependence of the neutrino energy density ρ_{ν} ,

$$\frac{1}{\rho_{\nu}} \frac{\mathrm{d}\rho_{\nu}}{\mathrm{d} \ln a} = -3[1 + w_{\nu}(a)], \tag{7.2}$$

with $w_{\nu} \equiv p_{\nu}/\rho_{\nu}$ the neutrino equation of state and p_{ν} the neutrino pressure. That is, the cosmological impact of neutrinos at the background level is fully determined by their energy density at an initial time (usually parametrized in terms of $N_{\rm eff}$) and their equation of state, which controls how fast ρ_{ν} dilutes.

Differences among particle physics models enter when specifying w_{ν} . For massive, non-interacting neutrinos that decoupled while being relativistic,

$$w_{\nu}(a, m_{\nu}) = \frac{1}{3} \frac{\int d^{3}\vec{p} \frac{\vec{p}^{2}}{\sqrt{\vec{p}^{2} + m_{\nu}^{2}}} f_{0}(a|\vec{p}|)}{\int d^{3}\vec{p} \sqrt{\vec{p}^{2} + m_{\nu}^{2}} f_{0}(a|\vec{p}|)} = \frac{1}{3} \frac{\int q^{2} dq \frac{q^{2}}{\sqrt{q^{2} + a^{2} m_{\nu}^{2}}} f_{0}(q)}{\int q^{2} dq \sqrt{q^{2} + a^{2} m_{\nu}^{2}} f_{0}(q)}, \quad (7.3)$$

with $ec{p}$ linear momentum, q the comoving linear momentum, $m_{
u}$ each neutrino mass and

$$f_0(q) = \frac{1}{(2\pi)^3} \frac{1}{e^{q/T_0^{\nu}} + 1} \tag{7.4}$$

Background effect $\sum m_{\nu} = 0.06 \text{ eV}_{\text{(ν oscillations)}}$ $\sum m_{\nu} = 0.24 \text{ eV}_{\text{(CMB)}}$ $\sum m_{\nu} = 1.35 \text{ eV}_{\text{(KATRIN)}}$ 0.2Recombination $10^{-4} \quad 10^{-3} \quad 10^{-2} \quad 10^{-1} \quad 1$ Scale factor, a

Figure 7.1: Impact of $\sum m_{\nu}$ on the neutrino equation of state w_{ν} , that controls how the neutrino energy density dilutes. When the neutrino temperature drops below their mass, w_{ν} varies from 1/3 (radiation) to 0 (matter). The only background effect of neutrino masses is to change how fast the neutrino energy dilutes, which modifies the expansion rate of the Universe.

a Fermi-Dirac distribution, with $T_0^{\nu} \simeq 1.9 \, \mathrm{K}$ the current neutrino temperature. Equation (7.3) encloses the only background effect of neutrino masses.

Figure 7.1 shows how, by changing the equation of state, $\sum m_{\nu}$ determines how fast the neutrino energy density dilutes. We plot the equation of state of non-interacting massive neutrinos for different total neutrino masses. The chosen values are the smallest value allowed by neutrino oscillation experiments, $\sum m_{\nu} > 0.06 \, \mathrm{eV}$ [21–23]; the current cosmological limit from Planck CMB data alone, $\sum m_{\nu} < 0.24 \, \mathrm{eV}$ [151]; and the current limit from the KATRIN experiment, $\sum m_{\nu} < 1.35 \, \mathrm{eV}$ [150].

As the figure shows, $\sum m_{\nu}$ controls at which time w_{ν} switches from 1/3 (radiation, $\rho_{\nu} \propto a^{-4}$) to 0 (matter, $\rho_{\nu} \propto a^{-3}$). The change happens earlier for higher $\sum m_{\nu}$, leading to a slower dilution of ρ_{ν} in eq. (7.1) due to the energy in neutrino masses. Hence, the only background effect of increasing neutrino masses, with other parameters fixed, is to increase the expansion rate of the Universe.

For instance, the background effect of a mass corresponding to current CMB limits (orange line) is that the neutrino energy density dilutes as radiation until $z \sim 10^3$. While in the minimal scenario only neutrino masses control this effect, it is rather indirect, and non-minimal cosmological extensions —either a different neutrino equation of state or additional background components— may mimic it [498, 499, 502–519].

Implementation. To implement these background effects, we parametrize w_{ν} as in the massive, non-interacting case $w_{\nu} = w_{\nu}(a, \sum m_{\nu}^{\text{Backg.}})$; with $\sum m_{\nu}^{\text{Backg.}}$ a parameter that we name *background neutrino mass*. Then, we solve eq. (7.2) for an equation of state of massive, non-interacting neutrinos with total mass $\sum m_{\nu}^{\text{Backg.}}$,

$$\rho_{\nu}(a) = \rho_{\nu}(a_1) \exp \left[-3 \int_{a_1}^{a} \frac{1 + w_{\nu}(a, \sum m_{\nu}^{\text{Backg.}})}{a} \, da \right], \tag{7.5}$$

where a_1 is an initial scale factor. For simplicity, we assume the standard initial energy density for three light neutrino species, [424]

$$\rho_{\nu}(a_1) = \frac{7\pi^2}{40a_1^4} (T_0^{\nu})^4, \qquad (7.6)$$

with the initial condition evaluated when neutrinos are ultrarelativistic, i.e., $T_0^{\nu}/a_1 \gg \sum m_{\nu}^{\text{Backg.}}$. The hereby computed neutrino energy density affects the expansion of the Universe via the Friedmann equation, eq. (7.1).

7.1.2 Evolution of perturbations

At the perturbations level, in the neutrino sector we define the energy density perturbation $\delta \rho_{\nu}$, the pressure perturbation δp_{ν} , the velocity divergence θ_{ν} , and the anisotropic stress σ_{ν} , following the definitions from eq. (6.32). These parameters source the perturbed Einstein eqs. (6.52) to (6.55). They evolve following energy-momentum conservation, which reads

$$\delta_{\nu}' = -(1 + w_{\nu})\theta_{\nu} + 3(1 + w_{\nu})\phi' - 3\mathcal{H}\left(c_{s,\nu}^2 - w_{\nu}\right)\delta_{\nu}, \qquad (7.7)$$

$$\theta_{\nu}' = -\mathcal{H}(1 - 3c_{\text{ad},\nu}^2)\theta + \frac{c_{s,\nu}^2}{1 + w_{\nu}}k^2\delta_{\nu} - k^2\sigma_{\nu} + k^2\psi, \qquad (7.8)$$

where $\delta_{\nu} \equiv \delta \rho_{\nu}/\rho_{\nu}$, $c_{\rm s,\nu}^2 \equiv \delta p_{\nu}/\delta \rho_{\nu}$ is the so-called squared sound-speed, and

$$c_{\text{ad},\nu}^2 \equiv \frac{p_{\nu}'}{\rho_{\nu}'} = w_{\nu} - \frac{w_{\nu}'}{3\mathcal{H}(1+w_{\nu})},$$
 (7.9)

is the so-called adiabatic squared sound-speed.

To solve these equations, c_s^2 and σ (together with the background quantity w_ν) have to be provided. An indeterminacy arises because c_s^2 is gauge-dependent, that is, its value depends on the coordinate system used to separate background from perturbations. As we have seen in section 6.2.2, for adiabatic perturbations, the evolution equations for small k should only depend on background quantities. This may enforce a consistency

relation between c_s^2 , σ , and w_v . In particular, adiabatic conditions impose eq. (6.45), which means,

$$\lim_{k \to 0} c_{s,\nu}^2 \equiv \lim_{k \to 0} \frac{\delta p_{\nu}}{\delta \rho_{\nu}} = \frac{p_{\nu}'}{\rho_{\nu}'} = w_{\nu} - \frac{w_{\nu}'}{3\mathcal{H}(1 + w_{\nu})} \equiv c_{\text{ad},\nu}^2$$
 (7.10)

This issue can be overcome if, instead of $c_{s,v}^2$, the equations are written in terms of the so-called effective sound-speed [523–525]

$$c_{\text{eff},\nu}^2 \equiv \frac{k^2 c_{s,\nu}^2 \delta_{\nu} + 3\mathcal{H}(1 + w_{\nu}) c_{\text{ad},\nu}^2 \theta_{\nu}}{k^2 \delta_{\nu} + 3\mathcal{H}(1 + w_{\nu}) \theta_{\nu}}.$$
 (7.11)

Physically, $c_{\text{eff},\nu}$ is the sound speed in a frame comoving with neutrinos. Firstly, from section 6.2.1, $c_{\text{eff},\nu}^2$ is gauge-invariant. Then, we can invert its definition to retrieve

$$c_{s,\nu}^2 = c_{\text{eff},\nu}^2 + (c_{\text{eff},\nu}^2 - c_{\text{ad},\nu}^2) \frac{3\mathcal{H}(1+w_{\nu})\theta_{\nu}}{k^2 \delta_{\nu}}.$$
 (7.12)

And, from eq. (6.50), in the $k \to 0$ limit this immediately means $c_{s,v} = c_{\text{ad},v}$. Therefore, when expressing the evolution equations in terms of $c_{\text{eff},v}$, adiabatic perturbations behave as background as $k \to 0$ regardless of the values of $c_{\text{eff},v}$, σ , and w_v .

Equations (7.7) and (7.8) always hold. Differences among particle physics models (including neutrino-mass effects) enter when specifying $c_{\text{eff},\nu}^2$ and σ . For massive, non-interacting neutrinos; they can be computed from the perturbed distribution function

$$f_{\nu}(\vec{k}, q, \hat{n}, \eta) = f_0(q) \left[1 + \Psi(\vec{k}, q, \hat{n}, \eta) \right].$$
 (7.13)

The explicit expression for the stress-energy tensor leads to [425]

$$\delta_{\nu} = \frac{a^{-4}}{\rho_{\nu}} \int q^2 \, \mathrm{d}q \, \mathrm{d}\Omega \, \sqrt{q^2 + a^2 m_{\nu}^2} f_0 \Psi \,, \tag{7.14}$$

$$\theta_{\nu} = \frac{a^{-4}}{\rho_{\nu} + p_{\nu}} \int q^{2} \mathrm{d}q \, \mathrm{d}\Omega \, (i\vec{k} \cdot \hat{n}) f_{0} \Psi \,, \tag{7.15}$$

$$\delta p_{\nu} = \frac{a^{-4}}{3} \int q^2 \mathrm{d}q \,\mathrm{d}\Omega \,qv f_0 \Psi \,, \tag{7.16}$$

$$\sigma_{\nu} = \frac{a^{-4}}{\rho_{\nu} + p_{\nu}} \int q^2 \mathrm{d}q \,\mathrm{d}\Omega \,qv \left[\frac{1}{3} - (\hat{k} \cdot \hat{n})^2\right] f_0 \Psi, \tag{7.17}$$

where $\epsilon = \sqrt{q^2 + a^2 m_{\nu}^2}$ is the comoving energy and $v = q/\epsilon$ is the neutrino velocity. These expressions explicitly show the physical meaning of θ , δP , and σ for massive, non-interacting neutrinos. We detail how do we obtain Ψ in the following subsection.

Comoving wavenumber, \boldsymbol{k} [Mpc⁻¹]

Perturbations effects $\sum m_{\nu} = 0.06 \,\mathrm{eV}_{(\nu \,\mathrm{oscillations})}$ $\sum m_{\nu} = 0.24 \,\mathrm{eV}_{(\mathrm{CMB})}$ $\sum m_{\nu} = 1.35 \,\mathrm{eV}_{(\mathrm{KATRIN})}$ $\equiv \delta(\text{Pressure}) / \delta(\text{Energy Density})$ --k=10⁻⁴ Mpc Fixed a = 1 $=10^{-}$ \equiv Anisotropic stress \equiv Anisotropic stress 0.04 0.1 0.2 0.02-0.1-0.210 10 10

Figure 7.2: Impact of $\sum m_{\nu}$ on the comoving neutrino squared-sound-speed $c_{\rm eff}^2$ [left] and anisotropic stress σ [center, for fixed scale and varying time; right, for fixed time and varying scale]. These parameters control all perturbations effects of neutrinos (see text). $c_{\rm eff,\nu}^2$ is essentially scale-independent and falls when the neutrino temperature drops below their mass. In turn, σ gets suppressed above a characteristic scale, the neutrino free-streaming length, that depends on the neutrino mass.

Scale factor, \boldsymbol{a}

Scale factor, \boldsymbol{a}

Figure 7.2 shows that the anisotropic stress contains the leading "kinematic" effects of $\sum m_{\nu}$. We plot the time- and scale-dependence of $c_{\rm eff,\nu}^2$ and σ (normalized to an initial comoving curvature perturbation $\mathcal{R}=1$) of non-interacting massive neutrinos, for the same total neutrino masses as in fig. 7.1. We fix other cosmological parameters to the best fit of the Planck 2018 CMB analysis [151].

The scale dependence can be understood in terms of the neutrino free-streaming wavenumber [424]

$$k_{\rm FS}(a) = \sqrt{\frac{3}{2}} \frac{\mathcal{H}}{c_{\rm S,v}} \simeq 0.776 \frac{a^2 H}{H_0} \left(\frac{m_v}{1 \,\text{eV}}\right) h \,\text{Mpc}^{-1} \,.$$
 (7.18)

Physically, if $k < k_{\rm FS}$, perturbations tend to collapse gravitationally; whereas if $k > k_{\rm FS}$, velocity dispersion inhibits gravitational collapse [424]. Thus, $k_{\rm FS}$ directly encodes the "kinematic" impact of $\sum m_{\nu} \neq 0$, i.e., that nonrelativistic neutrinos move at velocities much slower than the speed of light.

As the left panel of fig. 7.2 shows, the time dependence of $c_{\rm eff,\nu}^2$ resembles that of the equation of state, falling from 1/3 to 0 when neutrinos become non-relativistic. The scale dependence introduced by $k_{\rm FS}$ is subleading (see Ref. [526]). Physically, super-horizon adiabatic perturbations behave as background, $c_{\rm eff,\nu}^2 \rightarrow c_{\rm ad}^2$ at all scales, and scale dependence only appears after subleading sub-horizon evolution [526, 527].

The center and right panels of fig. 7.2 show that the evolution of σ_{ν} is much more scale-dependent, with a characteristic feature at $k=k_{\rm FS}$. As the center panel shows, at

early times σ_{ν} oscillates. These oscillations get steadily damped with time, as neutrino free-streaming steadily suppresses perturbations. However, when the mode becomes larger than the free-streaming scale (which shrinks with time as neutrinos become non-relativistic), i.e., when $k < k_{\rm FS}$; neutrinos cluster instead of free-streaming, the momentum flux diminishes, and σ_{ν} decays much faster. The right panel also shows the two distinct behaviors as a function of scale at fixed time. At scales below the free-streaming scale, $k > k_{\rm FS}$, σ_{ν} is larger at large scales, which had less time to evolve and are less damped by free-streaming. On the contrary, at scales above the free-streaming scale, $k < k_{\rm FS}$, σ_{ν} is smaller at large scales, where neutrino clustering reduces the momentum flux.

Implementation. To separate the background and perturbations effects of neutrino masses, we parametrize $c_{\rm eff,\nu}^2$ and σ_{ν} as in the massive, non-interacting case; computing them for a value of $\sum m_{\nu}$ that we name *perturbations neutrino mass*, $\sum m_{\nu}^{\rm Pert.}$. Technically, $c_{\rm eff,\nu}^2$ and σ depend on $\sum m_{\nu}^{\rm Pert.}$ as well as on the gravitational potentials ϕ and ψ . Physically, this captures the backreaction of gravity onto neutrinos, in the same way that the background equation of state w_{ν} depends both on the neutrino mass and on the scale factor a (see eq. (7.3)). To compute this dependence for massive, non-interacting neutrinos; we start from the collisionless Boltzmann equation (see eq. (6.29)) for the perturbed neutrino distribution Ψ as defined in eq. (7.13) [425],

$$\frac{\partial \Psi}{\partial x} + i\mu \frac{q}{\epsilon} \Psi = \frac{\mathrm{d} \ln f_0}{\mathrm{d} \ln q} \left(i\mu \frac{\epsilon}{q} \psi - \frac{\mathrm{d} \phi}{\mathrm{d} x} \right) . \tag{7.19}$$

Here, $x \equiv k\eta$ is the product of Fourier wavenumber and conformal time, and f_0 is given by eq. (7.4) in the main text. Following Refs. [526, 528], this equation can be implicitly solved in terms of ϕ and ψ . After expanding in Legendre polynomials and integrating by parts,

$$\Psi_{\ell}(x) = \Psi(0)j_{\ell}(y(0,x)) + \frac{\mathrm{d}\ln f_{0}}{\mathrm{d}\ln q} \left\{ \phi(0)j_{\ell}(y(0,x)) - \phi(x)j_{\ell}(0) - \int_{0}^{x} \mathrm{d}x' \left[\frac{\epsilon}{q} \psi(x') + \frac{q}{\epsilon} \phi(x') \right] j_{\ell}' \left(y(x',x) \right) \right\},$$

$$(7.20)$$

where

$$\Psi(k, q, \mu, x) \equiv \sum_{\ell=0}^{\infty} (-i)^{\ell} (2\ell + 1) \Psi_{\ell}(k, q, x) P_{\ell}(\mu), \qquad (7.21)$$

with P_{ℓ} the Legendre polynomials; $j_{\ell}(x)$ the spherical Bessel functions; and

$$y(x_1, x_2) \equiv \int_{x_1}^{x_2} \frac{q}{\epsilon(x')} dx',$$
 (7.22)

the distance traveled by neutrinos between times x_1/k and x_2/k , divided by the mode size. The super-horizon adiabatic initial condition for Ψ , assuming radiation domination and ultrarelativistic neutrinos, is [425]

$$\Psi(x=0) = \frac{1}{2}\psi(\eta=0)\frac{d\ln f_0}{d\ln q}.$$
 (7.23)

These equations allow to explicitly compute $\Psi(k,q,\mu,\eta)$ as a function of the gravitational potentials and the neutrino dispersion relation $\epsilon(q)$. The latter depends on the total perturbations mass $\sum m_{\nu}^{\rm Pert.}$, since $\epsilon(q)=\sqrt{q^2+a^2(m_{\nu}^{\rm Pert.})^2}$ with $m_{\nu}^{\rm Pert.}$ each individual perturbations neutrino mass. Once Ψ is known, $c_{\rm eff,\nu}^2$ and σ can be computed from eqs. (7.11) and (7.14) to (7.17). For instance,

$$\sigma = \frac{8\pi a^{-4}}{3[\rho_{\nu} + p_{\nu}]_{\text{pert.}}} \int dq \, q^{2} \frac{q^{2}}{\epsilon} f_{0}(q) \frac{d \ln f_{0}}{d \ln q} \left\{ \left(\frac{1}{2} \psi(0) + \phi(0) \right) j_{2} \left(\frac{1}{k} \int_{0}^{\tau} \frac{q}{\epsilon(\tau')} d\tau' \right) - \frac{1}{k} \int_{0}^{\tau} d\tau' j_{2}' \left(\frac{1}{k} \int_{\tau'}^{\tau} \frac{q}{\epsilon(\tau'')} d\tau'' \right) \left[\frac{\epsilon(\tau')}{q} \psi(k, \tau') + \frac{q}{\epsilon(\tau')} \phi(k, \tau') \right] \right\} (7.24)$$

with

$$[\rho_{\nu} + p_{\nu}]_{\text{pert.}} = 4\pi a^{-4} \int dq \left(q^2 \epsilon + \frac{q^4}{3\epsilon} \right) f_0(q). \tag{7.25}$$

Note that this definition of σ is also consistent with the background. Adiabatic perturbations behave as background at super-horizon scales, which implies a diagonal stress-energy tensor, i.e., $\sigma \to 0$ as $k \to 0$. Equations (7.17) and (7.20) trivially fulfill this, because $j_2(0) = 0$. That is, the anisotropic stress is non-zero only when the distance travelled by neutrinos is of the order of the mode size. Since σ is a gauge-invariant quantity, this is true in all gauges.

Then, to implement these perturbations effects, we compute at every time $c_{\rm eff,\nu}^2$ and σ_{ν} from eqs. (7.20) and (7.24), corresponding to neutrinos with total mass $\sum m_{\nu}^{\rm Pert.}$. At the practical level, this is equivalent to solving a Boltzmann tower of Legendre multipoles, as in the standard manner [425]. Then, we solve the fluid eqs. (7.7) and (7.8), which must necessarily be fulfilled from the conservation of energy and momentum, with these $c_{\rm eff,\nu}^2$ and σ_{ν} . This is the proper way to evolve perturbations separately from the background, but consistent with it. We set initial conditions corresponding to adiabatic perturbations of an ultrarelativistic relic from eq. (6.47). The hereby computed neutrino energy density and pressure perturbations $\delta \rho_{\nu}$ and δP_{ν} , velocity divergence θ_{ν} , and anisotropic stress σ_{ν} affect the evolution of the Universe via the perturbed Einstein equations.

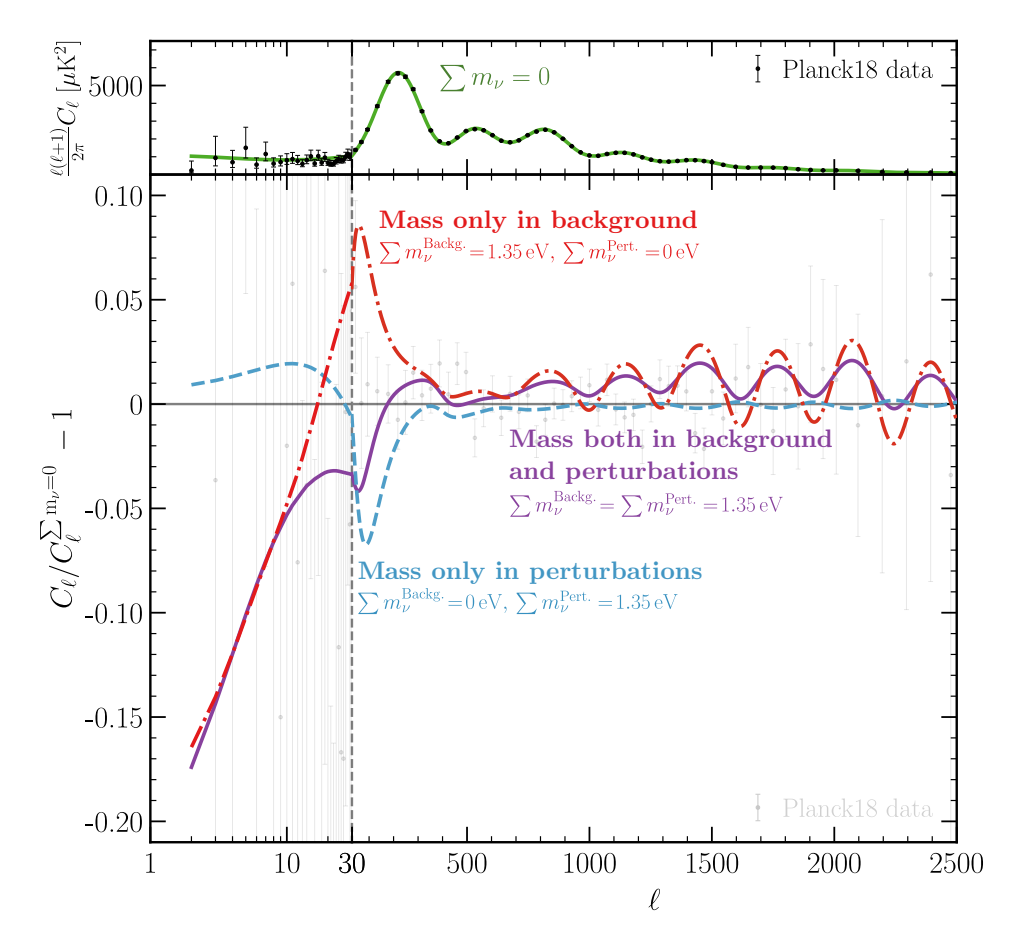


Figure 7.3: Background- and perturbations-induced impact of $\sum m_{\nu}$ on CMB anisotropies. As detailed in the main text; at low and high ℓ , the background affects the LISW effect, Silk damping, and lensing; at intermediate ℓ , both background and perturbations directly couple to photon-baryon oscillations via gravity. Most effects are background-induced. Perturbations-induced effects are mainly relevant at intermediate ℓ , where their effect is opposite to that of the background.

7.2 Physical effects on the CMB

In this Section we describe the different effects that $\sum m_{\nu}^{\text{Backg.}}$ and $\sum m_{\nu}^{\text{Pert.}}$ imprint on CMB anisotropies. All effects are collected in fig. 7.3, which already shows that $\sum m_{\nu}^{\text{Backg.}}$ and $\sum m_{\nu}^{\text{Pert.}}$ leave distinct signatures at different scales. To better represent the observable effects, in the figure we fix the well-measured cosmological parameters $\{100\theta_s, \omega_b, \omega_{\text{cdm}}, A_s, n_s, \tau_{\text{reio}}\}$ to the best fit of the Planck 2018 CMB analysis [151]. Below, we explore in detail the physical origin of the different effects at the different scales, while showing explicit checks and figures that illustrate them. To such purpose, it is convenient to separate the SW and ISW contributions, as defined in section 6.3.3, to distinguish between effects at recombination from effects after recombination. This is shown in fig. 7.4.

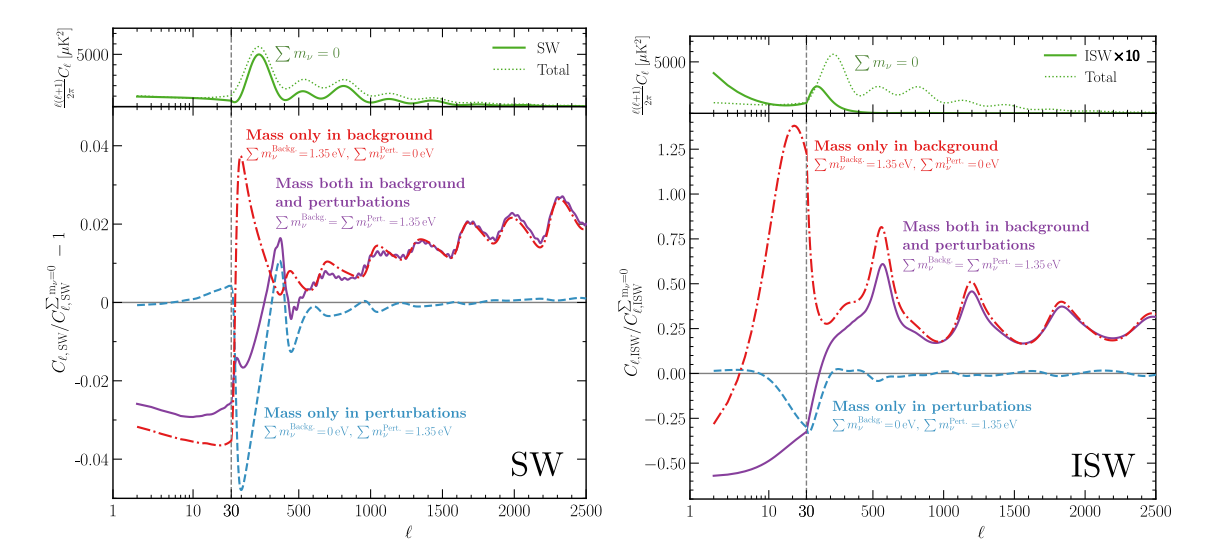


Figure 7.4: Background- and perturbations-induced impact of $\sum m_{\nu}$ on the Sachs-Wolfe (SW, left) and Integrated Sachs-Wolfe (ISW, right) effects as defined in eqs. (6.75) and (6.76), without including CMB lensing. The SW contribution can be understood as due to the temperature fluctuations at recombination, redshifted by the local gravitational potential. In turn, the ISW contribution can be understood as the accumulated gravitational redshift from recombination until today. Top plots show the contribution to the total CMB anisotropy power spectrum, and bottom plots the relative difference with respect to massless neutrinos. *The SW contribution, as defined in this work, only depends on background quantities as* $k \to 0$.

7.2.1 Low multipoles ($\ell \lesssim 10$)

Low multipoles correspond to modes that enter the horizon at very late times, when neutrinos constitute a subleading component of the energy density of the Universe. The main neutrino-mass effects in the CMB are induced in recombination, when the modes are larger than the horizon. Since, for adiabatic perturbations, the evolution of super-horizon modes depends only on background quantities, the effect of $\sum m_{\nu}^{\rm Pert.}$ at these scales is subdominant.

The main effect of $\sum m_{\nu}^{\text{Backg.}}$ is indirect and in the ISW effect. An increased $\sum m_{\nu}^{\text{Backg.}}$ slows down the dilution of the neutrino energy density, increasing H(z) and, in principle, modifying the observed angular scale of CMB peaks [424]

$$\theta_s = \frac{a(\eta_{\rm rec})r_s(\eta_{\rm rec})}{D_A(\eta_{\rm rec})} = \int_{z_{\rm rec}}^{\infty} \frac{c_{s,\gamma}(z)\,\mathrm{d}z}{H(z)} / \int_0^{z_{\rm rec}} \frac{\mathrm{d}z}{H(z)},\tag{7.26}$$

with $D_A(\eta_{\rm rec})$ the angular distance to recombination, $c_{s,\gamma}(z)$ the sound speed of the baryon-photon fluid and $z_{\rm rec}$ the redshift of recombination. Since θ_s is very-well measured, changes in it are compensated by modifying H_0 , which modifies the cosmological constant Λ . This changes the Λ -induced late-time boosting of large-scale anisotropies

through the late ISW. There is also a subleading ISW reduction caused by $\sum m_{\nu}^{\rm Pert.}$, as neutrino clustering slows down the Λ -induced decay of potentials. This effect is small, see figs. 7.3 and 7.4, and it is only present if $\sum m_{\nu}^{\rm Backg.} \neq 0$, because otherwise the neutrino energy density is too diluted at late times and neutrinos do not affect gravitational potentials.

However, the amplitude of super-horizon CMB perturbations also depends on the expansion rate of the Universe around recombination (see section 6.3) through the SW effect, which depends on $\sum m_{\nu}^{\rm Backg.}$ as shown in eq. (6.77). Increasing $\sum m_{\nu}^{\rm Backg.}$ reduces the neutrino contribution to $w_{\rm tot}$, reducing the $\ell \to 0$ limit of the SW contribution. In the left fig. 7.4, the blue line has the same background as $\sum m_{\nu} = 0$, and therefore the SW contribution is consequently suppressed as $\ell \to 0$. This only happens in our definition of $\Theta_{\gamma,\ell}^{\rm SW}$ in eq. (6.75), and shows that super-horizon modes can only depend on background quantities. The purple and red lines also share the same background evolution, but they have sub-percent differences as $\ell \to 0$. That is, there is a sub-percent effect of $\sum m_{\nu}^{\rm Pert.}$. This is reasonable, as these multipoles correspond to scales where $(k_{\ell=2}\eta_{\rm rec})^2 \sim 0.004$, so they are not completely out of the horizon around recombination, and already show partial sub-horizon evolution.

7.2.2 Intermediate multipoles ($10 \lesssim \ell \lesssim 500$)

Intermediate multipoles correspond to modes that are comparable with the horizon at recombination. Anisotropies at these scales are largely influenced by the gravitational potentials around recombination. These act as a driving term for photon-baryon acoustic oscillations, as seen in eq. (6.58). More precisely, decaying gravitational potentials increase the amplitude of oscillations. Physically, large initial potentials force the fluid into a highly compressed state. If they then decay, photon pressure overcomes gravity and the photon-baryon fluid oscillates with a larger amplitude. On top of that, decaying gravitational potentials reduce the redshift experienced by CMB photons as they leave the last-scattering surface, further increasing the anisotropies. For a detailed explanation of these effects, we refer to the work of Ref. [430]. Gravitational potentials decay in the radiation-dominated era [426], and since recombination happens soon after matter-radiation equality, they are still decaying when SW anisotropies get frozen (see fig. 7.5).

The effect of neutrino masses is then straightforward. A large $\sum m_{\nu}^{\text{Backg.}}$ increases the expansion rate of the Universe, boosting the decay of gravitational potentials, as shown in fig. 7.5; and increasing the SW contribution to CMB anisotropies, as shown in fig. 7.4. A large $\sum m_{\nu}^{\text{Pert.}}$ enhances neutrino clustering above the free-streaming scale, slowing down the decay of gravitational potentials, as shown in fig. 7.5; and decreasing the SW

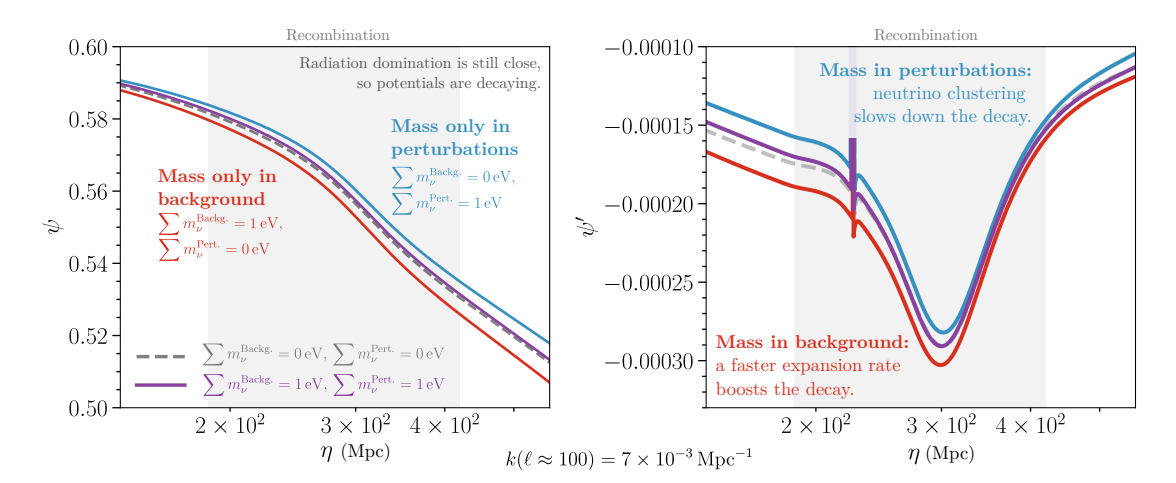


Figure 7.5: Gravitational potential ψ (left) and its derivative with respect to conformal time (right) for a mode entering the horizon ($k\eta_{\rm rec} \sim 1$) at the time of recombination. We normalize to an initial comoving curvature perturbation $\mathcal{R}=1$. This mode corresponds to $\ell \sim 100$. Background and perturbations neutrino masses affect intermediate- ℓ CMB anisotropies by boosting and slowing down the decay of ψ , respectively.

contribution to CMB anisotropies, as shown in fig. 7.4. On top of these effects, decaying gravitational potentials further increase the amplitude of CMB anisotropies through the integrated Sachs-Wolfe effect, boosting the aforementioned effects, as shown in fig. 7.4. In any case, background and perturbations-induced effects are opposite, and thus the net effect for standard massive neutrinos with $\sum m_{\nu}^{\rm Backg.} = \sum m_{\nu}^{\rm Pert.}$ is smaller, as shown in figs. 7.4 and 7.5. As we will show in the next Section, this leads to a partial degeneracy among both parameters in our data analysis.

Figure 7.6 shows the scale dependence of the clustering effect induced by $\sum m_{\nu}^{\text{Pert.}}$. As described in section 7.1.2, neutrino clustering is a scale-dependent "kinematic" effect that reflects that non-relativistic massive neutrinos move much slower than the speed of light. The characteristic scale, k_{FS} , is proportional to $\sum m_{\nu}^{\text{Pert.}}$, see eq. (7.18). As can be seen in fig. 7.6, if $\sum m_{\nu}^{\text{Pert.}}$ increases, the aforementioned depletion of CMB anisotropies affects higher multipoles.

We conclude that, while background effects are present at all multipoles, $\sum m_{\nu}^{\rm Pert.}$ on its own is mainly relevant at intermediate ℓ , where anisotropies are suppressed due to the direct gravitational impact of neutrino perturbations. Even if this effect can be partially hidden by a non-zero $\sum m_{\nu}^{\rm Backg.}$, unique background effects at high ℓ allow disentangling both.

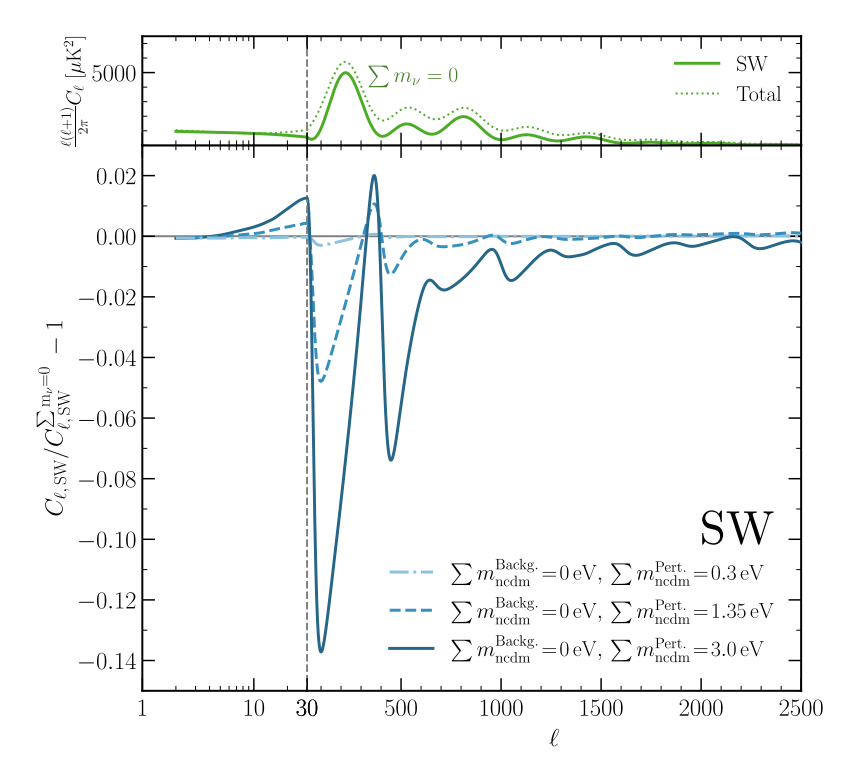


Figure 7.6: Scale-dependent impact of increasing $\sum m_{\nu}^{\text{Pert.}}$ on the SW contribution to CMB anisotropies. Larger $\sum m_{\nu}^{\text{Pert.}}$ slow down the decay of gravitational potentials through neutrino clustering (see fig. 7.5), reducing the amplitude of acoustic oscillations at recombination. Since neutrino clustering is a scale-dependent effect controlled by the free-streaming length, k_{FS} , eq. (7.18), larger perturbations masses increase k_{FS} and propagate the impact to higher multipoles.

7.2.3 High multipoles ($\ell \gtrsim 500$)

High multipoles correspond to modes that enter the horizon much before recombination. There are two main ways in which neutrino masses affect these modes, both of which are mainly sensitive to background effects. On the one hand, these modes are affected by diffusion damping due to the finite mean free path of photons before recombination. Modes are damped below the angular damping scale θ_D ,

$$\theta_D \sim \sqrt{\int_{z_{\text{rec}}}^{\infty} \frac{1+z}{n_e(z)\sigma_T} \frac{\mathrm{d}z}{H(z)}} / \int_0^{z_{\text{rec}}} \frac{\mathrm{d}z}{H(z)},$$
(7.27)

with n_e the electron density and σ_T the Thomson scattering cross section. Since θ_D only depends on background quantities, the high- ℓ contribution in fig. 7.4 depends only on $\sum m_{\nu}^{\rm Backg.}$ and not on $\sum m_{\nu}^{\rm Pert.}$. In particular, $\sum m_{\nu}^{\rm Backg.}$ slows down the dilution of the neutrino energy density, increasing H(z) both in the numerator and denominator. Overall, θ_D gets reduced, which is visible as an excess at high ℓ in fig. 7.3. This is purely an SW effect, and the ISW is negligible at high multipoles. We have checked that all

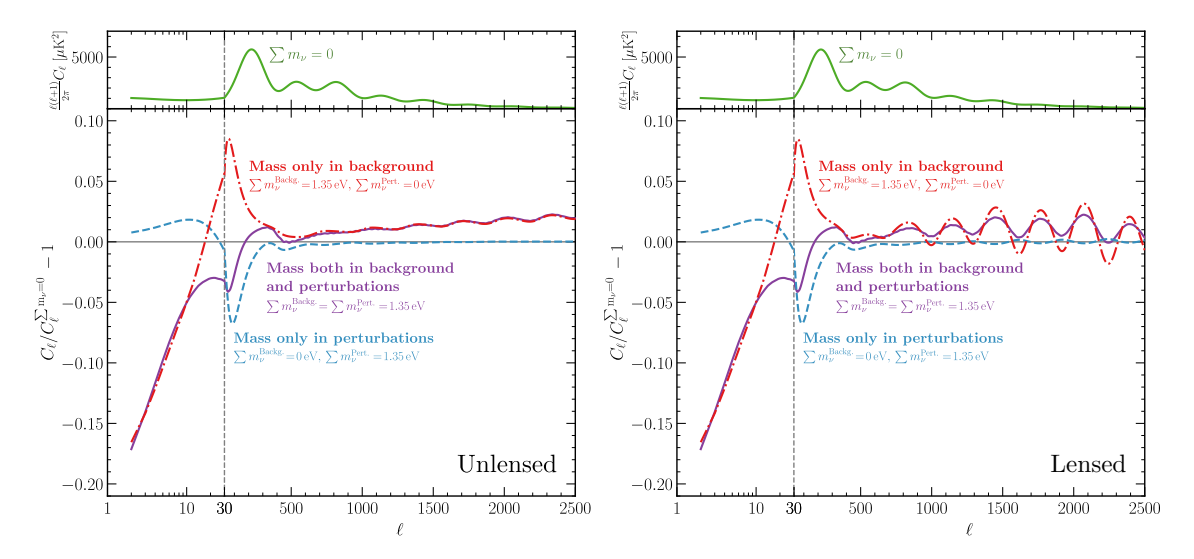


Figure 7.7: Impact of $\sum m_{\nu}^{\text{Backg.}}$ and $\sum m_{\nu}^{\text{Pert.}}$ on CMB anisotropies, with (left) and without (right) the effect of gravitational lensing. At high ℓ , unlensed anisotropies only depend on $\sum m_{\nu}^{\text{Backg.}}$ through diffusion damping. However, both $\sum m_{\nu}^{\text{Backg.}}$ and $\sum m_{\nu}^{\text{Pert.}}$ have an effect on the lensed anisotropies, and they do so in opposite directions. $\sum m_{\nu}^{\text{Backg.}}$ reduces CMB lensing, while $\sum m_{\nu}^{\text{Pert.}}$ enhances it.

the enhancement is due to a modified θ_D , because it can be completely removed by artificially keeping θ_D fixed (technically, this is achieved by changing the primordial Helium fraction Y_p , which rescales n_e in eq. (7.27) [424]).

On the other hand, high multipoles are affected by weak gravitational lensing, i.e., by the random gravitational deflection of CMB photons due to the large-scale structure of the Universe, as described in section 6.3.2. Lensing smooths out the power spectrum and transfers power from low multipoles to high multipoles [426]. Figure 7.7 shows how $\sum m_{\nu}^{\text{Backg.}}$ and $\sum m_{\nu}^{\text{Pert.}}$ control this effect. The left panel shows CMB anisotropies without lensing, while the right panel includes lensing. The high-\ell tail of the unlensed power spectrum only depends on $\sum m_{\nu}^{\text{Backg.}}$ through diffusion damping. Then, $\sum m_{\nu}^{\text{Backg.}}$ reduces CMB lensing by accelerating the expansion of the Universe, which suppresses structure formation. This is visible in fig. 7.7 as wiggles that are in phase with the CMB power spectrum. Weaker lensing also implies less power transferred to high multipoles, which leads to a slight depletion at $\ell \gtrsim 2000$. In turn, $\sum m_{\nu}^{\text{Pert.}}$ enhances neutrino clustering and structure growth, which enhances CMB lensing in a scale-dependent way. As $\sum m_{\nu}^{\rm Pert.}$ increases lensing, its effect is opposite to $\sum m_{\nu}^{\text{Backg.}}$, reducing the amplitude of the wiggles and slightly enhancing anisotropies in the $\ell \gtrsim 2000$ region. Perturbations mass effects are only relevant if $\sum m_{\nu}^{\text{Backg.}} \neq 0$, because otherwise the neutrino energy density is too diluted at late times and neutrinos do not affect gravitational potentials. Overall, the main impact of $\sum m_{
u}^{
m Pert.}$ on CMB lensing is to partially reduce the effect of $\sum m_{
u}^{
m Backg.}$ as

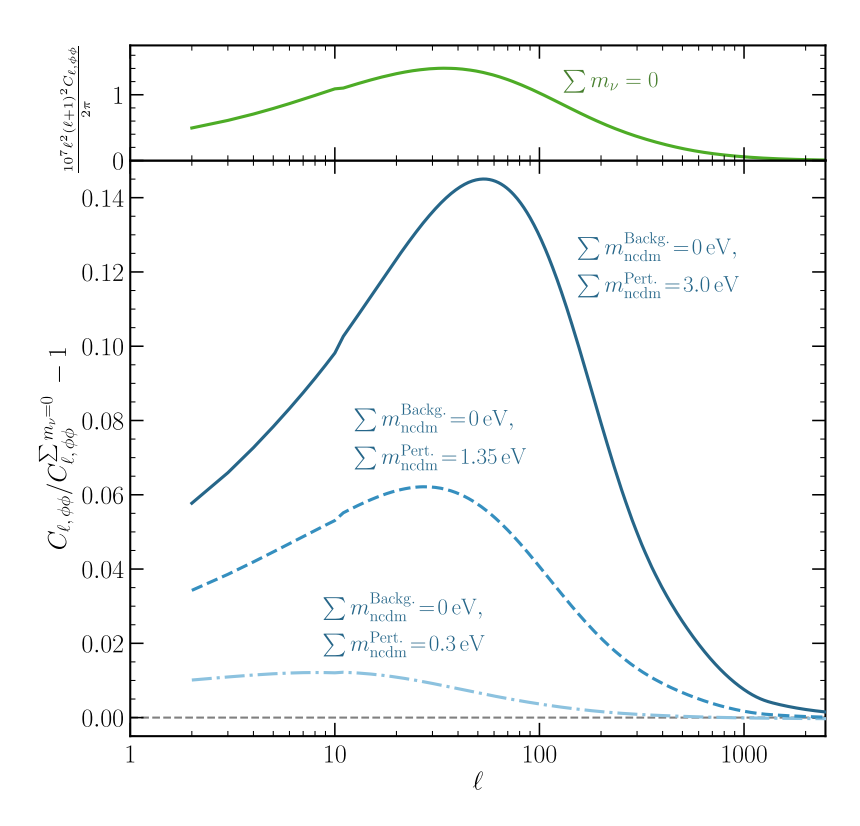


Figure 7.8: Scale-dependent impact of $\sum m_{\nu}^{\text{Pert.}}$ on the CMB lensing power spectrum. $\sum m_{\nu}^{\text{Pert.}}$ increases gravitational potentials through neutrino clustering, increasing CMB lensing. Neutrino clustering is a scale-dependent effect, controlled by the scale k_{FS} (see eq. (7.18)). A larger $\sum m_{\nu}^{\text{Pert.}}$ increases k_{FS} , shifting the impact of neutrino clustering to higher multipoles.

can be seen in fig. 7.3.

Finally, Figure 7.8 shows how the impact of $\sum m_{\nu}^{\text{Pert.}}$ is scale-dependent, with the characteristic scale k_{FS} being proportional to $\sum m_{\nu}^{\text{Pert.}}$ (see eq. (7.18)). We plot the power spectrum of the lensing potential, which is directly related to gravitational potentials [426, 432] (the scale dependence in CMB anisotropies is less evident, because lensing is nonlinear and the translation between k and ℓ is not straightforward). As the figure shows, $\sum m_{\nu}^{\text{Pert.}}$ enhances lensing, and increasing $\sum m_{\nu}^{\text{Pert.}}$ shifts its strongest impact to higher ℓ .

7.3 Constraints from Planck18 CMB data

In the Sections above, we have discussed how the different neutrino masses that we introduce affect the cosmological evolution. In short, $\sum m_{\nu}^{\rm Backg.}$ encodes the equation of state, i.e., how fast the neutrino energy density dilutes; while $\sum m_{\nu}^{\rm Pert.}$ contains a more direct "kinematic" effect related to the free-streaming nature of neutrinos. In this Section, we carry out an analysis of CMB data to quantify the allowed values of $\sum m_{\nu}^{\rm Backg.}$ and $\sum m_{\nu}^{\rm Pert.}$.

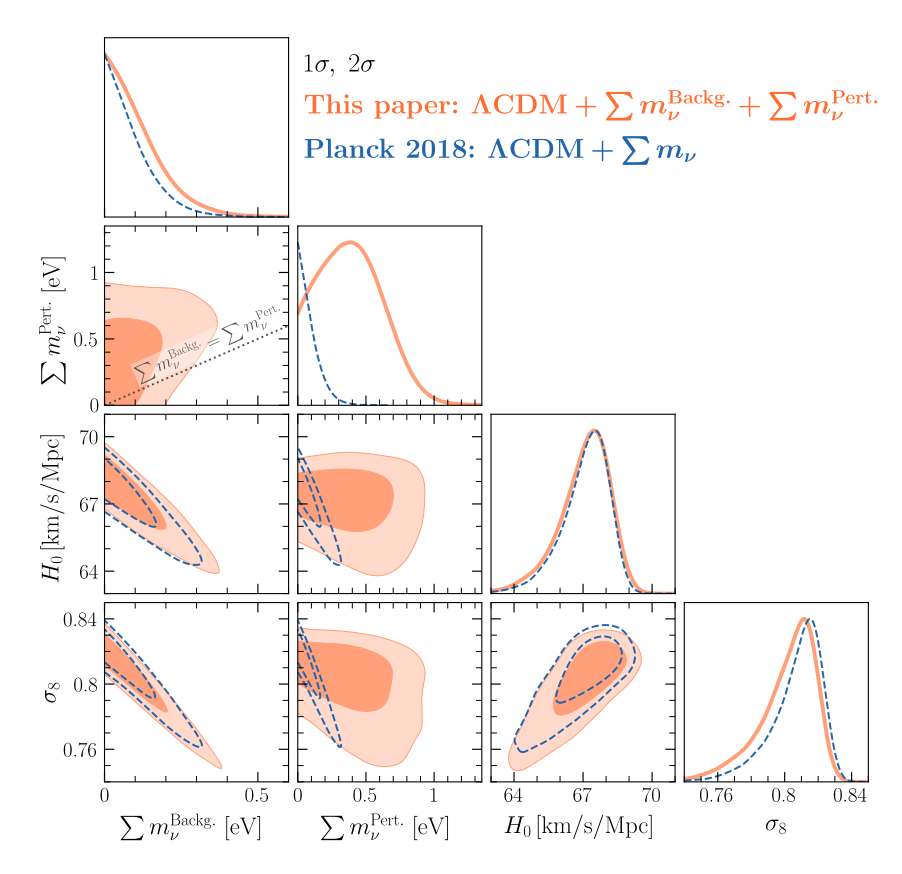


Figure 7.9: CMB limits on the separate neutrino-mass effects due to background and perturbations. The limit on $\sum m_{\nu}^{\text{Pert.}}$ gets strongly relaxed compared to that on $\sum m_{\nu}$. The CMB $\sum m_{\nu}$ limit is mostly a limit on background neutrino-mass effects.

7.3.1 Results

We analyze the Planck 2018 temperature, polarization, and lensing power spectra (TT, TE, EE+lowE+lensing in Ref. [151]). To do so, we modify the public code CLASS [527, 529–531], to solve the evolution of cosmological perturbations; and we explore the parameter space with the public Markov Chain Monte Carlo code COBAYA [532, 533]. Table 7.2 at the end of this chapter contains the priors on the cosmological parameters over which we scan.

Figure 7.9 shows that splitting neutrino mass effects among background and perturbations strongly increases the allowed perturbations effects. We show in solid the 1D posterior probabilities and 2D credible regions of our analysis for $\sum m_{\nu}^{\text{Backg.}}$, $\sum m_{\nu}^{\text{Pert.}}$, the Hubble parameter H_0 , and the amplitude parameter σ_8 . Dashed lines correspond to the standard scenario, i.e., $\sum m_{\nu}^{\text{Backg.}} = \sum m_{\nu}^{\text{Pert.}}$.

The $1-3\sigma$ credible intervals on the total neutrino mass, both for the standard scenario (where $\sum m_{\nu}^{\text{Backg.}} = \sum m_{\nu}^{\text{Pert.}}$) and for our analysis that splits among background and perturbations neutrino-mass effects, are found in table 7.1.

Planck 2018; 11, 1E, EE+lowE+lensing			
Mass type	68% CL	95% CL	99% CL
$\sum m_{\nu}$	< 0.11 eV	< 0.24 eV	< 0.35 eV
$\sum m_{ u}^{ m Backg.}$	< 0.13 eV	$< 0.29 \mathrm{eV}$	$< 0.40 \mathrm{eV}$
$\sum m_{ u}^{ ext{Pert.}}$	$0.40^{+0.19}_{-0.29}~{ m eV}$	< 0.79 eV	< 0.97 eV

Table 7.1: Neutrino-mass limits at different confidence levels. These results correspond to the posteriors shown in fig. 7.9. $\sum m_{\nu}$ refers to the standard scenario, $\sum m_{\nu}^{\text{Backg.}} = \sum m_{\nu}^{\text{Pert.}}$ [151].

That is, the standard limit on $\sum m_{\nu}$ is mostly a limit on $\sum m_{\nu}^{\rm Backg.}$ (the limit on the latter is slightly weaker due to a degeneracy with $\sum m_{\nu}^{\rm Pert.}$ that we discuss below). As the figure shows, the posterior probabilities of $\sum m_{\nu}$, in the standard analysis; and $\sum m_{\nu}^{\rm Backg.}$, in our analysis; almost match. The correspondence among $\sum m_{\nu}$ and $\sum m_{\nu}^{\rm Pert.}$, however, is null. In other words, CMB data tightly constraints the neutrino equation of state; but, compared to the standard scenario, the limit on "kinematic" effects of neutrino masses is relaxed by about a factor of 3.

The background neutrino mass is correlated with H_0 and σ_8 . These correlations are also present in the standard scenario, and they are due to the neutrino contribution to the total energy density of the Universe. Larger ρ_{ν} increases the expansion rate, which suppresses structure formation (i.e., σ_8); and, as described in the previous Section, modifies the angular scale of the CMB peaks that is degenerate with H_0 . These are both background effects, so $\sum m_{\nu}^{\text{Pert.}}$ is not strongly correlated with H_0 and σ_8 .

Finally, fig. 7.11 further includes the 1D posterior probabilities and 2D credible regions for all parameters in our analysis. All posteriors are well-contained within their priors, and the convergence of the MCMC run is determined by an R-1 < 0.02 Gelman-Rubin test [534, 535].

7.3.2 Discussion

Figure 7.10 (left) shows that intermediate- ℓ data constrains both perturbations and background mass effects, whereas high- ℓ data mainly constrains background-mass effects. In both cases, perturbations-mass effects can partially compensate background mass effects; we discuss this below. As in fig. 7.3, we fix $\{100\theta_s, \, \omega_b, \, \omega_{\rm cdm}, \, A_s, \, n_s, \, \tau_{\rm reio}\}$ to their Planck 2018 best-fit values [151]. The blue and purple lines are close to the 2σ allowed region in our analysis, whereas the red line is more strongly excluded.

As discussed in the previous Section, the sensitivity at intermediate multipoles is

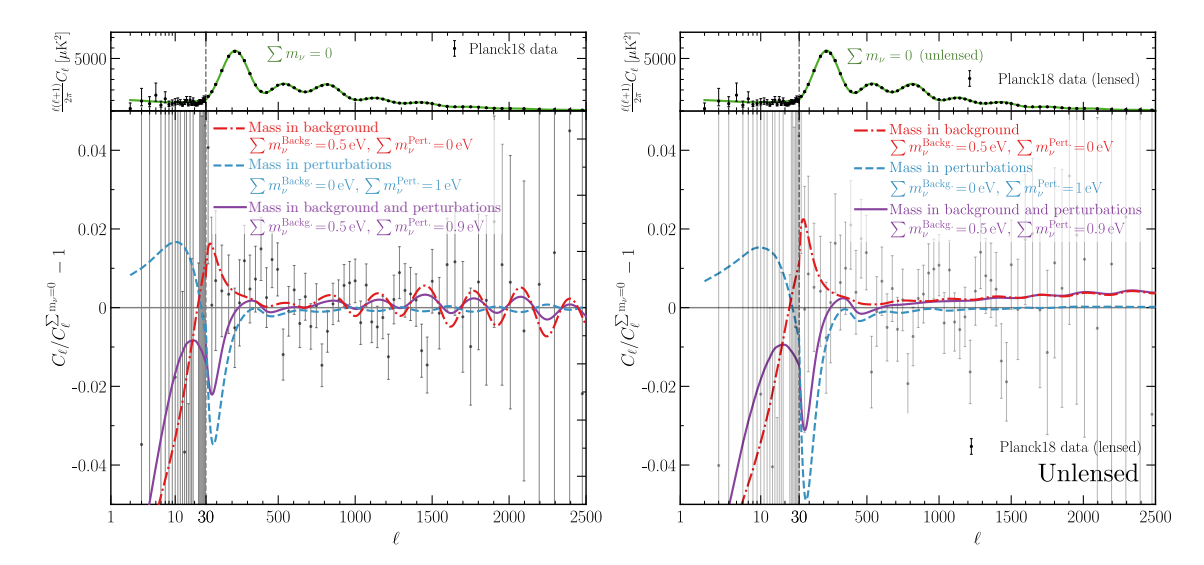


Figure 7.10: Impact on CMB anisotropies of parameters excluded by our analysis, with and without lensing effects. The left figure shows how background effects are most excluded by high- ℓ data (CMB lensing), and perturbations effects by intermediate- ℓ data (direct coupling via gravity). On the right, since the predictions are unlensed, but data is lensed, here the Planck18 data only shows visually the uncertainty of the measurements. Opposed physical effects induce a degeneracy between $\sum m_{\nu}^{\text{Pert.}}$ and $\sum m_{\nu}^{\text{Backg.}}$ (see text).

due to the direct impact of neutrino masses on the gravitational potentials. The high- ℓ sensitivity to background mass effects can be traced back to the impact on the damping tail and CMB lensing, as the right plot of fig. 7.10 shows. This is particularly relevant in light of the lensing anomaly: Planck 2018 data prefers more CMB lensing than what is present in the standard Λ CDM scenario [151, 495, 536–538] (see, however, Refs. [496, 497]). Since, as described in the previous Section, $\sum m_{\nu}^{\text{Backg.}}$ reduces CMB lensing, the anomaly enhances the high- ℓ constraints, and the resulting limit is somewhat stronger than what would be expected. This is visible in the bottom panel of fig. 7.10 as wiggles in the data that are out of phase with the effect of $\sum m_{\nu}^{\text{Backg.}}$. However, a value of $\sum m_{\nu}^{\text{Backg.}}$ that is excluded by our analysis predicts an unlensed damping tail well within error bars.

An interesting feature of fig. 7.9, also visible in fig. 7.10, is that when splitting neutrino masses into background and perturbations, $\sum m_{\nu}^{\text{Backg.}}$ and $\sum m_{\nu}^{\text{Pert.}}$ are partly degenerate. When $\sum m_{\nu}^{\text{Pert.}}$ increases, the limit over $\sum m_{\nu}^{\text{Backg.}}$ can relax by almost a factor of two. This is driven by opposite effects of background and perturbations: $\sum m_{\nu}^{\text{Backg.}}$ suppresses structure formation due to the increased expansion rate of the Universe, whereas $\sum m_{\nu}^{\text{Pert.}}$ enhances structure formation due to neutrinos clustering as matter. As described in the previous Section, this introduces opposite effects on the amplitude of CMB anisotropies, at intermediate ℓ ; and on CMB lensing, at high ℓ . The degener-

acy is not perfect, partly because increasing $\sum m_{\nu}^{\rm Backg.}$ also affects the CMB damping tail that is insensitive to $\sum m_{\nu}^{\rm Pert.}$. We also note from fig. 7.9 that the best fit for $\sum m_{\nu}^{\rm Pert.}$ is non-zero, with $\sum m_{\nu}^{\rm Pert.} = 0$ being excluded at $\sim 1\sigma$. This is driven by the lensing anomaly ($\sum m_{\nu}^{\rm Pert.}$ increases CMB lensing), but the result is not statistically significant.

Overall, our results explicitly show that the CMB bound on $\sum m_v$ is mainly a limit on background effects, i.e., on how the neutrino energy density evolves with time. Once we separate neutrino-mass effects into background and perturbations (the latter containing more direct "kinematic" signatures related to neutrino free-streaming), the limit on perturbations effects gets largely relaxed. This could serve as an insight for theories that evade cosmological neutrino mass bounds, as our results show that such theories should have a radiation-like dilution of the neutrino energy density until recombination.

7.4 Conclusions and Outlook

The absolute neutrino mass scale remains unknown. Cosmological surveys are close to either measuring it or excluding the lower limit set by oscillations. In this chapter, we explore the origin of the cosmological neutrino-mass bound from CMB data. Our results show that the driving constraint arises from the contribution of the energy in neutrino masses to the expansion of the Universe.

We focus on the macroscopic quantities that capture the cosmological impact of neutrinos. This enables us to explicitly discriminate, for the first time, between background and perturbations effects of neutrino masses. The separation can be understood in terms of standard "fluid" variables: the equation of state w_{ν} , which governs how fast the background neutrino energy density dilutes; the sound speed in the frame comoving with neutrinos $c_{\rm eff,\nu}^2$, which captures isotropic neutrino momentum flow; and the anisotropic stress σ , which captures anisotropic neutrino momentum flow. w_{ν} encloses all background effects, directly impacting the expansion rate of the Universe—which increases as $\sum m_{\nu}$ increases due to the energy in neutrino masses. In turn, $c_{\rm eff,\nu}^2$ and σ enclose the perturbations effects. $c_{\rm eff,\nu}^2$ is almost scale-independent, and σ contains the main "kinematic" impact of neutrino masses, related to the free-streaming scale set by neutrinos not moving at the speed of light.

Since our goal is to disentangle among background and perturbations effects, we explore two types of neutrino masses: the one that governs w_{ν} , that we name background neutrino mass $\sum m_{\nu}^{\rm Backg.}$; and the one that governs $c_{\rm eff,\nu}^2$ and σ , that we name perturbations neutrino mass $\sum m_{\nu}^{\rm Pert.}$. Although these parameters are phenomenological, they encode the distinct physical implications of neutrino masses in cosmology. Hence, they serve as a benchmark to understand the effects that cosmology is most sensitive

to, and to shed light on potential degeneracies of extended models with $\sum m_{\nu}$.

The effects on the CMB temperature anisotropies can be split into different multipole regions (see section 7.2). The low- ℓ region has a minor impact on the constraints due to cosmic variance. At high ℓ , $\sum m_{\nu}^{\rm Backg.}$ modifies the CMB damping tail, and both background and perturbations effects impact CMB lensing in opposite directions. While a larger $\sum m_{\nu}^{\rm Backg.}$ suppresses structure formation (and hence CMB lensing) by increasing the expansion rate of the Universe, a larger $\sum m_{\nu}^{\rm Pert.}$ enhances structure formation above the neutrino free-streaming scale. At intermediate ℓ , neutrino perturbations directly affect photon-baryon oscillations via gravity, where again the effects of $\sum m_{\nu}^{\rm Backg.}$ and $\sum m_{\nu}^{\rm Pert.}$ are opposite. As a consequence, there is a slight degeneracy among $\sum m_{\nu}^{\rm Backg.}$ and $\sum m_{\nu}^{\rm Pert.}$. Overall, high- ℓ data is mostly sensitive to background effects, whereas intermediate- ℓ data determines both background and perturbations effects.

We then carry out an analysis of Planck 2018 CMB data to shed light on the effects that observations constrain. We conclude that the Planck 2018 neutrino-mass bound is a bound on the background effects, i.e., on the evolution of the neutrino energy density. This provides a rule-of-thumb to understand if CMB data excludes a model with new physics in the neutrino sector: if its equation of state significantly deviates from $w_{\nu} = 1/3$ around recombination, the model is probably excluded.

The perturbations limit on "kinematic" effects of neutrino masses is consequently relaxed, $\sum m_{\nu}^{\rm Pert.} < 0.8$ eV. The limit is still competitive—models that dramatically affect free-streaming properties of neutrinos are still excluded—, and it is similar to the projected reach of KATRIN [150]; yet in the standard scenario such high neutrino masses are excluded within $\sim 7\sigma$. This result underscores the complementarity among laboratory and cosmological determinations of the neutrino mass.

In this work, we have focused on the consequences for the CMB of "energy-dilution" versus "kinematic" effects of neutrino masses. Since current and near-future observations of the matter power spectrum (particularly Baryon Acoustic Oscillation, BAO, measurements) have a strong impact on neutrino-mass determinations [153, 154], we will explore them in detail in incoming work [539]. For BAOs, which measure quantities that can be expressed in terms of background neutrino properties [498], we foresee a stronger impact on $\sum m_{\nu}^{\rm Backg.}$ than on $\sum m_{\nu}^{\rm Pert.}$.

Our separation among background and perturbation neutrino-mass effects opens many research avenues. The observed CMB-lensing excess drives the strong limit on $\sum m_{\nu}^{\text{Backg.}}$ and the best-fit for nonzero $\sum m_{\nu}^{\text{Pert.}}$ in fig. 7.9. In light of this, our framework could be explored with state-of-the-art CMB likelihoods where this anomaly is not present [421, 496, 497]. The opposite effects of $\sum m_{\nu}^{\text{Backg.}}$ and $\sum m_{\nu}^{\text{Pert.}}$ on CMB lensing, together with the scale-dependence of perturbations effects, could also be leveraged

to separate both effects in future high-precision determinations of CMB lensing [33, 34, 538, 540, 541]. Moreover, some cosmological tensions are correlated with neutrino masses, motivating new studies that address them in the context of our separation of neutrino-mass effects. This may shed light on the physics that can alleviate these tensions. Beyond pure cosmology studies, our results provide a benchmark to build models that evade the cosmological neutrino-mass bound. In short, the main way to relax the cosmological bound is by modifying the expansion history of the Universe, with the "kinematic" properties of the model being less important.

While we wait for a positive neutrino-mass signal from terrestrial experiments, cosmological measurements lead current limits. As they improve, we find ourselves in an era where cosmological limits are approaching values disfavored by oscillation experiments. If this tension grows, the solution may rely on a non-standard neutrino sector. If, in turn, a neutrino-mass signal is found, scrutinizing the robustness of this determination will be mandatory. In both cases, understanding the involved physical effects and degeneracies is key for solid progress in cosmology and particle physics. Future observations will guide the next steps for the physics of neutrinos, the first particle whose mass may be first measured outside laboratories.

Parameter	$\log(10^{10}A_{\mathrm{s}})$	n_{s}	$100\theta_{\mathrm{s}}$	$\omega_{ m b}$	$\omega_{ m cdm}$	$ au_{ m reio}$	$\sum m_{\nu}^{ m Backg.}$ [eV]	$\sum m_{\nu}^{\text{Pert.}} [\text{eV}]$
Prior	$\mathcal{U}[1.61, 3.91]$	\mathcal{U} [0.8, 1.2]	$\mathcal{U}[0.5, 10]$	$\mathcal{U}[0.005, 0.1]$	$\mathcal{U}[0.001, 0.99]$	$\mathcal{U}[0.01, 0.8]$	$\mathcal{U}[0.0, 3.0]$	$\mathcal{U}[0.0, 3.0]$

Table 7.2: Cosmological parameters that we scan over, and their corresponding priors. $\mathcal{U}[a, b]$ denotes a uniform distribution with lower limit a and upper limit b.

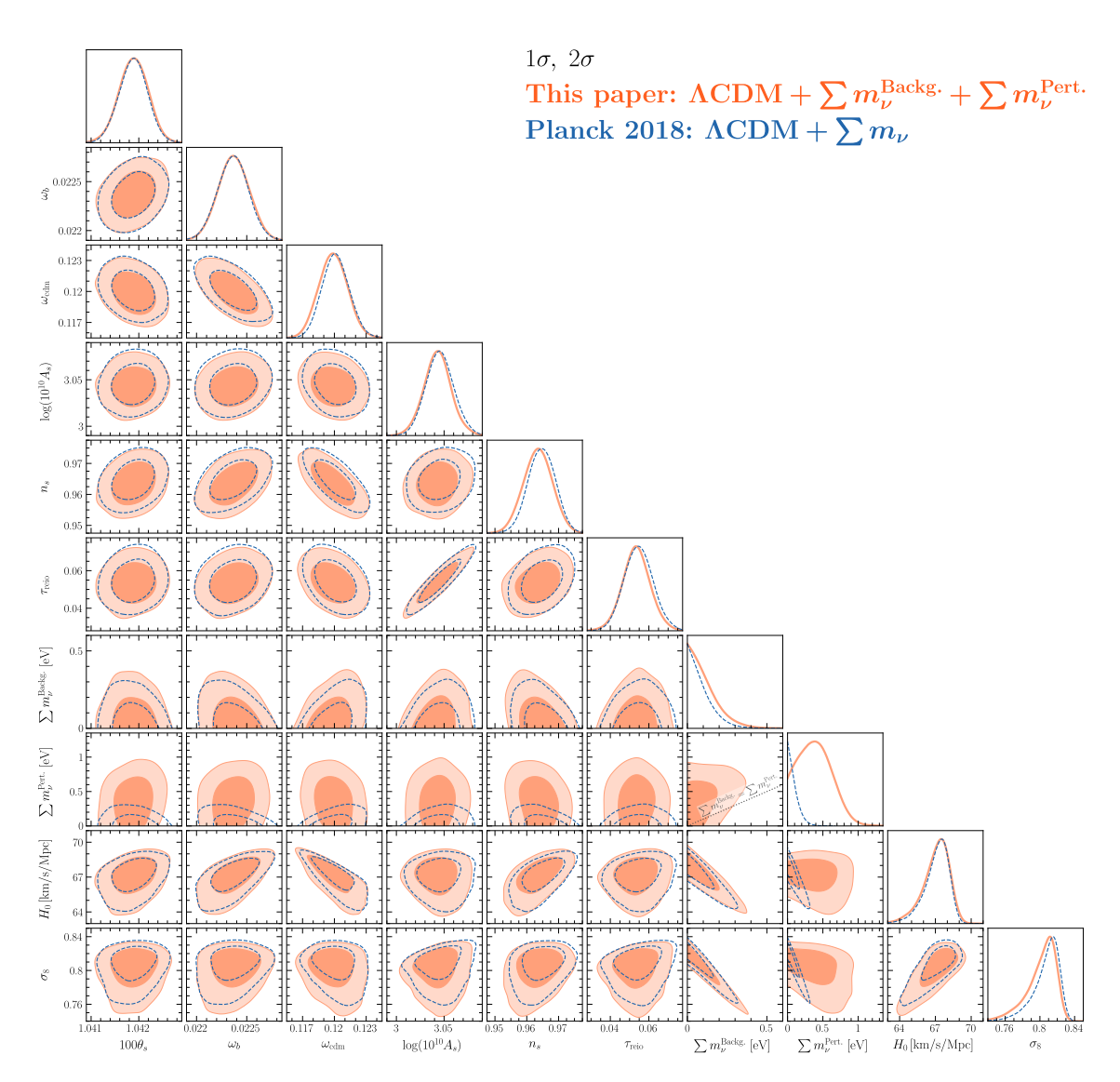


Figure 7.11: CMB 1σ and 2σ credible regions for all parameters in our analysis, together with individual posterior probabilities. Dashed lines correspond to the standard results, where neutrino-mass effects are not split between background and perturbations. In each subfigure, unshown parameters are marginalized over.

Chapter 7 Origin of cosmological neutrino mass bounds: background versus perturbations								

8 BBN bounds on neutrinophilic ultralight Dark Matter

Our technical discussion up to now has been limited to neutrinos alone, which indeed are a direct proof for the existence of BSM. But neutrinos are not alone. The existence of Dark Matter (DM) is also unexplained by the SM particle content, and is backed up by plenty of evidence [423]. Particle physics, astrophysics and cosmology have managed to greatly constrain the portals that can connect this dark sector with the SM [423, 542–544]. However, this is not the case for the neutrino portal, i.e., the possibility that DM is neutrinophilic and only interacts with the SM through neutrinos. Due to the elusive nature of neutrinos, current experimental and observational constraints on ν -DM couplings are much weaker than their electromagnetic counterpart.

One particularly interesting candidate to DM are ultralight scalar fields, which are predicted by many extensions to the SM [545–551]. Since they could be non-thermally produced through the misalignment mechanism –where the initial (random) value of the field is displaced from zero– [542, 552–555], these bosons could make up for the entirety of DM. When these bosons have mass $m_{\phi} \ll 1 \, \mathrm{eV}$, namely $m_{\phi} \sim 10^{-22} - 10^{-10} \, \mathrm{eV}$, they are called Ultra-Light Dark Matter (ULDM) candidates, and have their own distinct phenomenology [542, 555–570].

The unconstrained properties of neutrinos and DM make ν -ULDM interactions span a wide range of interesting phenomenology, from distorted neutrino oscillations to highenergy astrophysics [512, 571–606]. Here, in this work we are particularly interested in studying the cosmological evolution of ν -ULDM interactions.

One of the main interests of v-ULDM couplings is that neutrinos acquire a mass by propagating through a medium of ULDM. Hence, these models might be able to provide a joint explanation to neutrino masses and dark matter [512]. Since the DM number density increases to the early Universe as a^{-3} , these models predict a mass-varying neutrino with $m_v \sim a^{-3/2}$. If one then requires neutrino masses to have the right order of magnitude in terrestrial oscillation experiments, then this predicts $m_v \sim 10 \, \mathrm{eV}$ in the CMB epoch.

However, cosmology is not directly sensitive to the neutrino mass [3], as widely explained in chapter 7. In order to properly derive cosmological bounds, we must follow the evolution of the full neutrino fluid, i.e., its energy density and its pressure. To achieve that, one must understand the coupled evolution of neutrinos and ULDM. For instance, if neutrinos acquire a mass when the amplitude of ULDM increases, this will require an energy expense which will modify the dynamics of ULDM [593, 596]. As shown in [593], this modifies the neutrino mass scaling to $m_{\nu} \sim a^{-1}$.

In this work, we study the cosmological implications of a pseudoscalar coupling between neutrinos and the ULDM field, namely $ig\bar{\psi}\gamma^5\phi\psi$ [607, 608]. We quantitatively compute the background evolution of the coupled field, accounting for the fast oscillations of the ULDM with an adiabatic approximation. Apart from modifying the scaling of m_{ν} , this full calculation predicts additional relativistic degrees of freedom in the early Universe. These two effects allow to use primordial element abundances from Big Bang Nucleosynthesis to constrain the properties of the coupled ν -ULDM fluid and, thus, their coupling.

The outline of this chapter is as follows. In section 8.1, we introduce the lagrangian for the model and derive the equations of motion for both species. In section 8.2, we introduce the adiabatic approximation, a necessary ingredient to solve the equation of motion for an ULDM field. In section 8.3, we describe the cosmological implications of this model and its phenomenological signatures. In particular, in section 8.3.5 we discuss its effects on BBN. Finally, in section 8.4 we present our results and in section 8.5 we conclude.

8.1 Formalism

Let us consider the following action, in a curved spacetime background [609]

$$S = \int \sqrt{-\det g} \, d^4x \, \mathcal{L}(x) =$$

$$= \int \sqrt{-\det g} \, d^4x \left(-\frac{1}{2} D_{\mu} \hat{\phi} \, D^{\mu} \hat{\phi} - \frac{1}{2} m_{\phi}^2 \hat{\phi}^2 + \bar{\psi} \left[i \not \!\!D - m_0 + g \hat{\phi} \right] \psi \right) . \tag{8.1}$$

Here, \mathcal{L} is the Lagrangian density of the model, D_{μ} is a covariant derivative, det g is the metric determinant, $\bar{\psi} = \psi^{\dagger} \gamma^{0}$, m_{ϕ} is the bare mass of the pseudoscalar field, m_{0} the bare mass of the neutrino field and g the coupling between both fields. The pseudoscalar coupling between fermions (ψ) and ultralight bosons (ϕ) has already been extensively studied [607, 608]. Naively, gauge invariance asks that a coupling must exist both to electrons and to neutrinos. However, the coupling to electrons can be suppressed, for instance, if the ultralight pseudoscalar is coupled to a SM-singlet right-handed neutrino [572, 574]. Then, for now on ψ will refer to active neutrinos. Since we are interested in cosmological phenomenology, we choose a diagonal coupling. We expect similar results for a scalar coupling, but a detailed discussion on their differences is left for future work.

The equations of motions for the quantum fields from eq. (8.1) are

$$-\partial^{\mu}\partial_{\mu}\hat{\phi} + m_{\phi}^{2}\hat{\phi} = ig\bar{\psi}\gamma^{5}\psi, \qquad (8.2)$$

$$i\partial \psi - (m_0 - ig\hat{\phi}\gamma^5)\psi = 0. \tag{8.3}$$

However, when working within a cosmological framework, we can consider that the occupation number of the pseudoscalar field $\hat{\phi}$ is large, and that it can be described by a coherent state with a well-defined value. Furthermore, the coherence length of the fermion field is always much smaller than any considered distance. Then, we can describe the fermion field ψ as an ensemble of classical particles with a given momentum \vec{p} . In this framework, we can replace every quantum operator $\hat{\mathcal{O}}$ by its expectation value [498]

$$\langle \hat{\mathcal{O}} \rangle = \sum_{s} \int dP_1 dP_2 dP_3 \frac{1}{\sqrt{-\det g}} \frac{1}{2P^0} f(P, x, s) \langle \phi, P^s | \hat{\mathcal{O}} | \phi, P^s \rangle.$$
 (8.4)

As introduced in section 6.1.4, P^{μ} are the conjugate momenta to the positions x^{i} , s is the spin and f(P, x, s) the distribution function. $|\phi, P^{s}\rangle = |\phi\rangle \otimes |P^{s}\rangle$ is the product of a coherent state with field ϕ and a one-particle fermion state, given by [48, 610–612]

$$|\phi\rangle \equiv \exp\left\{-\frac{1}{2} \int \frac{\mathrm{d}^{3}\vec{k}}{(2\pi)^{3}} \frac{|\phi(K)|^{2}}{(2K^{0})^{5}}\right\} \exp\left\{\int \frac{\mathrm{d}^{3}\vec{k}}{(2\pi)^{3}} \frac{\phi(K)}{(2K^{0})^{5/2}} a_{K}^{\phi^{\dagger}}\right\} |0\rangle,$$

$$|P^{s}\rangle = \sqrt{2P^{0}} a_{P}^{s\dagger} |0\rangle.$$
(8.5)

Here, $|0\rangle$ is the vacuum state, a_P^s (a_K^ϕ) is the annihilation operator of the field ψ (ϕ), $K^\mu = (E_K, \vec{k})$ such that $K^2 = -m_\phi^2$, and $\phi(K)$ is the Fourier transform of the classical scalar field $\phi(x)$,

$$\phi(x) \equiv \int \frac{\mathrm{d}^3 \vec{k}}{(2\pi)^3} \frac{1}{(\sqrt{2}K^0)^3} \left[\phi(K) e^{-iKx} + \phi(K)^* e^{iKx} \right] . \tag{8.6}$$

8.1.1 Dirac equation and effective fermion mass

Let us analyze the equation of motion of free fermions, eq. (8.3), where for now we treat ϕ as a constant and homogeneous value. In order to transform this equation into something that we already know, we undergo the change of variables

$$\psi \to e^{i\alpha\gamma^5} \psi = (\cos \alpha + i\gamma^5 \sin \alpha) \psi,$$
 (8.7)

where then α is a constant parameter. The equation now becomes

$$(i\partial \!\!\!/ - (m_0 \cos \alpha - g\phi \sin \alpha) + i\gamma^5 (-m_0 \sin \alpha + g\phi \cos \alpha)) \psi = 0, \qquad (8.8)$$

where we have used $(\gamma^5)^2 = \mathbb{I}_4$, the 4x4 identity matrix. Now, by making the right choice,

$$\tan \alpha = \frac{g\phi}{m_0},\tag{8.9}$$

we convert this equation into

$$(i\partial \!\!\!/ - m_{\nu}) \psi = 0. \tag{8.10}$$

This is the standard Dirac equation with a mass term given by

$$m_{\nu} = \sqrt{m_0^2 + g^2 \phi^2} \,. \tag{8.11}$$

Now, this tells us that the eigenstates to the Dirac operator from eq. (8.3) are two states with the same mass, m_{ν} . For instance, one can use the Pauli-Dirac representation of the gamma matrices,

$$\gamma^{0} = \begin{pmatrix} \mathbb{I}_{2} & 0 \\ 0 & -\mathbb{I}_{2} \end{pmatrix}, \quad \gamma^{i} = \begin{pmatrix} 0 & \sigma^{i} \\ -\sigma^{i} & 0 \end{pmatrix}, \quad \gamma^{5} = \begin{pmatrix} 0 & \mathbb{I}_{2} \\ \mathbb{I}_{2} & 0 \end{pmatrix}, \tag{8.12}$$

with \mathbb{I}_2 the 2x2 identity matrix, and σ^i the Pauli matrices. Then, the positive and negative frequency solutions to eq. (8.10), with defined mass m_{ν} , are [46]

$$u_0^s(\vec{p}) = \begin{pmatrix} \sqrt{E_p + m_v} \, \xi^s \\ \vec{\sigma} \cdot \vec{p} \\ \sqrt{E_p + m_v} \, \xi^s \end{pmatrix}, \qquad v_0^s(\vec{p}) = \begin{pmatrix} \vec{\sigma} \cdot \vec{p} \\ \sqrt{E_p + m_v} \, \chi^s \\ \sqrt{E_p + m_v} \, \chi^s \end{pmatrix}, \tag{8.13}$$

respectively. Here $E_p=\sqrt{\vec{p}^2+m_0^2+g^2\phi^2}$, and ξ^s , χ^s are spinors corresponding to the eigenvectors of a Stern-Gerlach experiment in an arbitrary \hat{n} direction, with s=1,2 that differentiates between the two helicity eigenstates. These must fulfill $\xi^{s\dagger}\xi^s=\chi^{s\dagger}\chi^s=1$. Now, we must perform a chiral rotation to recover the plane wave solutions to eq. (8.3),

$$u^{s}(\vec{p}) = e^{i\alpha\gamma^{5}} u_{0}^{s}(\vec{p}), \qquad v^{s}(\vec{p}) = e^{i\alpha\gamma^{5}} v_{0}^{s}(\vec{p}),$$
 (8.14)

which compose the general solution

$$\psi = \int \frac{d^3\vec{p}}{(2\pi)^3} \frac{1}{\sqrt{2E_p}} \sum_{s=1,2} \left(e^{-iPx} a^s(\vec{p}) u^s(\vec{p}) + e^{iPx} b^{s\dagger}(\vec{p}) v^s(\vec{p}) \right) . \tag{8.15}$$

Here, $P^{\mu}=(E_p,\vec{p})$ and $a^s(P)$ and $b^s(P)$ are the annihilation operators to $u^s(\vec{p})$ and $v^s(\vec{p})$. Most importantly, the plane wave solutions fulfill

$$\bar{u}^s(\vec{p})\gamma^0 u^r(\vec{p}) = \bar{v}^s(\vec{p})\gamma^0 v^r(\vec{p}) = 2E\delta^{sr},$$

$$\bar{u}^s(\vec{p})\gamma^5 u^r(\vec{p}) = -\bar{v}^s(\vec{p})\gamma^5 v^r(\vec{p}) = 2ig\phi \delta^{sr}.$$
(8.16)

Evolution of the distribution function

The evolution in the neutrino sector is described by the evolution of the fermion distribution function, given by the geodesic eq. (6.27) and the Boltzmann eq. (6.29). However, in this model we are dealing with mass-varying neutrinos, $m_{\nu}(\eta) = \sqrt{m_0^2 + g^2 \phi(\eta)^2}$, which might make us wonder if $\mathrm{d}q/\mathrm{d}\eta = 0$ as we had assumed in the standard case. To first order, we would then have

$$\frac{\partial f_0}{\partial \eta} + \frac{\mathrm{d}q}{\mathrm{d}\eta} \frac{\partial f_0}{\partial q} = 0, \tag{8.17}$$

which could make $f_0(q)$ vary with time. For mass-varying neutrinos, the geodesic equation gets modified to [613]

$$P^{0} \frac{\mathrm{d}P^{\mu}}{\mathrm{d}\eta} + \Gamma^{\mu}_{\nu\rho} P^{\nu} P^{\rho} = -m_{\nu}^{2} \frac{\mathrm{d}\log m_{\nu}}{\mathrm{d}\phi} \frac{\partial\phi}{\partial x_{\mu}}. \tag{8.18}$$

After some algebra, in the 0th component of the geodesic equation the contribution from ϕ vanishes and we still get

$$\frac{\mathrm{d}q}{\mathrm{d}n} = 0. \tag{8.19}$$

Therefore, $\partial f_0/\partial \eta = 0$ and the shape of the momentum distribution function $f_0(q)$ does not vary with time, even for the mass-varying neutrinos from this model.

8.1.2 Pseudoscalar equation of motion

Now, we are ready to take the expectation value of eq. (8.2) assuming an homogeneous background field $\phi = \phi(t)$ and a collection of particles as in eq. (8.4), which leads to

$$-D_{\mu}D^{\mu}\phi + m_{\phi}^{2}\phi = ig\sum_{s} \int dP_{1}dP_{2}dP_{3} \frac{1}{\sqrt{-\det g}} \frac{1}{2P^{0}} f(P, x, s) \langle P^{s} | \bar{\psi} \gamma^{5} \psi | P^{s} \rangle.$$
 (8.20)

The expectation value in the right hand side gives

$$\langle P^s | \bar{\psi} \gamma^5 \psi | P^s \rangle = \bar{u}^s(P) \gamma^5 u^s(P) = 2ig\phi, \qquad (8.21)$$

with the same result for antiparticles. Plus, if f(P, x, s) = f(P, x) is spin-independent, the equation for the pseudoscalar field becomes

$$-D_{\mu}D^{\mu}\phi + m_{\phi}^{2}\phi = -2g^{2}\phi \,\mathfrak{g} \int dP_{1}dP_{2}dP_{3} \frac{1}{\sqrt{-\det g}} \frac{1}{2P^{0}} f(P,x), \qquad (8.22)$$

where \mathfrak{g} is the number of fermionic internal degrees of freedom: particles and antiparticles, and both spins. This is a spin-independent result, since the field is homogeneous. It is convenient to work in the comoving momentum q in order to explicitly show the scaling dependence of neutrino phase distribution integral,

$$\ddot{\phi} + 3H\dot{\phi} + m_{\phi}^2 \phi = -2g^2 \phi \,\mathfrak{g} \,a^{-2} \int 4\pi \,\mathrm{d}q \,q^2 \,\frac{1}{\sqrt{q^2 + a^2(m^2 + g^2\phi^2)}} f_0(q) \,. \tag{8.23}$$

Here, there are three characteristic timescales,

- the cosmological time, H^{-1} , which controls the Hubble friction term and the rate at which $f_0 = f_0(q)$ changes $(\frac{\mathrm{d}f_0}{\mathrm{d}t} = H \frac{\mathrm{d}f_0}{\mathrm{d}\log q})$.
- the characteristic oscillation time of ϕ . Naively, given by m_{ϕ} , but might be modified by the interactions.
- the timescale of neutrino dynamics, controlled by $E_p = \sqrt{\vec{p}^2 + m_0^2 + g^2 \phi^2}$.

In the regime $H\gg m_\phi$, then ϕ would be frozen to its value after inflation. Then, ϕ would be fixed to its initial non-zero value and behave as quintessence [613]. Instead, we are interested in the the regime where $m_\phi\gg H$, and thus it oscillates in scales much shorter than the cosmological expansion. In this limit, ϕ can be understood as a collection of CDM particles. Furthermore, we will also work in the limit $m_\phi\ll E_p$, the fermion sees the instantaneous value of ϕ as a constant, and thus the discussion of the previous subsection applies here.

The cosmological and oscillation timescales in eq. (8.23) are, in general, separated by many orders of magnitude. In usual standard cosmology, we average over the oscillation of the field which leads to ULDM behaving like CDM. However, here we want to follow the dynamics of the interaction between the field and the fermions, e.g., see if fermions backreact in the dynamics of the field. To such purpose, we will follow an adiabatic approximation [614].

8.2 Adiabatic approximation

In the framework of the adiabatic approximation, we define two different time variables. First, we parametrise the slow cosmological timescale H^{-1} with the scale factor a. Second, we will parametrise the timescale of the field oscillation with a proper time t. We will assume that, during an oscillation of ϕ (of timescale t), the scale factor a can be held constant, i.e. a' = 0. Thus, the equation of motion for ϕ becomes

$$\ddot{\phi} + m_{\phi}^2 \phi = -2g^2 \phi \, \mathfrak{g} \, a^{-2} \int 4\pi \, \mathrm{d}q \, q^2 \, \frac{1}{\sqrt{q^2 + a^2(m^2 + g^2 \phi^2)}} f_0(q) \,, \tag{8.24}$$

This is the equation of a one-dimensional non-relativistic particle moving on a potential well. The adiabatic approximation assumes that the real motion of ϕ is well described by this evolution, which assumes a constant in a complete period of oscillation t_{ϕ} .

In the adiabatic approximation, every observable \mathcal{O} at cosmological timescales is replaced by its value averaged over the oscillation,

$$\langle \mathcal{O} \rangle = \frac{1}{t_{\phi}} \int_{0}^{t_{\phi}} dt \, \mathcal{O}(\phi(t), \dot{\phi}(t)) = \frac{1}{t_{\phi}} \oint d\phi \, \frac{\mathcal{O}(\phi, \dot{\phi}(\phi))}{\dot{\phi}(\phi)}, \qquad (8.25)$$

where ϕ marks an integral over an oscillation of ϕ and t_{ϕ} is the period of the oscillation,

$$t_{\phi} = \int_0^{t_{\phi}} \mathrm{d}t = \oint \frac{\mathrm{d}\phi}{\dot{\phi}(\phi)}. \tag{8.26}$$

The period of oscillation would then define an oscillation frequency which we can interpret as an effective mass, $M_{\phi}=2\pi/t_{\phi}$.

One of our main interests is to find the evolution of the total energy density,

$$\rho(a,t) = \frac{1}{2}\dot{\phi}^2 - \frac{1}{2}m_{\phi}^2\phi^2 + \rho_{\nu}(a,\phi). \tag{8.27}$$

This is similar to the standard ULDM scenario, but with an additional term accounting for the energy in the fermion sector,

$$\rho_{\nu}(a,\phi) = a^{-4}\mathfrak{g} \int 4\pi \,\mathrm{d}q \,q^2 \sqrt{q^2 + a^2(m_0^2 + g^2\phi^2)} \,f_0(q) \,. \tag{8.28}$$

We can obtain the evolution equation for ρ by multiplying eq. (8.23) by $\dot{\phi}$, and rewriting it into

$$\frac{\mathrm{d}\rho(a,t)}{\mathrm{d}t} = H\left[\frac{\partial\rho_{\nu}}{\partial\log a} - 3\dot{\phi}^2\right],\tag{8.29}$$

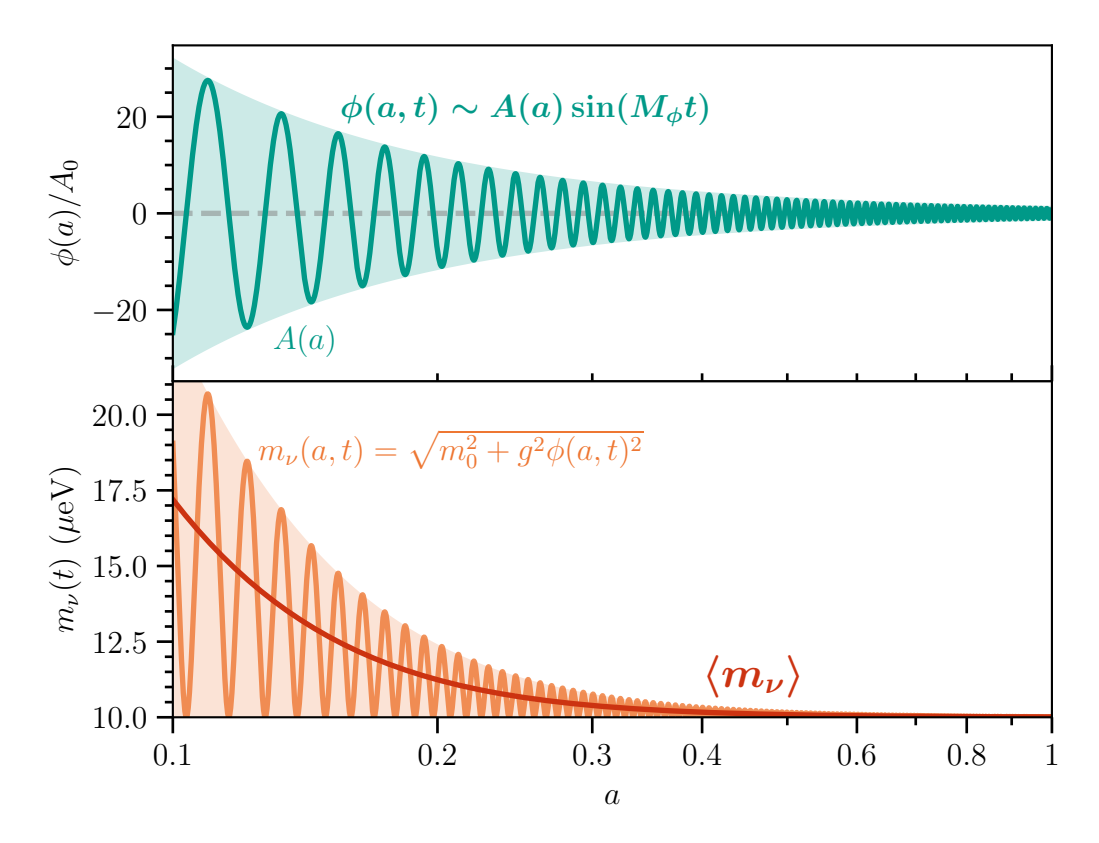


Figure 8.1: Illustration of the adiabatic approximation method. The top plot shows how the ULDM field $\phi(a,t)$ is oscillating rapidly around zero with amplitude A(a) and frequency M_{ϕ} . As a consequence of the oscillating field, the bottom plot shows how the mass of the neutrino, $m_{V}(a,t)$, also oscillates rapidly with time. The adiabatic approximation allows to compute the averaged neutrino mass, $\langle m_{V} \rangle$, or the average of any other observable \mathcal{O} as in eq. (8.25). Curves here correspond to $m_{0}=10~\mu\text{eV},~g=1.5\times10^{-20}$ and $m_{\phi}=10^{-19}~\text{eV},$ and $A_{0}\equiv A(a=1)$. For illustration purposes, the shown oscillation frequency is reduced by $\mathcal{O}(10^{21})$ compared to M_{ϕ} .

Within cosmological timescales, the energy density varies as

$$H\frac{\mathrm{d}\rho(a,t)}{\mathrm{d}\log a} = \frac{\mathrm{d}\rho(a,t)}{\mathrm{d}t}.$$
 (8.30)

In the adiabatic approximation, we replace $d\rho/dt$ by its averaged value over an oscillation,

$$H\frac{\mathrm{d}\rho}{\mathrm{d}\log a} = \left\langle \frac{\mathrm{d}\rho}{\mathrm{d}t} \right\rangle . \tag{8.31}$$

Now, plugging eq. (8.29) here,

$$\frac{\mathrm{d}\rho}{\mathrm{d}\log a} = \left\langle \frac{\partial \rho_{\nu}}{\partial \log a} \right\rangle - 3\langle \dot{\phi}^2 \rangle \,. \tag{8.32}$$

Within an oscillation we can treat the total energy as a constant of motion, $\rho(a, t) \simeq \langle \rho(a, t) \rangle \equiv \rho(a)$. This allows to use eq. (8.27) to find a closed expression for $\dot{\phi}$,

$$\dot{\phi} = \sqrt{2} \sqrt{\rho(a) - m_{\phi}^2 \phi^2 / 2 - \rho_{\nu}(\phi)}$$
 (8.33)

Then,

$$t_{\phi}\langle\dot{\phi}^{2}\rangle = \oint d\phi \,\dot{\phi} = \sqrt{2} \oint d\phi \,\sqrt{\rho(a) - \frac{1}{2}m_{\phi}^{2}\phi^{2} - \rho_{\nu}(\phi)}. \tag{8.34}$$

This is an important quantity, since we notice that

$$t_{\phi} \frac{\mathrm{d}\rho}{\mathrm{d}\log a} - t_{\phi} \left\langle \frac{\partial \rho_{\nu}}{\partial \log a} \right\rangle = \frac{1}{\sqrt{2}} \oint \mathrm{d}\phi \frac{\partial (\rho(a) - \rho_{\nu}(a, \phi))/\partial \log a}{\sqrt{\rho(a) - \frac{1}{2}m_{\phi}^{2}\phi^{2} - \rho_{\nu}(\phi)}} =$$

$$= \sqrt{2} \frac{\mathrm{d}}{\mathrm{d}\log a} \oint \mathrm{d}\phi \sqrt{\rho(a) - \frac{1}{2}m_{\phi}^{2}\phi^{2} - \rho_{\nu}(\phi)} =$$

$$= \frac{\mathrm{d}}{\mathrm{d}\log a} \left(t_{\phi} \langle \dot{\phi}^{2} \rangle \right) . \tag{8.35}$$

Plugging this result into eq. (8.32), we get that

$$\frac{\mathrm{d}}{\mathrm{d}\log a} \left(t_{\phi} \langle \dot{\phi}^2 \rangle \right) = -3t_{\phi} \langle \dot{\phi}^2 \rangle. \tag{8.36}$$

So,

$$\mathcal{I}(a) \equiv \frac{1}{\sqrt{2}} a^3 t_{\phi} \langle \dot{\phi}^2 \rangle = a^3 \oint d\phi \sqrt{\rho(a) - \frac{1}{2} m_{\phi}^2 \phi^2 - \rho_{\nu}(\phi)}$$
(8.37)

is an invariant quantity for the whole cosmological evolution, since $\mathrm{d}\mathcal{I}/\mathrm{d}a=0$. This adiabatic invariant allows to compute the total energy density $\rho(a)$ of the system as a function of the scale factor, given some initial conditions.

The framework of the adiabatic approximation allows to compute $\rho(a)$ at every time. However, for clarity we work in terms of the amplitude of oscillations of the pseudoscalar, A(a). In particular, $\phi = A$ is reached when $\dot{\phi} = 0$, and thus

$$\rho(a) = \frac{1}{2} m_{\phi}^2 A(a)^2 + \rho_{\nu}(a, A(a)). \tag{8.38}$$

Then, eq. (8.37) allows to compute the evolution of A(a). In the $g \to 0$ limit, the adiabatic invariant becomes

$$\mathcal{I}(a) = a^3 \oint d\phi \sqrt{\frac{1}{2} m_{\phi}^2 (A^2 - \phi^2)} = \frac{\pi}{2} m_{\phi} a^3 A^2, \tag{8.39}$$

which means that $A(a) \sim a^{-3/2}$. As expected, in the $g \to 0$ limit we retrieve that ϕ behaves as CDM, with $\rho(a) \sim a^{-3}$. In the limit where the interaction potential dominates, i.e. $m_{\phi}^2 A^2 \ll \rho_{\nu}(a,A(a))$, the adiabatic invariant becomes

$$\mathcal{I}(a) = a \oint d\phi \sqrt{g \int 4\pi q^2 dq \left(\sqrt{q^2 + g^2 a^2 A^2} - \sqrt{q^2 + g^2 a^2 \phi^2}\right) f_0(q)}.$$
 (8.40)

By making a change of variables to $\tilde{\phi}=a\phi$, one can check that $\mathcal{I}(a,A)=\mathcal{I}(aA)$, i.e., only the variable aA enters in the invariant, thus aA= constant. In the limit where the interaction potential dominates, the pseudoscalar field does not scale like CDM, but following $A(a)\sim a^{-1}$. This is due to the neutrino-dominated potential having a different scaling dependence to the m_{ϕ} potential. Let us look into this further.

8.3 Phenomenology

This adiabatic approximation now allows us to compute all the important cosmological variables, averaging-out the fast oscillations of the ULDM field. This has allowed us to fully follow the bidirectional feedback between the neutrino sector and the ULDM field. In particular, we have seen that the interaction can modify how does the field scale as the Universe expands. In this Section, we explore further the phenomenological consequences of this interaction into all the affected cosmological variables. All the shown results are computed in a modified version of CLASS [527, 529–531] which implements the full adiabatic approximation method.

8.3.1 Energy density and effective mass

From the energy-momentum tensor,

$$\rho(a) = \langle \rho(a,t) \rangle = \frac{1}{2} \langle \dot{\phi}^2 \rangle + \frac{1}{2} m_{\phi}^2 \langle \phi^2 \rangle + \langle \rho_{\nu}(a,\phi) \rangle \equiv \frac{1}{2} \langle \dot{\phi}^2 \rangle + \langle V(\phi) \rangle, , \qquad (8.41)$$

which has been checked to exactly coincide with eq. (8.38). We have defined the pseudoscalar potential

$$V(\phi) = \frac{1}{2} m_{\phi}^2 \phi^2 + \rho_{\nu}(a, \phi). \tag{8.42}$$

The shape and scaling of this potential at different epochs are shown in fig. 8.2. Firstly, $m_{\phi}^2 \phi^2$ is a quadratic potential, which scales as a^{-3} if ϕ behaves as standard CDM. Secondly, $\rho_{\nu} \sim a^{-4}$. Then, at some point in the past, defined as $a_{\rm tr}$ in fig. 8.2, $V(\phi)$ changes scaling from a^{-3} to a^{-4} , while still being quadratic. Finally, if $gA \gg |\vec{p}|$, neutrinos become non-relativistic, and then $V(\phi)$ becomes linear at large ϕ . The couplings required

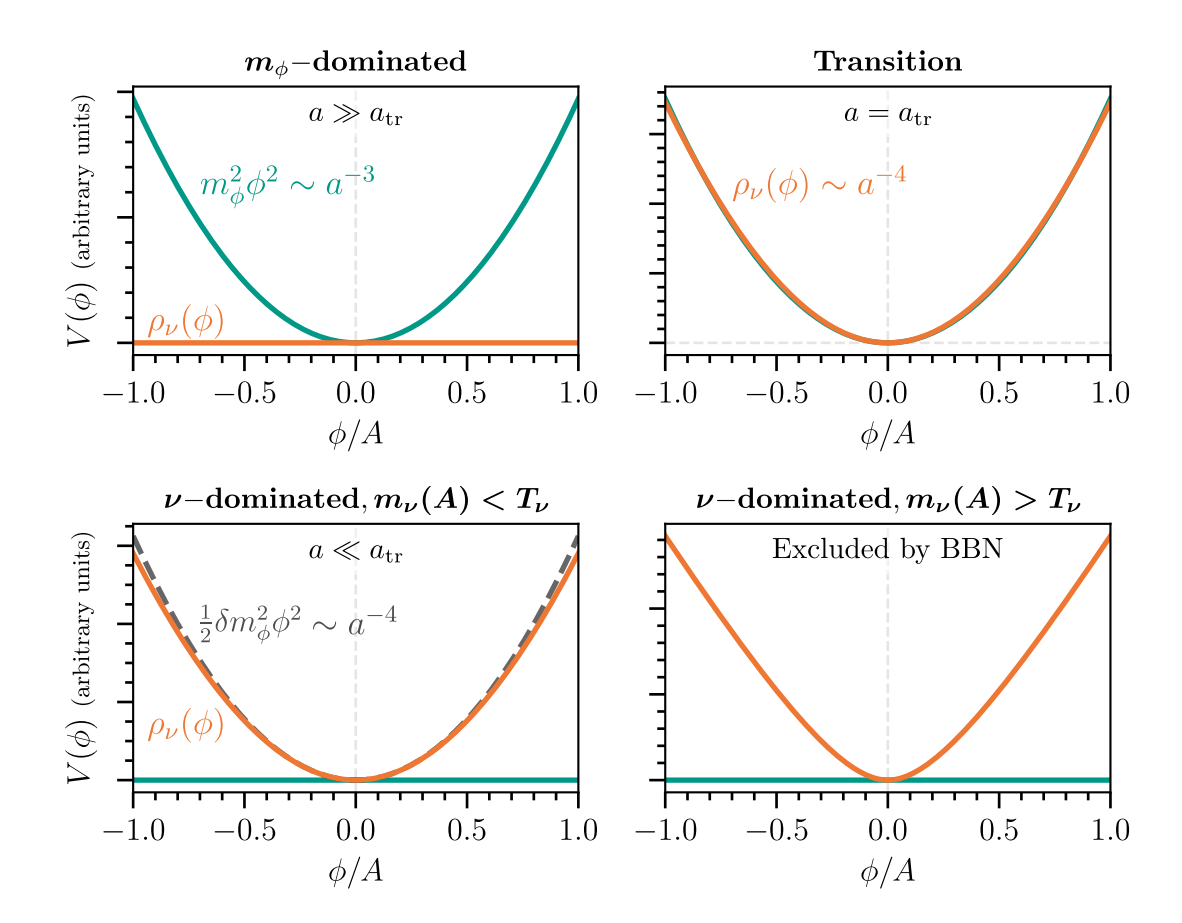


Figure 8.2: Evolution of the potential as in eq. (8.42). Left to right, top to bottom goes back in time. Today, the effect of neutrino interactions is negligible, and $V(\phi) = m_{\phi}^2 \phi^2/2$. However, $\rho_V(\phi)$ scales as a^{-4} , and therefore at some point $(a=a_{\rm tr})$ in the past the neutrino potential equals the bare- m_{ϕ} potential. From that time on, $V(\phi) \sim a^{-4}$ and the scaling of A(a) changes. If the momentum of neutrinos is larger than their effective mass, the $V(\phi)$ is quadratic, but if it becomes comparable, $V(\phi)$ becomes linear at large ϕ .

for this scenario are ruled out from the bounds obtained in section 8.4.

In a first approximation, we can assume that the linear momentum of neutrinos is much larger than their instantaneous mass, i.e., $T_{\nu} \gg gA$. We will refer to this regime as the linearised regime. In this limit, we can expand ρ_{ϕ} up to first order in ϕ and get

$$\rho(a,t) = \frac{1}{2}\dot{\phi}^2 + \frac{1}{2}m_{\phi}^2\phi^2 + \frac{1}{2}\delta m_{\phi}^2\phi^2 + \rho_{\nu}(a,0), \qquad (8.43)$$

where

$$\delta m_{\phi}^{2} = 2 \left. \frac{\partial \rho_{\nu}(a, \phi)}{\partial \phi^{2}} \right|_{\phi=0} = a^{-2} g^{2} g \int 4\pi dq q^{2} \frac{1}{\sqrt{q^{2} + a^{2} m_{0}^{2}}} f(q)$$
 (8.44)

is an effective pseudoscalar mass from the energy expense necessary to provide neutri-

nos their mass. This effective mass scales as $\delta m_\phi^2 \sim a^{-2}$, as follows. The energy of a single neutrino coupled to ϕ , when $T_\nu \gg g a A \gg m_0$, is

$$E_p = \sqrt{\vec{p}^2 + m_0^2 + g^2 \phi^2} \simeq |\vec{p}| + \frac{g^2 \phi^2}{2|\vec{p}|},$$
 (8.45)

which implies an increment in energy $\sim g^2\phi^2/|\vec{p}|$. For fixed ϕ , this scales as $\sim a$, but the number density of neutrinos which receive the mass scales with a^{-3} . Thus, $\delta m_\phi^2 \sim a^{-2}$.

Then, the total effective mass of the pseudoscalar field is given by

$$M_{\phi}^{2} = 2 \left. \frac{\partial^{2} V(\phi)}{\partial \phi^{2}} \right|_{\phi=0} = m_{\phi}^{2} + \delta m_{\phi}^{2} \sim \begin{cases} m_{\phi}^{2} \sim \text{constant} & a > a_{\text{tr}} \\ \delta m_{\phi}^{2} \sim a^{-2} & a < a_{\text{tr}} \end{cases},$$
 (8.46)

where $a_{
m tr}$ is quantitatively defined through $m_\phi = \delta m_\phi^2$,

$$a_{\rm tr}^2 = \frac{g^2}{m_\phi^2} \, \mathfrak{g} \int 4\pi \, \mathrm{d}q \, q^2 \frac{1}{\sqrt{q^2 + a^2 m_0^2}} f(q) \sim \left(8.4 \times 10^{-5} \, \frac{\mathrm{g/m_\phi}}{\mathrm{eV}^{-1}} \right)^2 \,,$$
 (8.47)

where we have used $T_{\nu,0} = 0.1681$ meV and $\mathfrak{g} = 6$ for the numerical estimate. Then, the equation of motion eq. (8.24) simplifies to

$$\ddot{\phi} + M_{\phi}^2 \phi = 0 \,, \tag{8.48}$$

which is the equation of a quadratic harmonic oscillator, with standard solution

$$\phi(a,t) = A(a)\sin(M_{\phi}t + \varphi_0), \tag{8.49}$$

with φ_0 an initial phase. In this case, it is trivial to average over an oscillation of the field, and for instance the total energy density is given by

$$\rho(a) = \frac{1}{2}M_{\phi}^2 A^2 + \rho_{\nu}(a,0), \qquad (8.50)$$

where $\rho_{\nu}(a,0)$ is the energy density of neutrinos as if they were decoupled. The evolution of this energy density is compared to standard $\nu+\text{ULDM}$ in fig. 8.3. While everything looks very similar, we can see that $\rho_{\phi} \equiv \frac{1}{2} \langle \dot{\phi}^2 \rangle + \frac{1}{2} m_{\phi}^2 \langle \phi^2 \rangle$ scales like radiation for $a < a_{\text{tr}}$.

The radiation behaviour of ρ_{ϕ} can be understood at the same time as one explains why $a_{\rm tr}$ also describes the transition between $A \sim a^{-3/2}$ and $A \sim a^{-1}$ from eq. (8.37). This stems from the conservation of the number of ϕ particles, i.e., the scaling of its number

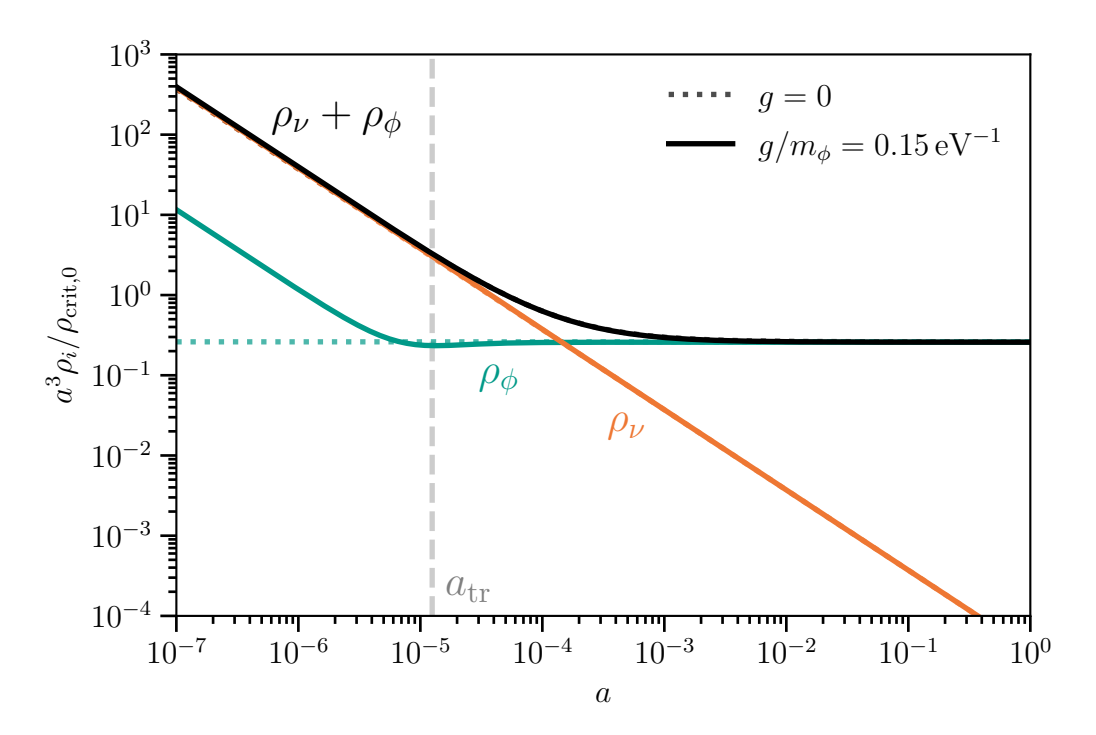


Figure 8.3: Evolution of the energy density of the $\nu+\text{ULDM}$ fluid, in the interacting scenario (solid) and in the decoupled scenario (dotted). In both cases, $m_0=10^{-5}\,\text{eV}$. A vertical dashed line shows the time of transition between m_ϕ -domination and ν -domination. As explained in Note 8.1, ρ_ϕ (teal) and ρ_ν (orange) can only be understood as independent fluids for $a\gg a_{\rm tr}$. For $a< a_{\rm tr}$, their separation is artificial.

density as $n_{\phi} \sim a^{-3}$ [593]. Its energy density is, in turn, $\rho_{\phi} = M_{\phi} n_{\phi}$. For $a > a_{\rm tr}$, M_{ϕ} is constant, and thus $\rho_{\phi} = m_{\phi} n_{\phi} \sim a^{-3}$. Since $\rho_{\phi} \equiv \frac{1}{2} m_{\phi}^2 A^2$, this means that $A \sim a^{-3/2}$, as standard CDM. However, when $a < a_{\rm tr}$, $\rho_{\phi} = \delta m_{\phi} n_{\phi} \sim a^{-4}$, as if it were radiation. Since $\rho_{\phi} \equiv \frac{1}{2} \delta m_{\phi}^2 A^2$, this means that $A \sim a^{-1}$. Since ϕ is homogeneous, we expect perturbations to still behave as CDM with zero momentum, but the exact treatment of perturbations is left for future research. In order to better understand the effect of this transition in the expansion history of the Universe, we now quantitatively compute the equation of state.

8.3.2 Pressure and equation of state

From the energy-momentum tensor, the pressure of the fermion-pseudoscalar fluid is

$$p(a) = \frac{1}{2} \langle \dot{\phi}^2 \rangle - \frac{1}{2} m_{\phi}^2 \langle \phi^2 \rangle + \langle p_{\nu}(a, \phi) \rangle, \qquad (8.51)$$

with

$$p_{\nu}(a,\phi) = \mathfrak{g} \int d^{3}\vec{p} \frac{p^{2}}{\sqrt{p^{2} + m_{0}^{2} + g^{2}\phi^{2}}} f_{0}(pa) = a^{-4}\mathfrak{g} \int \frac{4\pi dq \ q^{4}}{\sqrt{q^{2} + a^{2}(m_{0}^{2} + g^{2}\phi^{2})}} f_{0}(q).$$
(8.52)

In the linearised regime approximation, this can be simplified to

$$p(a,t) = \frac{1}{2}\dot{\phi}^2 - \frac{1}{2}m_{\phi}^2\phi^2 - \frac{1}{2}\delta\mu_{\phi}^2\phi^2 + p_{\nu}(a,0), \qquad (8.53)$$

where

$$\delta\mu_{\phi}^{2} = -2 \left. \frac{\partial p_{\nu}(a,\phi)}{\partial \phi^{2}} \right|_{\phi=0} = a^{-2} g^{2} \mathfrak{g} \int 4\pi \, \mathrm{d}q \, \frac{q^{4}}{(q^{2} + a^{2} m_{0}^{2})^{3/2}} f_{0}(q)$$
(8.54)

is a higher-order integral of the momentum distribution. Now, plugging the solution from eq. (8.49) and averaging over an oscillation,

$$p(a) = \frac{1}{4} \left(\delta m_{\phi}^2 - \delta \mu_{\phi}^2 \right) A^2 + p_{\nu}(a, 0).$$
 (8.55)

Since $\delta m_{\phi}^2 \geq \delta \mu_{\phi}^2$, the scalar part of the pressure is never negative. Then, one can define an equation of state for the total fluid,

$$w(a) = \frac{p(a)}{\rho(a)} = \frac{\left(\delta m_{\phi}^2 - \delta \mu_{\phi}^2\right) A^2 / 4 + p_{\nu}(a, 0)}{(m_{\phi}^2 + \delta m_{\phi}^2) A^2 / 2 + \rho_{\nu}(a, 0)}.$$
 (8.56)

Now, we can simplify this expression further. In the early universe, for allowed values of m_0 , $T_{\nu} \gg m_0$, and m_0 can be neglected in integrals over the distribution function. In this limit, $\delta m_{\phi}^2 = \delta \mu_{\phi}^2$, and therefore

$$p(a) = p_{\nu}(a,0) = \frac{1}{3}\rho_{\nu}(a,0),$$
 (8.57)

the pressure of the total fluid is only the pressure of the neutrino part, *as if they were uncoupled from the pseudoscalar field*, which are completely relativistic at early times. This simplifies the equation of state to

$$w(a) = \frac{1}{3} \frac{\rho_{\nu}(a,0)}{\rho_{\nu}(a,0) + (m_{\phi}^2 + \delta m_{\phi}^2)A^2/2} = \frac{1}{3} \left[1 - \left(1 + \frac{\rho_{\nu}(a,0)}{(m_{\phi}^2 + \delta m_{\phi}^2)A^2/2} \right)^{-1} \right]. \quad (8.58)$$

Figure 8.4 shows the evolution of w(a) for different couplings. For the standard scenario $g \to 0$, $\delta m_{\phi}^2 = 0$. Then, if $m_{\phi}^2 A^2 \gg \rho_{\nu}(a,0)$, w = 0 (CDM domination); and if $m_{\phi}^2 A^2 \ll \rho_{\nu}(a,0)$, w = 1/3 (relativistic neutrino domination). In the coupled scenario,

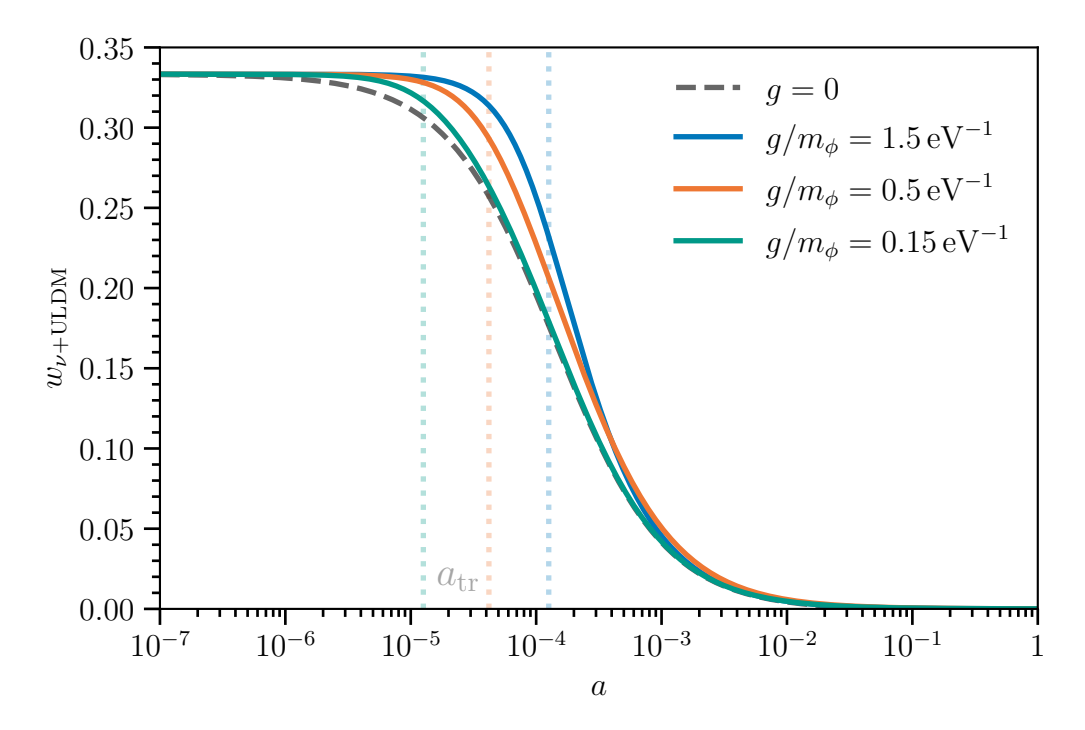


Figure 8.4: Evolution of the equation state of the $\nu+\text{ULDM}$ fluid for interacting scenarios (solid lines) and a decoupled scenario (dotted). Vertical dotted lines shows a_{tr} (transition between ν -domination and m_{ϕ} domination) for the different couplings, as in eq. (8.47). The coupled fluid stays relativistic for a longer period.

the modified scaling of A(a) makes w(a) grows faster to 1/3 than in the standard case. One of the consequences of the fluid staying relativistic for a longer time is that the time of equality between matter and radiation is delayed. However, for couplings allowed by BBN this is a subleading effect, as we will explore below.

Note 8.1. On the separation of the species

Looking at eqs. (8.50) and (8.55), one might be tempted to split the energy density and pressure as

$$\rho(a) = \rho_{\phi}(a) + \rho_{\nu}(a),
p(a) = \rho_{\phi}(a) + \rho_{\nu}(a),$$
(8.59)

where

$$\rho_{\phi}(a) \equiv \frac{1}{2} \langle \dot{\phi}^2 \rangle + \frac{1}{2} m_{\phi}^2 \langle \phi^2 \rangle,$$

$$p_{\phi}(a) \equiv \frac{1}{2} \langle \dot{\phi}^2 \rangle - \frac{1}{2} m_{\phi}^2 \langle \phi^2 \rangle.$$
(8.60)

However, in general the evolution of ρ_{ϕ} (p_{ϕ}) and ρ_{ν} (p_{ν}) is not physically separable, i.e. the pseudoscalar field and the fermion ensemble do not evolve as independent fluids. In fact, the conservation of the energy-momentum tensor only implies:

$$\frac{\partial \rho(a)}{\partial \log a} = \frac{\partial [\rho_{\phi}(a) + \rho_{\nu}(a)]}{\partial \log a} = -3 \left[(\rho_{\phi} + \rho_{\nu}) + (p_{\phi} + p_{\nu}) \right]. \tag{8.61}$$

All the time, ρ_{ν} and p_{ν} depend on the evolution of ϕ , and viceversa. Therefore, we cannot split this equation on two decoupled equations for $\partial \rho_{\phi}/\partial \log a$ and $\partial \rho_{\nu}/\partial \log a$.

8.3.3 Initial conditions

We want to impose that ϕ makes up all DM, namely $\Omega_{\phi,0}h^2 = \Omega_{c,0}h^2 = 0.1200$ [151]. This requires that the amplitude of the field today is

$$A(a=1) \equiv A_0 = \frac{\sqrt{2\Omega_{c,0} \rho_{\text{crit}}}}{m_{\phi}}, \qquad (8.62)$$

assuming $m_{\phi} > \delta m_{\phi}$ today. The value of A today fixes the value of the adiabatic invariant $\mathcal{I}(a) = \mathcal{I}_0$, and allows to compute A(a) at all times if we know $f_0(q)$. Since the coupling with ϕ does not change the evolution of $f_0(q)$, its shape is frozen from its initial conditions, i.e., neutrino decoupling.

The early-Universe physics and, in particular, decoupling depend on the time of the misalignment mechanism. In standard ULDM, oscillations start when the potential energy term is larger than the Hubble friction, i.e., $m_{\phi} > 3H$. However, the interaction modifies the condition to $M_{\phi} > 3H$. This advances misalignment, $a_{\rm mis}$, to earlier times, as shown in fig. 8.5.

Since $A_0 \propto m_\phi^{-1}$ and A always appears as gA, many of the cosmological observables depend only on g/m_ϕ . However, $\delta m_\phi^2 \sim g^2$ is independent of m_ϕ . Thus, the misalignment mechanism $3H < M_\phi$ breaks the degeneracy between g and m_ϕ . We find that, for couplings such that $\delta m_\phi^2 > m_\phi^2$, misalignment happens at

$$a_{\rm mis} \simeq 10^{-11} \left(\frac{5 \times 10^{-20}}{\rm g} \right) \,.$$
 (8.63)

Decoupling happens approximately at $T_{\gamma} \sim 2 \, \text{MeV}$, which –assuming a naive linear scaling for temperature– corresponds to $a \sim 10^{-11}$. That is, misalignment happens after

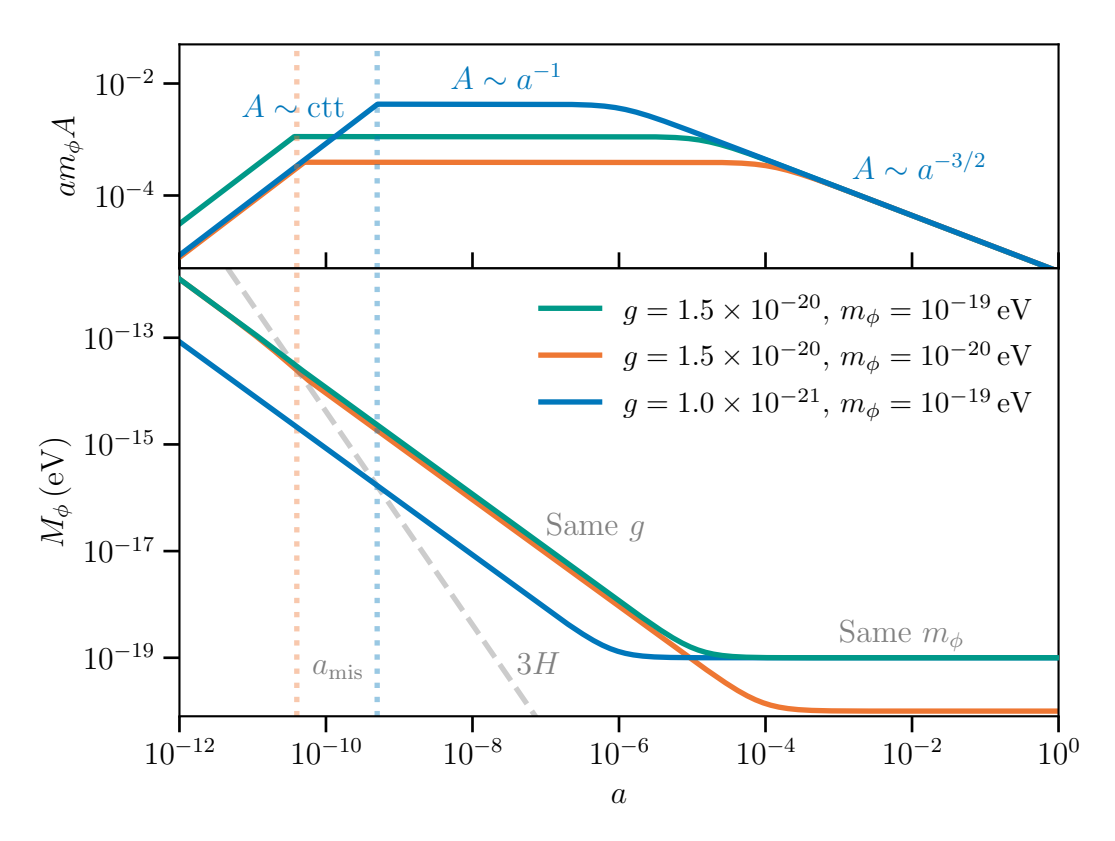


Figure 8.5: Effective mass M_{ϕ} , misalignment mechanism and evolution of the amplitude. From left to right, initially $3H > M_{\phi}$, and thus A(a) remains constant. At misalignment, $3H \sim M_{\phi}$, the field starts evolving as a^{-1} if $a < a_{\rm tr}$ or as $a^{-3/2}$ if $a > a_{\rm tr}$. Curves with the same coupling g satisfy the misalignment condition at similar times, while fields with the same m_{ϕ} arrive at the same point in M_{ϕ} . Here, the amplitude today is set to match the abundance of DM, and thus $A_0 \sim m_{\phi}^{-1}$.

decoupling roughly if $g \lesssim 5 \times 10^{-20}$. Two scenarios open up,

- Before misalignment, m_{ν} is constant, T_{ν}/m_{ν} grows to the past and neutrinos are relativistic soon before misalignment. If misalignment happens after decoupling, $g \lesssim 5 \times 10^{-20}$, then neutrinos are relativistic at decoupling and effects from the interaction are negligible. If they are, their distribution function at later times will be a relativistic Fermi-Dirac such as eq. (7.4).
- If misalignment happens while neutrinos are in thermal equilibrium with the baryon plasma, $g \gtrsim 5 \times 10^{-20}$, then the growth of A(a) might make them non-relativistic. Then, their distribution function will deviate from a Fermi-Dirac with m_{ν}/T_{ν} corrections. The full treatment requires thermal masses [597], but also to consider the effect of scatterings mediated by ϕ , far from the extent of this work.

With this in mind, we assume that misalignment happens after decoupling, and we approximate the misalignment to be instantaneous at $3H=M_{\phi}$. Before misalignment, we set $\phi=A$ and no oscillation is needed. At misalignment, ϕ starts to oscillate with M_{ϕ} and all observables are averaged as in eq. (8.25). This approximation produces an artificial discontinuity between unaveraged and averaged variables. A smooth misalignment should not strongly modify the results.

8.3.4 Massive neutrinos and $N_{\rm eff}$

The neutrino-feedback into the pseudoscalar field has two main phenomenological consequences, an increased effective mass for neutrinos and an increase of early radiation.

Firstly, neutrinos will acquire a mass given by

$$\langle m_{\nu} \rangle = \langle m_{\nu}(\phi) \rangle = \left\langle \sqrt{m_0^2 + g^2 \phi^2} \right\rangle ,$$
 (8.64)

where the average is taken over the oscillation of the field. In the linearized regime, and for early enough in the Universe, $\langle m_{\nu} \rangle \simeq gA/\sqrt{2}$. Figure 8.6 compares the evolution of the neutrino mass and T_{ν} , which is related to the mean momentum of the distribution. While early enough, the neutrino mass can reach $\mathcal{O}(1)$ MeV, the important quantity is the *relativisticness* (i.e., velocity) of neutrinos, $T_{\nu}/\langle m_{\nu} \rangle$. That is, the interaction with the field can make them non-relativistic, $\langle m_{\nu} \rangle \gg T_{\nu}$. Figure 8.6 also shows how $T_{\nu}/\langle m_{\nu} \rangle$ diminishes as $a^{-1/2}$ for $a > a_{\rm tr}$, while $T_{\nu}/\langle m_{\nu} \rangle$ becomes constant for $a < a_{\rm tr}$. At misalignment, ϕ freezes and neutrinos become relativistic soon enough.

Secondly, if we fix the right DM abundance today, a longer radiation epoch as shown in fig. 8.4 increases the amount of radiation in the early Universe. We quantify this by

$$\Delta N_{\rm eff} = N_{\rm eff} - 3.044$$
, (8.65)

with $N_{\rm eff}$ as defined in eq. (6.83). Figure 8.7 shows the evolution of $\Delta N_{\rm eff}$ in our model. The radiation excess is specially significant at the pre-CMB epoch, as expected from eq. (8.47). As a consequence, we expect BBN to put better constraints on the neutrino feedback of the model. Figure 8.7 also shows a short depletion of $N_{\rm eff}$ at the time of misalignment, which is an artifact of the instantaneous misalignment approximation. Namely, since at $a < a_{\rm mis}$ we set $\phi = A$ and skip oscillations, then $m_{\nu} = gA$ instead of $\langle m_{\nu} \rangle = gA/\sqrt{2}$, neutrinos become slightly non-relativistic and decrease $\rho_{\rm rad}$. However, as soon as the plasma heats the constant mass of neutrinos becomes negligible, thus making them relativistic and retrieving $\Delta N_{\rm eff} = 0$.

As explained in section 6.4, BBN constraints on $N_{\rm eff}$ are a derived result from the

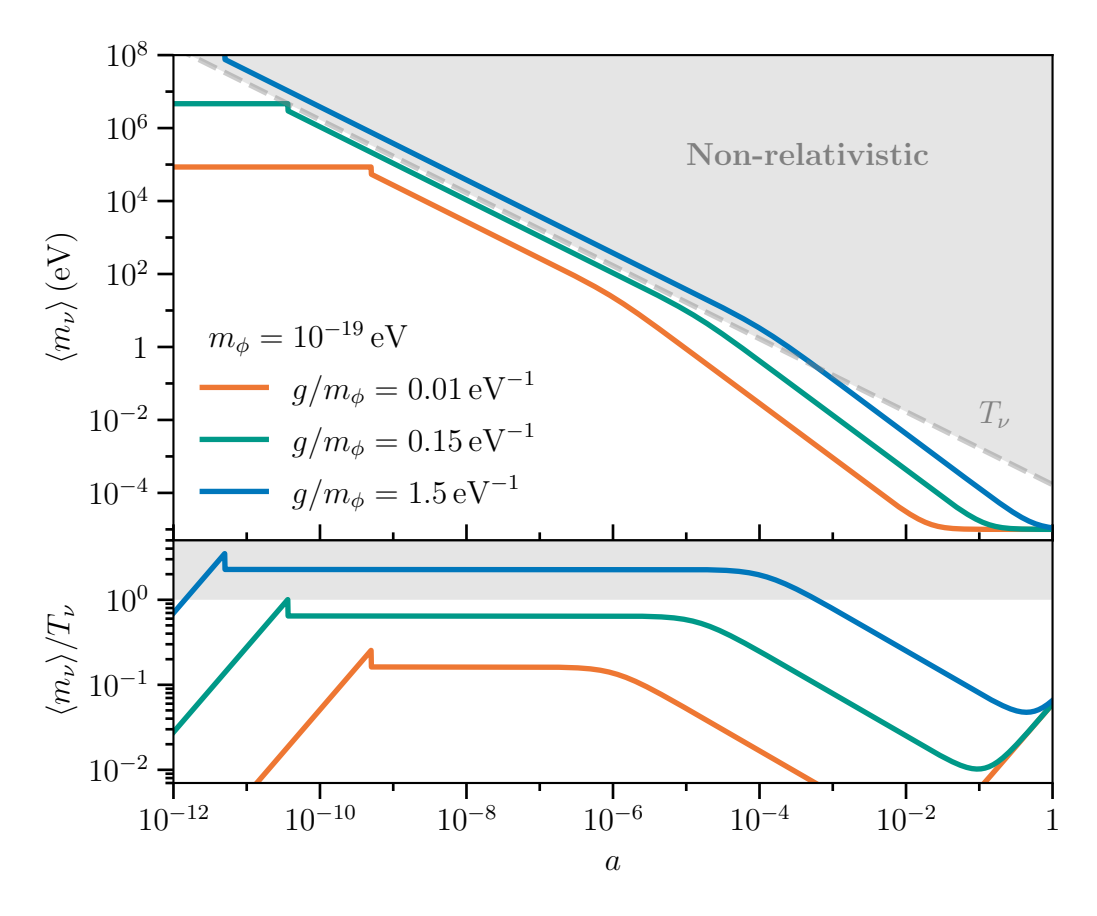


Figure 8.6: Evolution of average neutrino mass, $\langle m_{\nu} \rangle$, and its *non-relativisticness*, i.e., $\langle m_{\nu} \rangle / T_{\nu}$. Initially, $m_{\nu} \sim m_0 = 10^{-5} \, \text{eV}$, and soon $\langle m_{\nu} \rangle \sim gA/\sqrt{2}$. Thus, $\langle m_{\nu} \rangle$ follows A(a), shown in fig. 8.5. For large (excluded) couplings, neutrinos become non-relativistic. Since the linearised approximation is an expansion on $(\langle m_{\nu} \rangle / T_{\nu})^2$, the bottom plot justifies the validity of the approximation for non-excluded couplings.

observation of light element abundances and nucleosynthesis simulations. Since $N_{\rm eff}$ is not the only consequence of our model, we implement our model in the full calculation of the abundances and constrain the model from there.

8.3.5 Impact on Big Bang Nucleosynthesis

The impact of the model in BBN is two-fold. First, $\Delta N_{\rm eff}$ will increase the Hubble rate, thus making the processes in eq. (6.78) less efficient and modifying the duration of nucleosynthesis. Secondly, the non-zero mass of neutrinos will modify the kinematics of the reactions and thus the interaction rates Γ . For instance, if neutrinos had mass $m_{\nu} > \Delta - m_{e}$, with $\Delta = m_{n} - m_{p} \simeq 1.29333\,{\rm MeV}$, neutron decay would be forbidden, greatly increasing $Y_{\rm P}$.

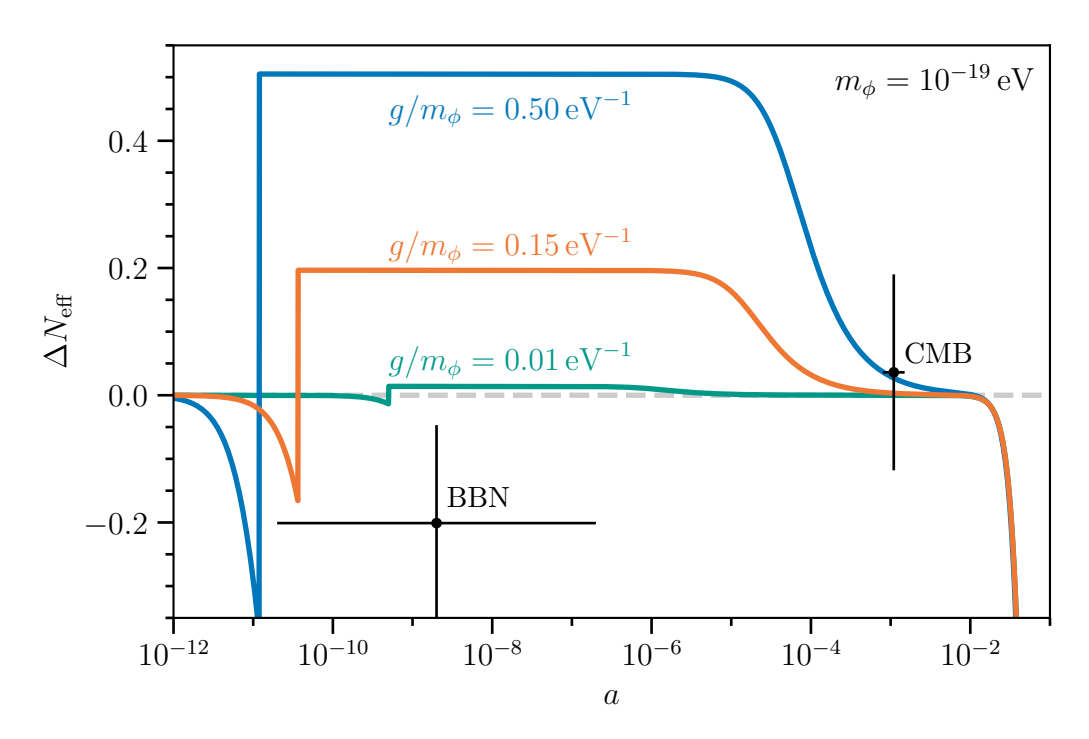


Figure 8.7: Number of relativistic neutrino species for different values of the coupling. The dilation of the radiation phase, shown in fig. 8.4, increases the amount of radiation in the early universe. Data points show the measurements of $N_{\rm eff}$ at CMB and BBN, with horizontal errorbars showing the approximate duration of each epoch. Couplings which have a significant impact on BBN are negligible at CMB. *BBN is the best epoch to constrain this model.*

In order to implement neutrino masses in $n \to p$ (and viceversa) interaction rates, we follow the Born approximation, where neutrons and protons are approximated to have infinite mass. In this limit, interaction rates from all the processes in eq. (6.78) are given by [615],

$$\Gamma_{n\to p} = \tilde{G}_F^2 \int_0^\infty dE_e \, E_e E_\nu^- \sqrt{E_e^2 - m_e^2} \sqrt{E_\nu^- - m_\nu^2} \left[f_\nu(E_\nu^-) f_e(-E_e) + f_\nu(-E_\nu^-) f_e(E_e) \right] ,$$

$$\Gamma_{p\to n} = \tilde{G}_F^2 \int_0^\infty dE_e \, E_e E_\nu^+ \sqrt{E_e^2 - m_e^2} \sqrt{E_\nu^+ - m_\nu^2} \left[f_\nu(E_\nu^+) f_e(-E_e) + f_\nu(-E_\nu^+) f_e(E_e) \right] .$$
(8.66)

Here, $\tilde{G}_F^2 = G_F V_{\rm ud} \sqrt{(1+3g_A^2)/(2\pi^3)}$ with G_F the Fermi constant, $V_{\rm ud}$ the Cabibbo angle and g_A the axial electroweak coupling; and $E_{\nu}^{\pm} = E_e \pm \Delta$. The distribution functions f_{ν} , f_e follow Fermi-Dirac distributions as in eq. (7.4), controlled by T_{ν} and T_{γ} , respectively. These implement the amount of allowed fermions for the interaction if in the initial state, or Pauli blocking if in the final state. While a modified neutrino mass will not modify the matrix element leading to Γ , further investigation is needed into whether the eigenstates of eq. (8.3) modify the interaction vertex. These rates are shown in fig. 8.8.

Now, $\Gamma = \Gamma(\phi)$ through $m_{\nu} = m_{\nu}(\phi)$. Before misalignment, $3H > M_{\phi}$, the field is

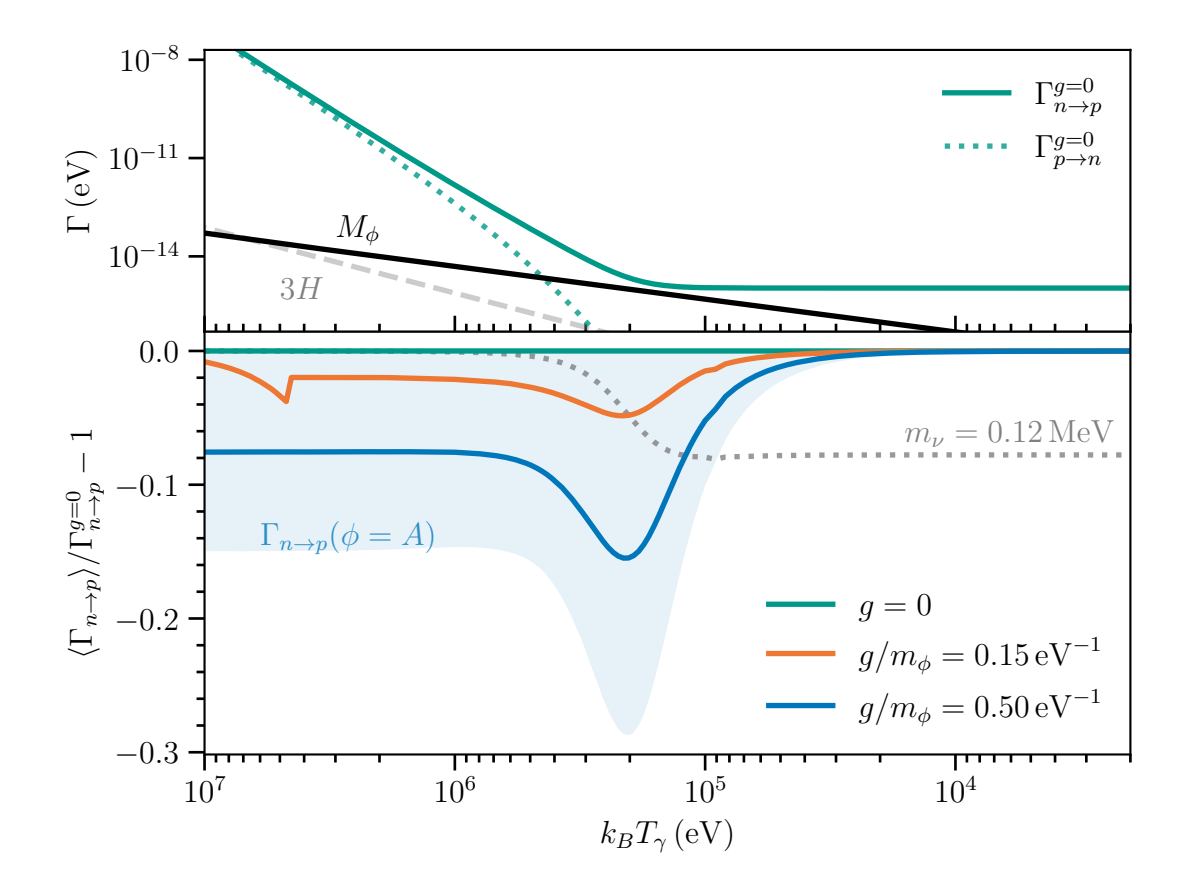


Figure 8.8: Neutron-to-proton (and viceversa) interaction rates $\Gamma_{n\to p}$ ($\Gamma_{p\to n}$) at the temperatures relevant for BBN, and the effect of v-ULDM interactions in them. In the top plot, we compare Γ to the other relevant timescales of the problem, and check that $3H > \Gamma$, M_{ϕ} ; which requires us to average over ϕ oscillations, as described in the main text. M_{ϕ} is shown for $g/m_{\phi} = 0.15 \, \text{eV}^{-1}$. In the bottom plot, we see how the coupling reduces the $n \to p$ interaction rate. For comparison, we show the effect of a constant mass $m_{v} = 0.12 \, \text{MeV}$ (dotted line). The blue shaded region encloses $\Gamma_{n\to p}(\phi)$ for all possible values of $\phi < A(a)$. Thus, the solid blue line is the average of the blue shaded region. A larger neutrino mass decreases the interaction rate, which will increase the helium and deuterium abundances.

frozen and oscillations need not be taken into account. However, after misalignment, the field oscillates and Γ needs to be averaged. Different timescales play a role here. First, the oscillation of the field is always much slower than the timescale of the electroweak vertex, $M_{\phi}^2 \ll G_F^{-1}$, and therefore electroweak interactions happen within a constant value of the field. Then, two regimes can follow,

- If $\Gamma > M_{\phi}$, many interactions happen within an oscillation of the field, and so eq. (8.66) can reach equilibrium within a constant m_{ν} . Since ϕ oscillates many times within cosmological timescales, we need to average Γ over each $m_{\nu}(\phi)$.
- If $\Gamma < M_{\phi}$, interactions happen only once every many oscillations. At cosmological

scale, with $\Gamma > H$, still many interactions happen, each of them effectively at a random value of $m_{\nu}(\phi)$. Then, the result is still an effective averaged Γ .

In any case, we must average as in eq. (8.25)

$$\langle \Gamma \rangle = t_{\phi}^{-1} \oint \frac{\Gamma(\phi)}{\dot{\phi}} \, \mathrm{d}\phi \,, \tag{8.67}$$

where $\Gamma(\phi)$ is given by eq. (8.66) with $m_{\nu}=m_{\nu}(\phi)$. Finally, neutrinos do not play a role in the subsequent thermonuclear interactions, and therefore hadronic rate are unmodified by non-zero m_{ν} . We implement the modified expansion history and expansion rates from eqs. (8.66) and (8.67) in the numerical code PRyMordial [615]. Figure 8.8 shows how the coupling reduces $\langle \Gamma_{n\to p} \rangle$. As a consequence, a reduced $n \to p$ interaction rate will then increase $Y_{\rm P}$.

8.4 Results

The modified version of PRyMordial allows to compute all the light element abundances. From the observed abundances given in eq. (6.82), we discard 3 He, for which only an upper limit exists, and 7 Li, which is currently anomalous. Thus, restricting the analysis to the 4 He (Y_P) and the deuterium (D/H) abundances makes it more conservative and robust. Figure 8.9 shows how an increased interaction rate increases the expected abundances, far above the observed values. The results also indicate that, while both $\Delta N_{\rm eff}$ and m_{ν} increase the final abundances, the Y_P result is more sensitive to m_{ν} than to $\Delta N_{\rm eff}$ and is the dominant quantity driving the constraints.

Then, for every point in the (g, m_{ϕ}) parameter space we can define a χ^2 function,

$$\chi^{2}(g, m_{\phi}) = \left(\frac{Y_{P}(g, m_{\phi}) - Y_{P}^{obs}}{\sigma_{Y_{P}}}\right)^{2} + \left(\frac{D/H(g, m_{\phi}) - (D/H)^{obs}}{\sigma_{D/H}}\right)^{2}, \tag{8.68}$$

where Y_P^{obs} ((D/H)^{obs}) is the observed value of the ⁴He (²H) abundance, and σ_{Y_P} ($\sigma_{D/H}$) its 1σ uncertainty, as given in eq. (6.82). As shown in fig. 8.9, there is percent discrepancy between the Born approximation and the result with next-to-leading order corrections (e.g., finite nucleon mass, bremsstrahlung losses [435]). We perform a hypothesis test by defining

$$\Delta \chi^2 \equiv \chi^2(g, m_\phi) - \chi^2_{NLO}(g = 0),$$
 (8.69)

where $\chi^2_{\rm NLO}(g=0)$ is the value of eq. (8.68) at g=0, including next-to-leading order corrections, i.e., the null hypothesis. The 95% C.L. contours of this function is presented in fig. 8.10. At $m_{\phi} \gtrsim 3 \times 10^{-20}$ eV, the bound is $g \lesssim 0.13 (m_{\phi}/{\rm eV})$. At this region,

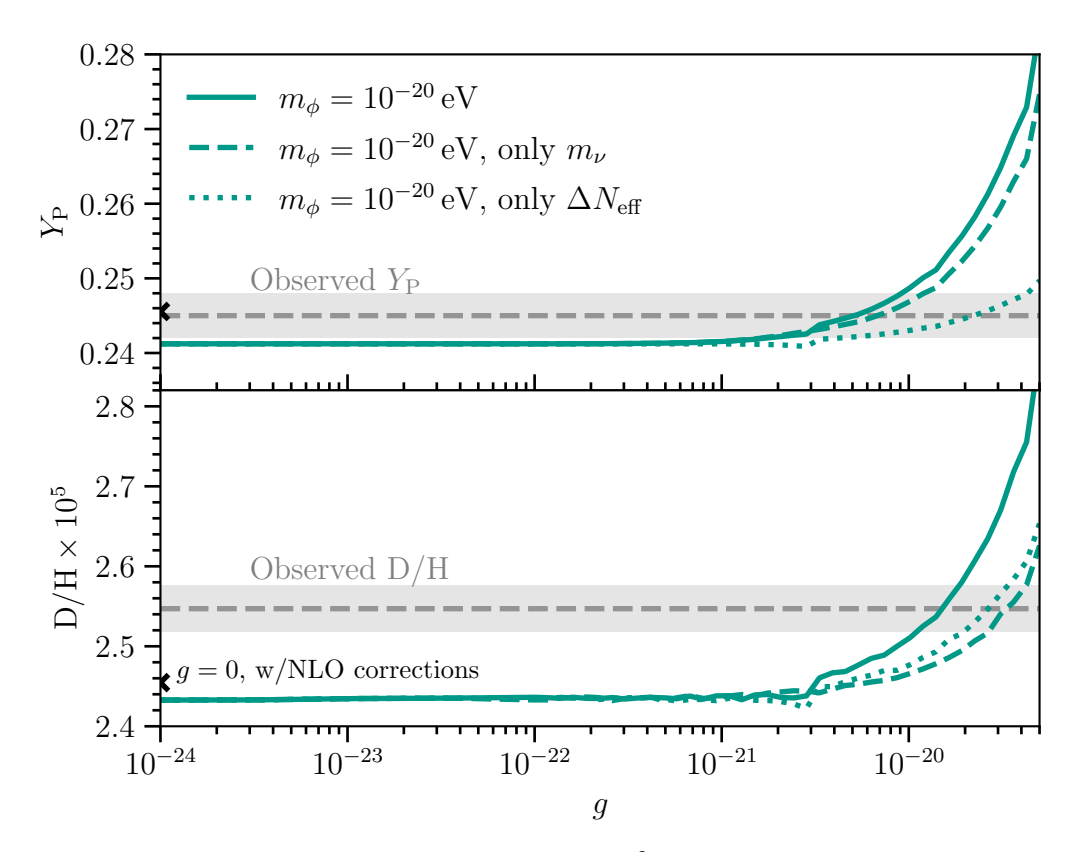


Figure 8.9: Prediction on primordial abundances of 3 He and deuterium for different values g, at $m_{\phi}=10^{-19}$ eV. Solid lines show the prediction including all effects of our model, while a dotted line includes only the modification of neutrino masses (i.e., $\Delta N_{\rm eff}=0$ artificially), and a dashed line only the modification of $N_{\rm eff}$ (i.e., $m_{\nu}=0$). A black cross shows the results at g=0 beyond the Born approximation, including next-to-leading order contributions, and a grey band shows the 1σ contours of the observed values [55].

misalignment happens before BBN, and all observable effects depend only on g/m_ϕ . However, as explained in section 8.3.3, bounds for $g \gtrsim 5 \times 10^{-20}$ depend on the physics of decoupling and might be corrected by thermal effects [596, 597]. At $m_\phi \lesssim 3 \times 10^{-20}$ eV, misalignment happens at some point in BBN. Previous to misalignment, the feedback effects disappear and BBN loses constraining power, thus weakening the bound to $g \lesssim 1.8 \times 10^{-11} \sqrt{m_\phi/\text{eV}}$.

Due to the Milky Way DM halo, the local DM density is larger than the cosmological mean field value that we have defined up to now. In particular, $\rho_{\rm DM}^{\odot} = 0.3 \, {\rm GeV \, cm^{-3}}$. Taking this into account, it would be specially interesting if this model could predict the right order of magnitude for neutrino masses without requiring the extra parameter m_0 .

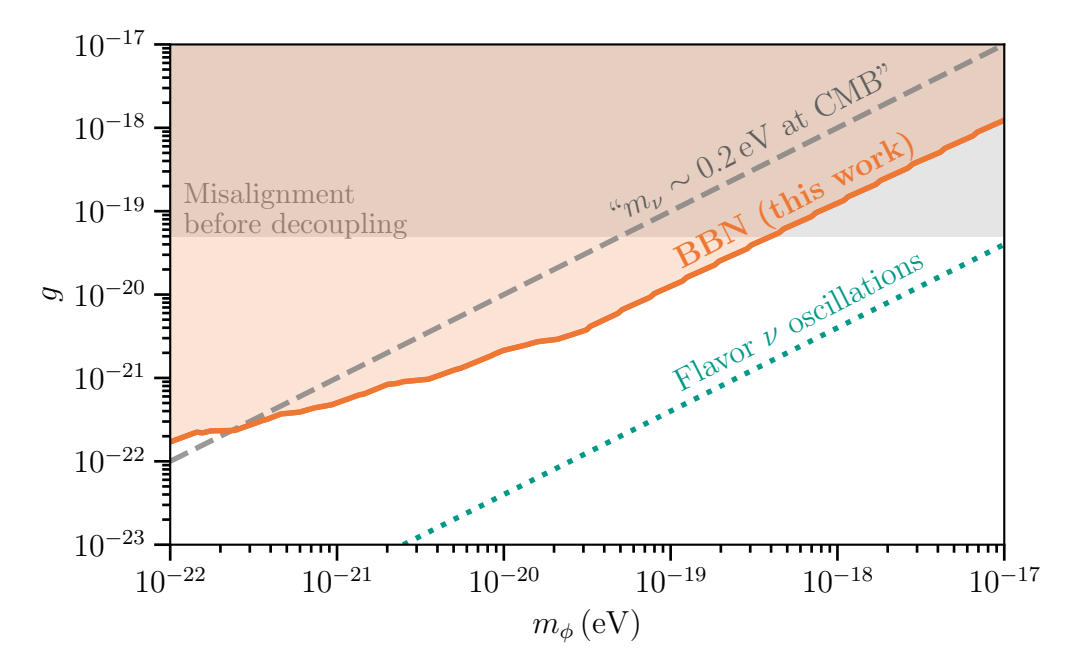


Figure 8.10: 95% C.L. exclusion regions for the $v-\phi$ coupling (as defined in eq. (8.1)), for the test statistic defined in eq. (8.69). A gray dashed line shows the bound for a scalar coupling to RHNs, assuming that $m_v(\phi) \lesssim 0.23\,\mathrm{eV}$ at CMB time [572]. A green dotted line shows a bound for this same model, assuming it has flavor structure and gives rise to time-dependent neutrino oscillations [572]. The gray shaded region corresponds to misalignment happening before neutrino decoupling, meaning neutrinos can be non-relativistic at decoupling and modify their distribution function from the here-assumed Fermi-Dirac.

Neglecting m_0 , this means

$$\langle m_{\nu}^{\odot} \rangle \simeq \frac{g}{m_{\phi}} \sqrt{\rho_{\rm DM}^{\odot}} = 2 \times 10^{-4} \left(\frac{g/m_{\phi}}{0.13 \,\mathrm{eV}^{-1}} \right) \,\mathrm{eV}.$$
 (8.70)

Setting the target neutrino mass to $m_{\nu}^{\odot} \sim \sqrt{|\Delta m_{3\ell}^2|} = 3 \times 10^{-3} \, \text{eV}$, this would only be reached at couplings saturating the bound for $m_{\phi} \sim 10^{-22} \, \text{eV}$.

8.5 Conclusions and outlook

The nature of DM and the origin of neutrino masses are two yet unsolved mysteries of particle physics. Models which connect both of these sectors are theoretically motivated and phenomenologically rich. In particular, models of ULDM are gaining interest in the community. In this chapter, we have explored the phenomenological implications of a coupling between ULDM and the neutrino sector in the early Universe. As a result, we have presented a quantitative bound from a full cosmological evolution of such models.

In this work we have quantitatively solved the equations of motion for the ULDM

field, which have a large separation of scales between the frequency of ϕ oscillations and cosmological evolution. To such purpose, we follow an adiabatic approximation which provides an invariant quantity with which to compute the amplitude of the field at every time. This method predicts that the scaling of the ULDM field changes when the neutrino interaction potential dominates over its mass potential, from $a^{-3/2}$ to a^{-1} .

Two observable consequences in the early Universe derive from this scaling transition. First, neutrino masses scale linearly with the scale factor, and thus their velocity, related to T_{ν}/m_{ν} , stays constant. This is shown in fig. 8.6. When compared to the naive scaling of $a^{-3/2}$, this weakens the effect of time-dependent neutrino masses in the early Universe. Second, the modified scaling also reduces the contribution of the bare-mass potential, $m_{\phi}^2 \phi^2$, to the total energy of the system. As a consequence, the coupled ν -ULDM stays relativistic for a longer time, as in fig. 8.4. If then we ask for ϕ to fulfill the totality of DM, this requires that the radiation energy density in the early Universe is slightly larger, which contributes positively to $\Delta N_{\rm eff}$, as in fig. 8.7.

Finally, we implement this two phenomenological consequences in Big Bang Nucleosynthesis using the PRyMordial code [615]. We modify the $n \to p$ and $p \to n$ interaction rates to account for a non-zero neutrino mass, following the Born approximation. Since these rates are faster than the oscillation frequencies and the cosmological evolution, we average them for the oscillation of the ULDM field. Using the modified rates and $N_{\rm eff}$, we compute the primordial element abundances for different (g, m_ϕ) , as in fig. 8.9. Comparing these to observations, we present our bounds on the parameter space of the model in fig. 8.10, which improve naive scaling bounds by up to an order of magnitude.

The non-trivial dynamics of the coupled fluid are an unexpected consequence of ν -ULDM which open new research possibilities. In particular, in this work we have focused on BBN consequences since we *a priori* expect it to provide further constraints on the model. However, to extend this framework to cosmological perturbations might bring about new unexpected consequences which make the CMB a better tool to constrain the model. In fact, to understand the dynamics of ν -ULDM perturbations is a problem sufficiently interesting on its own.

Furthermore, the exact coupling that we have used should be understood as a first approach to v-ULDM couplings with time-varying masses. Other couplings, which have more theoretically motivated SM extensions, have been proposed in the literature. Even if their phenomenological implications have already been explored [593, 596], it would be interesting to extend the quantitative analysis here presented into such models to place consistent bounds into them.

All in all, cosmology remains an exciting framework within which to look for signa-

tures of BSM particle physics models, specially for particles which interact extremely feebly. That is, the large particle number densities involved compensate for the small couplings. This is specially interesting for interactions which involve the neutrino sector. At the same time, cosmology is a complex science with a lot of subleties that must be under control in order to produce robust statements. In this work we have tried to clarify some of such details and to make claims on ν -ULDM claims consistent and quantitative.

Part IV Conclusions and appendices

9 Conclusions

Why should a man climb Everest?

- Because it is there.

- George Leigh Mallory, one of the first British to Everest.

Understanding the fundamental properties of Nature is a quest which requires the sum and interference of many different perspectives, expertises and methodologies. Experimentalists are essential to interrogate Nature and pave the way towards New Physics, while theorists must interpret the answers into the global picture. Lying in the middle, phenomenologists are the translators which bridge the gap between them. They are necessary to keep theories grounded, and to take the full potential of experiments beyond their original reach.

This thesis sums, and hopefully interferes constructively, to the enormous amount of work that has preceded it. We have tried to extend the frontiers of BSM searches using one of the richest and most diverse approaches to them, the neutrino sector. As reviewed in chapter 2, we know for sure that the neutrino sector must be extended in some manner, as neutrino oscillations have been our first hint of New Physics. Therefore, this was the first approach towards New Physics searches, and chapter 3 marked the beginning of this thesis. In this chapter, we reviewed how the bounds of reactor and gallium experiments varied if the wave packet width of sterile neutrinos were taken into account within experimental constraints, and how this could relieve their tension. While the experimental bounds on σ_x used are conventionally supposed to be far from the expected theoretical value, this work sparked lively discussion in the community. On the one hand, encouraging experimentalists to take σ_x as an unknown in sterile neutrino analysis; on the other hand, motivating theorists to undergo better calculations for σ_x and to think BSM models that could narrow the width down.

Neutrino oscillations were followed by ultra-high-energy astrophysics. In chapter 4, we reviewed the prediction of cosmogenic neutrinos and why they are useful to explore BSM at unprecedented energies. While this certainly is a promising field in the mid-future, it also brings interesting questions as of today. In chapter 5, we explore the anomalous ANITA-IV events and propose a general BSM explanation for them, simultaneously relaxing their tension with the silence from IceCube. On the one hand, our phenomenologist approach to this anomaly provides to model-builder theorists the requirements that their particular theory must fulfill. On the other hand, our exercise shows –with real data– what is the potential of UHE neutrino telescopes to constrain New Physics and how complementarity between experiments is essential for best re-

sults.

This thesis concludes with the third part, neutrino cosmology. In chapter 6 we review the basics that have lead cosmology into becoming a precision science, with the CMB as its most successful landmark. Chapter 7 then describes the role of neutrino masses in it, with a careful interpretation of their effect at the background and perturbations. This is a didactical work which elaborates not only on the datasets and measurements as many other works, but on the physical processes beneath them. On the one hand, this allows experimentalists to better understand the neutrino properties actually being measured, and understanding how to produce a more robust measurement of neutrino masses. On the other hand, it allows theorists to better understand cosmological bounds, and to visualize which kind of BSM physics could spoil the measure (and avoid a possible tension with terrestrial experiments). Finally, chapter 8 studies the cosmological consequences of a non-zero coupling between neutrinos and ultralight Dark Matter (ULDM). We describe how the scalar can give mass to the neutrinos and, as a consequence, its dynamics are affected by a neutrino-induced potential. We find that this interaction predicts mass-varying neutrinos and additional radiation in the early Universe. This modifies the primordial abundances of the light elements, which we then use to set quantitative and competitive bounds for the coupling. These bounds difficult the understanding of the measured neutrino masses as a direct coupling to ULDM.

All in all, this thesis collects different research works which bridge the gap between theory and experiment in a satisfactory manner. It manages to answer each of the the scientifical questions that are addressed, while opening opportunities for new research and future prospects. To me, this thesis has the intrinsic value of approaching neutrino BSM from three completely distinct fields, which require different theoretical knowledge and methodologies, and which engage completely different communities. Beyond the produced work that forms this thesis, these four years have equipped me with a broad perspective of the current status of neutrino physics, and with the baggage to tackle new problems, even beyond neutrinos. In any case, obtaining the complete description of Nature will still require further constructive interference. Hopefully, this thesis is just the beginning to my contribution to it.

A UHE particle propagation inside the Earth

In order to measure UHE neutrino properties it is essential to take into account the physical processes during the neutrino and charged lepton propagations, e.g., scattering cross-sections, inelasticities, energy losses and regeneration processes.

Since these are stochastic processes, a Montecarlo method is necessary to compute the flux of particles at a detector, given an incoming astrophysical flux. This is the case of PROPOSAL [616], NuPropEarth [617] TauRunner [618], NuPyProp [619] or NuLeptonSim [620]. In chapter 5 we introduce a BSM scheme which emulates this propagation in a simplified manner. In this appendix, we write down the probabilities for the arrival of the different particles. In particular, we call N a BSM neutrino-like particle which can interact with ordinary matter with a cross-section σ , to produce a secondary T particle through N+N \rightarrow T+X. Then, T –with a laboratory lifetime τ –, can propagate and in average decay after a distance $c\tau$.

Geometry

We use analytic estimates by approximating the Preliminary Earth Reference Model (PREM) parametrization of the Earth density [621] by a set of homogeneous layers (although the results from chapter 5 are robust against different parametrizations). For a given trajectory inside a spherical Earth with exit angle θ , the particle changes layers at

$$x_i^{\pm} = R_{\oplus} \cos \theta \pm \frac{\sqrt{2}}{2} \sqrt{2r_i^2 - R_{\oplus}^2 (1 - \cos 2\theta)},$$
 (A.1)

with r_i the radii of the discontinuities between layers and R_{\oplus} the radius of the Earth. The width of each layer is $\Delta l_i = x_{i+1} - x_i$.

In ANITA, the total travelled distance is the chord length inside Earth, $L(\theta) = 2R_{\oplus}\cos\theta$. In IceCube the trajectory must finish at the detector, before leaving Earth. The distance between the detector and the exit point is

$$2R_{\oplus}^{2}[1-\cos(\theta-\alpha(\theta))] - 2R_{\oplus}D[1-\cos(\theta-\alpha(\theta))] + D^{2} \equiv a(\theta), \qquad (A.2)$$

where D = 1 km is the depth of the detector.

We compute all probabilities in terms of the zenith angle θ of the particle T at its exit point. For ANITA, this is related to the elevation angle α as

$$\sin \theta = \cos \alpha \left(1 + \frac{h_{\text{ant}}}{R_{\oplus}} \right) , \tag{A.3}$$

with $h_{\rm ant}$ the height of the ANITA antenna and R_{\oplus} the Earth radius. However, radio

waves are refracted during propagation, which modifies the relation between θ and the observed elevation. We implement this by effectively increasing the Earth radius by a fudge factor 1.13 that reproduces the horizon elevation angle as a function of $h_{\rm ant}$ as provided by the ANITA collaboration (see Table 1 in Ref. [372]). For instance, the distance $d(\theta)$ between the detector and the exit point of the T particle –which enters in the detection probability– is

$$d(\theta) = -R_{\oplus} \frac{\cos(\theta - \alpha(\theta))}{\cos \alpha(\theta)} \sim \mathcal{O}(500 \text{ km}). \tag{A.4}$$

For the IceCube experiment, the relation between angles is

$$\sin \theta = -\cos \alpha \left(1 - \frac{h_{\rm exp}}{R_{\oplus}} \right) , \qquad (A.5)$$

with $h_{\text{exp}} = 1 \text{ km}$ the depth of IceCube.

N exit probability

The probability for a particle N to interact with a nucleus in a medium after travelling a distance x is $p_{\lambda}(x;\lambda) = e^{-x/\lambda}/\lambda$, where $\lambda^{-1} = n\sigma$ is the mean free path and n the nucleon number density. The probability for N to leave a uniform medium of depth Δl is $P(X_{\rm int} > \Delta l) = \int_{\Lambda l}^{\infty} p_{\lambda}(x;\lambda) \, \mathrm{d}x = e^{-\Delta l/\lambda}$, and the probability to escape all the layers is

$$P_{\text{exit}}^{\text{N}} = \prod_{i=1}^{m} P(X_{\text{int}}^{(i)} > \Delta l_i) = \prod_{i=1}^{m} e^{-\Delta l_i/\lambda_i},$$
 (A.6)

with m the number of layers crossed in the trajectory. In order to account for N regeneration, we add two additional terms,

$$P_{\text{exit}}^{\text{N}} = \prod_{i=1}^{m} P(X_{\text{int}}^{(i)} > \Delta l_i) + \\ + \sum_{i=1}^{m} \left(\prod_{k < i} P(X_{\text{int}}^{(k)} > \Delta l_k) \right) \times \left(\prod_{k > i} P(X_{\text{int}}^{(k)} > \Delta l_k) \right) \times \\ \times \int_{0}^{\Delta l_i} P(X_{\text{int}}^{(i)} = x) \, \mathrm{d}x \int_{x}^{\Delta l_i} P(Y_{\text{dec}}^{(i)} > y - x) P(Y_{\text{int}}^{(i)} = y - x) P(X_{\text{int}}^{(i)} > \Delta l_i - y) \, \mathrm{d}y + \\ \text{In the layer } i, \text{ N produces a T that produces another N}$$

$$+\sum_{i=1}^{m}\sum_{j>i}^{m}\left(\prod_{k< i}P(X_{\mathrm{int}}^{(k)}>\Delta l_{k})\right)\times\left(\prod_{k>j}P(X_{\mathrm{int}}^{(k)}>\Delta l_{k})\right)\times\\ N \text{ survives all layers before }i\right)\times\left(\prod_{k>j}P(X_{\mathrm{int}}^{(k)}>\Delta l_{k})\right)\times\\ \times\int_{0}^{\Delta l_{i}}P(X_{\mathrm{int}}=x)P(Y_{\mathrm{decay}}>\Delta l_{i}-x)P(Y_{\mathrm{int}}>\Delta l_{i}-x)\,\mathrm{d}x\times\\ N \text{ interacts at layer }i\text{ and T leaves the layer}\\ \times\left(\prod_{k=i+1}^{j-1}P(Y_{\mathrm{decay}}^{(k)}>\Delta l_{k})P(Y_{\mathrm{int}}^{(k)}>\Delta l_{k})\right)\times\\ T \text{ survives all layers between }i\text{ and }j$$

$$\times\int_{0}^{\Delta l_{j}}P(Y_{\mathrm{decay}}^{(j)}>y)P(Y_{\mathrm{int}}^{(j)}=y)P(X_{\mathrm{int}}^{(j)}>\Delta l_{j}-y)\,\mathrm{d}y$$

$$T \text{ produces a N in layer }i\text{ and N leaves}$$

The first term describes N exiting without interaction. The second term introduces one intermediate T which is created and destroyed in the same layer. In the third term, the T is created and destroyed in different layers. This gives

$$P_{\text{exit}}^{\text{N}} = \left(\prod_{k=1}^{m} e^{-\Delta l_k/\lambda_k}\right) \left[1 + \sum_{i=1}^{m} \left(\frac{c\tau}{\lambda_i}\right)^2 \left(\frac{\Delta l_i}{c\tau} + e^{-\Delta l_i/c\tau} - 1\right) + \left(\frac{\Delta l_i}{c\tau}\right)^2 \left(\frac{\Delta l_i}{c\tau} + e^{-\Delta l_i/c\tau}\right) + \sum_{i,j>i}^{m} \left(\prod_{k>i,k$$

We find that one regeneration process is enough to describe the dominant contributions.

T exit probability

In order for a T particle to exit a medium, we need the parent N to interact, and T not to decay nor interact before it leaves the medium. We define

$$P(Y_{\text{decay}} > \Delta x) \equiv \int_{\Delta x}^{\infty} p_{\tau}(x, \tau) \, \mathrm{d}x = e^{-\Delta x/c\tau}, \ P(Y_{\text{int}} > \Delta x) \equiv \int_{\Delta x}^{\infty} p_{\lambda}(x, \tau) \, \mathrm{d}x = e^{-\Delta x/\lambda}. \tag{A.9}$$

Treating Earth as a multi-layered medium, the total exit probability is

$$P_{\text{exit}}^{\text{T}} = \sum_{i=1}^{m} \left(\prod_{j < i} P(X_{\text{int}}^{(j)} > \Delta l_j) \right) \times \left(\prod_{j > i} P(Y_{\text{decay}}^{(j)} > \Delta l_j) P(Y_{\text{int}}^{(j)} > \Delta l_j) \right)$$

$$\times \int_{0}^{\Delta l_i} P(X_{\text{int}} = x) P(Y_{\text{decay}} > \Delta l_i - x) P(Y_{\text{int}} > \Delta l_i - x) \, \mathrm{d}x \,. \tag{A.10}$$

$$\times \int_{0}^{\Delta l_i} P(X_{\text{int}} = x) P(Y_{\text{decay}} > \Delta l_i - x) P(Y_{\text{int}} > \Delta l_i - x) \, \mathrm{d}x \,.$$

This gives

$$P_{\text{exit}}^{\text{T}} = \left(\prod_{j=1}^{m} e^{-\Delta l_j/\lambda_j}\right) \left(\prod_{j>i} e^{-\Delta l_j/c\tau}\right) \sum_{i=1}^{m} \frac{c\tau}{\lambda_i} \left(1 - e^{-\Delta l_i/c\tau}\right) . \tag{A.11}$$

Bibliography

- [1] Carlos A. Argüelles, Toni Bertólez-Martínez, and Jordi Salvado. "Impact of wave packet separation in low-energy sterile neutrino searches". In: *Phys. Rev. D* 107.3 (2023), p. 036004. DOI: 10.1103/PhysRevD.107.036004. arXiv: 2201.05108 [hep-ph].
- [2] Toni Bertólez-Martínez et al. "IceCube and the origin of ANITA-IV events". In: *JHEP* 07 (2023), p. 005. DOI: 10.1007/JHEP07 (2023) 005. arXiv: 2305.03746 [hep-ph].
- [3] Toni Bertólez-Martínez et al. "Origin of cosmological neutrino mass bounds: background *versus* perturbations". In: (Nov. 2024). arXiv: 2411.14524 [astro-ph.CO].
- [4] Virgile Dandoy, Toni Bertólez-Martínez, and Francesco Costa. "High Frequency Gravitational Wave bounds from galactic neutron stars". In: *JCAP* 12 (2024), p. 023. DOI: 10. 1088/1475-7516/2024/12/023. arXiv: 2402.14092 [gr-qc].
- [5] Wolfgang Pauli. "Aufsätze und Vorträge über Physik und Erkenntnistheorie". In: *Braunschweig (1961); Collected Scientific Papers, volume 2, Interscience (1964) page 1313* ().
- [6] F. J. Hasert et al. "Observation of Neutrino Like Interactions Without Muon Or Electron in the Gargamelle Neutrino Experiment". In: *Phys. Lett. B* 46 (1973), pp. 138–140. DOI: 10.1016/0370-2693(73)90499-1.
- [7] G. Arnison et al. "Experimental Observation of Isolated Large Transverse Energy Electrons with Associated Missing Energy at $\sqrt{s} = 540$ GeV". In: *Phys. Lett. B* 122 (1983), pp. 103–116. DOI: 10.1016/0370-2693(83)91177-2.
- [8] G. Arnison et al. "Experimental Observation of Lepton Pairs of Invariant Mass Around 95-GeV/c**2 at the CERN SPS Collider". In: *Phys. Lett. B* 126 (1983), pp. 398–410. DOI: 10.1016/0370-2693(83)90188-0.
- [9] P. Bagnaia et al. "Evidence for $Z^0 \to e^+e^-$ at the CERN $\bar{p}p$ Collider". In: *Phys. Lett. B* 129 (1983), pp. 130–140. DOI: 10.1016/0370–2693(83)90744–X.
- [10] M. Banner et al. "Observation of Single Isolated Electrons of High Transverse Momentum in Events with Missing Transverse Energy at the CERN anti-p p Collider". In: *Phys. Lett. B* 122 (1983), pp. 476–485. DOI: 10.1016/0370-2693(83)91605-2.
- [11] John N. Bahcall and Roger K. Ulrich. "Solar Models, Neutrino Experiments and Helioseismology". In: *Rev. Mod. Phys.* 60 (1988), pp. 297–372. DOI: 10.1103/RevModPhys.60.297.
- [12] John N. Bahcall and M. H. Pinsonneault. "Standard solar models, with and without helium diffusion and the solar neutrino problem". In: *Rev. Mod. Phys.* 64 (1992), pp. 885–926. DOI: 10.1103/RevModPhys.64.885.
- [13] C. V. Achar et al. "Detection of muons produced by cosmic ray neutrinos deep underground". In: *Phys. Lett.* 18 (1965), pp. 196–199. DOI: 10.1016/0031-9163(65)90712-2.
- [14] F. Reines et al. "Evidence for high-energy cosmic ray neutrino interactions". In: *Phys. Rev. Lett.* 15 (1965), pp. 429–433. DOI: 10.1103/PhysRevLett.15.429.
- [15] Y. Fukuda et al. "Evidence for oscillation of atmospheric neutrinos". In: *Phys. Rev. Lett.* 81 (1998), pp. 1562–1567. DOI: 10.1103/PhysRevLett.81.1562. arXiv: hep-ex/9807003.
- [16] Q. R. Ahmad et al. "Direct evidence for neutrino flavor transformation from neutral current interactions in the Sudbury Neutrino Observatory". In: *Phys. Rev. Lett.* 89 (2002), p. 011301. DOI: 10.1103/PhysRevLett.89.011301. arXiv: nucl-ex/0204008.
- [17] K. Eguchi et al. "First results from KamLAND: Evidence for reactor anti-neutrino disappearance". In: *Phys. Rev. Lett.* 90 (2003), p. 021802. DOI: 10.1103/PhysRevLett.90.021802. arXiv: hep-ex/0212021.

- [18] S. H. Ahn et al. "Detection of accelerator produced neutrinos at a distance of 250 km". In: *Phys. Lett. B* 511 (2001), pp. 178–184. DOI: 10.1016/S0370-2693(01)00647-5. arXiv: hep-ex/0103001.
- [19] P. Adamson et al. "Measurement of Neutrino and Antineutrino Oscillations Using Beam and Atmospheric Data in MINOS". In: *Phys. Rev. Lett.* 110.25 (2013), p. 251801. DOI: 10.1103/PhysRevLett.110.251801. arXiv: 1304.6335 [hep-ex].
- [20] Markus Ackermann et al. "High-energy and ultra-high-energy neutrinos: A Snowmass white paper". In: *JHEAp* 36 (2022), pp. 55–110. DOI: 10.1016/j.jheap.2022.08.001. arXiv: 2203.08096 [hep-ph].
- [21] Ivan Esteban et al. "NuFit-6.0: Updated global analysis of three-flavor neutrino oscillations". In: (Oct. 2024). arXiv: 2410.05380 [hep-ph].
- [22] P. F. de Salas et al. "2020 global reassessment of the neutrino oscillation picture". In: *JHEP* 02 (2021), p. 071. DOI: 10.1007/JHEP02(2021)071. arXiv: 2006.11237 [hep-ph].
- [23] F. Capozzi et al. "Current unknowns in the three neutrino framework". In: *Prog. Part. Nucl. Phys.* 102 (2018), pp. 48–72. DOI: 10.1016/j.ppnp.2018.05.005. arXiv: 1804.09678 [hep-ph].
- [24] K. Abe et al. "Measurements of neutrino oscillation parameters from the T2K experiment using 3.6×10^{21} protons on target". In: *Eur. Phys. J. C* 83.9 (2023), p. 782. DOI: 10.1140/epjc/s10052-023-11819-x. arXiv: 2303.03222 [hep-ex].
- [25] M. A. Acero et al. "Improved measurement of neutrino oscillation parameters by the NOvA experiment". In: *Phys. Rev. D* 106.3 (2022), p. 032004. DOI: 10.1103/PhysRevD. 106.032004. arXiv: 2108.08219 [hep-ex].
- [26] Fengpeng An et al. "Neutrino Physics with JUNO". In: *J. Phys. G* 43.3 (2016), p. 030401. DOI: 10.1088/0954-3899/43/3/030401. arXiv: 1507.05613 [physics.ins-det].
- [27] K. Abe et al. "Hyper-Kamiokande Design Report". In: (May 2018). arXiv: 1805.04163 [physics.ins-det].
- [28] Babak Abi et al. "Deep Underground Neutrino Experiment (DUNE), Far Detector Technical Design Report, Volume II: DUNE Physics". In: (Feb. 2020). arXiv: 2002.03005 [hep-ex].
- [29] R. Acciarri et al. "Long-Baseline Neutrino Facility (LBNF) and Deep Underground Neutrino Experiment (DUNE): Conceptual Design Report, Volume 4 The DUNE Detectors at LBNF". In: (Jan. 2016). arXiv: 1601.02984 [physics.ins-det].
- [30] K. Abe et al. "Physics potential of a long-baseline neutrino oscillation experiment using a J-PARC neutrino beam and Hyper-Kamiokande". In: *PTEP* 2015 (2015), p. 053C02. DOI: 10.1093/ptep/ptv061. arXiv: 1502.05199 [hep-ex].
- [31] M. Archidiacono et al. "Euclid preparation. Sensitivity to neutrino parameters". In: (May 2024). arXiv: 2405.06047 [astro-ph.CO].
- [32] Amir Aghamousa et al. "The DESI Experiment Part I: Science, Targeting, and Survey Design". In: (Oct. 2016). arXiv: 1611.00036 [astro-ph.IM].
- [33] Peter Ade et al. "The Simons Observatory: Science goals and forecasts". In: *JCAP* 02 (2019), p. 056. DOI: 10.1088/1475-7516/2019/02/056. arXiv: 1808.07445 [astro-ph.CO].
- [34] E. Allys et al. "Probing Cosmic Inflation with the LiteBIRD Cosmic Microwave Background Polarization Survey". In: *PTEP* 2023.4 (2023), 042F01. DOI: 10.1093/ptep/ptac150.arXiv: 2202.02773 [astro-ph.IM].
- [35] F. Agostini et al. "Sensitivity of the DARWIN observatory to the neutrinoless double beta decay of ¹³⁶Xe". In: *Eur. Phys. J. C* 80.9 (2020). [Erratum: Eur.Phys.J.C 83, 996 (2023)], p. 808. DOI: 10.1140/epjc/s10052-020-8196-z. arXiv: 2003.13407 [physics.ins-det].

- [36] C. Adams et al. "Sensitivity of a tonne-scale NEXT detector for neutrinoless double beta decay searches". In: *JHEP* 2021.08 (2021), p. 164. DOI: 10.1007/JHEP08 (2021) 164. arXiv: 2005.06467 [physics.ins-det].
- [37] M. Agostini et al. "Final Results of GERDA on the Search for Neutrinoless Double- β Decay". In: *Phys. Rev. Lett.* 125.25 (2020), p. 252502. DOI: 10.1103/PhysRevLett.125. 252502. arXiv: 2009.06079 [nucl-ex].
- [38] M. G. Aartsen et al. "IceCube-Gen2: the window to the extreme Universe". In: *J. Phys. G* 48.6 (2021), p. 060501. DOI: 10 . 1088 / 1361 6471 / abbd48. arXiv: 2008 . 04323 [astro-ph.HE].
- [39] E. Baracchini et al. "PTOLEMY: A Proposal for Thermal Relic Detection of Massive Neutrinos and Directional Detection of MeV Dark Matter". In: (Aug. 2018). arXiv: 1808. 01892 [physics.ins-det].
- [40] Martin Bauer and Jack D. Shergold. "Limits on the cosmic neutrino background". In: *JCAP* 01 (2023), p. 003. DOI: 10.1088/1475-7516/2023/01/003. arXiv: 2207.12413 [hep-ph].
- [41] M. Herrero. "The Standard Model". In: *NATO Sci. Ser. C* 534 (1999). Ed. by T. Ferbel, pp. 1-59. doi: 10.1007/978-94-011-4689-0_1. arXiv: hep-ph/9812242. URL: https://arxiv.org/abs/hep-ph/9812242.
- [42] Scott Willenbrock. "Symmetries of the Standard Model". Oct. 2004. DOI: 10.48550 / ARXIV.HEP-PH/0410370. arXiv: hep-ph/0410370.
- [43] Michael Spira and Peter M. Zerwas. "Electroweak Symmetry Breaking and Higgs Physics". In: vol. 512. 1998, pp. 161–225. DOI: 10.1007/BFb0106895. arXiv: hep-ph/9803257. (Visited on 04/14/2025).
- [44] Antonio Pich. "The Standard model of electroweak interactions". In: 2006 European School of High-Energy Physics. 2007, pp. 1–49. arXiv: 0705.4264 [hep-ph].
- [45] Paul Langacker. "Introduction to the Standard Model and Electroweak Physics". In: *The Dawn of the LHC Era*. Aug. 2010, pp. 3–48. DOI: 10.1142/9789812838360_0001. arXiv: 0901.0241 [hep-ph]. (Visited on 04/14/2025).
- [46] F. Halzen and Alan D. Martin. *Quarks and Leptons: an introductory course in modern Particle Physics.* 1984. ISBN: 978-0-471-88741-6.
- [47] Brian Robert Martin and Graham Shaw. Particle physics. 2008. ISBN: 978-0-470-03294-7.
- [48] Michael E. Peskin and Daniel V. Schroeder. *An Introduction to quantum field theory*. Reading, USA: Addison-Wesley, 1995. ISBN: 978-0-201-50397-5, 978-0-429-50355-9, 978-0-429-49417-8. DOI: 10.1201/9780429503559.
- [49] Steven Weinberg. "The Making of the standard model". In: *Eur. Phys. J. C* 34 (2004). Ed. by G. 't Hooft, pp. 5–13. DOI: 10.1140/epjc/s2004-01761-1. arXiv: hep-ph/0401010.
- [50] Steven Weinberg. "Essay: Half a Century of the Standard Model". In: *Phys. Rev. Lett.* 121 (22 Nov. 2018), p. 220001. DOI: 10.1103/PhysRevLett.121.220001. URL: https://link.aps.org/doi/10.1103/PhysRevLett.121.220001.
- [51] *The Rise of the Standard Model: A History of Particle Physics from 1964 to 1979.* Cambridge University Press, 1997.
- [52] Steven Weinberg. "A Model of Leptons". In: *Phys. Rev. Lett.* 19 (1967), pp. 1264–1266. DOI: 10.1103/PhysRevLett.19.1264.
- [53] Abdus Salam. "Weak and Electromagnetic Interactions". In: *Conf. Proc. C* 680519 (1968), pp. 367–377. DOI: 10.1142/9789812795915_0034.
- [54] S. L. Glashow. "Partial Symmetries of Weak Interactions". In: *Nucl. Phys.* 22 (1961), pp. 579–588. DOI: 10.1016/0029-5582(61)90469-2.

- [55] S. Navas et al. "Review of particle physics". In: *Phys. Rev. D* 110.3 (2024), p. 030001. DOI: 10.1103/PhysRevD.110.030001.
- [56] H. Fritzsch, Murray Gell-Mann, and H. Leutwyler. "Advantages of the Color Octet Gluon Picture". In: *Phys. Lett. B* 47 (1973), pp. 365–368. DOI: 10.1016/0370-2693 (73) 90625-4.
- [57] D. J. Gross and Frank Wilczek. "Asymptotically Free Gauge Theories I". In: *Phys. Rev. D* 8 (1973), pp. 3633–3652. DOI: 10.1103/PhysRevD.8.3633.
- [58] Steven Weinberg. "Nonabelian Gauge Theories of the Strong Interactions". In: *Phys. Rev. Lett.* 31 (1973), pp. 494–497. DOI: 10.1103/PhysRevLett.31.494.
- [59] F. Englert and R. Brout. "Broken Symmetry and the Mass of Gauge Vector Mesons". In: *Phys. Rev. Lett.* 13 (1964). Ed. by J. C. Taylor, pp. 321–323. DOI: 10.1103/PhysRevLett. 13.321.
- [60] Peter W. Higgs. "Broken Symmetries and the Masses of Gauge Bosons". In: *Phys. Rev. Lett.* 13 (1964). Ed. by J. C. Taylor, pp. 508–509. DOI: 10.1103/PhysRevLett.13.508.
- [61] G. S. Guralnik, C. R. Hagen, and T. W. B. Kibble. "Global Conservation Laws and Massless Particles". In: *Phys. Rev. Lett.* 13 (1964). Ed. by J. C. Taylor, pp. 585–587. DOI: 10.1103/PhysRevLett.13.585.
- [62] Georges Aad et al. "Observation of a new particle in the search for the Standard Model Higgs boson with the ATLAS detector at the LHC". In: *Phys. Lett. B* 716 (2012), pp. 1–29. DOI: 10.1016/j.physletb.2012.08.020. arXiv: 1207.7214 [hep-ex].
- [63] Serguei Chatrchyan et al. "Observation of a New Boson at a Mass of 125 GeV with the CMS Experiment at the LHC". In: *Phys. Lett. B* 716 (2012), pp. 30–61. DOI: 10.1016/j.physletb.2012.08.021. arXiv: 1207.7235 [hep-ex].
- [64] S. Schael et al. "Precision electroweak measurements on the Z resonance". In: *Phys. Rept.* 427 (2006), pp. 257-454. DOI: 10.1016/j.physrep.2005.12.006. arXiv: hep-ex/0509008.
- [65] Feng Peng An et al. "Measurement of electron antineutrino oscillation based on 1230 days of operation of the Daya Bay experiment". In: *Phys. Rev. D* 95.7 (2017), p. 072006. DOI: 10.1103/PhysRevD.95.072006. arXiv: 1610.04802 [hep-ex].
- [66] R. Abbasi et al. "Measurement of atmospheric neutrino mixing with improved IceCube DeepCore calibration and data processing". In: *Phys. Rev. D* 108.1 (2023), p. 012014. DOI: 10.1103/PhysRevD.108.012014. arXiv: 2304.12236 [hep-ex].
- [67] Ivan Esteban. "Leptonic CP Violation and its Origin". PhD thesis. Barcelona U., Oct. 2020. arXiv: 2010.00440 [hep-ph].
- [68] R. N. Mohapatra and P. B. Pal. *Massive neutrinos in physics and astrophysics. Second edition.* Vol. 60. 1998.
- [69] E. Kh Akhmedov. *Neutrino Physics*. Jan. 2000. DOI: 10.48550/arXiv.hep-ph/0001264. arXiv: hep-ph/0001264. (Visited on 04/14/2025).
- [70] J. Schechter and J. W. F. Valle. "Neutrinoless Double beta Decay in SU(2) x U(1) Theories". In: *Phys. Rev. D* 25 (1982), p. 2951. DOI: 10.1103/PhysRevD.25.2951.
- [71] W. Buchmuller and D. Wyler. "Effective Lagrangian Analysis of New Interactions and Flavor Conservation". In: *Nucl. Phys. B* 268 (1986), pp. 621–653. DOI: 10.1016/0550–3213(86)90262–2.
- [72] B. Grzadkowski et al. "Dimension-Six Terms in the Standard Model Lagrangian". In: *JHEP* 10 (2010), p. 085. DOI: 10.1007/JHEP10(2010)085. arXiv: 1008.4884 [hep-ph].
- [73] Steven Weinberg. "Baryon and Lepton Nonconserving Processes". In: *Phys. Rev. Lett.* 43 (1979), pp. 1566–1570. DOI: 10.1103/PhysRevLett.43.1566.

- [74] Pierre Ramond. "The Family Group in Grand Unified Theories". In: *International Symposium on Fundamentals of Quantum Theory and Quantum Field Theory*. Feb. 1979. arXiv: hep-ph/9809459.
- [75] Murray Gell-Mann, Pierre Ramond, and Richard Slansky. "Complex Spinors and Unified Theories". In: Conf. Proc. C 790927 (1979), pp. 315–321. arXiv: 1306.4669 [hep-th].
- [76] Rabindra N. Mohapatra and Goran Senjanovic. "Neutrino Mass and Spontaneous Parity Nonconservation". In: *Phys. Rev. Lett.* 44 (1980), p. 912. DOI: 10.1103/PhysRevLett.44. 912.
- [77] M. Magg and C. Wetterich. "Neutrino Mass Problem and Gauge Hierarchy". In: *Phys. Lett. B* 94 (1980), pp. 61–64. DOI: 10.1016/0370-2693(80)90825-4.
- [78] J. Schechter and J. W. F. Valle. "Neutrino Masses in SU(2) x U(1) Theories". In: *Phys. Rev.* D 22 (1980), p. 2227. DOI: 10.1103/PhysRevD.22.2227.
- [79] Robert Foot et al. "Seesaw Neutrino Masses Induced by a Triplet of Leptons". In: *Z. Phys. C* 44 (1989), p. 441. DOI: 10.1007/BF01415558.
- [80] C. Giunti and C. W. Kim. "Coherence of neutrino oscillations in the wave packet approach". In: *Phys. Rev. D* 58 (1998), p. 017301. DOI: 10.1103/PhysRevD.58.017301. arXiv: hep-ph/9711363.
- [81] S. Nussinov. "Solar Neutrinos and Neutrino Mixing". In: *Phys. Lett. B* 63 (1976), pp. 201–203. DOI: 10.1016/0370-2693(76)90648-1.
- [82] Boris Kayser. "On the Quantum Mechanics of Neutrino Oscillation". In: *Phys. Rev. D* 24 (1981), p. 110. DOI: 10.1103/PhysRevD.24.110.
- [83] Ken Kiers, Shmuel Nussinov, and Nathan Weiss. "Coherence effects in neutrino oscillations". In: *Phys. Rev. D* 53 (1996), pp. 537–547. DOI: 10.1103/PhysRevD.53.537. arXiv: hep-ph/9506271.
- [84] Mikael Beuthe. "Oscillations of neutrinos and mesons in quantum field theory". In: *Phys. Rept.* 375 (2003), pp. 105–218. DOI: 10.1016/S0370-1573(02)00538-0. arXiv: hep-ph/0109119.
- [85] Evgeny Akhmedov, Daniel Hernandez, and Alexei Smirnov. "Neutrino production coherence and oscillation experiments". In: *JHEP* 04 (2012), p. 052. DOI: 10.1007/JHEP04(2012) 052. arXiv: 1201.4128 [hep-ph].
- [86] Evgeny Akhmedov, Joachim Kopp, and Manfred Lindner. "Collective neutrino oscillations and neutrino wave packets". In: *JCAP* 09 (2017), p. 017. DOI: 10.1088/1475-7516/2017/09/017. arXiv: 1702.08338 [hep-ph].
- [87] B. Pontecorvo. "Inverse beta processes and nonconservation of lepton charge". In: *Zh. Eksp. Teor. Fiz.* 34 (1957), p. 247.
- [88] Z. Maki, M. Nakagawa, and S. Sakata. "Remarks on the unified model of elementary particles". In: 11th International Conference on High-energy Physics. 1962, pp. 663–666.
- [89] Francesco Capozzi et al. "Unfinished fabric of the three neutrino paradigm". In: *Phys. Rev. D* 104.8 (2021), p. 083031. DOI: 10.1103/PhysRevD.104.083031. arXiv: 2107.00532 [hep-ph].
- [90] Evgeny Kh. Akhmedov and Alexei Yu. Smirnov. "Paradoxes of neutrino oscillations". In: *Phys. Atom. Nucl.* 72 (2009), pp. 1363–1381. DOI: 10.1134/S1063778809080122. arXiv: 0905.1903 [hep-ph].
- [91] C. Giunti. "Neutrino wave packets in quantum field theory". In: *JHEP* 11 (2002), p. 017. DOI: 10.1088/1126-6708/2002/11/017. arXiv: hep-ph/0205014.

- [92] Evgeny Kh. Akhmedov and Joachim Kopp. "Neutrino Oscillations: Quantum Mechanics vs. Quantum Field Theory". In: *JHEP* 04 (2010). [Erratum: JHEP 10, 052 (2013)], p. 008. DOI: 10.1007/JHEP04(2010)008. arXiv: 1001.4815 [hep-ph].
- [93] Bruno de S. L. Torres et al. "Neutrino flavor oscillations without flavor states". In: *Phys. Rev. D* 102.9 (2020), p. 093003. DOI: 10.1103/PhysRevD.102.093003. arXiv: 2009. 10165 [hep-ph].
- [94] Evgeny Akhmedov and Alexei Y. Smirnov. "Damping of neutrino oscillations, decoherence and the lengths of neutrino wave packets". In: (Aug. 2022). arXiv: 2208.03736 [hep-ph].
- [95] John N. Bahcall, Aldo M. Serenelli, and Sarbani Basu. "New solar opacities, abundances, helioseismology, and neutrino fluxes". In: *Astrophys. J. Lett.* 621 (2005), pp. L85–L88. DOI: 10.1086/428929. arXiv: astro-ph/0412440.
- [96] Aldo M. Serenelli, W. C. Haxton, and Carlos Pena-Garay. "Solar models with accretion. I. Application to the solar abundance problem". In: *Astrophys. J.* 743 (2011), p. 24. DOI: 10.1088/0004-637X/743/1/24. arXiv: 1104.1639 [astro-ph.SR].
- [97] S. P. Mikheyev and A. Yu. Smirnov. "Resonance Amplification of Oscillations in Matter and Spectroscopy of Solar Neutrinos". In: *Sov. J. Nucl. Phys.* 42 (1985), pp. 913–917.
- [98] L. Wolfenstein. "Neutrino Oscillations in Matter". In: *Phys. Rev. D* 17 (1978), pp. 2369–2374. DOI: 10.1103/PhysRevD.17.2369.
- [99] B. T. Cleveland et al. "Measurement of the solar electron neutrino flux with the Homestake chlorine detector". In: *Astrophys. J.* 496 (1998), pp. 505–526. DOI: 10.1086/305343.
- [100] J. N. Abdurashitov et al. "Measurement of the solar neutrino capture rate with gallium metal. III: Results for the 2002–2007 data-taking period". In: *Phys. Rev. C* 80 (2009), p. 015807. DOI: 10.1103/PhysRevC.80.015807. arXiv: 0901.2200 [nucl-ex].
- [101] W. Hampel et al. "GALLEX solar neutrino observations: Results for GALLEX IV". In: *Phys. Lett. B* 447 (1999), pp. 127–133. DOI: 10.1016/S0370–2693(98)01579–2.
- [102] J. Hosaka et al. "Solar neutrino measurements in super-Kamiokande-I". In: *Phys. Rev. D* 73 (2006), p. 112001. DOI: 10.1103/PhysRevD.73.112001. arXiv: hep-ex/0508053.
- [103] Q. R. Ahmad et al. "Measurement of the rate of $v_e + d \rightarrow p + p + e^-$ interactions produced by ⁸B solar neutrinos at the Sudbury Neutrino Observatory". In: *Phys. Rev. Lett.* 87 (2001), p. 071301. DOI: 10.1103/PhysRevLett.87.071301. arXiv: nucl-ex/0106015.
- [104] T. Araki et al. "Measurement of neutrino oscillation with KamLAND: Evidence of spectral distortion". In: *Phys. Rev. Lett.* 94 (2005), p. 081801. DOI: 10.1103/PhysRevLett.94. 081801. arXiv: hep-ex/0406035.
- [105] G. Bellini et al. "Final results of Borexino Phase-I on low energy solar neutrino spectroscopy". In: *Phys. Rev. D* 89.11 (2014), p. 112007. DOI: 10.1103/PhysRevD.89.112007. arXiv: 1308.0443 [hep-ex].
- [106] D. Casper et al. "Measurement of atmospheric neutrino composition with IMB-3". In: *Phys. Rev. Lett.* 66 (1991), pp. 2561–2564. DOI: 10.1103/PhysRevLett.66.2561.
- [107] Y. Fukuda et al. "Atmospheric muon-neutrino / electron-neutrino ratio in the multiGeV energy range". In: *Phys. Lett. B* 335 (1994), pp. 237–245. DOI: 10.1016/0370-2693(94) 91420-6.
- [108] M Ambrosio et al. "Measurement of the atmospheric neutrino induced upgoing muon flux using MACRO". In: *Phys. Lett. B* 434 (1998), pp. 451–457. DOI: 10.1016/S0370–2693(98)00885–5. arXiv: hep-ex/9807005.

- [109] W. W. M. Allison et al. "Measurement of the L/E distributions of atmospheric neutrinos in Soudan 2 and their interpretation as neutrino oscillations". In: *Phys. Rev. D* 68 (2003), p. 113004. DOI: 10.1103/PhysRevD.68.113004. arXiv: hep-ex/0307069.
- [110] S. Adrian-Martinez et al. "Letter of intent for KM3NeT 2.0". In: *J. Phys. G* 43.8 (2016), p. 084001. DOI: 10.1088/0954-3899/43/8/084001. arXiv: 1601.07459 [astro-ph.IM].
- [111] S. Aiello et al. "Measurement of neutrino oscillation parameters with the first six detection units of KM3NeT/ORCA". In: *JHEP* 10 (2024), p. 206. DOI: 10.1007/JHEP10(2024) 206. arXiv: 2408.07015 [hep-ex].
- [112] C. Athanassopoulos et al. "Evidence for anti-muon-neutrino —> anti-electron-neutrino oscillations from the LSND experiment at LAMPF". In: *Phys. Rev. Lett.* 77 (1996), pp. 3082–3085. DOI: 10.1103/PhysRevLett.77.3082. arXiv: nucl-ex/9605003.
- [113] A. Aguilar-Arevalo et al. "Evidence for neutrino oscillations from the observation of $\bar{\nu}_e$ appearance in a $\bar{\nu}_\mu$ beam". In: *Phys. Rev. D* 64 (2001), p. 112007. DOI: 10.1103/PhysRevD. 64.112007. arXiv: hep-ex/0104049.
- [114] A. A. Aguilar-Arevalo et al. "Improved Search for $\bar{v}_{\mu} \rightarrow \bar{v}_{e}$ Oscillations in the MiniBooNE Experiment". In: *Phys. Rev. Lett.* 110 (2013), p. 161801. DOI: 10.1103/PhysRevLett.110. 161801. arXiv: 1303.2588 [hep-ex].
- [115] A. A. Aguilar-Arevalo et al. "Significant Excess of ElectronLike Events in the MiniBooNE Short-Baseline Neutrino Experiment". In: *Phys. Rev. Lett.* 121.22 (2018), p. 221801. DOI: 10.1103/PhysRevLett.121.221801. arXiv: 1805.12028 [hep-ex].
- [116] Henso Abreu et al. "First Direct Observation of Collider Neutrinos with FASER at the LHC". In: *Phys. Rev. Lett.* 131.3 (2023), p. 031801. DOI: 10.1103/PhysRevLett.131.031801. arXiv: 2303.14185 [hep-ex].
- [117] Eduardo Cortina Gil et al. "First detection of a tagged neutrino in the NA62 experiment". In: *Phys. Lett. B* 863 (2025), p. 139345. DOI: 10.1016/j.physletb.2025.139345. arXiv: 2412.04033 [hep-ex].
- [118] Mathieu Perrin-Terrin. "Neutrino tagging: a new tool for accelerator based neutrino experiments". In: *Eur. Phys. J. C* 82.5 (2022), p. 465. DOI: 10.1140/epjc/s10052-022-10397-8. arXiv: 2112.12848 [hep-ex].
- [119] Th. A. Mueller et al. "Improved Predictions of Reactor Antineutrino Spectra". In: *Phys. Rev. C* 83 (2011), p. 054615. DOI: 10.1103/PhysRevC.83.054615. arXiv: 1101.2663 [hep-ex].
- [120] Patrick Huber. "On the determination of anti-neutrino spectra from nuclear reactors". In: *Phys. Rev. C* 84 (2011). [Erratum: Phys.Rev.C 85, 029901 (2012)], p. 024617. DOI: 10. 1103/PhysRevC.85.029901. arXiv: 1106.0687 [hep-ph].
- [121] K. Schreckenbach et al. "Determination of the anti-neutrino spectrum from U-235 thermal neutron fission products up to 9.5-Mev". In: *Phys. Lett. B* 160 (1985), pp. 325–330. DOI: 10.1016/0370-2693(85)91337-1.
- [122] F. Von Feilitzsch, A. A. Hahn, and K. Schreckenbach. "Experimental beta spectra from Pu-239 and U-235 thermal neutron fission products and their correlated anti-neutrinos spectra". In: *Phys. Lett. B* 118 (1982), pp. 162–166. DOI: 10.1016/0370-2693 (82) 90622-0.
- [123] A. A. Hahn et al. "Anti-neutrino Spectra From ²⁴¹Pu and ²³⁹Pu Thermal Neutron Fission Products". In: *Phys. Lett. B* 218 (1989), pp. 365–368. DOI: 10.1016/0370-2693(89) 91598-0.

- [124] D. Adey et al. "Improved Measurement of the Reactor Antineutrino Flux at Daya Bay". In: *Phys. Rev. D* 100.5 (2019), p. 052004. DOI: 10.1103/PhysRevD.100.052004. arXiv: 1808.10836 [hep-ex].
- [125] H. Almazán et al. "Accurate Measurement of the Electron Antineutrino Yield of ²³⁵U Fissions from the STEREO Experiment with 119 Days of Reactor-On Data". In: *Phys. Rev. Lett.* 125.20 (2020), p. 201801. DOI: 10.1103/PhysRevLett.125.201801. arXiv: 2004.04075 [hep-ex].
- [126] G. Mention et al. "The Reactor Antineutrino Anomaly". In: *Phys. Rev. D* 83 (2011), p. 073006. DOI: 10.1103/PhysRevD.83.073006. arXiv: 1101.2755 [hep-ex].
- [127] V. Kopeikin, M. Skorokhvatov, and O. Titov. "Reevaluating reactor antineutrino spectra with new measurements of the ratio between U235 and Pu239 β spectra". In: *Phys. Rev. D* 104.7 (2021), p. L071301. DOI: 10.1103/PhysRevD.104.L071301. arXiv: 2103.01684 [nucl-ex].
- [128] C. Giunti et al. "Reactor antineutrino anomaly in light of recent flux model refinements". In: *Phys. Lett. B* 829 (2022), p. 137054. DOI: 10.1016/j.physletb.2022.137054. arXiv: 2110.06820 [hep-ph].
- [129] Jeffrey M. Berryman and Patrick Huber. "Sterile Neutrinos and the Global Reactor Antineutrino Dataset". In: *JHEP* 01 (2021), p. 167. DOI: 10.1007/JHEP01(2021)167. arXiv: 2005.01756 [hep-ph].
- [130] Feng Peng An et al. "Improved Search for a Light Sterile Neutrino with the Full Configuration of the Daya Bay Experiment". In: *Phys. Rev. Lett.* 117.15 (2016), p. 151802. DOI: 10.1103/PhysRevLett.117.151802. arXiv: 1607.01174 [hep-ex].
- [131] Y. J. Ko et al. "Sterile Neutrino Search at the NEOS Experiment". In: *Phys. Rev. Lett.* 118.12 (2017), p. 121802. DOI: 10.1103/PhysRevLett.118.121802. arXiv: 1610.05134 [hep-ex].
- [132] M. Andriamirado et al. "Improved short-baseline neutrino oscillation search and energy spectrum measurement with the PROSPECT experiment at HFIR". In: *Phys. Rev. D 103*, 032001 (2021) 103.3 (Feb. 2021), p. 032001. DOI: 10.1103/physrevd.103.032001. arXiv: https://arxiv.org/abs/2006.11210 [hep-ex].
- [133] I Alekseev et al. "Search for sterile neutrinos at the DANSS experiment". In: *Phys. Lett. B* 787 (2018), pp. 56–63. DOI: 10.1016/j.physletb.2018.10.038. arXiv: 1804.04046 [hep-ex].
- [134] H. Almazán et al. "Improved sterile neutrino constraints from the STEREO experiment with 179 days of reactor-on data". In: *Phys. Rev. D* 102.5 (2020), p. 052002. DOI: 10.1103/PhysRevD.102.052002. arXiv: 1912.06582 [hep-ex].
- [135] A. P. Serebrov et al. "Search for sterile neutrinos with the Neutrino-4 experiment and measurement results". In: *Physical Review D* 104.3 (Aug. 2021). ISSN: 2470-0029. DOI: 10. 1103/physrevd.104.032003. URL: http://dx.doi.org/10.1103/PhysRevD.104.032003.
- [136] M. A. Acero et al. "White paper on light sterile neutrino searches and related phenomenology". In: *J. Phys. G* 51.12 (2024), p. 120501. DOI: 10.1088/1361-6471/ad307f. arXiv: 2203.07323 [hep-ex].
- [137] Jeffrey M. Berryman et al. "Statistical significance of the sterile-neutrino hypothesis in the context of reactor and gallium data". In: *JHEP* 02 (2022), p. 055. DOI: 10.1007/JHEP02(2022)055. arXiv: 2111.12530 [hep-ph].
- [138] V. V. Barinov et al. "Results from the Baksan Experiment on Sterile Transitions (BEST)". In: (Sept. 2021). arXiv: 2109.11482 [nucl-ex].

- [139] Carlo Giunti and Marco Laveder. "Statistical Significance of the Gallium Anomaly". In: *Phys. Rev. C* 83 (2011), p. 065504. DOI: 10.1103/PhysRevC.83.065504. arXiv: 1006. 3244 [hep-ph].
- [140] C. Giunti et al. "Gallium Anomaly: critical view from the global picture of v_e and \overline{v}_e disappearance". In: *JHEP* 10 (2022), p. 164. DOI: 10.1007/JHEP10(2022) 164. arXiv: 2209.00916 [hep-ph].
- [141] J. N. Abdurashitov et al. "Measurement of the response of a Ga solar neutrino experiment to neutrinos from an Ar-37 source". In: *Phys. Rev. C* 73 (2006), p. 045805. DOI: 10.1103/PhysRevC.73.045805. arXiv: nucl-ex/0512041.
- [142] J. N. Abdurashitov et al. "Measurement of the response of the Russian-American gallium experiment to neutrinos from a Cr-51 source". In: *Phys. Rev. C* 59 (1999), pp. 2246–2263. DOI: 10.1103/PhysRevC.59.2246. arXiv: hep-ph/9803418.
- [143] John N. Bahcall, P. I. Krastev, and E. Lisi. "Limits on electron-neutrino oscillations from the GALLEX Cr-51 source experiment". In: *Phys. Lett. B* 348 (1995), pp. 121–123. DOI: 10.1016/0370-2693(95)00111-W. arXiv: hep-ph/9411414.
- [144] W. Hampel et al. "Final results of the Cr-51 neutrino source experiments in GALLEX". In: *Phys. Lett. B* 420 (1998), pp. 114–126. DOI: 10.1016/S0370-2693(97)01562-1.
- [145] F. Kaether et al. "Reanalysis of the GALLEX solar neutrino flux and source experiments". In: *Phys. Lett. B* 685 (2010), pp. 47–54. DOI: 10.1016/j.physletb.2010.01.030. arXiv: 1001.2731 [hep-ex].
- [146] Vladislav Barinov and Dmitry Gorbunov. "BEST Impact on Sterile Neutrino Hypothesis". In: (Sept. 2021). arXiv: 2109.14654 [hep-ph].
- [147] V. V. Barinov et al. "Search for electron-neutrino transitions to sterile states in the BEST experiment". In: *Phys. Rev. C* 105.6 (2022), p. 065502. DOI: 10.1103/PhysRevC.105.065502. arXiv: 2201.07364 [nucl-ex].
- [148] Edoardo Vitagliano, Irene Tamborra, and Georg Raffelt. "Grand Unified Neutrino Spectrum at Earth: Sources and Spectral Components". In: *Rev. Mod. Phys.* 92 (2020), p. 45006. DOI: 10.1103/RevModPhys.92.045006. arXiv: 1910.11878 [astro-ph.HE].
- [149] A. Osipowicz et al. "KATRIN: A Next generation tritium beta decay experiment with sub-eV sensitivity for the electron neutrino mass. Letter of intent". In: (Sept. 2001). arXiv: hep-ex/0109033.
- [150] M. Aker et al. "Direct neutrino-mass measurement based on 259 days of KATRIN data". In: (June 2024). arXiv: 2406.13516 [nucl-ex].
- [151] N. Aghanim et al. "Planck 2018 results. VI. Cosmological parameters". In: *Astron. Astrophys.* 641 (2020). [Erratum: Astron. Astrophys. 652, C4 (2021)], A6. DOI: 10.1051/0004-6361/201833910. arXiv: 1807.06209 [astro-ph.C0].
- [152] W. Elbers et al. "Constraints on Neutrino Physics from DESI DR2 BAO and DR1 Full Shape". In: (Mar. 2025). arXiv: 2503.14744 [astro-ph.C0].
- [153] A. G. Adame et al. "DESI 2024 VII: Cosmological Constraints from the Full-Shape Modeling of Clustering Measurements". In: (Nov. 2024). arXiv: 2411.12022 [astro-ph.CO].
- [154] A. G. Adame et al. "DESI 2024 VI: Cosmological Constraints from the Measurements of Baryon Acoustic Oscillations". In: (Apr. 2024). arXiv: 2404.03002 [astro-ph.CO].
- [155] Yuval Grossman. "Nonstandard neutrino interactions and neutrino oscillation experiments". In: *Phys. Lett. B* 359 (1995), pp. 141–147. DOI: 10.1016/0370-2693(95)01069-3. arXiv: hep-ph/9507344.

- [156] N. Fornengo et al. "Probing neutrino nonstandard interactions with atmospheric neutrino data". In: *Phys. Rev. D* 65 (2002), p. 013010. DOI: 10.1103/PhysRevD.65.013010. arXiv: hep-ph/0108043.
- [157] S. Davidson et al. "Present and future bounds on nonstandard neutrino interactions". In: JHEP 03 (2003), p. 011. DOI: 10 . 1088 / 1126 6708 / 2003 / 03 / 011. arXiv: hep-ph/0302093.
- [158] Joachim Kopp et al. "Non-standard neutrino interactions in reactor and superbeam experiments". In: *Phys. Rev. D* 77 (2008), p. 013007. DOI: 10.1103/PhysRevD.77.013007. arXiv: 0708.0152 [hep-ph].
- [159] Y. Farzan and M. Tortola. "Neutrino oscillations and Non-Standard Interactions". In: Front. in Phys. 6 (2018), p. 10. DOI: 10.3389/fphy.2018.00010. arXiv: 1710.09360 [hep-ph].
- [160] Ivan Esteban et al. "Updated constraints on non-standard interactions from global analysis of oscillation data". In: *JHEP* 08 (2018). [Addendum: JHEP 12, 152 (2020)], p. 180. DOI: 10.1007/JHEP08(2018) 180. arXiv: 1805.04530 [hep-ph].
- [161] John N. Bahcall. "Gallium solar neutrino experiments: Absorption cross sections, neutrino spectra, and predicted event rates". In: *Phys. Rev. C* 56 (6 Dec. 1997), pp. 3391–3409. DOI: 10.1103/PhysRevC.56.3391. URL: https://link.aps.org/doi/10.1103/PhysRevC.56.3391.
- [162] H. Almazan et al. ""Sterile Neutrino Constraints from the STEREO Experiment with 66 Days of Reactor-On Data"". In: *Phys. Rev. Lett.* 121.16 (2018), p. 161801. DOI: 10.1103/PhysRevLett.121.161801. arXiv: 1806.02096 [hep-ex].
- [163] Luis Manzanillas. "Performance of the SoLid Reactor Neutrino Detector". In: 39th International Conference on High Energy Physics (ICHEP 2018) Seoul, Gangnam-Gu, Korea, Republic of, July 4-11, 2018. 2018. arXiv: 1811.05694 [physics.ins-det].
- [164] J. H. Choi et al. "Search for Sub-eV Sterile Neutrinos at RENO". In: *Phys. Rev. Lett.* 125 (19 Nov. 2020), p. 191801. DOI: 10.1103/PhysRevLett.125.191801. URL: https://link.aps.org/doi/10.1103/PhysRevLett.125.191801.
- [165] Mikhail Danilov and Nataliya Skrobova. "New results from the DANSS experiment". In: European Physical Society Conference on High Energy Physics 2021. Dec. 2021. arXiv: 2112.13413 [hep-ex].
- [166] Kim Goldhagen et al. "Testing sterile neutrino mixing with present and future solar neutrino data". In: Eur. Phys. J. C 82.2 (2022), p. 116. DOI: 10.1140/epjc/s10052-022-10052-2. arXiv: 2109.14898 [hep-ph].
- [167] P. Abratenko et al. "Search for an anomalous excess of charged-current quasi-elastic v_e interactions with the MicroBooNE experiment using Deep-Learning-based reconstruction". In: (Oct. 2021). arXiv: 2110.14080 [hep-ex].
- [168] P. Abratenko et al. "Search for an anomalous excess of inclusive charged-current v_e interactions in the MicroBooNE experiment using Wire-Cell reconstruction". In: (Oct. 2021). arXiv: 2110.13978 [hep-ex].
- [169] P. Abratenko et al. "Search for an Excess of Electron Neutrino Interactions in Micro-BooNE Using Multiple Final State Topologies". In: (Oct. 2021). arXiv: 2110.14054 [hep-ex].
- [170] P. Abratenko et al. "Search for an anomalous excess of charged-current v_e interactions without pions in the final state with the MicroBooNE experiment". In: (Oct. 2021). arXiv: 2110.14065 [hep-ex].
- [171] Peter B. Denton. "Sterile Neutrino Searches with MicroBooNE: Electron Neutrino Disappearance". In: (Nov. 2021). arXiv: 2111.05793 [hep-ph].

- [172] C. A. Argüelles et al. "MicroBooNE and the v_e Interpretation of the MiniBooNE Low-Energy Excess". In: (Nov. 2021). arXiv: 2111.10359 [hep-ph].
- [173] A. A. Aguilar-Arevalo et al. "MiniBooNE and MicroBooNE Joint Fit to a 3+1 Sterile Neutrino Scenario". In: (Jan. 2022). arXiv: 2201.01724 [hep-ex].
- [174] P. Adamson et al. "Search for sterile neutrinos in MINOS and MINOS+ using a two-detector fit". In: *Phys. Rev. Lett.* 122.9 (2019), p. 091803. DOI: 10.1103/PhysRevLett. 122.091803. arXiv: 1710.06488 [hep-ex].
- [175] M. G. Aartsen et al. "Searches for Sterile Neutrinos with the IceCube Detector". In: *Phys. Rev. Lett.* 117.7 (2016), p. 071801. DOI: 10.1103/PhysRevLett.117.071801. arXiv: 1605.01990 [hep-ex].
- [176] M. G. Aartsen et al. "Searching for eV-scale sterile neutrinos with eight years of atmospheric neutrinos at the IceCube Neutrino Telescope". In: *Phys. Rev. D* 102.5 (2020), p. 052009. DOI: 10.1103/PhysRevD.102.052009. arXiv: 2005.12943 [hep-ex].
- [177] M. G. Aartsen et al. "eV-Scale Sterile Neutrino Search Using Eight Years of Atmospheric Muon Neutrino Data from the IceCube Neutrino Observatory". In: *Phys. Rev. Lett.* 125.14 (2020), p. 141801. DOI: 10.1103/PhysRevLett.125.141801. arXiv: 2005.12942 [hep-ex].
- [178] Mona Dentler et al. "Updated Global Analysis of Neutrino Oscillations in the Presence of eV-Scale Sterile Neutrinos". In: *JHEP* 08 (2018), p. 010. DOI: 10.1007/JHEP08 (2018) 010. arXiv: 1803.10661 [hep-ph].
- [179] Carlo Giunti and T. Lasserre. "eV-scale Sterile Neutrinos". In: *Ann. Rev. Nucl. Part. Sci.* 69 (2019), pp. 163-190. DOI: 10.1146/annurev-nucl-101918-023755. arXiv: 1901. 08330 [hep-ph].
- [180] A. Diaz et al. "Where Are We With Light Sterile Neutrinos?" In: *Phys. Rept.* 884 (2020), pp. 1–59. DOI: 10.1016/j.physrep.2020.08.005. arXiv: 1906.00045 [hep-ex].
- [181] Sebastian Böser et al. "Status of Light Sterile Neutrino Searches". In: *Prog. Part. Nucl. Phys.* 111 (2020), p. 103736. DOI: 10.1016/j.ppnp.2019.103736. arXiv: 1906.01739 [hep-ex].
- [182] Shalom Eliezer and Arthur R. Swift. "Experimental Consequences of electron Neutrino-Muon-neutrino Mixing in Neutrino Beams". In: *Nucl. Phys. B* 105 (1976), pp. 45–51. DOI: 10.1016/0550-3213(76)90059-6.
- [183] Harald Fritzsch and Peter Minkowski. "Vector-Like Weak Currents, Massive Neutrinos, and Neutrino Beam Oscillations". In: *Phys. Lett. B* 62 (1976), pp. 72–76. DOI: 10.1016/0370-2693(76)90051-4.
- [184] Samoil M. Bilenky and B. Pontecorvo. "Again on Neutrino Oscillations". In: Lett. Nuovo Cim. 17 (1976), p. 569. DOI: 10.1007/BF02746567.
- [185] Evgeny Akhmedov. "Quantum mechanics aspects and subtleties of neutrino oscillations". In: *International Conference on History of the Neutrino: 1930-2018.* Jan. 2019. arXiv: 1901. 05232 [hep-ph].
- [186] C. Giunti. "Coherence and wave packets in neutrino oscillations". In: Found. Phys. Lett. 17 (2004), pp. 103–124. DOI: 10.1023/B:FOPL.0000019651.53280.31. arXiv: hep-ph/0302026.
- [187] Carlo Giunti and Chung W. Kim. Fundamentals of Neutrino Physics and Astrophysics. 2007. ISBN: 978-0-19-850871-7.
- [188] Alex E. Bernardini and Stefano De Leo. "An Analytic approach to the wave packet formalism in oscillation phenomena". In: *Phys. Rev. D* 70 (2004), p. 053010. DOI: 10.1103/PhysRevD.70.053010. arXiv: hep-ph/0411134.

- [189] D. V. Naumov and V. A. Naumov. "A Diagrammatic treatment of neutrino oscillations". In: *J. Phys. G* 37 (2010), p. 105014. DOI: 10.1088/0954-3899/37/10/105014. arXiv: 1008.0306 [hep-ph].
- [190] B. J. P. Jones. "Dynamical pion collapse and the coherence of conventional neutrino beams". In: *Phys. Rev. D* 91.5 (2015), p. 053002. DOI: 10.1103/PhysRevD.91.053002. arXiv: 1412.2264 [hep-ph].
- [191] Feng Peng An et al. "Study of the wave packet treatment of neutrino oscillation at Daya Bay". In: Eur. Phys. J. C 77.9 (2017), p. 606. DOI: 10.1140/epjc/s10052-017-4970-y. arXiv: 1608.01661 [hep-ex].
- [192] B. J. P. Jones. "Comment on "Damping of neutrino oscillations, decoherence and the lengths of neutrino wave packets"". In: (Sept. 2022). arXiv: 2209.00561 [hep-ph].
- [193] B. J. P. Jones, E. Marzec, and J. Spitz. "The Width of a Beta-decay-induced Antineutrino Wavepacket". In: (Oct. 2022). arXiv: 2211.00026 [hep-ph].
- [194] André de Gouvêa, Valentina De Romeri, and Christoph A. Ternes. "Combined analysis of neutrino decoherence at reactor experiments". In: *JHEP* 06 (2021), p. 042. DOI: 10.1007/JHEP06 (2021) 042. arXiv: 2104.05806 [hep-ph].
- [195] Leo Stodolsky. "The Unnecessary wave packet". In: *Phys. Rev. D* 58 (1998), p. 036006. DOI: 10.1103/PhysRevD.58.036006. arXiv: hep-ph/9802387.
- [196] C. Giunti, C. W. Kim, and U. W. Lee. "When do neutrinos really oscillate?: Quantum mechanics of neutrino oscillations". In: *Phys. Rev. D* 44 (1991), pp. 3635–3640. DOI: 10. 1103/PhysRevD.44.3635.
- [197] Evgeny Akhmedov. "Do non-relativistic neutrinos oscillate?" In: *JHEP* 07 (2017), p. 070. DOI: 10.1007/JHEP07 (2017) 070. arXiv: 1703.08169 [hep-ph].
- [198] Patrick Huber. "The 5 MeV bump a nuclear whodunit mystery". In: *Phys. Rev. Lett. 118*, 042502 (2017) (Sept. 2016). DOI: 10.1103/PhysRevLett.118.042502. arXiv: 1609.03910 [hep-ph].
- [199] Mona Dentler et al. "Sterile neutrinos or flux uncertainties? Status of the reactor antineutrino anomaly". In: *JHEP* 11 (2017), p. 099. DOI: 10.1007/JHEP11(2017)099. arXiv: 1709.04294 [hep-ph].
- [200] A Oralbaev, M Skorokhvatov, and O Titov. "The inverse beta decay: a study of cross section". In: Journal of Physics: Conference Series 675.1 (Feb. 2016), p. 012003. DOI: 10. 1088 / 1742 6596 / 675 / 1 / 012003. URL: https://doi.org/10.1088 / 1742 6596 / 675 / 1 / 012003.
- [201] Ivan Esteban et al. "The fate of hints: updated global analysis of three-flavor neutrino oscillations". In: 2020.9 (Sept. 2020). DOI: 10.1007/jhep09(2020)178. arXiv: http://arxiv.org/abs/2007.14792 [hep-ph].
- [202] Hyunsoo Kim. "Search for Sterile Neutrino at NEOS Experiment". In: 13th Recontres du Vietnam (2017).
- [203] Seok-Gyeong Yoon. "Search for sterile neutrinos at RENO". In: XIX International Workshop on Neutrino Telescopes (2021).
- [204] Eric Marzec and Joshua Spitz. "Neutrino decoherence and the mass hierarchy in the JUNO experiment". In: *Phys. Rev. D* 106.5 (2022), p. 053007. DOI: 10.1103/PhysRevD. 106.053007. arXiv: 2208.04277 [hep-ph].
- [205] Evgeny Akhmedov and Alexei Y. Smirnov. "Reply to "Comment on "Damping of neutrino oscillations, decoherence and the lengths of neutrino wave packets"." In: (Oct. 2022). arXiv: 2210.01547 [hep-ph].

- [206] Raphael Krueger and Thomas Schwetz. "Decoherence effects in reactor and Gallium neutrino oscillation experiments: a QFT approach". In: *Eur. Phys. J. C* 83.7 (2023), p. 578. DOI: 10.1140/epjc/s10052-023-11711-8. arXiv: 2303.15524 [hep-ph].
- [207] Joseph Smolsky et al. "Direct experimental constraints on the spatial extent of a neutrino wavepacket". In: *Nature* 638.8051 (2025), pp. 640–644. DOI: 10 . 1038 / s41586 024 08479–6. arXiv: 2404.03102 [nucl-ex].
- [208] B. J. P. Jones, E. Marzec, and J. Spitz. "The Width of an Electron-Capture Neutrino Wave Packet". In: (Apr. 2024). arXiv: 2404.19746 [hep-ph].
- [209] Hannah Banks, Kevin J. Kelly, and Matthew McCullough. "How broad is a neutrino?" In: *JHEP* 02 (2023), p. 136. DOI: 10.1007/JHEP02 (2023) 136. arXiv: 2209.11270 [hep-ph].
- [210] Hannah Banks et al. "Broad sterile neutrinos & the reactor/gallium tension". In: JHEP 04 (2024), p. 096. DOI: 10.1007/JHEP04(2024)096. arXiv: 2311.06352 [hep-ph].
- [211] J. Alonso et al. "Neutrino physics opportunities with the IsoDAR source at Yemilab". In: *Phys. Rev. D* 105.5 (2022), p. 052009. DOI: 10.1103/PhysRevD.105.052009. arXiv: 2111.09480 [hep-ex].
- [212] J. M. Hardin et al. "New Clues about light sterile neutrinos: preference for models with damping effects in global fits". In: *JHEP* 09 (2023), p. 058. DOI: 10.1007/JHEP09 (2023) 058. arXiv: 2211.02610 [hep-ph].
- [213] Yasaman Farzan and Thomas Schwetz. "A decoherence explanation of the gallium neutrino anomaly". In: *SciPost Phys.* 15.4 (2023), p. 172. DOI: 10.21468/SciPostPhys.15.4.172. arXiv: 2306.09422 [hep-ph].
- [214] Thomas K. Gaisser, Ralph Engel, and Elisa Resconi. *Cosmic Rays and Particle Physics: 2nd Edition.* Cambridge University Press, June 2016. ISBN: 978-0-521-01646-9.
- [215] F. Oikonomou. "Constraining the sources of ultra-high energy cosmic rays with multi-messenger data". PhD thesis. University Coll. London, 2014.
- [216] M. Ackermann et al. "The spectrum of isotropic diffuse gamma-ray emission between 100 MeV and 820 GeV". In: *Astrophys. J.* 799 (2015), p. 86. DOI: 10.1088/0004-637X/799/1/86. arXiv: 1410.3696 [astro-ph.HE].
- [217] M. G. Aartsen et al. "Detection of a particle shower at the Glashow resonance with Ice-Cube". In: *Nature* 591.7849 (2021). [Erratum: Nature 592, E11 (2021)], pp. 220–224. DOI: 10.1038/s41586-021-03256-1. arXiv: 2110.15051 [hep-ex].
- [218] M. G. Aartsen et al. "Characteristics of the diffuse astrophysical electron and tau neutrino flux with six years of IceCube high energy cascade data". In: *Phys. Rev. Lett.* 125.12 (2020), p. 121104. DOI: 10.1103/PhysRevLett.125.121104. arXiv: 2001.09520 [astro-ph.HE].
- [219] R. Abbasi et al. "Improved Characterization of the Astrophysical Muon-neutrino Flux with 9.5 Years of IceCube Data". In: *Astrophys. J.* 928.1 (2022), p. 50. DOI: 10.3847/1538-4357/ac4d29. arXiv: 2111.10299 [astro-ph.HE].
- P. Abreu et al. "The energy spectrum of cosmic rays beyond the turn-down around 10¹⁷ eV as measured with the surface detector of the Pierre Auger Observatory". In: *Eur. Phys. J. C* 81.11 (2021), p. 966. DOI: 10.1140/epjc/s10052-021-09700-w. arXiv: 2109.13400 [astro-ph.HE].
- [221] Dmitri Ivanov. "Energy Spectrum Measured by the Telescope Array". In: *PoS* ICRC2019 (2019), p. 298. DOI: 10.22323/1.358.0298.
- [222] Silvia Vernetto and Paolo Lipari. "Absorption of very high energy gamma rays in the Milky Way". In: *Phys. Rev. D* 94.6 (2016), p. 063009. DOI: 10.1103/PhysRevD.94.063009. arXiv: 1608.01587 [astro-ph.HE].

- [223] Zhen Cao et al. "Ultrahigh-energy photons up to 1.4 petaelectronvolts from 12 γ -ray Galactic sources". In: *Nature* 594.7861 (2021), pp. 33–36. DOI: 10.1038/s41586-021-03498-z.
- [224] Zhen Cao et al. "Measurement of Ultra-High-Energy Diffuse Gamma-Ray Emission of the Galactic Plane from 10 TeV to 1 PeV with LHAASO-KM2A". In: Phys. Rev. Lett. 131.15 (2023), p. 151001. DOI: 10.1103/PhysRevLett.131.151001. arXiv: 2305.05372 [astro-ph.HE].
- [225] Zhen Cao et al. "The First LHAASO Catalog of Gamma-Ray Sources". In: *Astrophys. J. Suppl.* 271.1 (2024), p. 25. DOI: 10.3847/1538-4365/acfd29. arXiv: 2305.17030 [astro-ph.HE].
- [226] Zhen Cao et al. "An ultrahigh-energy γ -ray bubble powered by a super PeVatron". In: *Sci. Bull.* 69.4 (2024), pp. 449–457. DOI: 10.1016/j.scib.2023.12.040. arXiv: 2310.10100 [astro-ph.HE].
- [227] D. J. Bird et al. "Detection of a cosmic ray with measured energy well beyond the expected spectral cutoff due to cosmic microwave radiation". In: *Astrophys. J.* 441 (1995), pp. 144–150. DOI: 10.1086/175344. arXiv: astro-ph/9410067.
- [228] Rafael Alves Batista et al. "Open Questions in Cosmic-Ray Research at Ultrahigh Energies". In: Front. Astron. Space Sci. 6 (2019), p. 23. DOI: 10.3389/fspas.2019.00023. arXiv: 1903.06714 [astro-ph.HE].
- [229] A. Coleman et al. "Ultra high energy cosmic rays The intersection of the Cosmic and Energy Frontiers". In: *Astropart. Phys.* 149 (2023), p. 102819. DOI: 10.1016/j.astropartphys. 2023.102819. arXiv: 2205.05845 [astro-ph.HE].
- [230] A. M. Hillas. "The Origin of Ultra-High-Energy Cosmic Rays". In: *Ann. Rev. Astron. Astro- phys.* 22.Volume 22, 1984 (1984), pp. 425–444. ISSN: 1545-4282. DOI: 10.1146/annurev. aa.22.090184.002233.
- [231] A. R. Bell. "The acceleration of cosmic rays in shock fronts I". In: *Mon. Not. Roy. Astron. Soc.* 182.2 (1978), pp. 147–156. DOI: 10.1093/mnras/182.2.147.
- [232] Anatoly Spitkovsky. "Particle acceleration in relativistic collisionless shocks: Fermi process at last?" In: *Astrophys. J. Lett.* 682 (2008), p. L5. DOI: 10.1086/590248. arXiv: 0802. 3216 [astro-ph].
- [233] Karl Mannheim, R. J. Protheroe, and Jorg P. Rachen. "On the cosmic ray bound for models of extragalactic neutrino production". In: *Phys. Rev. D* 63 (2001), p. 023003. DOI: 10.1103/PhysRevD.63.023003. arXiv: astro-ph/9812398.
- [234] U. F. Katz and Ch. Spiering. "High-Energy Neutrino Astrophysics: Status and Perspectives". In: *Prog. Part. Nucl. Phys.* 67 (2012), pp. 651–704. DOI: 10.1016/j.ppnp.2011.12.001. arXiv: 1111.0507 [astro-ph.HE].
- [235] Eli Waxman and John N. Bahcall. "High-energy neutrinos from astrophysical sources: An Upper bound". In: *Phys. Rev. D* 59 (1999), p. 023002. DOI: 10.1103/PhysRevD.59.023002. arXiv: hep-ph/9807282.
- [236] M. G. Aartsen et al. "Observation and Characterization of a Cosmic Muon Neutrino Flux from the Northern Hemisphere using six years of IceCube data". In: *Astrophys. J.* 833.1 (2016), p. 3. DOI: 10.3847/0004-637X/833/1/3. arXiv: 1607.08006 [astro-ph.HE].
- [237] Kenneth Greisen. "End to the cosmic ray spectrum?" In: *Phys. Rev. Lett.* 16 (1966), pp. 748–750. DOI: 10.1103/PhysRevLett.16.748.
- [238] G. T. Zatsepin and V. A. Kuzmin. "Upper limit of the spectrum of cosmic rays". In: *JETP Lett.* 4 (1966), pp. 78–80.

- [239] J. A. Formaggio and G. P. Zeller. "From eV to EeV: Neutrino Cross Sections Across Energy Scales". In: *Rev. Mod. Phys.* 84 (2012), pp. 1307–1341. DOI: 10.1103/RevModPhys.84. 1307. arXiv: 1305.7513 [hep-ex].
- [240] Ivan Esteban, Steven Prohira, and John F. Beacom. "Detector requirements for model-independent measurements of ultrahigh energy neutrino cross sections". In: *Phys. Rev. D* 106.2 (2022), p. 023021. DOI: 10.1103/PhysRevD.106.023021. arXiv: 2205.09763 [hep-ph].
- [241] Alexander Kusenko and Thomas J. Weiler. "Neutrino cross-sections at high-energies and the future observations of ultrahigh-energy cosmic rays". In: *Phys. Rev. Lett.* 88 (2002), p. 161101. DOI: 10.1103/PhysRevLett.88.161101. arXiv: hep-ph/0106071.
- [242] Amy Connolly, Robert S. Thorne, and David Waters. "Calculation of High Energy Neutrino-Nucleon Cross Sections and Uncertainties Using the MSTW Parton Distribution Functions and Implications for Future Experiments". In: *Phys. Rev. D* 83 (2011), p. 113009. DOI: 10.1103/PhysRevD.83.113009. arXiv: 1102.0691 [hep-ph].
- [243] Amanda Cooper-Sarkar, Philipp Mertsch, and Subir Sarkar. "The high energy neutrino cross-section in the Standard Model and its uncertainty". In: *JHEP* 08 (2011), p. 042. DOI: 10.1007/JHEP08(2011)042. arXiv: 1106.3723 [hep-ph].
- [244] Valerio Bertone, Rhorry Gauld, and Juan Rojo. "Neutrino Telescopes as QCD Microscopes". In: JHEP 01 (2019), p. 217. DOI: 10.1007/JHEP01 (2019) 217. arXiv: 1808.02034 [hep-ph].
- [245] Luis A. Anchordoqui, Carlos García Canal, and Jorge F. Soriano. "Probing strong dynamics with cosmic neutrinos". In: *Phys. Rev. D* 100.10 (2019), p. 103001. DOI: 10.1103/PhysRevD.100.103001. arXiv: 1902.10134 [hep-ph].
- [246] Luis A. Anchordoqui. "Ultra-High-Energy Cosmic Rays". In: *Phys. Rept.* 801 (2019), pp. 1–93. DOI: 10.1016/j.physrep.2019.01.002. arXiv: 1807.09645 [astro-ph.HE].
- [247] Luis A. Anchordoqui et al. "Black holes from cosmic rays: Probes of extra dimensions and new limits on TeV scale gravity". In: *Phys. Rev. D* 65 (2002), p. 124027. DOI: 10.1103/PhysRevD.65.124027. arXiv: hep-ph/0112247.
- [248] Spencer R. Klein. "Probing high-energy interactions of atmospheric and astrophysical neutrinos". In: 2020. DOI: 10.1142/9789813275027_0004. arXiv: 1906.02221 [astro-ph.HE].
- [249] Jaime Alvarez-Muniz et al. "Detecting microscopic black holes with neutrino telescopes". In: *Phys. Rev. D* 65 (2002), p. 124015. DOI: 10.1103/PhysRevD.65.124015. arXiv: hep-ph/0202081.
- [250] J. Alvarez-Muniz et al. "Phenomenology of high-energy neutrinos in low scale quantum gravity models". In: *Phys. Rev. Lett.* 88 (2002), p. 021301. DOI: 10.1103/PhysRevLett. 88.021301. arXiv: hep-ph/0107057.
- [251] Jeffrey M. Berryman et al. "Neutrino self-interactions: A white paper". In: *Phys. Dark Univ.* 42 (2023), p. 101267. DOI: 10.1016/j.dark.2023.101267. arXiv: 2203.01955 [hep-ph].
- [252] Mar Císcar-Monsalvatje, Gonzalo Herrera, and Ian M. Shoemaker. "Upper limits on the cosmic neutrino background from cosmic rays". In: *Phys. Rev. D* 110.6 (2024), p. 063036. DOI: 10.1103/PhysRevD.110.063036. arXiv: 2402.00985 [hep-ph].
- [253] Dan Hooper. "Detecting MeV Gauge Bosons with High-Energy Neutrino Telescopes". In: *Phys. Rev. D* 75 (2007), p. 123001. DOI: 10.1103/PhysRevD.75.123001. arXiv: hep-ph/0701194.

- [254] Kunihto loka and Kohta Murase. "IceCube PeV-EeV neutrinos and secret interactions of neutrinos". In: *PTEP* 2014.6 (2014), 061E01. DOI: 10.1093/ptep/ptu090. arXiv: 1404. 2279 [astro-ph.HE].
- [255] Kenny C. Y. Ng and John F. Beacom. "Cosmic neutrino cascades from secret neutrino interactions". In: *Phys. Rev. D* 90.6 (2014). [Erratum: Phys.Rev.D 90, 089904 (2014)], p. 065035. DOI: 10.1103/PhysRevD.90.065035. arXiv: 1404.2288 [astro-ph.HE].
- [256] Mauricio Bustamante et al. "Bounds on secret neutrino interactions from high-energy astrophysical neutrinos". In: *Phys. Rev. D* 101.12 (2020), p. 123024. DOI: 10.1103/PhysRevD. 101.123024. arXiv: 2001.04994 [astro-ph.HE].
- [257] Cyril Creque-Sarbinowski, Jeffrey Hyde, and Marc Kamionkowski. "Resonant neutrino self-interactions". In: *Phys. Rev. D* 103.2 (2021), p. 023527. DOI: 10.1103/PhysRevD.103.023527. arXiv: 2005.05332 [hep-ph].
- [258] Kohta Murase and Ian M. Shoemaker. "Neutrino Echoes from Multimessenger Transient Sources". In: *Phys. Rev. Lett.* 123.24 (2019), p. 241102. DOI: 10.1103/PhysRevLett.123. 241102. arXiv: 1903.08607 [hep-ph].
- [259] Anthony DiFranzo and Dan Hooper. "Searching for MeV-Scale Gauge Bosons with Ice-Cube". In: *Phys. Rev. D* 92.9 (2015), p. 095007. DOI: 10.1103/PhysRevD.92.095007. arXiv: 1507.03015 [hep-ph].
- [260] Ivan Esteban et al. "Probing secret interactions of astrophysical neutrinos in the high-statistics era". In: *Phys. Rev. D* 104.12 (2021), p. 123014. DOI: 10.1103/PhysRevD.104. 123014. arXiv: 2107.13568 [hep-ph].
- [261] Christian Döring and Stefan Vogl. "Testing secret interaction with astrophysical neutrino point sources". In: *JCAP* 07 (2024), p. 015. DOI: 10.1088/1475-7516/2024/07/015. arXiv: 2304.08533 [hep-ph].
- [262] Jose Alonso Carpio and Kohta Murase. "Simulating neutrino echoes induced by secret neutrino interactions". In: *JCAP* 02 (2023), p. 042. DOI: 10.1088/1475-7516/2023/02/042. arXiv: 2204.09029 [hep-ph].
- [263] Kevin J. Kelly and Pedro A. N. Machado. "Multimessenger Astronomy and New Neutrino Physics". In: *JCAP* 10 (2018), p. 048. DOI: 10.1088/1475-7516/2018/10/048. arXiv: 1808.02889 [hep-ph].
- [264] Luighi P. S. Leal, Daniel Naredo-Tuero, and Renata Zukanovich Funchal. "Cosmogenic neutrinos as probes of new physics". In: (Apr. 2025). arXiv: 2504.10576 [hep-ph].
- [265] Rasmus W. Rasmussen et al. "Astrophysical neutrinos flavored with Beyond the Standard Model physics". In: *Phys. Rev. D* 96.8 (2017), p. 083018. DOI: 10.1103/PhysRevD. 96.083018. arXiv: 1707.07684 [hep-ph].
- [266] R. Abbasi et al. "Searches for connections between dark matter and high-energy neutrinos with IceCube". In: *JCAP* 10 (2023), p. 003. DOI: 10.1088/1475-7516/2023/10/003. arXiv: 2205.12950 [hep-ex].
- [267] Francesc Ferrer, Gonzalo Herrera, and Alejandro Ibarra. "New constraints on the dark matter-neutrino and dark matter-photon scattering cross sections from TXS 0506+056". In: *JCAP* 05 (2023), p. 057. DOI: 10.1088/1475-7516/2023/05/057. arXiv: 2209.06339 [hep-ph].
- [268] G. D. Zapata, J. Jones-Pérez, and A. M. Gago. "Bounds on neutrino-DM interactions from TXS 0506+056 neutrino outburst". In: (Mar. 2025). arXiv: 2503.03823 [hep-ph].
- [269] James M. Cline et al. "Blazar Constraints on Neutrino-Dark Matter Scattering". In: *Phys. Rev. Lett.* 130.9 (2023), p. 091402. DOI: 10.1103/PhysRevLett.130.091402. arXiv: 2209.02713 [hep-ph].

- [270] James M. Cline and Matteo Puel. "NGC 1068 constraints on neutrino-dark matter scattering". In: *JCAP* 06 (2023), p. 004. doi: 10.1088/1475-7516/2023/06/004. arXiv: 2301.08756 [hep-ph].
- [271] Motoko Fujiwara, Gonzalo Herrera, and Shunsaku Horiuchi. "Neutrino Diffusion within Dark Matter Spikes". In: (Dec. 2024). arXiv: 2412.00805 [hep-ph].
- [272] Motoko Fujiwara and Gonzalo Herrera. "Tidal disruption events and dark matter scatterings with neutrinos and photons". In: *Phys. Lett. B* 851 (2024), p. 138573. DOI: 10.1016/j.physletb.2024.138573. arXiv: 2312.11670 [hep-ph].
- [273] Carlos A. Argüelles, Ali Kheirandish, and Aaron C. Vincent. "Imaging Galactic Dark Matter with High-Energy Cosmic Neutrinos". In: *Phys. Rev. Lett.* 119.20 (2017), p. 201801. DOI: 10.1103/PhysRevLett.119.201801. arXiv: 1703.00451 [hep-ph].
- [274] Carlos A. Argüelles, Kareem Farrag, and Teppei Katori. "Ultra-light Dark Matter Limits from Astrophysical Neutrino Flavor". In: (Apr. 2024). arXiv: 2404.10926 [hep-ph].
- [275] Niki Klop and Shin'ichiro Ando. "Effects of a neutrino-dark energy coupling on oscillations of high-energy neutrinos". In: *Phys. Rev. D* 97.6 (2018), p. 063006. DOI: 10.1103/PhysRevD.97.063006. arXiv: 1712.05413 [hep-ph].
- [276] Shin'ichiro Ando, Marc Kamionkowski, and Irina Mocioiu. "Neutrino Oscillations, Lorentz/CPT Violation, and Dark Energy". In: *Phys. Rev. D* 80 (2009), p. 123522. DOI: 10.1103/PhysRevD. 80.123522. arXiv: 0910.4391 [hep-ph].
- [277] Peter B. Denton and Irene Tamborra. "Invisible Neutrino Decay Could Resolve IceCube's Track and Cascade Tension". In: *Phys. Rev. Lett.* 121.12 (2018), p. 121802. DOI: 10.1103/PhysRevLett.121.121802. arXiv: 1805.05950 [hep-ph].
- [278] Asli Abdullahi and Peter B. Denton. "Visible Decay of Astrophysical Neutrinos at Ice-Cube". In: *Phys. Rev. D* 102.2 (2020), p. 023018. DOI: 10.1103/PhysRevD.102.023018. arXiv: 2005.07200 [hep-ph].
- [279] John F. Beacom et al. "Decay of High-Energy Astrophysical Neutrinos". In: *Phys. Rev. Lett.* 90 (2003), p. 181301. DOI: 10.1103/PhysRevLett.90.181301. arXiv: hep-ph/0211305.
- [280] John F. Beacom et al. "Sensitivity to θ_{13} and δ in the Decaying Astrophysical Neutrino Scenario". In: *Phys. Rev. D* 69 (2004), p. 017303. DOI: 10.1103/PhysRevD.69.017303. arXiv: hep-ph/0309267.
- [281] Philipp Baerwald, Mauricio Bustamante, and Walter Winter. "Neutrino Decays over Cosmological Distances and the Implications for Neutrino Telescopes". In: *JCAP* 10 (2012), p. 020. DOI: 10.1088/1475-7516/2012/10/020. arXiv: 1208.4600 [astro-ph.CO].
- [282] Mauricio Bustamante, John F. Beacom, and Kohta Murase. "Testing decay of astrophysical neutrinos with incomplete information". In: *Phys. Rev. D* 95.6 (2017), p. 063013. DOI: 10.1103/PhysRevD.95.063013. arXiv: 1610.02096 [astro-ph.HE].
- [283] P. S. Bhupal Dev, Pedro A. N. Machado, and Ivan Martinez-Soler. "Pseudo-Dirac neutrinos and relic neutrino matter effect on the high-energy neutrino flavor composition". In: *Phys. Lett. B* 862 (2025), p. 139306. DOI: 10.1016/j.physletb.2025.139306. arXiv: 2406.18507 [hep-ph].
- [284] Mauricio Bustamante, John F. Beacom, and Walter Winter. "Theoretically palatable flavor combinations of astrophysical neutrinos". In: *Phys. Rev. Lett.* 115.16 (2015), p. 161302. DOI: 10.1103/PhysRevLett.115.161302. arXiv: 1506.02645 [astro-ph.HE].
- [285] Markus Ahlers, Mauricio Bustamante, and Niels Gustav Nortvig Willesen. "Flavors of astrophysical neutrinos with active-sterile mixing". In: *JCAP* 07 (2021), p. 029. DOI: 10. 1088/1475-7516/2021/07/029. arXiv: 2009.01253 [hep-ph].

- [286] Markus Ahlers, Mauricio Bustamante, and Siqiao Mu. "Unitarity Bounds of Astrophysical Neutrinos". In: *Phys. Rev. D* 98.12 (2018), p. 123023. DOI: 10.1103/PhysRevD.98. 123023. arXiv: 1810.00893 [astro-ph.HE].
- [287] M. C. Gonzalez-Garcia et al. "Non-standard neutrino interactions in the Earth and the flavor of astrophysical neutrinos". In: *Astropart. Phys.* 84 (2016), pp. 15–22. DOI: 10.1016/j.astropartphys.2016.07.001. arXiv: 1605.08055 [hep-ph].
- [288] Ian M. Shoemaker and Kohta Murase. "Probing BSM Neutrino Physics with Flavor and Spectral Distortions: Prospects for Future High-Energy Neutrino Telescopes". In: *Phys. Rev. D* 93.8 (2016), p. 085004. DOI: 10.1103/PhysRevD.93.085004. arXiv: 1512.07228 [astro-ph.HE].
- [289] Carlos A. Argüelles, Teppei Katori, and Jordi Salvado. "New Physics in Astrophysical Neutrino Flavor". In: *Phys. Rev. Lett.* 115 (2015), p. 161303. DOI: 10.1103/PhysRevLett. 115.161303. arXiv: 1506.02043 [hep-ph].
- [290] Poonam Mehta and Walter Winter. "Interplay of energy dependent astrophysical neutrino flavor ratios and new physics effects". In: *JCAP* 03 (2011), p. 041. DOI: 10.1088/1475-7516/2011/03/041. arXiv: 1101.2673 [hep-ph].
- [291] M. Bustamante, A. M. Gago, and Joel Jones Perez. "SUSY Renormalization Group Effects in Ultra High Energy Neutrinos". In: *JHEP* 05 (2011), p. 133. DOI: 10.1007/JHEP05 (2011) 133. arXiv: 1012.2728 [hep-ph].
- [292] M. Bustamante, A. M. Gago, and C. Pena-Garay. "Energy-Independent New Physics in the Flavour Ratios of High-Energy Astrophysical Neutrinos". In: *JHEP* 04 (2010), p. 066. DOI: 10.1007/JHEP04(2010)066. arXiv: 1001.4878 [hep-ph].
- [293] Sandip Pakvasa, Werner Rodejohann, and Thomas J. Weiler. "Flavor Ratios of Astrophysical Neutrinos: Implications for Precision Measurements". In: *JHEP* 02 (2008), p. 005. DOI: 10.1088/1126-6708/2008/02/005. arXiv: 0711.4517 [hep-ph].
- [294] A. Albert et al. "Combined search for neutrinos from dark matter self-annihilation in the Galactic Center with ANTARES and IceCube". In: *Phys. Rev. D* 102.8 (2020), p. 082002. DOI: 10.1103/PhysRevD.102.082002. arXiv: 2003.06614 [astro-ph.HE].
- [295] R. Abbasi et al. "Search for GeV-scale dark matter annihilation in the Sun with IceCube DeepCore". In: *Phys. Rev. D* 105.6 (2022), p. 062004. DOI: 10.1103/PhysRevD.105.062004. arXiv: 2111.09970 [astro-ph.HE].
- [296] R. Abbasi et al. "Search for neutrino lines from dark matter annihilation and decay with IceCube". In: *Phys. Rev. D* 108.10 (2023), p. 102004. DOI: 10 . 1103 / PhysRevD . 108 . 102004. arXiv: 2303.13663 [astro-ph.HE].
- [297] R. Abbasi et al. "Search for dark matter from the center of the Earth with ten years of IceCube data". In: (Dec. 2024). arXiv: 2412.12972 [astro-ph.HE].
- [298] Carlos A. Argüelles et al. "Dark matter annihilation to neutrinos". In: *Rev. Mod. Phys.* 93.3 (2021), p. 035007. DOI: 10.1103/RevModPhys.93.035007. arXiv: 1912.09486 [hep-ph].
- [299] Yicong Sui and P. S. Bhupal Dev. "A Combined Astrophysical and Dark Matter Interpretation of the IceCube HESE and Throughgoing Muon Events". In: *JCAP* 07 (2018), p. 020. DOI: 10.1088/1475-7516/2018/07/020. arXiv: 1804.04919 [hep-ph].
- [300] Marco Chianese, Gennaro Miele, and Stefano Morisi. "Interpreting IceCube 6-year HESE data as an evidence for hundred TeV decaying Dark Matter". In: *Phys. Lett. B* 773 (2017), pp. 591–595. DOI: 10.1016/j.physletb.2017.09.016. arXiv: 1707.05241 [hep-ph].

- [301] Nagisa Hiroshima et al. "High-energy neutrinos from multibody decaying dark matter". In: *Phys. Rev. D* 97.2 (2018), p. 023006. DOI: 10.1103/PhysRevD.97.023006. arXiv: 1705.04419 [hep-ph].
- [302] P. S. Bhupal Dev et al. "Heavy right-handed neutrino dark matter and PeV neutrinos at IceCube". In: *JCAP* 08 (2016), p. 034. DOI: 10.1088/1475-7516/2016/08/034. arXiv: 1606.04517 [hep-ph].
- [303] Timothy Cohen et al. "γ -ray Constraints on Decaying Dark Matter and Implications for IceCube". In: *Phys. Rev. Lett.* 119.2 (2017), p. 021102. DOI: 10.1103/PhysRevLett.119. 021102. arXiv: 1612.05638 [hep-ph].
- [304] Sofiane M. Boucenna et al. "Decaying Leptophilic Dark Matter at IceCube". In: *JCAP* 12 (2015), p. 055. DOI: 10.1088/1475-7516/2015/12/055. arXiv: 1507.01000 [hep-ph].
- [305] Luis A. Anchordoqui et al. "IceCube neutrinos, decaying dark matter, and the Hubble constant". In: *Phys. Rev. D* 92.6 (2015). [Erratum: Phys.Rev.D 94, 069901 (2016)], p. 061301. DOI: 10.1103/PhysRevD.94.069901. arXiv: 1506.08788 [hep-ph].
- [306] Kohta Murase et al. "Testing the Dark Matter Scenario for PeV Neutrinos Observed in IceCube". In: *Phys. Rev. Lett.* 115.7 (2015), p. 071301. DOI: 10.1103/PhysRevLett.115. 071301. arXiv: 1503.04663 [hep-ph].
- [307] Chee Sheng Fong et al. "Possible Interpretations of IceCube High-Energy Neutrino Events". In: JHEP 02 (2015), p. 189. DOI: 10.1007/JHEP02 (2015) 189. arXiv: 1411.5318 [hep-ph].
- [308] Jesús Zavala. "Galactic PeV neutrinos from dark matter annihilation". In: *Phys. Rev. D* 89.12 (2014), p. 123516. DOI: 10 . 1103 / PhysRevD . 89 . 123516. arXiv: 1404 . 2932 [astro-ph.HE].
- [309] Emilian Dudas, Yann Mambrini, and Keith A. Olive. "Monochromatic neutrinos generated by dark matter and the seesaw mechanism". In: *Phys. Rev. D* 91 (2015), p. 075001. DOI: 10.1103/PhysRevD.91.075001. arXiv: 1412.3459 [hep-ph].
- [310] Carsten Rott, Kazunori Kohri, and Seong Chan Park. "Superheavy dark matter and Ice-Cube neutrino signals: Bounds on decaying dark matter". In: *Phys. Rev. D* 92.2 (2015), p. 023529. DOI: 10.1103/PhysRevD.92.023529. arXiv: 1408.4575 [hep-ph].
- [311] Tetsutaro Higaki, Ryuichiro Kitano, and Ryosuke Sato. "Neutrinoful Universe". In: JHEP 07 (2014), p. 044. DOI: 10.1007/JHEP07 (2014) 044. arXiv: 1405.0013 [hep-ph].
- [312] Arman Esmaili and Pasquale Dario Serpico. "Are IceCube neutrinos unveiling PeV-scale decaying dark matter?" In: *JCAP* 11 (2013), p. 054. doi: 10.1088/1475-7516/2013/11/054. arXiv: 1308.1105 [hep-ph].
- [313] Brian Feldstein et al. "Neutrinos at IceCube from Heavy Decaying Dark Matter". In: *Phys. Rev. D* 88.1 (2013), p. 015004. DOI: 10.1103/PhysRevD.88.015004. arXiv: 1303.7320 [hep-ph].
- [314] Kazunori Kohri, Partha Kumar Paul, and Narendra Sahu. "Super heavy dark matter origin of the PeV neutrino event: KM3-230213A". In: (Mar. 2025). arXiv: 2503.04464 [hep-ph].
- [315] Debasish Borah et al. "Possible origin of the KM3-230213A neutrino event from dark matter decay". In: (Feb. 2025). arXiv: 2503.00097 [hep-ph].
- [316] Basabendu Barman et al. "Hunting for heavy Z' with IceCube neutrinos and gravitational waves". In: (Feb. 2025). arXiv: 2502.13217 [hep-ph].
- [317] Kim V. Berghaus, Dan Hooper, and Emily R. Simon. "Searching For Superheavy Decaying Particles With Ultra-High-Energy Neutrino Observatories". In: (Feb. 2025). arXiv: 2502. 12238 [hep-ph].

- [318] Qinrui Liu, Ningqiang Song, and Aaron C. Vincent. "Constraints on Heavy Asymmetric and Symmetric Dark Matter from the Glashow Resonance". In: (June 2024). arXiv: 2406. 14602 [hep-ph].
- [319] Saikat Das, Jose Alonso Carpio, and Kohta Murase. "Probing superheavy dark matter through lunar radio observations of ultrahigh-energy neutrinos and the impacts of neutrino cascades". In: *Phys. Rev. D* 111.8 (2025), p. 083007. DOI: 10.1103/PhysRevD.111. 083007. arXiv: 2405.06382 [hep-ph].
- [320] M. G. Aartsen et al. "Measurements using the inelasticity distribution of multi-TeV neutrino interactions in IceCube". In: *Phys. Rev. D* 99.3 (2019), p. 032004. DOI: 10.1103/PhysRevD.99.032004. arXiv: 1808.07629 [hep-ex].
- [321] Sheldon L. Glashow. "Resonant Scattering of Antineutrinos". In: *Phys. Rev.* 118 (1960), pp. 316–317. DOI: 10.1103/PhysRev.118.316.
- [322] M. Ageron et al. "ANTARES: the first undersea neutrino telescope". In: *Nucl. Instrum. Meth. A* 656 (2011), pp. 11–38. DOI: 10.1016/j.nima.2011.06.103. arXiv: 1104.1607 [astro-ph.IM].
- [323] Thomas Gaisser and Francis Halzen. "IceCube". In: Annual Review of Nuclear and Particle Science 64. Volume 64, 2014 (2014), pp. 101-123. ISSN: 1545-4134. DOI: https://doi.org/10.1146/annurev-nucl-102313-025321. URL: https://www.annualreviews.org/content/journals/10.1146/annurev-nucl-102313-025321.
- [324] Francis Halzen and Spencer R. Klein. "IceCube: An Instrument for Neutrino Astronomy". In: *Rev. Sci. Instrum.* 81 (2010), p. 081101. DOI: 10.1063/1.3480478. arXiv: 1007.1247 [astro-ph.HE].
- [325] M. G. Aartsen et al. "Evidence for High-Energy Extraterrestrial Neutrinos at the IceCube Detector". In: *Science* 342 (2013), p. 1242856. DOI: 10.1126/science.1242856. arXiv: 1311.5238 [astro-ph.HE].
- [326] R. Abbasi et al. "Measurement of the atmospheric neutrino energy spectrum from 100 GeV to 400 TeV with IceCube". In: *Phys. Rev. D* 83 (2011), p. 012001. DOI: 10.1103/PhysRevD.83.012001. arXiv: 1010.3980 [astro-ph.HE].
- [327] M. G. Aartsen et al. "Neutrino emission from the direction of the blazar TXS 0506+056 prior to the IceCube-170922A alert". In: *Science* 361.6398 (2018), pp. 147-151. DOI: 10. 1126/science.aat2890. arXiv: 1807.08794 [astro-ph.HE].
- [328] R. Abbasi et al. "Evidence for neutrino emission from the nearby active galaxy NGC 1068". In: *Science* 378.6619 (2022), pp. 538-543. DOI: 10.1126/science.abg3395. arXiv: 2211.09972 [astro-ph.HE].
- [329] M. G. Aartsen et al. "Multimessenger observations of a flaring blazar coincident with high-energy neutrino lceCube-170922A". In: *Science* 361.6398 (2018), eaat1378. DOI: 10.1126/science.aat1378. arXiv: 1807.08816 [astro-ph.HE].
- [330] R. Abbasi et al. "The IceCube high-energy starting event sample: Description and flux characterization with 7.5 years of data". In: *Phys. Rev. D* 104 (2021), p. 022002. DOI: 10. 1103/PhysRevD.104.022002. arXiv: 2011.03545 [astro-ph.HE].
- [331] R. Abbasi et al. "Observation of high-energy neutrinos from the Galactic plane". In: *Science* 380.6652 (2023), adc9818. DOI: 10.1126/science.adc9818. arXiv: 2307.04427 [astro-ph.HE].
- [332] V'eronique Van Elewyck. "The Antares And Km3Net Neutrino Telescopes: Status And Outlook For Acoustic Studies". In: *EPJ Web of Conferences* (2019). URL: https://api.semanticscholar.org/CorpusID:204197309.

- [333] S. Aiello et al. "Observation of an ultra-high-energy cosmic neutrino with KM3NeT". In: *Nature* 638.8050 (2025). [Erratum: Nature 640, E3 (2025)], pp. 376–382. DOI: 10.1038/s41586-024-08543-1.
- O. Adriani et al. "The ultra-high-energy event KM3-230213A within the global neutrino landscape". In: (Feb. 2025). arXiv: 2502.08173 [astro-ph.HE].
- [335] Shirley Weishi Li et al. "Clash of the Titans: ultra-high energy KM3NeT event versus IceCube data". In: (Feb. 2025). arXiv: 2502.04508 [astro-ph.HE].
- [336] A. D. Avrorin et al. "Baikal-GVD: status and prospects". In: *EPJ Web Conf.* 191 (2018). Ed. by V. E. Volkova et al., p. 01006. DOI: 10.1051/epjconf/201819101006. arXiv: 1808.10353 [astro-ph.IM].
- [337] Matteo Agostini et al. "The Pacific Ocean Neutrino Experiment". In: *Nature Astron.* 4.10 (2020), pp. 913–915. DOI: 10.1038/s41550-020-1182-4. arXiv: 2005.09493 [astro-ph.HE].
- [338] Z. P. Ye et al. "A multi-cubic-kilometre neutrino telescope in the western Pacific Ocean". In: *Nature Astron.* 7.12 (2023), pp. 1497–1505. DOI: 10.1038/s41550-023-02087-6. arXiv: 2207.04519 [astro-ph.HE].
- [339] Lisa Johanna Schumacher et al. "Beyond first light: global monitoring for high-energy neutrino astronomy". In: (Mar. 2025). arXiv: 2503.07549 [astro-ph.HE].
- [340] Marco Stein Muzio, Glennys R. Farrar, and Michael Unger. "Probing the environments surrounding ultrahigh energy cosmic ray accelerators and their implications for astrophysical neutrinos". In: *Phys. Rev. D* 105.2 (2022), p. 023022. DOI: 10.1103/PhysRevD. 105.023022. arXiv: 2108.05512 [astro-ph.HE].
- [341] Arjen van Vliet, Rafael Alves Batista, and Jörg R. Hörandel. "Determining the fraction of cosmic-ray protons at ultrahigh energies with cosmogenic neutrinos". In: *Phys. Rev. D* 100.2 (2019), p. 021302. DOI: 10.1103/PhysRevD.100.021302. arXiv: 1901.01899 [astro-ph.HE].
- [342] G. A. Askar'yan. "Excess negative charge of an electron-photon shower and its coherent radio emission". In: *Zh. Eksp. Teor. Fiz.* 41 (1961), pp. 616–618.
- [343] E. Zas, F. Halzen, and T. Stanev. "Electromagnetic pulses from high-energy showers: Implications for neutrino detection". In: *Phys. Rev. D* 45 (1992), pp. 362–376. DOI: 10.1103/PhysRevD.45.362.
- [344] J. Alvarez-Muniz and E. Zas. "Cherenkov radio pulses from Eev neutrino interactions: The LPM effect". In: *Phys. Lett. B* 411 (1997), pp. 218–224. DOI: 10.1016/S0370-2693(97) 01009-5. arXiv: astro-ph/9706064.
- [345] F. D. Kahn and I. Lerche. "Radiation from Cosmic Ray Air Showers". In: *Proceedings of the Royal Society of London Series A* 289.1417 (Jan. 1966), pp. 206–213. DOI: 10.1098/rspa.1966.0007.
- [346] O. Scholten, K. Werner, and F. Rusydi. "A Macroscopic Description of Coherent Geo-Magnetic Radiation from Cosmic Ray Air Showers". In: *Astropart. Phys.* 29 (2008), pp. 94– 103. DOI: 10.1016/j.astropartphys.2007.11.012. arXiv: 0709.2872 [astro-ph].
- [347] Krijn D. de Vries et al. "The cosmic-ray air-shower signal in Askaryan radio detectors". In: *Astropart. Phys.* 74 (2016), pp. 96–104. DOI: 10.1016/j.astropartphys.2015.10.003. arXiv: 1503.02808 [astro-ph.HE].
- [348] Daniele Fargion. "Discovering Ultra High Energy Neutrinos by Horizontal and Upward tau Air-Showers: Evidences in Terrestrial Gamma Flashes?" In: *Astrophys. J.* 570 (2002), pp. 909–925. DOI: 10.1086/339772. arXiv: astro-ph/0002453.

- [349] Alexander Aab et al. "Probing the origin of ultra-high-energy cosmic rays with neutrinos in the EeV energy range using the Pierre Auger Observatory". In: *JCAP* 10 (2019), p. 022. DOI: 10.1088/1475-7516/2019/10/022. arXiv: 1906.07422 [astro-ph.HE].
- [350] P. Allison et al. "Performance of two Askaryan Radio Array stations and first results in the search for ultrahigh energy neutrinos". In: *Phys. Rev. D* 93.8 (2016), p. 082003. DOI: 10.1103/PhysRevD.93.082003. arXiv: 1507.08991 [astro-ph.HE].
- [351] A. Anker et al. "Targeting ultra-high energy neutrinos with the ARIANNA experiment". In: *Adv. Space Res.* 64 (2019), pp. 2595–2609. DOI: 10.1016/j.asr.2019.06.016. arXiv: 1903.01609 [astro-ph.IM].
- [352] J. A. Aguilar et al. "Design and Sensitivity of the Radio Neutrino Observatory in Greenland (RNO-G)". In: *JINST* 16.03 (2021). [Erratum: JINST 18, E03001 (2023)], P03025. DOI: 10.1088/1748-0221/16/03/P03025. arXiv: 2010.12279 [astro-ph.IM].
- [353] P. W. Gorham et al. "The Antarctic Impulsive Transient Antenna Ultra-high Energy Neutrino Detector Design, Performance, and Sensitivity for 2006-2007 Balloon Flight". In: *Astropart. Phys.* 32 (2009), pp. 10–41. DOI: 10.1016/j.astropartphys.2009.05.003. arXiv: 0812.1920 [astro-ph].
- [354] Q. Abarr et al. "The Payload for Ultrahigh Energy Observations (PUEO): a white paper". In: JINST 16.08 (2021), P08035. DOI: 10.1088/1748-0221/16/08/P08035. arXiv: 2010.02892 [astro-ph.IM].
- [355] Daniel Southall et al. "Searching for RF-Only Triggered Cosmic Ray Events with the High-Elevation BEACON Prototype". In: *PoS* ICRC2021 (2021), p. 1084. DOI: 10.22323/1.395.1084.
- [356] Shih-Hao Wang et al. "TAROGE-M: radio antenna array on antarctic high mountain for detecting near-horizontal ultra-high energy air showers". In: *JCAP* 11 (2022), p. 022. DOI: 10.1088/1475-7516/2022/11/022. arXiv: 2207.10616 [astro-ph.HE].
- [357] Jaime Álvarez-Muñiz et al. "The Giant Radio Array for Neutrino Detection (GRAND): Science and Design". In: Sci. China Phys. Mech. Astron. 63.1 (2020), p. 219501. DOI: 10.1007/s11433-018-9385-7. arXiv: 1810.09994 [astro-ph.HE].
- [358] Andres Romero-Wolf et al. "An Andean Deep-Valley Detector for High-Energy Tau Neutrinos". In: *Latin American Strategy Forum for Research Infrastructure*. Feb. 2020. arXiv: 2002.06475 [astro-ph.IM].
- [359] A. Nepomuk Otte et al. "Trinity: An Air-Shower Imaging System for the Detection of Ultrahigh Energy Neutrinos". In: *PoS* ICRC2019 (2020), p. 976. DOI: 10.22323/1.358.0976. arXiv: 1907.08732 [astro-ph.IM].
- [360] A. V. Olinto et al. "The POEMMA (Probe of Extreme Multi-Messenger Astrophysics) observatory". In: *JCAP* 06 (2021), p. 007. DOI: 10.1088/1475-7516/2021/06/007. arXiv: 2012.07945 [astro-ph.IM].
- [361] P. W. Gorham et al. "Observation of an Unusual Upward-going Cosmic-ray-like Event in the Third Flight of ANITA". In: *Phys. Rev. Lett.* 121.16 (2018), p. 161102. DOI: 10.1103/PhysRevLett.121.161102. arXiv: 1803.05088 [astro-ph.HE].
- [362] A. Romero-Wolf et al. "Comprehensive analysis of anomalous ANITA events disfavors a diffuse tau-neutrino flux origin". In: *Phys. Rev. D* 99.6 (2019), p. 063011. DOI: 10.1103/PhysRevD.99.063011. arXiv: 1811.07261 [astro-ph.HE].
- [363] Ivan Esteban et al. "Looking at the axionic dark sector with ANITA". In: *Eur. Phys. J. C* 80.3 (2020), p. 259. DOI: 10.1140/epjc/s10052-020-7816-y. arXiv: 1905.10372 [hep-ph].

- [364] James M. Cline, Christian Gross, and Wei Xue. "Can the ANITA anomalous events be due to new physics?" In: *Phys. Rev. D* 100.1 (2019), p. 015031. DOI: 10.1103/PhysRevD. 100.015031. arXiv: 1904.13396 [hep-ph].
- [365] Lucien Heurtier, Yann Mambrini, and Mathias Pierre. "Dark matter interpretation of the ANITA anomalous events". In: *Phys. Rev. D* 99.9 (2019), p. 095014. DOI: 10.1103/PhysRevD.99.095014. arXiv: 1902.04584 [hep-ph].
- [366] Guo-yuan Huang. "Sterile neutrinos as a possible explanation for the upward air shower events at ANITA". In: *Phys. Rev. D* 98.4 (2018), p. 043019. DOI: 10.1103/PhysRevD.98. 043019. arXiv: 1804.05362 [hep-ph].
- [367] John F. Cherry and Ian M. Shoemaker. "Sterile neutrino origin for the upward directed cosmic ray showers detected by ANITA". In: *Phys. Rev. D* 99.6 (2019), p. 063016. DOI: 10.1103/PhysRevD.99.063016. arXiv: 1802.01611 [hep-ph].
- [368] Luis A. Anchordoqui and Ignatios Antoniadis. "Supersymmetric sphaleron configurations as the origin of the perplexing ANITA events". In: *Phys. Lett. B* 790 (2019), pp. 578–582. DOI: 10.1016/j.physletb.2019.02.003. arXiv: 1812.01520 [hep-ph].
- [369] Bhavesh Chauhan and Subhendra Mohanty. "Leptoquark solution for both the flavor and ANITA anomalies". In: *Phys. Rev. D* 99.9 (2019), p. 095018. DOI: 10.1103/PhysRevD. 99.095018. arXiv: 1812.00919 [hep-ph].
- [370] Jack H. Collins, P. S. Bhupal Dev, and Yicong Sui. "R-parity Violating Supersymmetric Explanation of the Anomalous Events at ANITA". In: *Phys. Rev. D* 99.4 (2019), p. 043009. DOI: 10.1103/PhysRevD.99.043009. arXiv: 1810.08479 [hep-ph].
- [371] Derek B. Fox et al. "The ANITA Anomalous Events as Signatures of a Beyond Standard Model Particle, and Supporting Observations from IceCube". In: (Sept. 2018). arXiv: 1809.09615 [astro-ph.HE].
- [372] P. W. Gorham et al. "Unusual Near-Horizon Cosmic-Ray-like Events Observed by ANITA-IV". In: *Phys. Rev. Lett.* 126.7 (2021), p. 071103. DOI: 10.1103/PhysRevLett.126.071103. arXiv: 2008.05690 [astro-ph.HE].
- [373] R. Prechelt et al. "Analysis of a tau neutrino origin for the near-horizon air shower events observed by the fourth flight of the Antarctic Impulsive Transient Antenna". In: *Phys. Rev. D* 105.4 (2022), p. 042001. DOI: 10.1103/PhysRevD.105.042001. arXiv: 2112.07069 [astro-ph.HE].
- [374] Peter B. Denton and Yves Kini. "Ultra-High-Energy Tau Neutrino Cross Sections with GRAND and POEMMA". In: *Phys. Rev. D* 102 (2020), p. 123019. DOI: 10.1103/PhysRevD. 102.123019. arXiv: 2007.10334 [astro-ph.HE].
- [375] Guo-yuan Huang et al. "Probing new physics at future tau neutrino telescopes". In: *JCAP* 02.02 (2022), p. 038. DOI: 10.1088/1475-7516/2022/02/038. arXiv: 2112.09476 [hep-ph].
- [376] Victor Branco Valera, Mauricio Bustamante, and Christian Glaser. "The ultra-high-energy neutrino-nucleon cross section: measurement forecasts for an era of cosmic EeV-neutrino discovery". In: *JHEP* 06 (2022), p. 105. DOI: 10.1007/JHEP06(2022) 105. arXiv: 2204. 04237 [hep-ph].
- [377] Dan Hooper et al. "Superheavy dark matter and ANITA's anomalous events". In: *Phys. Rev. D* 100.4 (2019), p. 043019. DOI: 10.1103/PhysRevD.100.043019. arXiv: 1904. 12865 [astro-ph.HE].
- [378] L. A. Anchordoqui et al. "The pros and cons of beyond standard model interpretations of ANITA events". In: *PoS* ICRC2019 (2020), p. 884. DOI: 10.22323/1.358.0884. arXiv: 1907.06308 [hep-ph].

- [379] Luis A. Anchordoqui et al. "Upgoing ANITA events as evidence of the CPT symmetric universe". In: *LHEP* 1.1 (2018), pp. 13–16. DOI: 10.31526/LHEP.1.2018.03. arXiv: 1803.11554 [hep-ph].
- [380] Emilian Dudas et al. "Gravitino decay in high scale supersymmetry with R-parity violation". In: *Phys. Rev. D* 98.1 (2018), p. 015030. DOI: 10.1103/PhysRevD.98.015030. arXiv: 1805.07342 [hep-ph].
- [381] Amy Connolly, Patrick Allison, and Oindree Banerjee. "On ANITA's sensitivity to long-lived, charged massive particles". In: (July 2018). arXiv: 1807.08892 [astro-ph.HE].
- [382] Shoshana Chipman et al. "Anomalous ANITA air shower events and tau decays". In: *Phys. Rev. D* 100.6 (2019), p. 063011. DOI: 10.1103/PhysRevD.100.063011. arXiv: 1906.11736 [astro-ph.HE].
- [383] Mohammad Abdullah et al. " $(g-2)_{\mu,e}$ and the ANITA anomalous events in a three-loop neutrino mass model". In: *Phys. Rev. D* 100.11 (2019), p. 115006. DOI: 10.1103/PhysRevD. 100.115006. arXiv: 1907.08109 [hep-ph].
- [384] Debasish Borah et al. "Connecting ANITA anomalous events to a nonthermal dark matter scenario". In: *Phys. Rev. D* 101.7 (2020), p. 075039. DOI: 10.1103/PhysRevD.101.075039. arXiv: 1907.02740 [hep-ph].
- [385] Arman Esmaili and Yasaman Farzan. "Explaining the ANITA events by a L_e-L_τ gauge model". In: *JCAP* 12 (2019), p. 017. DOI: 10 . 1088/1475-7516/2019/12/017. arXiv: 1909.07995 [hep-ph].
- [386] Lucien Heurtier et al. "Explaining the ANITA Anomaly with Inelastic Boosted Dark Matter". In: *Phys. Rev. D* 100.5 (2019), p. 055004. DOI: 10.1103/PhysRevD.100.055004. arXiv: 1905.13223 [hep-ph].
- [387] Wolfgang Altmannshofer et al. "Addressing $R_{D^{(*)}}$, $R_{K^{(*)}}$, muon g-2 and ANITA anomalies in a minimal R-parity violating supersymmetric framework". In: *Phys. Rev. D* 102.1 (2020), p. 015031. DOI: 10.1103/PhysRevD.102.015031. arXiv: 2002.12910 [hep-ph].
- [388] Xunyu Liang and Ariel Zhitnitsky. "ANITA anomalous events and axion quark nuggets". In: *Phys. Rev. D* 106.6 (2022), p. 063022. DOI: 10.1103/PhysRevD.106.063022. arXiv: 2105.01668 [hep-ph].
- [389] Stephanie Wissel et al. "Concept Study for the Beamforming Elevated Array for Cosmic Neutrinos (BEACON)". In: *PoS* ICRC2019 (2020), p. 1033. DOI: 10.22323/1.358.1033.
- [390] S. Prohira et al. "The Radar Echo Telescope for Cosmic Rays: Pathfinder experiment for a next-generation neutrino observatory". In: *Phys. Rev. D* 104.10 (2021), p. 102006. DOI: 10.1103/PhysRevD.104.102006. arXiv: 2104.00459 [astro-ph.IM].
- [391] Antonio Marinelli, Pasquale Migliozzi, and Andreino Simonelli. "Acoustic neutrino detection in a Adriatic multidisciplinary observatory (ANDIAMO)". In: *Astropart. Phys.* 143 (2022), p. 102760. DOI: 10.1016/j.astropartphys.2022.102760. arXiv: 2109.15199 [astro-ph.IM].
- [392] M. G. Aartsen et al. "Constraints on Ultrahigh-Energy Cosmic-Ray Sources from a Search for Neutrinos above 10 PeV with IceCube". In: *Phys. Rev. Lett.* 117.24 (2016). [Erratum: Phys.Rev.Lett. 119, 259902 (2017)], p. 241101. DOI: 10.1103/PhysRevLett.117.241101. arXiv: 1607.05886 [astro-ph.HE].
- [393] Alfonso Garcia Soto et al. "Probing quantum gravity with elastic interactions of ultrahighenergy neutrinos". In: *Phys. Rev. D* 107.3 (2023), p. 033009. DOI: 10.1103/PhysRevD.107.033009. arXiv: 2209.06282 [hep-ph].

- [394] Sergio Palomares-Ruiz, Aaron C. Vincent, and Olga Mena. "Spectral analysis of the high-energy IceCube neutrinos". In: *Phys. Rev. D* 91.10 (2015), p. 103008. DOI: 10.1103/PhysRevD.91.103008. arXiv: 1502.02649 [astro-ph.HE].
- [395] Ibrahim Safa et al. "Observing EeV neutrinos through Earth: GZK and the anomalous ANITA events". In: *JCAP* 01 (2020), p. 012. DOI: 10.1088/1475-7516/2020/01/012. arXiv: 1909.10487 [hep-ph].
- [396] M. G. Aartsen et al. "A search for IceCube events in the direction of ANITA neutrino candidates". In: (Jan. 2020). DOI: 10.3847/1538-4357/ab791d. arXiv: 2001.01737 [astro-ph.HE].
- [397] Carlos A. Argüelles et al. "PeV Tau Neutrinos to Unveil Ultra-High-Energy Sources". In: (Mar. 2022). arXiv: 2203.13827 [astro-ph.HE].
- [398] M. G. Aartsen et al. "Differential limit on the extremely-high-energy cosmic neutrino flux in the presence of astrophysical background from nine years of IceCube data". In: *Phys. Rev. D* 98.6 (2018), p. 062003. DOI: 10.1103/PhysRevD.98.062003. arXiv: 1807.01820 [astro-ph.HE].
- [399] P. W. Gorham et al. "Characteristics of Four Upward-pointing Cosmic-ray-like Events Observed with ANITA". In: *Phys. Rev. Lett.* 117.7 (2016), p. 071101. DOI: 10.1103/PhysRevLett. 117.071101. arXiv: 1603.05218 [astro-ph.HE].
- [400] Marco Cirelli et al. "PPPC 4 DM ID: A Poor Particle Physicist Cookbook for Dark Matter Indirect Detection". In: *JCAP* 03 (2011). [Erratum: JCAP 10, E01 (2012)], p. 051. DOI: 10. 1088/1475-7516/2012/10/E01. arXiv: 1012.4515 [hep-ph].
- [401] S. Alvi et al. "Do you smell something decaying? Updated linear constraints on decaying dark matter scenarios". In: *JCAP* 11 (2022), p. 015. DOI: 10.1088/1475-7516/2022/11/015. arXiv: 2205.05636 [astro-ph.CO].
- [402] Bob Holdom. "Two U(1)'s and Epsilon Charge Shifts". In: *Phys. Lett. B* 166 (1986), pp. 196–198. DOI: 10.1016/0370-2693(86)91377-8.
- [403] L. B. Okun. "Limits of electrodynamics: paraphotons?" In: *Sov. Phys. JETP* 56 (1982), p. 502.
- [404] Martina Mongillo et al. "Constraining Light Thermal Inelastic Dark Matter with NA64". In: (Feb. 2023). arXiv: 2302.05414 [hep-ph].
- [405] David Tucker-Smith and Neal Weiner. "Inelastic dark matter". In: *Phys. Rev. D* 64 (2001), p. 043502. doi: 10.1103/PhysRevD.64.043502. arXiv: hep-ph/0101138.
- [406] Gopolang Mohlabeng. "Revisiting the dark photon explanation of the muon anomalous magnetic moment". In: *Phys. Rev. D* 99.11 (2019), p. 115001. DOI: 10.1103/PhysRevD. 99.115001. arXiv: 1902.05075 [hep-ph].
- [407] Asli M. Abdullahi et al. "Semi-Visible Dark Photons below the Electroweak Scale". In: (Feb. 2023). arXiv: 2302.05410 [hep-ph].
- [408] Edward W. Kolb and Andrew J. Long. "Superheavy dark matter through Higgs portal operators". In: *Phys. Rev. D* 96.10 (2017), p. 103540. DOI: 10.1103/PhysRevD.96.103540. arXiv: 1708.04293 [astro-ph.CO].
- [409] Brian R. Greene, Tomislav Prokopec, and Thomas G. Roos. "Inflaton decay and heavy particle production with negative coupling". In: *Phys. Rev. D* 56 (1997), pp. 6484–6507. DOI: 10.1103/PhysRevD.56.6484. arXiv: hep-ph/9705357.
- [410] Daniel J. H. Chung, Edward W. Kolb, and Antonio Riotto. "Nonthermal supermassive dark matter". In: *Phys. Rev. Lett.* 81 (1998), pp. 4048–4051. DOI: 10.1103/PhysRevLett. 81.4048. arXiv: hep-ph/9805473.

- [411] Daniel J. H. Chung, Edward W. Kolb, and Antonio Riotto. "Production of massive particles during reheating". In: *Phys. Rev. D* 60 (1999), p. 063504. DOI: 10.1103/PhysRevD.60.063504. arXiv: hep-ph/9809453.
- [412] Kristjan Kannike, Antonio Racioppi, and Martti Raidal. "Super-heavy dark matter Towards predictive scenarios from inflation". In: *Nucl. Phys. B* 918 (2017), pp. 162–177. DOI: 10.1016/j.nuclphysb.2017.02.019. arXiv: 1605.09378 [hep-ph].
- [413] Fred Hoyle. "The Big Bang in Astronomy". In: New Scientist 92 (Dec. 1981), pp. 521–524.
- [414] Pedro G. Ferreira, William J. Wolf, and James Read. "The Spectre of Underdetermination in Modern Cosmology". In: (Jan. 2025). arXiv: 2501.06095 [physics.hist-ph].
- [415] Alexander Friedman. "Über die Krümmung des Raumes". In: *Z. Physik 10, 377-386* (1922). DOI: https://doi.org/10.1007/BF01332580.
- [416] Nils Schöneberg et al. "The H0 Olympics: A fair ranking of proposed models". In: *Phys. Rept.* 984 (2022), pp. 1–55. DOI: 10.1016/j.physrep.2022.07.001. arXiv: 2107.10291 [astro-ph.C0].
- [417] Jian-Ping Hu and Fa-Yin Wang. "Hubble Tension: The Evidence of New Physics". In: *Universe* 9.2 (2023), p. 94. DOI: 10.3390/universe9020094. arXiv: 2302.05709 [astro-ph.CO].
- [418] Dillon Brout et al. "The Pantheon+ Analysis: Cosmological Constraints". In: *Astrophys. J.* 938.2 (2022), p. 110. DOI: 10.3847/1538-4357/ac8e04. arXiv: 2202.04077 [astro-ph.CO].
- [419] M. Abdul Karim et al. "DESI DR2 Results II: Measurements of Baryon Acoustic Oscillations and Cosmological Constraints". In: (Mar. 2025). arXiv: 2503.14738 [astro-ph.C0].
- [420] K. Lodha et al. "Extended Dark Energy analysis using DESI DR2 BAO measurements". In: (Mar. 2025). arXiv: 2503.14743 [astro-ph.C0].
- [421] Daniel Naredo-Tuero et al. "Living at the Edge: A Critical Look at the Cosmological Neutrino Mass Bound". In: (July 2024). arXiv: 2407.13831 [astro-ph.CO].
- [422] Daniel Green and Joel Meyers. "The Cosmological Preference for Negative Neutrino Mass". In: (July 2024). arXiv: 2407.07878 [astro-ph.CO].
- [423] Marco Cirelli, Alessandro Strumia, and Jure Zupan. "Dark Matter". In: (June 2024). arXiv: 2406.01705 [hep-ph].
- [424] Julien Lesgourgues et al. *Neutrino Cosmology*. Cambridge University Press, Feb. 2013. ISBN: 978-1-108-70501-1, 978-1-139-60341-6.
- [425] Chung-Pei Ma and Edmund Bertschinger. "Cosmological perturbation theory in the synchronous and conformal Newtonian gauges". In: *Astrophys. J.* 455 (1995), pp. 7–25. DOI: 10.1086/176550. arXiv: astro-ph/9506072.
- [426] Scott Dodelson and Fabian Schmidt. *Modern Cosmology, 2nd Edition.* Academic Press, Apr. 2020. ISBN: 9780128159484, 9780128159491.
- [427] Viatcheslav Mukhanov. *Physical Foundations of Cosmology*. Cambridge University Press, 2005.
- [428] Emory F. Bunn and David W. Hogg. "The Kinematic origin of the cosmological redshift". In: *Am. J. Phys.* 77 (2009), pp. 688–694. DOI: 10.1119/1.3129103. arXiv: 0808.1081 [physics.pop-ph].
- [429] D. J. Fixsen. "The Temperature of the Cosmic Microwave Background". In: *Astrophys. J.* 707 (2009), pp. 916–920. DOI: 10.1088/0004-637X/707/2/916. arXiv: 0911.1955 [astro-ph.CO].
- [430] Wayne Hu, Naoshi Sugiyama, and Joseph Silk. "The Physics of microwave background anisotropies". In: *Nature* 386 (1997), pp. 37–43. DOI: 10.1038/386037a0. arXiv: astro-ph/9604166.

- [431] R. K. Sachs and A. M. Wolfe. "Perturbations of a cosmological model and angular variations of the microwave background". In: *Astrophys. J.* 147 (1967), pp. 73–90. DOI: 10. 1007/s10714-007-0448-9.
- [432] Antony Lewis and Anthony Challinor. "Weak gravitational lensing of the CMB". In: *Phys. Rept.* 429 (2006), pp. 1–65. DOI: 10.1016/j.physrep.2006.03.002. arXiv: astro-ph/0601594.
- [433] James M. Bardeen. "Gauge-invariant cosmological perturbations". In: *Phys. Rev. D* 22 (8 Oct. 1980), pp. 1882–1905. DOI: 10.1103/PhysRevD.22.1882. URL: https://link.aps.org/doi/10.1103/PhysRevD.22.1882.
- [434] Hideo Kodama and Misao Sasaki. "Cosmological Perturbation Theory". In: *Prog. Theor. Phys. Suppl.* 78 (1984), pp. 1–166. DOI: 10.1143/PTPS.78.1.
- [435] Cyril Pitrou et al. "Precision Big Bang Nucleosynthesis with Improved Helium-4 Predictions". In: *Phys. Rept.* 754 (2018), pp. 1–66. DOI: 10.1016/j.physrep.2018.04.005.
- [436] Erik Aver et al. "Improving helium abundance determinations with Leo P as a case study". In: *JCAP* 03 (2021), p. 027. DOI: 10.1088/1475-7516/2021/03/027. arXiv: 2010.04180 [astro-ph.CO].
- [437] Mabel Valerdi et al. "Determination of the Primordial Helium Abundance Based on NGC 346, an H ii Region of the Small Magellanic Cloud". In: *Astrophys. J.* 876.2 (2019), p. 98. DOI: 10.3847/1538-4357/ab14e4. arXiv: 1904.01594 [astro-ph.GA].
- [438] Vital Fernández et al. "A Bayesian direct method implementation to fit emission line spectra: Application to the primordial He abundance determination". In: *Mon. Not. Roy. Astron. Soc.* 487.3 (2019), pp. 3221–3238. DOI: 10.1093/mnras/stz1433. arXiv: 1905. 09215 [astro-ph.GA].
- [439] O. A. Kurichin et al. "A new determination of the primordial helium abundance using the analyses of H II region spectra from SDSS". In: *Mon. Not. Roy. Astron. Soc.* 502.2 (2021), pp. 3045–3056. DOI: 10.1093/mnras/stab215. arXiv: 2101.09127 [astro-ph.CO].
- [440] Tiffany Hsyu et al. "The PHLEK Survey: A New Determination of the Primordial Helium Abundance". In: ApJ 896.1, 77 (June 2020), p. 77. doi: 10.3847/1538-4357/ab91af. arXiv: 2005.12290 [astro-ph.GA].
- [441] Ryan Cooke et al. "Precision measures of the primordial abundance of deuterium". In: *Astrophys. J.* 781.1 (2014), p. 31. DOI: 10.1088/0004-637X/781/1/31. arXiv: 1308.3240 [astro-ph.CO].
- [442] Ryan J. Cooke et al. "The primordial deuterium abundance of the most metal-poor damped Ly α system". In: *Astrophys. J.* 830.2 (2016), p. 148. DOI: 10.3847/0004-637X/830/2/148. arXiv: 1607.03900 [astro-ph.CO].
- [443] S. A. Balashev et al. "The primordial deuterium abundance: subDLA system at $z_{\rm abs}=2.437$ towards the QSO J 1444+2919". In: *Mon. Not. Roy. Astron. Soc.* 458.2 (2016), pp. 2188–2198. DOI: 10.1093/mnras/stw356. arXiv: 1511.01797 [astro-ph.GA].
- [444] S. Riemer-Sørensen et al. "A precise deuterium abundance: remeasurement of the z = 3.572 absorption system towards the quasar PKS1937-101". In: *Mon. Not. Roy. Astron. Soc.* 468.3 (2017), pp. 3239-3250. DOI: 10.1093/mnras/stx681. arXiv: 1703.06656 [astro-ph.CO].
- [445] Dana S. Balser and T. M. Bania. "Green Bank Telescope Observations of ³He⁺: H II Regions". In: AJ 156.6, 280 (Dec. 2018), p. 280. DOI: 10.3847/1538-3881/aaeb2b. arXiv: 1810.09422 [astro-ph.GA].

- [446] T. M. Bania, Robert T. Rood, and Dana S. Balser. "The cosmological density of baryons from observations of ³He⁺ in the Milky Way". In: Nature 415.6867 (Jan. 2002), pp. 54–57. DOI: 10.1038/415054a.
- [447] Wako Aoki et al. "Lithium Abundances of Extremely Metal-Poor Turnoff Stars". In: ApJ 698.2 (June 2009), pp. 1803-1812. DOI: 10.1088/0004-637X/698/2/1803. arXiv: 0904.1448 [astro-ph.SR].
- [448] L. Sbordone et al. "The metal-poor end of the Spite plateau. I. Stellar parameters, metallicities, and lithium abundances". In: A&A 522, A26 (Nov. 2010), A26. DOI: 10.1051/0004-6361/200913282. arXiv: 1003.4510 [astro-ph.GA].
- [449] Henrique Reggiani et al. "Constraining cosmic scatter in the Galactic halo through a differential analysis of metal-poor stars". In: A&A 608, A46 (Dec. 2017), A46. DOI: 10. 1051/0004-6361/201730750. arXiv: 1709.03750 [astro-ph.SR].
- [450] Brian D. Fields. "The primordial lithium problem". In: *Ann. Rev. Nucl. Part. Sci.* 61 (2011), pp. 47–68. DOI: 10.1146/annurev-nucl-102010-130445. arXiv: 1203.3551 [astro-ph.CO].
- [451] Scott Dodelson and Michael S. Turner. "Nonequilibrium neutrino statistical mechanics in the expanding universe". In: *Phys. Rev. D* 46 (1992), pp. 3372–3387. DOI: 10.1103/PhysRevD.46.3372.
- [452] Mattia Cielo et al. "Neff in the Standard Model at NLO is 3.043". In: *Phys. Rev. D* 108.12 (2023), p. L121301. DOI: 10.1103/PhysRevD.108.L121301. arXiv: 2306.05460 [hep-ph].
- [453] Marco Drewes et al. "Towards a precision calculation of $N_{\rm eff}$ in the Standard Model IV: Impact of positronium formation". In: (Nov. 2024). arXiv: 2411.14091 [hep-ph].
- [454] Brian D. Fields et al. "Big-Bang Nucleosynthesis after Planck". In: *JCAP* 03 (2020). [Erratum: JCAP 11, E02 (2020)], p. 010. DOI: 10.1088/1475-7516/2020/03/010. arXiv: 1912.01132 [astro-ph.CO].
- [455] Jun-Qian Jiang et al. "Neutrino cosmology after DESI: tightest mass upper limits, preference for the normal ordering, and tension with terrestrial observations". In: (July 2024). arXiv: 2407.18047 [astro-ph.CO].
- [456] Deng Wang et al. "Updating neutrino mass constraints with Background measurements". In: (May 2024). arXiv: 2405.03368 [astro-ph.CO].
- [457] Shouvik Roy Choudhury and Teppei Okumura. "Updated Cosmological Constraints in Extended Parameter Space with Planck PR4, DESI Baryon Acoustic Oscillations, and Supernovae: Dynamical Dark Energy, Neutrino Masses, Lensing Anomaly, and the Hubble Tension". In: *Astrophys. J. Lett.* 976.1 (2024), p. L11. DOI: 10.3847/2041-8213/ad8c26. arXiv: 2409.13022 [astro-ph.CO].
- [458] Steen Hannestad. "Neutrino masses and the dark energy equation of state Relaxing the cosmological neutrino mass bound". In: *Phys. Rev. Lett.* 95 (2005), p. 221301. DOI: 10. 1103/PhysRevLett.95.221301. arXiv: astro-ph/0505551.
- [459] Weiqiang Yang et al. "Emergent Dark Energy, neutrinos and cosmological tensions". In: *Phys. Dark Univ.* 31 (2021), p. 100762. DOI: 10.1016/j.dark.2020.100762. arXiv: 2007.02927 [astro-ph.CO].
- [460] Sunny Vagnozzi et al. "Constraints on the sum of the neutrino masses in dynamical dark energy models with $w(z) \ge -1$ are tighter than those obtained in Λ CDM". In: *Phys. Rev. D* 98.8 (2018), p. 083501. DOI: 10 . 1103 / PhysRevD . 98 . 083501. arXiv: 1801 . 08553 [astro-ph.CO].
- [461] Shouvik Roy Choudhury and Abhishek Naskar. "Strong Bounds on Sum of Neutrino Masses in a 12 Parameter Extended Scenario with Non-Phantom Dynamical Dark En-

- ergy $(w(z) \ge -1)$ with CPL parameterization". In: *Eur. Phys. J. C* 79.3 (2019), p. 262. DOI: 10.1140/epjc/s10052-019-6762-z. arXiv: 1807.02860 [astro-ph.CO].
- [462] Eleonora di Valentino, Stefano Gariazzo, and Olga Mena. "Model marginalized constraints on neutrino properties from cosmology". In: *Phys. Rev. D* 106.4 (2022), p. 043540. DOI: 10.1103/PhysRevD.106.043540. arXiv: 2207.05167 [astro-ph.CO].
- [463] Ming-Ming Zhao et al. "Constraining neutrino mass and extra relativistic degrees of freedom in dynamical dark energy models using Planck 2015 data in combination with low-redshift cosmological probes: basic extensions to ΛCDM cosmology". In: *Mon. Not. Roy. Astron. Soc.* 469.2 (2017), pp. 1713–1724. DOI: 10.1093/mnras/stx978. arXiv: 1608. 01219 [astro-ph.CO].
- [464] Xin Zhang. "Impacts of dark energy on weighing neutrinos after Planck 2015". In: *Phys. Rev. D* 93.8 (2016), p. 083011. DOI: 10.1103/PhysRevD.93.083011. arXiv: 1511.02651 [astro-ph.CO].
- [465] Rui-Yun Guo, Jing-Fei Zhang, and Xin Zhang. "Exploring neutrino mass and mass hierarchy in the scenario of vacuum energy interacting with cold dark matte". In: *Chin. Phys. C* 42.9 (2018), p. 095103. DOI: 10.1088/1674-1137/42/9/095103. arXiv: 1803.06910 [astro-ph.CO].
- [466] Shouvik Roy Choudhury and Steen Hannestad. "Updated results on neutrino mass and mass hierarchy from cosmology with Planck 2018 likelihoods". In: *JCAP* 07 (2020), p. 037. DOI: 10.1088/1475-7516/2020/07/037. arXiv: 1907.12598 [astro-ph.CO].
- [467] Hong Li and Xin Zhang. "Constraining dynamical dark energy with a divergence-free parametrization in the presence of spatial curvature and massive neutrinos". In: *Phys. Lett. B* 713 (2012), pp. 160–164. DOI: 10.1016/j.physletb.2012.06.030. arXiv: 1202.4071 [astro-ph.CO].
- [468] Yun-He Li et al. "Holographic dark energy in a Universe with spatial curvature and massive neutrinos: a full Markov Chain Monte Carlo exploration". In: *JCAP* 02 (2013), p. 033. DOI: 10.1088/1475-7516/2013/02/033. arXiv: 1207.6679 [astro-ph.CO].
- [469] Jing-Fei Zhang, Yun-He Li, and Xin Zhang. "Cosmological constraints on neutrinos after BICEP2". In: Eur. Phys. J. C 74 (2014), p. 2954. DOI: 10.1140/epjc/s10052-014-2954-8. arXiv: 1404.3598 [astro-ph.CO].
- [470] Jing-Fei Zhang et al. "Neutrinos in the holographic dark energy model: constraints from latest measurements of expansion history and growth of structure". In: *JCAP* 04 (2015), p. 038. DOI: 10.1088/1475-7516/2015/04/038. arXiv: 1502.04028 [astro-ph.CO].
- [471] Chao-Qiang Geng et al. "Observational constraints on varying neutrino-mass cosmology". In: *JCAP* 01 (2016), p. 049. DOI: 10.1088/1475-7516/2016/01/049. arXiv: 1504.08141 [astro-ph.CO].
- [472] Yun Chen and Lixin Xu. "Galaxy clustering, CMB and supernova data constraints on ϕ CDM model with massive neutrinos". In: *Phys. Lett. B* 752 (2016), pp. 66–75. DOI: 10. 1016/j.physletb.2015.11.022. arXiv: 1507.02008 [astro-ph.CO].
- [473] Arthur Loureiro et al. "On The Upper Bound of Neutrino Masses from Combined Cosmological Observations and Particle Physics Experiments". In: *Phys. Rev. Lett.* 123.8 (2019), p. 081301. DOI: 10.1103/PhysRevLett.123.081301. arXiv: 1811.02578 [astro-ph.CO].
- [474] Sai Wang et al. "Impacts of dark energy on weighing neutrinos: mass hierarchies considered". In: *Phys. Rev. D* 94.8 (2016), p. 083519. DOI: 10.1103/PhysRevD.94.083519. arXiv: 1608.00672 [astro-ph.CO].

- [475] Weiqiang Yang et al. "Effects of neutrino mass hierarchies on dynamical dark energy models". In: *Phys. Rev. D* 95.10 (2017), p. 103522. DOI: 10.1103/PhysRevD.95.103522. arXiv: 1703.02556 [astro-ph.CO].
- [476] Qing-Guo Huang, Ke Wang, and Sai Wang. "Constraints on the neutrino mass and mass hierarchy from cosmological observations". In: *Eur. Phys. J. C* 76.9 (2016), p. 489. DOI: 10.1140/epjc/s10052-016-4334-z. arXiv: 1512.05899 [astro-ph.CO].
- [477] Ravi Kumar Sharma, Kanhaiya Lal Pandey, and Subinoy Das. "Implications of an Extended Dark Energy Model with Massive Neutrinos". In: *Astrophys. J.* 934.2 (2022), p. 113. DOI: 10.3847/1538-4357/ac7a33. arXiv: 2202.01749 [astro-ph.CO].
- [478] Ming Zhang, Jing-Fei Zhang, and Xin Zhang. "Impacts of dark energy on constraining neutrino mass after Planck 2018". In: *Commun. Theor. Phys.* 72.12 (2020), p. 125402. DOI: 10.1088/1572-9494/abbb84. arXiv: 2005.04647 [astro-ph.C0].
- [479] Ali Rida Khalifeh and Raul Jimenez. "Distinguishing Dark Energy models with neutrino oscillations". In: *Phys. Dark Univ.* 34 (2021), p. 100897. DOI: 10.1016/j.dark.2021. 100897. arXiv: 2105.07973 [astro-ph.CO].
- [480] Yun Chen et al. "Constraints on non-flat cosmologies with massive neutrinos after Planck 2015". In: *Astrophys. J.* 829.2 (2016), p. 61. DOI: 10.3847/0004-637X/829/2/61. arXiv: 1603.07115 [astro-ph.CO].
- [481] Elena Giusarma, Roland De Putter, and Olga Mena. "Testing standard and nonstandard neutrino physics with cosmological data". In: *Phys. Rev. D* 87.4 (2013), p. 043515. DOI: 10.1103/PhysRevD.87.043515. arXiv: 1211.2154 [astro-ph.CO].
- [482] Ian G. Mccarthy et al. "The BAHAMAS project: the CMB-large-scale structure tension and the roles of massive neutrinos and galaxy formation". In: *Mon. Not. Roy. Astron. Soc.* 476.3 (2018), pp. 2999-3030. DOI: 10.1093/mnras/sty377. arXiv: 1712.02411 [astro-ph.CO].
- [483] Kevork N. Abazajian and Alexander Kusenko. "Hidden treasures: Sterile neutrinos as dark matter with miraculous abundance, structure formation for different production mechanisms, and a solution to the σ_8 problem". In: *Phys. Rev. D* 100.10 (2019), p. 103513. DOI: 10.1103/PhysRevD.100.103513. arXiv: 1907.11696 [hep-ph].
- [484] Elcio Abdalla et al. "Cosmology intertwined: A review of the particle physics, astrophysics, and cosmology associated with the cosmological tensions and anomalies". In: *JHEAp* 34 (2022), pp. 49–211. DOI: 10.1016/j.jheap.2022.04.002. arXiv: 2203.06142 [astro-ph.CO].
- [485] Eleonora Di Valentino et al. "In the realm of the Hubble tension—a review of solutions". In: *Class. Quant. Grav.* 38.15 (2021), p. 153001. DOI: 10.1088/1361-6382/ac086d. arXiv: 2103.01183 [astro-ph.CO].
- [486] L. Verde, T. Treu, and A. G. Riess. "Tensions between the Early and the Late Universe". In: *Nature Astron.* 3 (2019), p. 891. DOI: 10.1038/s41550-019-0902-0. arXiv: 1907.10625 [astro-ph.CO].
- [487] Licia Verde, Nils Schöneberg, and Héctor Gil-Marín. "A tale of many H_0 ". In: (Nov. 2023). arXiv: 2311.13305 [astro-ph.CO].
- [488] Eleonora Di Valentino et al. "Cosmology Intertwined III: $f\sigma_8$ and S_8 ". In: Astropart. Phys. 131 (2021), p. 102604. DOI: 10.1016/j.astropartphys.2021.102604. arXiv: 2008. 11285 [astro-ph.CO].
- [489] Shouvik Roy Choudhury and Sandhya Choubey. "Updated Bounds on Sum of Neutrino Masses in Various Cosmological Scenarios". In: *JCAP* 09 (2018), p. 017. DOI: 10.1088/1475-7516/2018/09/017. arXiv: 1806.10832 [astro-ph.CO].

- [490] Eleonora Di Valentino and Alessandro Melchiorri. "Neutrino Mass Bounds in the Era of Tension Cosmology". In: *Astrophys. J. Lett.* 931.2 (2022), p. L18. DOI: 10.3847/2041-8213/ac6ef5. arXiv: 2112.02993 [astro-ph.C0].
- [491] William Giarè, Olga Mena, and Eleonora Di Valentino. "Lensing impact on cosmic relics and tensions". In: *Phys. Rev. D* 108.10 (2023), p. 103539. DOI: 10.1103/PhysRevD.108. 103539. arXiv: 2307.14204 [astro-ph.CO].
- [492] Nathaniel Craig et al. "No vs is Good News". In: (May 2024). arXiv: 2405.00836 [astro-ph.CO].
- [493] Marilena Loverde and Zachary J. Weiner. "Massive neutrinos and cosmic composition". In: (Sept. 2024). arXiv: 2410.00090 [astro-ph.CO].
- [494] Itamar J. Allali and Alessio Notari. "Neutrino mass bounds from DESI 2024 are relaxed by Planck PR4 and cosmological supernovae". In: (June 2024). arXiv: 2406.14554 [astro-ph.CO].
- [495] Pavel Motloch and Wayne Hu. "Tensions between direct measurements of the lens power spectrum from Planck data". In: *Phys. Rev. D* 97.10 (2018), p. 103536. DOI: 10.1103/PhysRevD.97.103536. arXiv: 1803.11526 [astro-ph.CO].
- [496] M. Tristram et al. "Cosmological parameters derived from the final Planck data release (PR4)". In: Astron. Astrophys. 682 (2024), A37. DOI: 10.1051/0004-6361/202348015. arXiv: 2309.10034 [astro-ph.CO].
- [497] Erik Rosenberg, Steven Gratton, and George Efstathiou. "CMB power spectra and cosmological parameters from Planck PR4 with CamSpec". In: *Mon. Not. Roy. Astron. Soc.* 517.3 (2022), pp. 4620–4636. DOI: 10.1093/mnras/stac2744. arXiv: 2205.10869 [astro-ph.CO].
- [498] Ivan Esteban and Jordi Salvado. "Long Range Interactions in Cosmology: Implications for Neutrinos". In: *JCAP* 05 (2021), p. 036. DOI: 10.1088/1475-7516/2021/05/036. arXiv: 2101.05804 [hep-ph].
- [499] Ivan Esteban, Olga Mena, and Jordi Salvado. "Nonstandard neutrino cosmology dilutes the lensing anomaly". In: *Phys. Rev. D* 106.8 (2022), p. 083516. DOI: 10.1103/PhysRevD. 106.083516. arXiv: 2202.04656 [astro-ph.CO].
- [500] Christina D. Kreisch, Francis-Yan Cyr-Racine, and Olivier Doré. "Neutrino puzzle: Anomalies, interactions, and cosmological tensions". In: *Phys. Rev. D* 101.12 (2020), p. 123505. DOI: 10.1103/PhysRevD.101.123505. arXiv: 1902.00534 [astro-ph.CO].
- [501] Massimiliano Lattanzi and Martina Gerbino. "Status of neutrino properties and future prospects Cosmological and astrophysical constraints". In: *Front. in Phys.* 5 (2018), p. 70. DOI: 10.3389/fphy.2017.00070. arXiv: 1712.07109 [astro-ph.CO].
- [502] Zackaria Chacko et al. "Cosmological Limits on the Neutrino Mass and Lifetime". In: *JHEP* 04 (2020), p. 020. DOI: 10.1007/JHEP04 (2020) 020. arXiv: 1909.05275 [hep-ph].
- [503] Zackaria Chacko et al. "Determining the Neutrino Lifetime from Cosmology". In: *Phys. Rev. D* 103.4 (2021), p. 043519. DOI: 10.1103/PhysRevD.103.043519. arXiv: 2002.08401 [astro-ph.CO].
- [504] Miguel Escudero et al. "Relaxing Cosmological Neutrino Mass Bounds with Unstable Neutrinos". In: JHEP 12 (2020), p. 119. DOI: 10.1007/JHEP12(2020)119. arXiv: 2007. 04994 [hep-ph].
- [505] Guillermo Franco Abellán et al. "Improved cosmological constraints on the neutrino mass and lifetime". In: *JHEP* 08 (2022), p. 076. DOI: 10.1007/JHEP08(2022)076. arXiv: 2112.13862 [hep-ph].
- [506] Nicola Bellomo et al. "Hiding neutrino mass in modified gravity cosmologies". In: *JCAP* 02 (2017), p. 043. DOI: 10 . 1088 / 1475 7516 / 2017 / 02 / 043. arXiv: 1612 . 02598 [astro-ph.CO].

- [507] Gia Dvali and Lena Funcke. "Small neutrino masses from gravitational θ -term". In: *Phys. Rev. D* 93.11 (2016), p. 113002. DOI: 10.1103/PhysRevD.93.113002. arXiv: 1602.03191 [hep-ph].
- [508] Christiane S. Lorenz et al. "Time-varying neutrino mass from a supercooled phase transition: current cosmological constraints and impact on the Ω_m - σ_8 plane". In: *Phys. Rev.* D 99.2 (2019), p. 023501. DOI: 10.1103/PhysRevD.99.023501. arXiv: 1811.01991 [astro-ph.CO].
- [509] Gia Dvali, Lena Funcke, and Tanmay Vachaspati. "Time- and Space-Varying Neutrino Mass Matrix from Soft Topological Defects". In: *Phys. Rev. Lett.* 130.9 (2023), p. 091601. DOI: 10.1103/PhysRevLett.130.091601. arXiv: 2112.02107 [hep-ph].
- [510] Christiane S. Lorenz et al. "Reconstruction of the neutrino mass as a function of redshift". In: *Phys. Rev. D* 104.12 (2021), p. 123518. DOI: 10.1103/PhysRevD.104.123518. arXiv: 2102.13618 [astro-ph.CO].
- [511] Miguel Escudero, Thomas Schwetz, and Jorge Terol-Calvo. "A seesaw model for large neutrino masses in concordance with cosmology". In: *JHEP* 02 (2023). [Addendum: JHEP 06, 119 (2024)], p. 142. DOI: 10.1007/JHEP02 (2023) 142. arXiv: 2211.01729 [hep-ph].
- [512] Manibrata Sen and Alexei Y. Smirnov. "Refractive neutrino masses, ultralight dark matter and cosmology". In: *JCAP* 01 (2024), p. 040. DOI: 10.1088/1475-7516/2024/01/040. arXiv: 2306.15718 [hep-ph].
- [513] Yasaman Farzan and Steen Hannestad. "Neutrinos secretly converting to lighter particles to please both KATRIN and the cosmos". In: *JCAP* 02 (2016), p. 058. DOI: 10.1088/1475-7516/2016/02/058. arXiv: 1510.02201 [hep-ph].
- [514] James Alvey et al. "Cosmic neutrino background detection in large-neutrino-mass cosmologies". In: *Phys. Rev. D* 105.6 (2022), p. 063501. DOI: 10 . 1103 / PhysRevD . 105 . 063501. arXiv: 2111.14870 [hep-ph].
- [515] Isabel M. Oldengott et al. "How to relax the cosmological neutrino mass bound". In: *JCAP* 04 (2019), p. 049. DOI: 10.1088/1475-7516/2019/04/049. arXiv: 1901.04352 [astro-ph.CO].
- [516] James Alvey, Miguel Escudero, and Nashwan Sabti. "What can CMB observations tell us about the neutrino distribution function?" In: *JCAP* 02.02 (2022), p. 037. DOI: 10.1088/1475-7516/2022/02/037. arXiv: 2111.12726 [astro-ph.CO].
- [517] Alessandro Cuoco et al. "Do observations prove that cosmological neutrinos are thermally distributed?" In: *Phys. Rev. D* 71 (2005), p. 123501. DOI: 10.1103/PhysRevD.71. 123501. arXiv: astro-ph/0502465.
- [518] Itamar J. Allali, Daniel Aloni, and Nils Schöneberg. "Cosmological probes of Dark Radiation from Neutrino Mixing". In: *JCAP* 09 (2024), p. 019. DOI: 10.1088/1475-7516/2024/09/019. arXiv: 2404.16822 [astro-ph.CO].
- [519] Cristina Benso, Thomas Schwetz, and Drona Vatsyayan. "Large neutrino mass in cosmology and keV sterile neutrino dark matter from a dark sector". In: (Oct. 2024). arXiv: 2410.23926 [hep-ph].
- [520] Wayne T. Hu. "Wandering in the Background: A CMB Explorer". PhD thesis. University of California at Berkeley, Aug. 1995. arXiv: astro-ph/9508126.
- [521] Benjamin Audren et al. "Robustness of cosmic neutrino background detection in the cosmic microwave background". In: *JCAP* 03 (2015), p. 036. DOI: 10.1088/1475-7516/2015/03/036. arXiv: 1412.5948 [astro-ph.CO].

- [522] Julien Lesgourgues and Sergio Pastor. "Neutrino cosmology and Planck". In: New J. Phys. 16 (2014), p. 065002. DOI: 10.1088/1367-2630/16/6/065002. arXiv: 1404.1740 [hep-ph].
- [523] Wayne Hu. "Crossing the phantom divide: Dark energy internal degrees of freedom". In: *Phys. Rev. D* 71 (2005), p. 047301. DOI: 10.1103/PhysRevD.71.047301. arXiv: astro-ph/0410680.
- [524] Jaume Garriga and Viatcheslav F. Mukhanov. "Perturbations in k-inflation". In: *Phys. Lett. B* 458 (1999), pp. 219–225. DOI: 10.1016/S0370-2693(99)00602-4. arXiv: hep-th/9904176.
- [525] Wayne Hu. "Structure formation with generalized dark matter". In: *Astrophys. J.* 506 (1998), pp. 485–494. DOI: 10.1086/306274. arXiv: astro-ph/9801234.
- [526] Caio Nascimento. "Accurate fluid approximation for massive neutrinos in cosmology". In: *Phys. Rev. D* 108.2 (2023), p. 023505. DOI: 10.1103/PhysRevD.108.023505. arXiv: 2303.09580 [astro-ph.CO].
- [527] Julien Lesgourgues and Thomas Tram. "The Cosmic Linear Anisotropy Solving System (CLASS) IV: efficient implementation of non-cold relics". In: *JCAP* 09 (2011), p. 032. DOI: 10.1088/1475-7516/2011/09/032. arXiv: 1104.2935 [astro-ph.CO].
- [528] Masatoshi Shoji and Eiichiro Komatsu. "Massive Neutrinos in Cosmology: Analytic Solutions and Fluid Approximation". In: *Phys. Rev. D* 81 (2010). [Erratum: Phys.Rev.D 82, 089901 (2010)], p. 123516. DOI: 10.1103/PhysRevD.81.123516. arXiv: 1003.0942 [astro-ph.CO].
- [529] Julien Lesgourgues. "The Cosmic Linear Anisotropy Solving System (CLASS) I: Overview". In: (Apr. 2011). arXiv: 1104.2932 [astro-ph.IM].
- [530] Diego Blas, Julien Lesgourgues, and Thomas Tram. "The Cosmic Linear Anisotropy Solving System (CLASS) II: Approximation schemes". In: *JCAP* 07 (2011), p. 034. DOI: 10. 1088/1475-7516/2011/07/034. arXiv: 1104.2933 [astro-ph.CO].
- [531] Julien Lesgourgues. "The Cosmic Linear Anisotropy Solving System (CLASS) III: Comparision with CAMB for LambdaCDM". In: (Apr. 2011). arXiv: 1104.2934 [astro-ph.CO].
- [532] Jesus Torrado and Antony Lewis. "Cobaya: Code for Bayesian Analysis of hierarchical physical models". In: *JCAP* 05 (2021), p. 057. DOI: 10.1088/1475-7516/2021/05/057. arXiv: 2005.05290 [astro-ph.IM].
- [533] Jesús Torrado and Antony Lewis. *Cobaya: Bayesian analysis in cosmology.* Astrophysics Source Code Library, record ascl:1910.019. Oct. 2019.
- [534] Antony Lewis. "Efficient sampling of fast and slow cosmological parameters". In: *Phys. Rev. D* 87.10 (2013), p. 103529. DOI: 10.1103/PhysRevD.87.103529. arXiv: 1304.4473 [astro-ph.CO].
- [535] Andrew Gelman and Donald B. Rubin. "Inference from Iterative Simulation Using Multiple Sequences". In: *Statistical Science* 7.4 (1992), pp. 457–472. DOI: 10.1214/ss/1177011136. URL: https://doi.org/10.1214/ss/1177011136.
- [536] Pavel Motloch and Wayne Hu. "Lensinglike tensions in the *Planck* legacy release". In: *Phys. Rev. D* 101.8 (2020), p. 083515. DOI: 10.1103/PhysRevD.101.083515. arXiv: 1912.06601 [astro-ph.CO].
- [537] George Efstathiou and Steven Gratton. "A Detailed Description of the CamSpec Likelihood Pipeline and a Reanalysis of the Planck High Frequency Maps". In: (Oct. 2019). DOI: 10.21105/astro.1910.00483. arXiv: 1910.00483 [astro-ph.CO].
- [538] F. Ge et al. "Cosmology From CMB Lensing and Delensed EE Power Spectra Using 2019-2020 SPT-3G Polarization Data". In: (Nov. 2024). arXiv: 2411.06000 [astro-ph.CO].

- [539] T. Bertólez-Martínez et al. In: (2024). To appear (2024).
- [540] B. A. Benson et al. "SPT-3G: A Next-Generation Cosmic Microwave Background Polarization Experiment on the South Pole Telescope". In: *Proc. SPIE Int. Soc. Opt. Eng.* 9153 (2014), 91531P. DOI: 10.1117/12.2057305. arXiv: 1407.2973 [astro-ph.IM].
- [541] A. I. Lonappan et al. "LiteBIRD science goals and forecasts: a full-sky measurement of gravitational lensing of the CMB". In: JCAP 06 (2024), p. 009. DOI: 10.1088/1475-7516/2024/06/009. arXiv: 2312.05184 [astro-ph.CO].
- [542] Ciaran A. J. O'Hare. "Cosmology of axion dark matter". In: *PoS* COSMICWISPers (2024), p. 040. DOI: 10.22323/1.454.0040. arXiv: 2403.17697 [hep-ph].
- [543] Giorgio Arcadi et al. "The Waning of the WIMP: Endgame?" In: (Mar. 2024). arXiv: 2403. 15860 [hep-ph].
- [544] Marco Fabbrichesi, Emidio Gabrielli, and Gaia Lanfranchi. "The Dark Photon". In: (May 2020). DOI: 10.1007/978-3-030-62519-1. arXiv: 2005.01515 [hep-ph].
- [545] Peter Svrcek and Edward Witten. "Axions In String Theory". In: *JHEP* 06 (2006), p. 051. DOI: 10.1088/1126-6708/2006/051. arXiv: hep-th/0605206.
- [546] Michael B. Green, J. H. Schwarz, and Edward Witten. *Superstring theory. Vol. 2: loop amplitudes, anomalies and phenomenology.* July 1988. ISBN: 978-0-521-35753-1.
- [547] Asimina Arvanitaki et al. "String Axiverse". In: *Phys. Rev. D* 81 (2010), p. 123530. DOI: 10.1103/PhysRevD.81.123530. arXiv: 0905.4720 [hep-th].
- [548] Michael Dine. *Supersymmetry and String Theory: Beyond the Standard Model.* Oxford University Press, 2016. ISBN: 978-1-107-04838-6, 978-1-316-40530-7, 978-1-009-29088-3, 978-1-009-29092-0, 978-1-009-29089-0. DOI: 10.1017/9781009290883.
- [549] James Halverson, Cody Long, and Pran Nath. "Ultralight axion in supersymmetry and strings and cosmology at small scales". In: *Phys. Rev. D* 96.5 (2017), p. 056025. DOI: 10. 1103/PhysRevD.96.056025. arXiv: 1703.07779 [hep-ph].
- [550] Thomas C. Bachlechner et al. "Axion Landscape Cosmology". In: *JCAP* 09 (2019), p. 062. DOI: 10.1088/1475-7516/2019/09/062. arXiv: 1810.02822 [hep-th].
- [551] Rouven Essig et al. "Working Group Report: New Light Weakly Coupled Particles". In: Snowmass 2013: Snowmass on the Mississippi. Oct. 2013. arXiv: 1311.0029 [hep-ph].
- [552] John Preskill, Mark B. Wise, and Frank Wilczek. "Cosmology of the Invisible Axion". In: *Phys. Lett. B* 120 (1983). Ed. by M. A. Srednicki, pp. 127–132. DOI: 10.1016/0370-2693(83)90637-8.
- [553] L. F. Abbott and P. Sikivie. "A Cosmological Bound on the Invisible Axion". In: *Phys. Lett. B* 120 (1983). Ed. by M. A. Srednicki, pp. 133–136. DOI: 10.1016/0370-2693 (83) 90638-X.
- [554] Michael Dine and Willy Fischler. "The Not So Harmless Axion". In: *Phys. Lett. B* 120 (1983). Ed. by M. A. Srednicki, pp. 137–141. DOI: 10.1016/0370-2693(83)90639-1.
- [555] Michael S. Turner. "Coherent Scalar Field Oscillations in an Expanding Universe". In: *Phys. Rev. D* 28 (1983), p. 1243. DOI: 10.1103/PhysRevD.28.1243.
- [556] Lam Hui et al. "Ultralight scalars as cosmological dark matter". In: *Phys. Rev. D* 95.4 (2017), p. 043541. DOI: 10.1103/PhysRevD.95.043541. arXiv: 1610.08297 [astro-ph.CO].
- [557] Lam Hui. "Wave Dark Matter". In: *Ann. Rev. Astron. Astrophys.* 59 (2021), pp. 247–289. DOI: 10.1146/annurev-astro-120920-010024. arXiv: 2101.11735 [astro-ph.CO].
- [558] David J. E. Marsh. "Axion Cosmology". In: *Phys. Rept.* 643 (2016), pp. 1–79. DOI: 10.1016/j.physrep.2016.06.005. arXiv: 1510.07633 [astro-ph.CO].

- [559] Wayne Hu, Rennan Barkana, and Andrei Gruzinov. "Cold and fuzzy dark matter". In: *Phys. Rev. Lett.* 85 (2000), pp. 1158–1161. DOI: 10.1103/PhysRevLett.85.1158. arXiv: astro-ph/0003365.
- [560] Sang-Jin Sin. "Late time cosmological phase transition and galactic halo as Bose liquid". In: *Phys. Rev. D* 50 (1994), pp. 3650–3654. DOI: 10.1103/PhysRevD.50.3650. arXiv: hep-ph/9205208.
- [561] P. J. E. Peebles. "Fluid dark matter". In: *Astrophys. J. Lett.* 534 (2000), p. L127. DOI: 10. 1086/312677. arXiv: astro-ph/0002495.
- [562] William H. Press, Barbara S. Ryden, and David N. Spergel. "Single Mechanism for Generating Large Scale Structure and Providing Dark Missing Matter". In: *Phys. Rev. Lett.* 64 (1990), p. 1084. DOI: 10.1103/PhysRevLett.64.1084.
- [563] M. R. Baldeschi, R. Ruffini, and G. B. Gelmini. "On massive fermions and bosons in galactic halos". In: *Phys. Lett. B* 122 (1983), pp. 221–224. DOI: 10.1016/0370-2693(83) 90688-3.
- [564] Jeremy Goodman. "Repulsive dark matter". In: *New Astron.* 5 (2000), p. 103. DOI: 10. 1016/S1384-1076(00)00015-4. arXiv: astro-ph/0003018.
- [565] Alexandre Arbey, Julien Lesgourgues, and Pierre Salati. "Galactic halos of fluid dark matter". In: *Phys. Rev. D* 68 (2003), p. 023511. DOI: 10.1103/PhysRevD.68.023511. arXiv: astro-ph/0301533.
- [566] Luca Amendola and Riccardo Barbieri. "Dark matter from an ultra-light pseudo-Goldsone-boson". In: *Phys. Lett. B* 642 (2006), pp. 192–196. DOI: 10.1016/j.physletb.2006.08. 069. arXiv: hep-ph/0509257.
- [567] Pierre-Henri Chavanis. "Mass-radius relation of Newtonian self-gravitating Bose-Einstein condensates with short-range interactions. I. Analytical results". In: Phys. Rev. D 84.4, 043531 (Aug. 2011), p. 043531. DOI: 10.1103/PhysRevD.84.043531. arXiv: 1103.2050 [astro-ph.C0].
- [568] Abril Suarez and Tonatiuh Matos. "Structure Formation with Scalar Field Dark Matter: The Fluid Approach". In: *Mon. Not. Roy. Astron. Soc.* 416 (2011), p. 87. DOI: 10.1111/j. 1365-2966.2011.19012.x. arXiv: 1101.4039 [gr-qc].
- [569] Lasha Berezhiani and Justin Khoury. "Theory of dark matter superfluidity". In: *Phys. Rev. D* 92 (2015), p. 103510. DOI: 10.1103/PhysRevD.92.103510. arXiv: 1507.01019 [astro-ph.CO].
- [570] JiJi Fan. "Ultralight Repulsive Dark Matter and BEC". In: *Phys. Dark Univ.* 14 (2016), pp. 84–94. DOI: 10.1016/j.dark.2016.10.005. arXiv: 1603.06580 [hep-ph].
- [571] M. Blennow et al. "Neutrino Portals to Dark Matter". In: *Eur. Phys. J. C* 79.7 (2019), p. 555. DOI: 10.1140/epjc/s10052-019-7060-5. arXiv: 1903.00006 [hep-ph].
- [572] Asher Berlin. "Neutrino Oscillations as a Probe of Light Scalar Dark Matter". In: *Phys. Rev. Lett.* 117.23 (2016), p. 231801. DOI: 10.1103/PhysRevLett.117.231801. arXiv: 1608.01307 [hep-ph].
- [573] Abhish Dev, Pedro A. N. Machado, and Pablo Martínez-Miravé. "Signatures of ultralight dark matter in neutrino oscillation experiments". In: *JHEP* 01 (2021), p. 094. DOI: 10. 1007/JHEP01(2021)094. arXiv: 2007.03590 [hep-ph].
- [574] Gordan Krnjaic, Pedro A. N. Machado, and Lina Necib. "Distorted neutrino oscillations from time varying cosmic fields". In: *Phys. Rev. D* 97.7 (2018), p. 075017. DOI: 10.1103/PhysRevD.97.075017. arXiv: 1705.06740 [hep-ph].

- [575] V. Barger, Patrick Huber, and Danny Marfatia. "Solar mass-varying neutrino oscillations". In: *Phys. Rev. Lett.* 95 (2005), p. 211802. DOI: 10.1103/PhysRevLett.95.211802. arXiv: hep-ph/0502196.
- [576] Vedran Brdar et al. "Fuzzy dark matter and nonstandard neutrino interactions". In: *Phys. Rev. D* 97.4 (2018), p. 043001. DOI: 10.1103/PhysRevD.97.043001. arXiv: 1705.09455 [hep-ph].
- [577] Marta Losada et al. "Probing scalar dark matter oscillations with neutrino oscillations". In: JHEP 04 (2022), p. 030. DOI: 10 . 1007 / JHEP04(2022) 030. arXiv: 2107 . 10865 [hep-ph].
- [578] Francesco Capozzi, Ian M. Shoemaker, and Luca Vecchi. "Neutrino Oscillations in Dark Backgrounds". In: *JCAP* 07 (2018), p. 004. DOI: 10.1088/1475-7516/2018/07/004. arXiv: 1804.05117 [hep-ph].
- [579] Andrew Cheek, Luca Visinelli, and Hong-Yi Zhang. "Testing the dark origin of neutrino masses with oscillation experiments". In: (Mar. 2025). arXiv: 2503.08439 [hep-ph].
- [580] YeolLin ChoeJo, Yechan Kim, and Hye-Sung Lee. "Dirac-Majorana neutrino type oscillation induced by a wave dark matter". In: *Phys. Rev. D* 108.9 (2023), p. 095028. DOI: 10.1103/PhysRevD.108.095028. arXiv: 2305.16900 [hep-ph].
- [581] Eung Jin Chun. "Neutrino Transition in Dark Matter". In: (Dec. 2021). arXiv: 2112.05057 [hep-ph].
- [582] Ki-Young Choi, Eung Jin Chun, and Jongkuk Kim. "Neutrino Oscillations in Dark Matter". In: *Phys. Dark Univ.* 30 (2020), p. 100606. DOI: 10.1016/j.dark.2020.100606. arXiv: 1909.10478 [hep-ph].
- [583] Jiajun Liao, Danny Marfatia, and Kerry Whisnant. "Light scalar dark matter at neutrino oscillation experiments". In: *JHEP* 04 (2018), p. 136. DOI: 10.1007/JHEP04(2018) 136. arXiv: 1803.01773 [hep-ph].
- [584] Shao-Feng Ge and Hitoshi Murayama. "Apparent CPT Violation in Neutrino Oscillation from Dark Non-Standard Interactions". In: (Apr. 2019). arXiv: 1904.02518 [hep-ph].
- [585] Clara Murgui and Ryan Plestid. "Coleman-Weinberg dynamics of ultralight scalar dark matter and GeV-scale right-handed neutrinos". In: *JHEP* 08 (2024), p. 168. DOI: 10.1007/ JHEP08 (2024) 168. arXiv: 2306.13799 [hep-ph].
- [586] Shao-Feng Ge, Chui-Fan Kong, and Alexei Y. Smirnov. "Testing the Origins of Neutrino Mass with Supernova-Neutrino Time Delay". In: *Phys. Rev. Lett.* 133.12 (2024), p. 121802. DOI: 10.1103/PhysRevLett.133.121802. arXiv: 2404.17352 [hep-ph].
- [587] Matías M. Reynoso and Oscar A. Sampayo. "Propagation of high-energy neutrinos in a background of ultralight scalar dark matter". In: *Astropart. Phys.* 82 (2016), pp. 10–20. DOI: 10.1016/j.astropartphys.2016.05.004. arXiv: 1605.09671 [hep-ph].
- [588] Matías M. Reynoso, Oscar A. Sampayo, and Agustín M. Carulli. "Neutrino interactions with ultralight axion-like dark matter". In: *Eur. Phys. J. C* 82.3 (2022), p. 274. DOI: 10. 1140/epjc/s10052-022-10228-w. arXiv: 2203.11642 [hep-ph].
- [589] Gaetano Lambiase and Tanmay Kumar Poddar. "Pulsar kicks in ultralight dark matter background induced by neutrino oscillation". In: *JCAP* 01 (2024), p. 069. DOI: 10.1088/1475-7516/2024/01/069. arXiv: 2307.05229 [hep-ph].
- [590] Sujata Pandey, Siddhartha Karmakar, and Subhendu Rakshit. "Interactions of astrophysical neutrinos with dark matter: a model building perspective". In: *JHEP* 01 (2019). [Erratum: JHEP 11, 215 (2021)], p. 095. DOI: 10.1007/JHEP11(2021)215. arXiv: 1810.04203 [hep-ph].

- [591] Yasaman Farzan and Sergio Palomares-Ruiz. "Flavor of cosmic neutrinos preserved by ultralight dark matter". In: *Phys. Rev. D* 99.5 (2019), p. 051702. doi: 10.1103/PhysRevD. 99.051702. arXiv: 1810.00892 [hep-ph].
- [592] Guo-Yuan Huang and Newton Nath. "Neutrinophilic Axion-Like Dark Matter". In: *Eur. Phys. J. C* 78.11 (2018), p. 922. DOI: 10.1140/epjc/s10052-018-6391-y. arXiv: 1809.01111 [hep-ph].
- [593] Guo-yuan Huang and Newton Nath. "Neutrino meets ultralight dark matter: $0\nu\beta\beta$ decay and cosmology". In: *JCAP* 05.05 (2022), p. 034. DOI: 10.1088/1475-7516/2022/05/034. arXiv: 2111.08732 [hep-ph].
- [594] Guo-yuan Huang et al. "Cosmology-friendly time-varying neutrino masses via the sterile neutrino portal". In: *Phys. Rev. D* 106.3 (2022), p. 033004. DOI: 10.1103/PhysRevD.106. 033004. arXiv: 2205.08431 [hep-ph].
- [595] Abhish Dev et al. "Constraining feeble neutrino interactions with ultralight dark matter". In: *Phys. Rev. D* 107.3 (2023), p. 035006. DOI: 10.1103/PhysRevD.107.035006. arXiv: 2205.06821 [hep-ph].
- [596] Ryan Plestid and Sophia Tevosyan. "The cosmology of ultralight scalar dark matter coupled to right-handed neutrinos". In: (Sept. 2024). arXiv: 2409.17396 [hep-ph].
- [597] Jorge Venzor, Abdel Pérez-Lorenzana, and Josue De-Santiago. "Bounds on neutrino-scalar nonstandard interactions from big bang nucleosynthesis". In: *Phys. Rev. D* 103.4 (2021), p. 043534. DOI: 10.1103/PhysRevD.103.043534. arXiv: 2009.08104 [hep-ph].
- [598] Hooman Davoudiasl, Gopolang Mohlabeng, and Matthew Sullivan. "Galactic Dark Matter Population as the Source of Neutrino Masses". In: *Phys. Rev. D* 98.2 (2018), p. 021301. DOI: 10.1103/PhysRevD.98.021301. arXiv: 1803.00012 [hep-ph].
- [599] Alexei Y. Smirnov and Victor B. Valera. "Resonance refraction and neutrino oscillations". In: JHEP 09 (2021), p. 177. doi: 10.1007/JHEP09(2021) 177. arXiv: 2106.13829 [hep-ph].
- [600] Pablo Martínez-Miravé, Yuber F. Perez-Gonzalez, and Manibrata Sen. "Effects of neutrinoultralight dark matter interaction on the cosmic neutrino background". In: *Phys. Rev. D* 110.5 (2024), p. 055005. DOI: 10.1103/PhysRevD.110.055005. arXiv: 2406.01682 [hep-ph].
- [601] Yechan Kim and Hye-Sung Lee. "Oscillating scalar potential and its implications for cosmic neutrino background searches". In: (Mar. 2025). arXiv: 2503.04949 [hep-ph].
- [602] K. S. Babu, Garv Chauhan, and P. S. Bhupal Dev. "Neutrino nonstandard interactions via light scalars in the Earth, Sun, supernovae, and the early Universe". In: *Phys. Rev. D* 101.9 (2020), p. 095029. DOI: 10.1103/PhysRevD.101.095029. arXiv: 1912.13488 [hep-ph].
- [603] Manibrata Sen and Alexei Y. Smirnov. "Neutrinos with refractive masses and the DESI BAO results". In: (July 2024). arXiv: 2407.02462 [hep-ph].
- [604] Jae-Weon Lee. "Neutrino mass and ultralight dark matter mass from the Higgs mechanism". In: (Oct. 2024). arXiv: 2410.02842 [hep-ph].
- [605] Ernest Ma. "Common origin of neutrino mass, dark matter, and baryogenesis". In: *Mod. Phys. Lett. A* 21 (2006), pp. 1777–1782. DOI: 10.1142/S0217732306021141. arXiv: hep-ph/0605180.
- [606] Asher Berlin and Dan Hooper. "Axion-Assisted Production of Sterile Neutrino Dark Matter". In: *Phys. Rev. D* 95.7 (2017), p. 075017. DOI: 10.1103/PhysRevD.95.075017. arXiv: 1610.03849 [hep-ph].

- [607] J. Moody and Frank Wilczek. "New Macroscopic Forces?" In: *Physical Review D* 30.1 (July 1984), pp. 130–138. doi: 10.1103/physrevd.30.130.
- [608] Jihn E. Kim. "Light Pseudoscalars, Particle Physics and Cosmology". In: *Phys. Rept.* 150 (1987), pp. 1–177. DOI: 10.1016/0370-1573(87)90017-2.
- [609] Leonard Parker and David Toms. *Quantum Field Theory in Curved Spacetime: Quantized Fields and Gravity*. Cambridge Monographs on Mathematical Physics. Cambridge University Press, 2009.
- [610] E. C. G. Sudarshan. "Equivalence of semiclassical and quantum mechanical descriptions of statistical light beams". In: *Phys. Rev. Lett.* 10 (1963), pp. 277–279. DOI: 10.1103/PhysRevLett.10.277.
- [611] Roy J. Glauber. "Coherent and incoherent states of the radiation field". In: *Phys. Rev.* 131 (1963), pp. 2766–2788. DOI: 10.1103/PhysRev.131.2766.
- [612] Roy J. Glauber. "The Quantum theory of optical coherence". In: *Phys. Rev.* 130 (1963), pp. 2529–2539. DOI: 10.1103/PhysRev.130.2529.
- [613] Anthony W. Brookfield et al. "Cosmology of mass-varying neutrinos driven by quintessence: theory and observations". In: *Phys. Rev. D* 73 (2006). [Erratum: Phys.Rev.D 76, 049901 (2007)], p. 083515. DOI: 10.1103/PhysRevD.73.083515. arXiv: astro-ph/0512367.
- [614] L. D. Landau and E. M. Lifshitz. *Mechanics, Third Edition: Volume 1 (Course of Theoretical Physics).* 3rd ed. Butterworth-Heinemann, Jan. 1976. ISBN: 0750628960.
- [615] Anne-Katherine Burns, Tim M. P. Tait, and Mauro Valli. "PRyMordial: the first three minutes, within and beyond the standard model". In: *Eur. Phys. J. C* 84.1 (2024), p. 86. DOI: 10.1140/epjc/s10052-024-12442-0. arXiv: 2307.07061 [hep-ph].
- [616] J. H. Koehne et al. "PROPOSAL: A tool for propagation of charged leptons". In: *Comput. Phys. Commun.* 184 (2013), pp. 2070–2090. DOI: 10.1016/j.cpc.2013.04.001.
- [617] Alfonso Garcia et al. "Complete predictions for high-energy neutrino propagation in matter". In: *JCAP* 09 (2020), p. 025. DOI: 10.1088/1475-7516/2020/09/025. arXiv: 2004.04756 [hep-ph].
- [618] Ibrahim Safa et al. "TauRunner: A public Python program to propagate neutral and charged leptons". In: *Comput. Phys. Commun.* 278 (2022), p. 108422. DOI: 10.1016/j.cpc.2022.108422. arXiv: 2110.14662 [hep-ph].
- [619] Diksha Garg et al. "Neutrino propagation in the Earth and emerging charged leptons with nuPyProp". In: *JCAP* 01 (2023), p. 041. DOI: 10.1088/1475-7516/2023/01/041. arXiv: 2209.15581 [astro-ph.HE].
- [620] Austin Cummings, Abigail Bishop, and Ryan Krebsaand William Luszczak. "NuLepton-Sim: A practical use of a neutrino propagation code as event generator". In: *PoS* ARENA2022 (2023), p. 014. DOI: 10.22323/1.424.0014.
- [621] A. M. Dziewonski and D. L. Anderson. "Preliminary reference earth model". In: *Phys. Earth Planet. Interiors* 25 (1981), pp. 297–356. DOI: 10.1016/0031-9201(81)90046-7.

Agraiments

Bé, has arribat fins aquí. O potser aquesta és l'única secció que has decidit llegir. Sigui com sigui, has fet bé, és la que considero més important. Estic molt orgullós de la recerca que s'inscriu en aquesta tesi, i també dels aprenentatges i les oportunitats que ha implicat. Però, molt per sobre d'això, estic inabastablement orgullós de totes les persones que m'han acompanyat –en menor o major mesura– fins on soc ara. Dels seus creixements i dels seus èxits, de ser on són.

És ara, en acabat d'escriure la tesi, que puc mirar enrere i agrair. Primer de tot, agrairme a mi, per ser, per escoltar-me i per cuidar-me. Jo mateix soc un dels aprenentatges que m'emporto d'aquests anys. Dues frases per a mi, i totes aquestes darreres pàgines per a vosaltres. Aparegui el vostre nom en aquestes pàgines o no, us hi agraeixo la immensa sort de tenir-vos a prop, físicament o al cor: us estimo. Ara, seieu, que va per llarg.

Als mentors

El jo científic que soc és qui és gràcies a la persona que li ha ensenyat tot el que sap. Jordi, espero haver estat un bon primer doctorand, i espero que jo t'hagi també permès aprendre algunes coses, així com tu me n'has fet aprendre a mi. Gràcies per la llibertat que m'has donat aquests cinc anys, per confiar en mi des del primer dia, per sempre estar disposat a escoltar (encara que pensis que soc massa patidor) i per saber-me donar espai. Per estar orgullós de mi encara que no m'ho hagis dit mai, i per donar-me esperança en què hi ha una altra manera de fer les coses i que aquesta manera també pot tenir èxit a l'acadèmia. Però, sobretot, gràcies per la bondat. Sota una capa de melapelisme bastant necessària, ets una persona intuïtivament bona, i m'has fet intentar ser-ho també. Ara em toca seguir les teves passes tot intentant diferenciar-me, però ja passaré a visitar.

Si, durant aquests cinc anys en Jordi no m'ha fotut massa canya, l'Iván ja s'ha encarregat de fer-ho. Iván, ets l'altra persona amb qui més he treballat, i de les que més he après. Gràcies per l'atenció als petits detalls, pel temps dedicat a donar-me consells i suggerències en llocs on ningú altre hi hauria parat, per ensenyar-me quines són les petites coses que fan que un article estigui ben presentat, i per explicar-me què és l'espí. Gràcies també al meu altre gran col·laborador, en Carlos, per sempre obrir-me les portes del teu institut i de la teva gent, ser inclusiu i fer-me sentir com a casa. Tots els meus amics flipaven quan els deia que anava a Harvard. Gràcies per la confiança que has tingut en mi, m'has ajudat a passar millor la síndrome de l'impostor.

Més enllà dels meus col·laboradors amb qui he col·laborat, una de les persones que més admiro ets tu, Miguel. Ets el referent de tantes persones, i ho ets per tants motius.

Per la passió, pel carisma, per la bondat, per la confiança que contagies i per, malgrat ser tan bo, mantenir els peus a terra. Conèixer-te a tu, i a en Xabi, és un pol Nord on apuntar la brúixola.

Als passadissos de la Facultat també hi ha moltes persones a qui agrair. Primer de tot, a tu, Concha, per ventilar-me la boira que m'ha encegat quan tocava prendre decisions, per la generositat, i per l'empenta que sempre m'has donat per impulsar la meva carrera. També al Josep, per sempre tenir llesta una broma i una batalleta, i al Justo, per ensenyar-me més que física.

Finalment, no només de física s'aprèn a l'acadèmia. Molts dels meus aprenentatges els he fet a la Comissió d'Equitat (DEIC), de lluitar per allò que és just. Assumpta, gràcies per mostrar-nos que hi ha lloc per a la vertadera força, la de saber-se i mostrar-se vulnerable i tot i així seguir endavant; i per fer del teu despatx un espai de cures. Companyes del DEIC, gràcies per ser referents.

Als amics (acadèmics)

Sobre el paper, l'objectiu d'un doctorat és aprendre a fer ciència. Ara bé, també cal assolir un sentiment de pertinença a la comunitat amb qui tens aquesta aventura en comú. Per mi això ha estat possible gràcies als amics que he fet pel camí, que m'han ajudat a sentirme un més de la ciència, i que són de les coses més boniques que m'emporto d'aquests quatre anys. N'he tingut a casa i enfora, i aquí us en parlo.

De la mateixa manera que a la carrera les forces per anar a classe venien de veure els amics, al doctorat ho feien els dinars al solet del balcó. He tingut la sort de compartir des del principi el camí amb l'Ana, la Carla, en Carlos, en Dani, en David, l'Emanuele, la Itziar, en Joao, en Jordi, en Julien, la Lucía, en Marcel, en Sergi i l'Stefan. També els més grans, que m'han fet de germans grans doctorals: en Dani, l'Edgar, en Josep, la Irina; i en especial als màquines, l'Óscar i en Quim. Gràcies a qui m'heu acompanyat en la quotidianitat del doctorat, en els moments difícils però sobretot en els feliços. Treure un article és un moment especial, però no seria possible sense el suport i companyia en els llargs dies frustrants que calen per arribar-hi. Gràcies per haver construït plegats un espai de trobada i cures a la facultat, us ho dic des del cor quan us dic que trobaré a faltar les vostres abraçades. Gràcies també a totes les que heu vingut darrere nostre, especialment a l'Adri i l'Elena, i que em doneu la confiança que la facultat (i tot en general) estarà en bones mans per anys i anys. Dins el balcó, menció especial per a la Mar. Em vas dir que en començar el doctorat tenies la intuïció que ens acompanyaríem molt bé, i això hem fet. Ja saps que estic infinitament orgullós de veure com has crescut en aquests anys, i amb moltes ganes de seguir admirant la teva llum en el futur.

Gràcies als meus companys de despatx per donar-li vidilla i que no m'hi tornés boig.

Gràcies Stefan i Sandra; i en especial a la Keyun, per la teva generositat i bondat, i per donar-me sempre el bon dia amb una llum a la mirada. Gràcies també als particuleros-cosmòlegs, Neus, Arianna i Àlex, per aguantar les converses del·lusionals. Gràcies a l'Anne-Katherine per la comprensió i el suport en l'època de postdocs. També, guardaré prop del meu cor a la tassa que em van fer les meves estudiants de Mètodes I, gràcies.

Al meu doctorat li estic agraït que m'hagi donat l'oportunitat de sortir de la facultat, per a crèixer com a científic, però sobretot per a conèixer persones precioses. Per començar per algun lloc, hi ha aquells amics a qui també puc anomenar col·laboradors. Virgile i Francesco, gràcies per llançar-vos a la piscina amb mi i ensenyar-me a fer ciència col·laborant de tu a tu, i per ser tan bons companys. Seguiré a la ciència gràcies a vosaltres. Jorge i Gonzalo, gràcies per la motivació constant i per donar els millors consells en aquest caos que és la carrera acadèmica. Rasmi, gràcies per fer el mateix camí alhora que jo, haver après i crescut alhora, i ser un mirall on entendre'm. Que bons amics que som, que bé que ens ho passem.

A en Jack i la Mar, gràcies per mantenir-nos cuidant des del primer dia que vam sortir enfora, ara ja fa tres anys. A la Sílvia i l'Ángel, els catalans adoptius que han fet de Barcelona un lloc més bonic (i una mica més astroparticulero, que ja tocava). A en George, l'Androniki i la Sara, gràcies per entendre'ns tan bé i per les situacions surrealistes en què ens hem trobat. A qui van fer de la meva estada al mojón de Fermilab fins i tot enyorable, i a qui tornaré a veure als EUA, l'Elias, en Gian i la Jamie. Hi ha tanta gent bonica a la física, que no acabaria mai. Gràcies per coincidir, Ana, Arturo, Asli, Daniel, Denise, Dom, Federica, Jaime, Kylar, Rebeca, Salva(s), entre molts altres.

Als amics (d'arreu)

La tesi és un viatge. Quan et perds entre neutrins i lagrangians, és una sort poder comptar amb una xarxa de persones que esclaten la bombolla i et fan tocar de peus a terra. Gràcies a totes les persones que, des de fora, m'ajuden a recordar per què estic fent tot això i quines són les coses vertaderament importants. Sé que totes vosaltres m'admireu d'una manera o altra, i aquesta admiració m'empeny a ser qui soc. A totes vosaltres: jo també us admiro molt, gràcies.

Per més hores de ser-hi, començo pels companys de Can Sadíssim. Pau, Maria i Noe, gràcies per les estones de caliu, les d'estiu a la terrassa i les d'hivern ajustats al sofà. Em considero molt afortunat d'haver trobat aquest pis, i el creixement d'aquests quatre anys també ha estat per ser-hi. A les gates, especialetes les dues, gràcies pels mimus bonics i pels tristos (i per preferir-me per davant del Pau).

Deu anys a la facultat donen per estimar a moltes persones, i de fer-ho amb molta intensitat. Als Ferdis, gràcies per ser-hi des d'aquell primer dia, estic orgullosíssim del vostre creixement com a persones i de la sort de poder-vos tenir encara al meu costat en aquest moment que ens fem –ara sí– grans. Andrea, Guillem, Irene, Maria i Maria, Marta, Neus, Pau i Pau, Pol i Sandra, us estimo molt. També a tots els que els heu vingut a acompanyar, com l'Ignasi, la Margot, la Valeria i en Xavier, i especialment a la Isona, a qui he conegut una hora i ja estimo irracionalment. També a la universitat, gràcies a l'Aina, per fer-ho tot tan fàcil; a la Núria, per ensenyar-me a ser-hi en la distància; a l'Emma i a la Marina. També, a la Carmen pel sucre en vena i els somriures.

Dono gràcies també a la divulgació, on he après tant i he conegut a gent increïble. Vaig començar el doctorat al Cosmo, d'on m'emporto companyes brillants com l'Abril o la Irena, i endinsant-me en Neurones Fregides. A totes les neurones, gràcies per ensenyar-me tantes coses i per haver-me acompanyat en una aventura tan preciosa i necessària. En especial, a en Miquel pels dinars a biologia i els esmorzars a la Montferry; i a la Cristina i a la Núria, per treure'm de casa i cuidar-me sense pretendre-ho del tot. Aprofito també per donar les gràcies a totes aquelles persones boniques que, en algun moment o altre, m'ha fet arribar els seus ànims a través de les xarxes: han servit.

La vida també m'ha creuat amb gent molt bonica. Gràcies a la Judit, per compartir amb mi l'estima al Montseny; i a l'Anna i la Laura, per compartir amb mi l'estima, en general. També a la Cris, per ajudar-me a ser. Castellers de Sarrià sempre ha sigut casa, i els agraeixo l'estima que em tenen i que de vegades no acabo d'entendre com la mereixo. Gràcies pels vespres de desconnectar dels neutrins, i per demanar-me sempre que torni. El mateix per a Endavant, Sisplau.

Finalment, als amics que fa més temps que tinc. De l'escola, tots hem seguit ja camins diferents, però us he sentit sempre ben a prop, i estic content d'anar-nos trobant per compartir-nos un cop més. Menció especial a la Marta per ajuntar-nos sempre, i a en Pau per confiar en nosaltres i pel creixement que està fent. Sobretot, però, gràcies a en Poti per ser la meva amistat més estable i duradora i per entendre'ns sense paraules, fins i tot quan discutim. Al final tot es remunta al capitalisme, oi?

A les lluitadores

I, com tot es remunta al capitalisme, també vull donar gràcies per allò que se n'allunya. L'acadèmia és un sistema reservat per a aquelles persones en unes condicions socials i econòmiques que els permeten superar els estudis; fer una carrera científica suposa un esforç i sacrifici pels quals no tothom pot trobar el suport. Aquesta tesi és possible gràcies a un privilegi que soc afortunat de tenir i que agraeixo per a visibilitzar-lo.

Per aquest motiu, agraeixo a totes les persones que han lluitat i lluiten per a fer la nostra societat més justa i més coherent amb la vida. Agraeixo a la lluita per l'educació i la sanitat públiques que posen la llavor i la cuiden mentre creix; per l'ecologisme i

la protecció del medi ambient que m'ha permès baixar pulsacions; i per la universitat pública, que és –tot i les moltes mancances– un dels pilars bàsics d'una societat formada. En concret, gràcies als professors que m'han inspirat, al col·lectiu de Doctorandes en Lluita per la vostra força; i a Alexandra Elbakyan per obrir els candaus de la ciència. Amb tot el que m'heu ensenyat, permès i donat, ho faré el millor que pugui.

A la família

Per acabar, el suport que hi ha estat sempre. De nou, per a poder dedicar-se a l'acadèmia cal un cert privilegi, i jo he tingut el privilegi i la sort de créixer a la meva família. Una família que m'ha donat tot el que he necessitat, però sobretot que m'ha estimat incondicionalment i m'ha empentat per a perseguir allò que sentís (fins i tot la carrera acadèmica, que toca a prop). A casa els agraïments i l'estima són més tàcits que explícits, així que aquest espai és una oportunitat perquè quedin escrits per a sempre.

A Aiguafreda hi tinc una àvia que és una força de la natura. Fa els millors arrossos que he tastat mai, i sempre té una ració preparada per a què repeteixi o me n'emporti una carmanyola. Sempre està molt contenta que la vingui a veure, fins i tot si vinc amb les mans buides, i jo també estic molt content d'anar-hi. Sento que està orgullosa de mi, encara que no entengui del tot el que faig, i jo també ho estic molt d'ella. La incapacitat de parar de fer coses, transversal a tota la família, ve d'ella. Gràcies àvia, t'estimo molt.

A banda i banda de la Península hi tinc tiets i tietes que també em fan sentir estimat. Gràcies a la Cuqui, el Jordi, la Mimi i la Xell, així com la Marta i el Ramis, per recordar-me que soc el nen petit de la família, i mimar-me com a tal. Al meu germà gran, usualment no tan mimat, el Guille, també li estic molt agraït. No som de moltes paraules, i tots dos ho fem tan bé com sabem. Però sé que ens tenim l'un a l'altre pel que faci falta quan faci falta, que ell m'estima i jo l'estimo a ell. Gràcies per deixar-me crèixer al teu costat i per cobrir-me les esquenes.

Finalment, acabo la tesi com l'he començada. Gràcies infinites als meus pares. Gràcies a tots dos per estimular-me des de ben petit i acompanyar-me fins convertir-me en qui soc. Poc a poc m'adono que és molt difícil ser pare, però trobo que jo no hauria fet millor que vosaltres. Al papa, per totes les vegades que has mostrat l'estima en les petites coses: els taxis, els pastissos o els talls de cabell. Gràcies per ensenyar-me a creure en un món més just i sensat, i per transmetre'm els valors amb què havies crescut. A la mama, gràcies per tot. Tot, en el sentit més complet i ample de la paraula. Si soc una persona que sovint pensa més en els altres que en un mateix, per a bé i per a mal, és culpa teva. Gràcies per sempre cuidar-nos, pels sacrificis que inevitablement has hagut de fer per nosaltres, per haver-ho tirat tot endavant. Ets la major referent de la meva vida.